

CR112177
N73-20011

TR- 3720291



Viking'75 Project

BALLOON LAUNCHED DECELERATOR TEST PROGRAM
POST- FLIGHT TEST REPORT
BLDT VEHICLE AV- 2

**CASE FILE
COPY**

NAS1-9000

MARTIN MARIETTA

TR-3720291

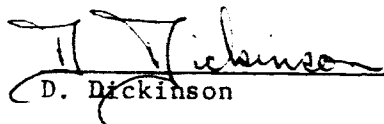
15 December 1972

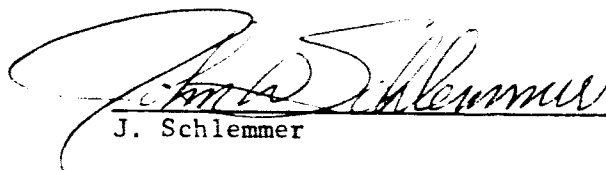
DRL Line Item No.: N3-T040


BALLOON LAUNCHED DECELERATOR
TEST PROGRAM
POST-TEST TEST PROGRAM
(45 day)

BLDT VEHICLE AV-2

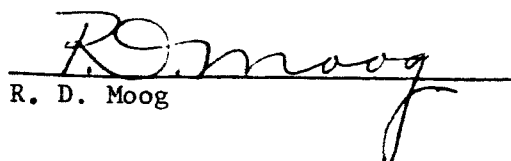
prepared by:


D. Dickinson


J. Schlemmer

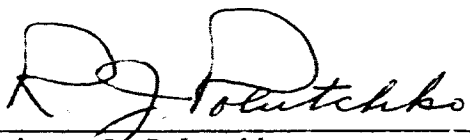

F. Hicks


F. Michel

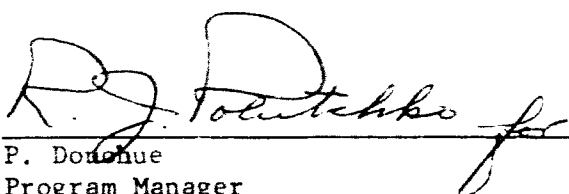

R. D. Moog

PREPARED UNDER CONTRACT NAS1-9000 BY
MARTIN MARIETTA CORPORATION
DENVER DIVISION
P. O. Box 179
DENVER, COLORADO 80201

APPROVAL SHEET


 Robert J. Polutchko
 Project Engineer
 Viking Vehicle Engineering

12/15/72
 Date


 P. Donohue
 Program Manager
 BLDT Program

12/15/72
 Date

TABLE OF CONTENTS

	<u>PAGE</u>
APPROVAL SHEET	i
TABLE OF CONTENTS	iii
SECTION	TITLE
I.	PURPOSE OF REPORT I-1
II.	MISSION OBJECTIVES II-1
III.	DECELERATOR OPERATIONS SUMMARY III-1
	A. Operations Summary III-1
	B. Vehicle Performance Summary III-2
	C. Decelerator System Summary III-2
IV.	MISSION OPERATIONS IV-1
	A. Flight Readiness Test and Launch IV-1
	B. Ascent and Float IV-1
	C. Vehicle Flight IV-3
	D. Recovery Operations IV-4
V.	DECELERATOR SYSTEM ANALYSIS V-1
	A. System Description V-1
	B. Mortar Fire Conditions V-2
	C. Mortar Performance V-3
	D. Decelerator Inflation Sequence V-4
	E. Opening Load V-6
	F. Vehicle Stability V-8
	G. Parachute Drag Performance V-9
	H. Aeroshell Separation V-12
	I. Parachute Recovery Assessment V-14

TABLE OF CONTENTS (CONTINUED)

	<u>PAGE</u>
VI. VEHICLE PERFORMANCE ANALYSIS	VI-1
A. Flight Dynamics	VI-1
B. Capsule Aerodynamic Characteristics	VI-11
C. Thermal Control Subsystem	VI-13
D. Structural Subsystem	VI-15
E. Propulsion, Azimuth Pointing and Ordnance Subsystems	VI-16
F. Electrical Subsystem	VI-19
G. Instrumentation Subsystem	VI-19
H. RF Subsystem	VI-20
I. TSE/OSE	VI-20
J. Mass Properties	VI-21
VII. MISSION CONCLUSIONS AND RECOMMENDATIONS	VII-1
VIII. REFERENCES AND OTHER DATA SOURCES	VIII-1
A. References	VIII-1
B. Abbreviations	VIII-2
APPENDIX A - Description of Balloon Launched Decelerator Test Vehicle	A-1
APPENDIX B - Description of BLDT System Mission	B-1
APPENDIX C - GAC Post-Test Failure Analysis	C-1
APPENDIX D - Parachute Dimensional Survey	D-1
APPENDIX E - BLDT Computer Software	E-1

LIST OF ILLUSTRATIONS

<u>FIGURE</u>	<u>TITLE</u>	<u>PAGE</u>
II - 1	BLDT AV-2 Test Conditions	II-3
IV - 1	Mission Ground Track AV-2	IV-8
IV - 2	Balloon Altitude Profile	IV-9
IV - 3	Pointing Pressure Profile	IV-10
IV - 4	Mortar Fire Command System Operation	IV-11
V - 1	Viking Decelerator System	V-17
V - 2	Ejected Weight Distribution	V-18
V - 3	On-Board Camera Photographs	V-19
V - 4	Canopy Growth Parameter	V-23
V - 5	Canopy Area Oscillations	V-24
V - 6	Parachute Filling Time from Line Stretch	V-25
V - 7	Parachute Opening Load, 0 - 10 Seconds	V-26
V - 8	Parachute Opening Load, 0 - 50 Seconds	V-27
V - 9	Tensiometer Readings	V-28
V - 10	Parachute Pull Angle, Pitch Plane	V-29
V - 11	Parachute Pull Angle, Yaw Plane	V-30
V - 12	Parachute Total Pull Angle	V-31
V - 13	Longitudinal Acceleration	V-32
V - 14	Transverse Acceleration	V-33
V - 15	Normal Acceleration	V-34
V - 16	Vehicle Pitch Rate	V-35
V - 17	Vehicle Roll Rate	V-36
V - 18	Vehicle Yaw Rate	V-37
V - 19	Parachute Lifting During Descent	V-38
V - 20	Parachute Force Coefficient (Accelerometer Data)	V-39
V - 21	Parachute Force Coefficient (Tensiometer Data)	V-40
V - 22	Parachute Force Coefficient (Accelerometer Data)	V-41
V - 23	Parachute Force Coefficient (Tensiometer Data)	V-42
V - 24	Dynamic Pressure Time-History	V-43
V - 25	Mach Number Time-History	V-44

LIST OF ILLUSTRATIONS (CONTINUED)

<u>FIGURE</u>	<u>TITLE</u>	<u>PAGE</u>
V - 26	Flight Path Angle	V-45
V - 27	Aeroshell Separation Distance, 0 - 3 Seconds	V-46
V - 28	Extensiometer Separation Distance	V-47
V - 29	Extensiometer and Guide Rail Location	V-48
V - 30	Relative Angular Motion between Aeroshell and Lander	V-49
VI - 1	BLDT AV-2 Test Conditions	VI-26
VI - 2	WSMR Map Showing Telemetry and Radar Sites	VI-27
VI - 3	Gyro Data Prior to Drop	VI-28
VI - 4	Accelerometer Data Prior to Drop	VI-29
VI - 5	Gyro Data During Powered Flight	VI-30
VI - 6	Accelerometer Data During Powered Flight	VI-31
VI - 7	Comparison Between Radar Data (R125 transformed to R123)	VI-32
VI - 8	Comparison Between Radar Data (R128 transformed to R123)	VI-33
VI - 9	Radar (R125) Velocity vs. Flight Time	VI-34
VI - 10	Radar (R125) Flight Path Angle vs. Flight Time	VI-35
VI - 11	Radar (R123) Altitude (MSL) vs. Flight Time	VI-36
VI - 12	Step Trajectory Reconstruction of Altitude and Velocity	VI-37
VI - 13	Step Trajectory Reconstruction of Mach Number	VI-38
VI - 14	Step Trajectory Reconstruction of Vehicle Attitude and Flight Path Angle	VI-39
VI - 15	Step Trajectory Reconstruction of the Body Heading and Velocity Heading	VI-40
VI - 16	Step Trajectory Reconstruction of Angle of Attack and Sideslip	VI-41
VI - 17	Step Trajectory Reconstruction of Total Angle of Attack	VI-42
VI - 18	Body Attitudes from Aft Looking Camera (Milliken)	VI-43
VI - 19	Angles of Attack and Sideslip and Axial Force Coefficient at Mortar Fire	VI-44

LIST OF ILLUSTRATIONS (CONCLUDED)

<u>FIGURE</u>	<u>TITLE</u>	<u>PAGE</u>
VI - 20	Mission Ascent Profiles	VI-45
VI - 21	Base Cover Temperature History	VI-46
VI - 22	Rocket Motor Support Structure Temperature History	VI-47
VI - 23	Aeroshell Temperature History	VI-48
VI - 24	S-Band Transmitter	VI-49
VI - 25	BLDT AV-2 Vehicle Azimuth Heading	VI-50
VI - 26	BLDT AV-2 Torsional Stiffness	VI-51

LIST OF TABLES

<u>TABLE</u>	<u>TITLE</u>	<u>PAGE</u>
IV - 1	AV-2 Vehicle Flight Sequence of Events	IV-6
IV - 2	Summary of Flight Parameters	IV-7
V - 1	Parachute Geometric Properties	V-16
VI - 1	BLDT AV-2 Atmospheric Properties	VI-22
VI - 2	State Vector Data	VI-23
VI - 3	Battery Performance Data	VI-24
VI - 4	Final BLDT Mass Properties, AV-2	VI-25

I. PURPOSE OF REPORT

The purpose of this report is to document the pertinent events concerned with the launch, float and flight of Balloon Launched Decelerator Test Vehicle AV-2 and the performance of the Decelerator System installed therein. The report will describe and provide data pertinent to the flight trajectory and decelerator test points at the time of decelerator deployment as well as a description of the time history of vehicle events and anomalies encountered during the mission.

The final test reports for BLDT Vehicles AV-1, AV-3 and AV-4 are contained in the following documents:

- AV-1 - Document number TR-3720289
- AV-3 - Document number TR-3720293
- AV-4 - Document number TR-3720295

II. MISSION OBJECTIVES

The mission objective for the BLDT program is to subject the Viking Decelerator System to qualification test requirements at simulated Mars entry conditions and in the wake of a full scale blunt body which simulates the Viking Lander Capsule. The program test requirements provide for parachute qualification at simulated Mars atmospheric conditions which are consistent with parachute deployment at supersonic, transonic and subsonic conditions.

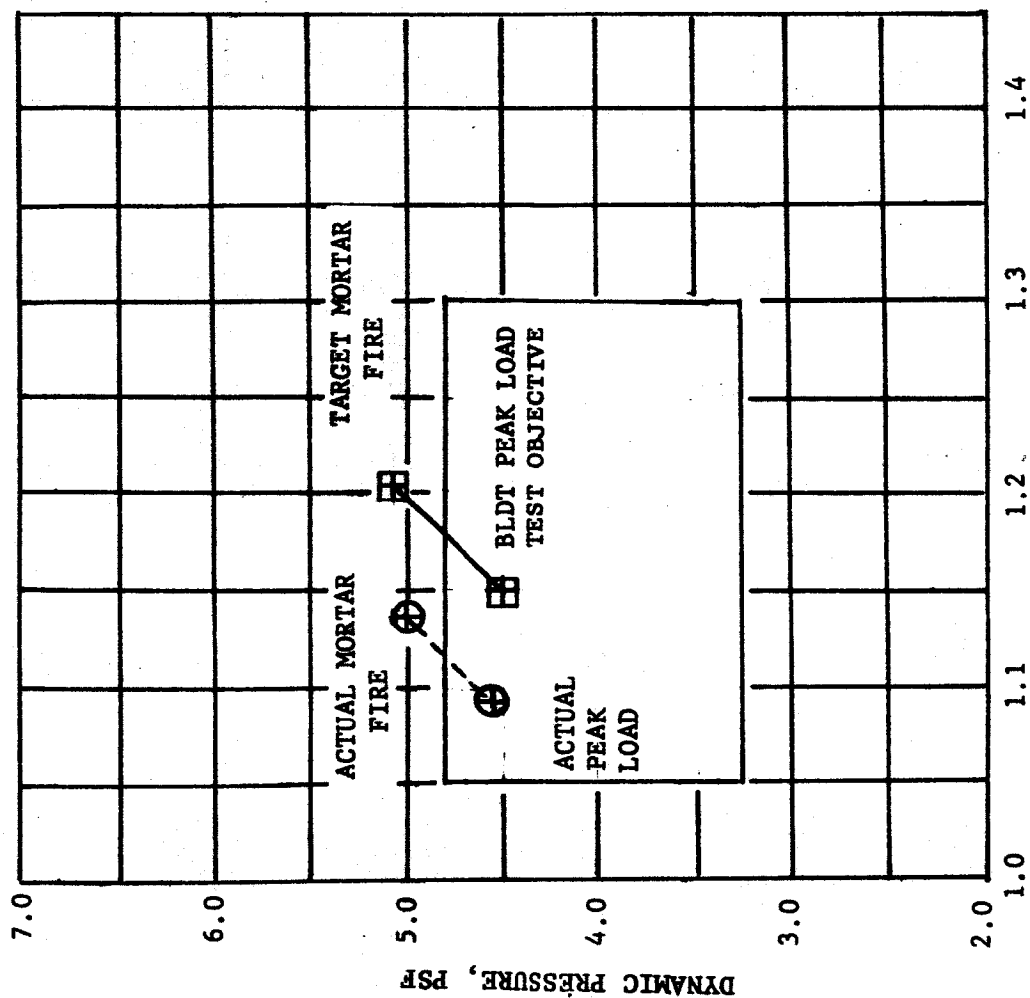
The flight of vehicle AV-2 provides for deployment of the decelerator under the simulated Mars atmospheric conditions equivalent to a transonic case. The Mach number and dynamic pressure resulting from this simulated entry condition are shown on Figure II-1. The total vehicle requirements described in Paragraph 3.3 of "Parachute Test Objectives and Requirements Document for BLDT Program" (RD-3720247) are:

Angle of Attack at Mortar Fire	$\leq 21^{\circ}$
Residual Spin Rate	$\leq 100^{\circ}/\text{second}$
Parachute Temperature at Mortar Fire	$\leq 80^{\circ}\text{F}$
Simulated Mach Number/"q" Conditions	See Figure II-1

In order to provide the velocity/atmospheric density equivalent to a transonic Mars entry, the BLDT vehicle was lifted to high altitude (approximately 120,000 feet) beneath a balloon system. Once at the correct altitude and over the White Sands Missile Range, the flight vehicle was released from the balloon load bar and under control of airborne programming, the vehicle was boosted by solid rocket motors to the altitude (density)/velocity equivalent of the transonic test condition.

It was also a goal of this mission to separate the vehicle aeroshell following decelerator deployment in order to obtain a time/ distance history of the separation function.

A description of the BLDT vehicle, which served as the qualification test bed, is included in Appendix A of this report. A description of the BLDT mission is provided in Appendix B.



MACH NUMBER

FIGURE II-1 BLDT AV-2 TEST CONDITIONS

III. DECELERATOR QUALIFICATION SUMMARY

The following is a summary of program events, pertinent to the decelerator system, occurring from the time of decelerator system installation in the BLDT vehicle through the recovery of the decelerator system at the point of payload impact.

A. Operations Summary

The decelerator system was installed in the base cover of vehicle AV-2 prior to final vehicle assembly for Flight Readiness Test. The system was Martin Marietta Corporation Serial Number 0000074 (GAC System S/N 14) with a system weight of 125.12# and a total ejected weight of 97#. Following decelerator installation in the BLDT however, it was necessary to remove the decelerator breach and orifice to assure that the orifice was installed correctly. The orifice assembly was replaced and the breach assembly reinstalled.

During vehicle stand time while awaiting satisfactory meteorological conditions for launch, conditioned air was applied to the vehicle in order to maintain the vehicle interior, including the decelerator cannister, at a temperature below 80°F.

The decelerator system was subject to cooling during the ascent and float phases of the mission with pertinent decelerator temperatures just prior to release from the load bar as follows:

<u>Sensor Location</u>	<u>Spec. Req'd (°F)</u>	<u>Actual Temp (°F)</u>
*Bridle #1	+210 to -90	+46
*Bridle #2	+210 to -90	+46
*Bridle #3	+210 to -90	+45
Mortar Cannister #1	+80 (No Min)	+48
Mortar Cannister #2	+80 (No Min)	+45
Mortar Breach	+175 to +25	+49 (automatic heater controlled)
Mortar Breach Flange	+74 to +25	+45

*Temperature measured on the base cover interior beneath the bridle leg.

B. Vehicle Performance Summary

The AV-2 vehicle performed normally and all anticipated functions occurred. Mortar fire was commanded from the ground at the proper flight conditions for the decelerator test. The flight conditions at mortar fire were:

	<u>TARGET</u>	<u>ACTUAL</u>
Mach Number	1.208	1.135
Dynamic Pressure (PSF)	5.07	5.01
Residual Spin Rate (Deg/Sec)	+100	-62
Total Angle of Attack (Deg)	<21	7.1

There was no vehicle induced damage to the decelerator system.

C. Decelerator System Summary

Test conditions at peak load fell within the envelope of Mach number and dynamic pressure shown in Figure II-1. Mortar velocity of 106.5 FPS was lower than expected but above the minimum required for Viking. Bag strip and parachute inflation were normal with little unsymmetrical loading in evidence.

The maximum parachute opening load of 9009 lbs. occurred shortly before first full inflation. After a short period of area fluctuations, the canopy reached stable inflation and showed good stability for the remainder of the flight. No damage, other than a few black smudges, was sustained by the parachute.

Parachute drag exceeded expectations over most of the Mach number range. Some drag reduction occurred near Mach 1.0 as predicted by wind tunnel testing.

The parachute opening transient induced vehicle attitude rates as high as 92 degrees/second initially, which damped to below 50 degrees/second in 10 seconds. The damping characteristics of the parachute, as experienced on other BLDT flights, are not as good as expected.

Aeroshell separation was successfully demonstrated at a dynamic pressure of 1.43 psf and a Mach number of .615. The separation distance of 120 feet in 3 seconds was adequate to meet the minimum system requirement of 50 feet in 3 seconds. All separation hardware performed satisfactorily.

IV. MISSION OPERATIONS

The following is a summary of the program events occurring from the time of vehicle AV-2 flight Readiness Test through Recovery Operations.

A. Flight Readiness Test and Launch

BLDT Vehicle AV-2 completed Flight Readiness Test #1 on July 22, 1972 with data review being completed on July 23. The airborne batteries were activated on July 20, and installed prior to FRT.

The launch was initiated during the evening of July 25, for a launch on the morning of July 26. This launch attempt resulted in vehicle launch at 1403 hours Z on July 26.

Balloon winch up and system launch were smooth and without incident with launch winds (surface to 1000 ft) of approximately 17 to 18 knots.

During the pre-launch vehicle checkout, a high current was noted on the E-31 umbilical ground instrument power supply. The umbilical was disconnected, at both the van and vehicle, inspected and reconnected. The inspection and reconnection of the umbilical revealed that the high current condition no longer existed. Post flight inspection located a cut umbilical which caused intermittent shorting. The umbilical was repaired prior to the launch of vehicle AV-4.

B. Ascent and Float

The balloon ground track during ascent and float was as shown on Figure IV-1. The float track to range, range intersect point and float heading at range were in general agreement with the pre-launch prediction for these parameters.

Figure IV-2 presents the ascent profile of altitude versus time of day. It can be seen that the predicted profile of 1000 feet/minute was not quite met with a result that drop altitude was attained slightly late. Unlike vehicle AV-1 where the system was porpoising approximately 1200 feet at vehicle release from the load bar, vehicle AV-2 system was very stable at float with porpoising at drop in the order of 200 feet. The reduced porpoising was probably due to a more timely arrival at float altitude and system ballasting earlier in the ascent phase for vehicle AV-2.

During the ascent phase, the vehicle was intermittently acquired by range telemetry at approximately 14:23 hours Z and a balloon altitude of approximately 18,000 feet. The vehicle beacon was acquired by range radar at 14:29 hours Z and an altitude of approximately 22,000 feet. The vehicle command system was captured at approximately 14:54 hours Z and at an altitude of approximately 47,000 feet. Command system operation was verified at 14:59 hours Z by sending vehicle safe and safe backup commands and monitoring airborne receipt of the commands on the vehicle TM data and the command reception indicator panel. Vehicle azimuth pointing operations, just prior to drop, are covered in Section VI - Vehicle Performance Analysis.

Two anomalies occurred during the ascent phase of the mission which were:

1. Interruption of the TDC magnetometer data stream between the TDC computer and the 1108 real time computer with loss of the interface for approximately 10 minutes.
2. Loss of azimuth pointing system pressure.

Post flight analysis of the TDC computer to real time computer problem revealed that the interruption was due to a synchronization problem between

the two computers. A revision was made to the 1108 software to provide automatic resynchronization in the event of any future interruptions. Procedures were also prepared to manually resynchronize the interface. This anomaly did not reoccur during the remaining BLDT flights.

As previously stated, during the ascent and float phase, the azimuth pointing system lost system pressure. The pressure decay was approximately as shown in Figure IV-3. Clockwise and counter-clockwise pointing commands were issued when system pressure had decayed to approximately 1200 psi, in an attempt to reduce system leakage. Cycling of the system reduced the pressure decay rate from approximately 11 psi/min to approximately 1 psi/min. The tank pressure finally stabilized at about 1080 psi.

The fact that the system pressure decay proceeded without any thruster operation and the decay rate decreased when the system was operated indicated that the leak was probably from the system relief valve and due to contamination at the system regulation valve seat. Since this anomaly was judged to be unique to the AV-2 system and since this system was not to be flown on subsequent mission, no further failure analysis was performed.

C. Vehicle Flight

All airborne and ground functions occurred as planned during the vehicle flight portion of the mission. The real time mortar fire command was issued by the WSMR ground computer based on radar tracking and T-24 hour meteorological data. The computer software used is described in Appendix E. The real time computed dynamic pressure is compared to the actual (T-1 hour meteorological data and reconstructed post flight trajectory) and also to the reference dynamic pressure (software reference) in Figure IV-4. The

difference in the real time computed and reference dynamic pressure was used to predict the time when the desired dynamic pressure (5.05 PSF) would be obtained. When the real time prediction matched this value, the computer fired the mortar through the command system. The variation in this predicted mortar fire time just prior to mortar fire is also shown in Figure IV-4.

A variation in real time computed dynamic pressure at 36 seconds caused the mortar fire program to (properly) delay the mortar fire time such that the predicted dynamic pressure was 2% below the target.

The programmed sequence of flight events and actual event times for the vehicle flight are provided in Table IV-1. Table IV-2 contains a summary of predicted and actual flight parameters.

During this phase of the mission, the decelerator was deployed as planned. The analysis of the decelerator performance is provided in Section V.

It was a requirement during this phase of the mission to separate the aeroshell from the BLDT test bed in order to obtain a separation time-distance history. The analysis of the flight film covered in Section V of this report, reveals that the actual separation rate exceeded the minimum requirement of 50 feet in 3 seconds.

Inspection of the recovered vehicle indicated -

1. All ordnance functions occurred with no damage to the vehicle due to separation processes or vehicle ordnance functions.

D. Recovery Operations

The vehicle flight path was such that the payload impacted approximately 12 miles southwest of the vehicle drop point (See Figure IV-1). The

point of impact on the range was in sandy terrain and close to a major range road which minimized vehicle damage and provided easy access for recovering the expended vehicle and decelerator. All recovery operations were completed on the launch day.

TABLE IV-1

AV-2 VEHICLE FLIGHT SEQUENCE OF EVENTS

	Programmed Time (Seconds)	Actual Time (Seconds)	Source
1. Drop from Load Bar/ Initiate A/B Programmer	0	0	Ground Command
2. Ignite Spin Motors/ Enable Boost Motors	+1	1.01	A/B Programmer
3. Ignite Boost Motors	+2	2.04	A/B Programmer
4. Ignite Despin Motors/ Release Camera Lens Covers/ Start Aft Milliken Camera	+33	33.23	A/B Programmer
5. Initiate Mortar Fire/ Start Aft Photosonics Camera/ Start Forward Milliken Camera	33.5 to 39.5	38.22	Ground Command
6. Initiate Mortar Fire Backup/ Start Aft Photosonics Camera B/U/ Start Forward Milliken Camera B/U	39	39.24	A/B Programmer
7. Separate Aeroshell	47	47.32	A/B Programmer

TABLE IV-2

SUMMARY OF FLIGHT PARAMETERS

	<u>PREDICTED</u>	<u>ACTUAL</u>
A. Drop Time, GMT	--	16:55:33.65
B. Drop Conditions		
1. Longitude (DEG)	--	106.235
2. Latitude (DEG)	--	33.256
3. Altitude, Geometric (FT)	122,500	120,900
4. Drop Azimuth (DEG)	--	210.4
C. Spin/Despin		
1. Spin-up Rate (DEG/SEC)	212	224
2. Spin Rate at Despin (DEG/SEC)	111	118
3. Residual Spin Rate (DEG/SEC)	-61	-62
D. Maximum Flight Conditions		
1. Maximum Q/V	29.0	28.6
a. Time from Drop (SEC)	7.92	8.215
b. Max. Q (PSF)	1451	1396
c. Velocity (FPS)		
2. Maximum Acceleration		
a. Time from Drop (SEC)	14.50	14.0
b. Max. Longitudinal Acceleration (g's)	2.84	2.79
E. Mortar Fire Conditions		
1. Mach Number	1.208	1.133
2. Dynamic Pressure (PSF)	5.07	5.00
3. Velocity (FPS)	1267	1194
4. Axial Acceleration (g's)	-0.41	-0.40
5. Altitude (FEET)	137,500	135,368
6. Angle of Attack (DEG)	-3.0	5.4
7. Angle of Yaw (DEG)	0.0	-4.9
F. Aeroshell Separation Conditions		
1. Mach Number	0.67	.615
2. Dynamic Pressure (PSF)	1.46	1.43
3. Time for 1 Foot (SEC)	0.18	0.18
4. Time for 50 Feet (SEC)	3.0	1.9
6. Distance at 3 Seconds (FEET)	50.0	120.0

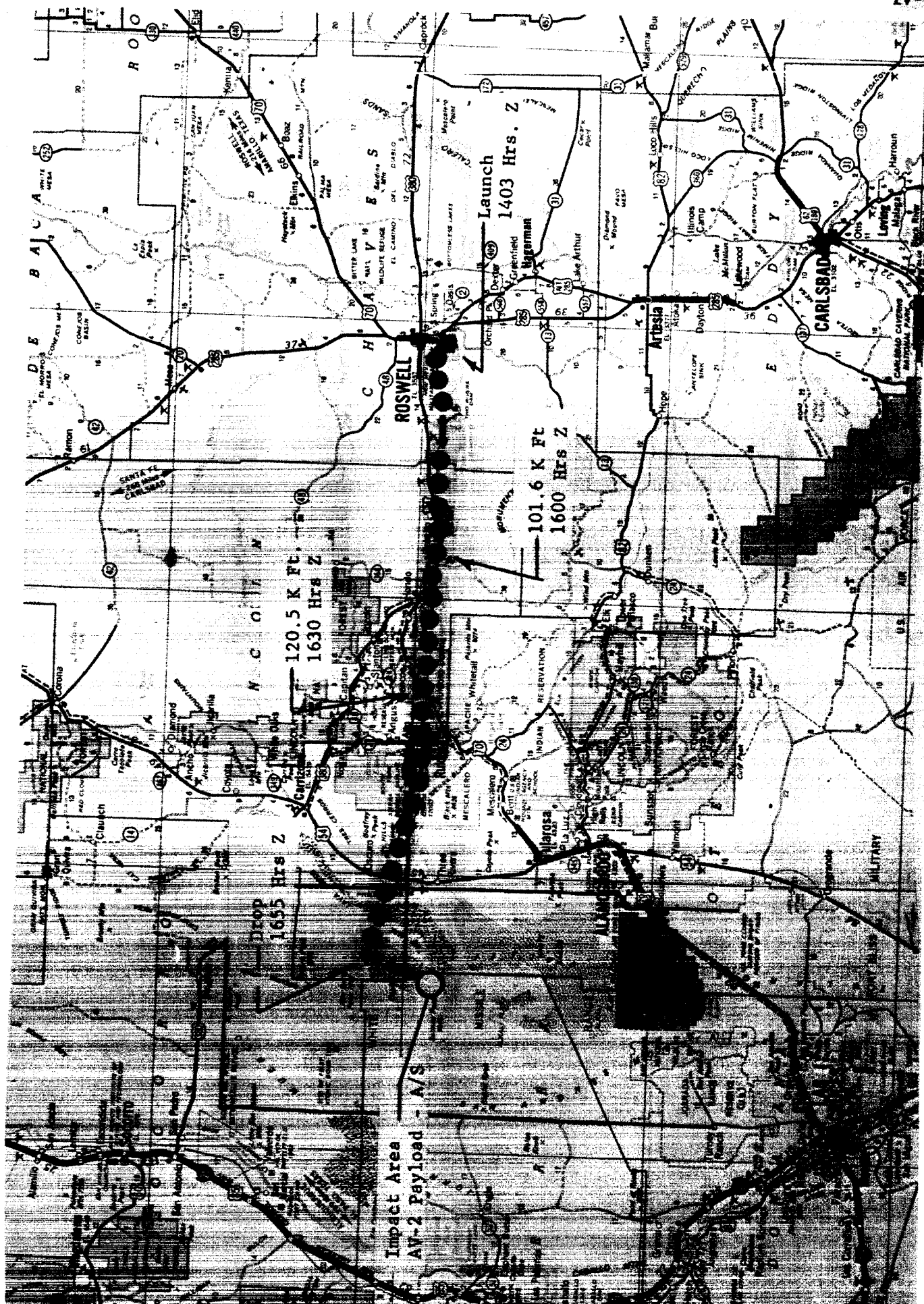


FIGURE IV-1
MISSION GROUND TRACK AV2

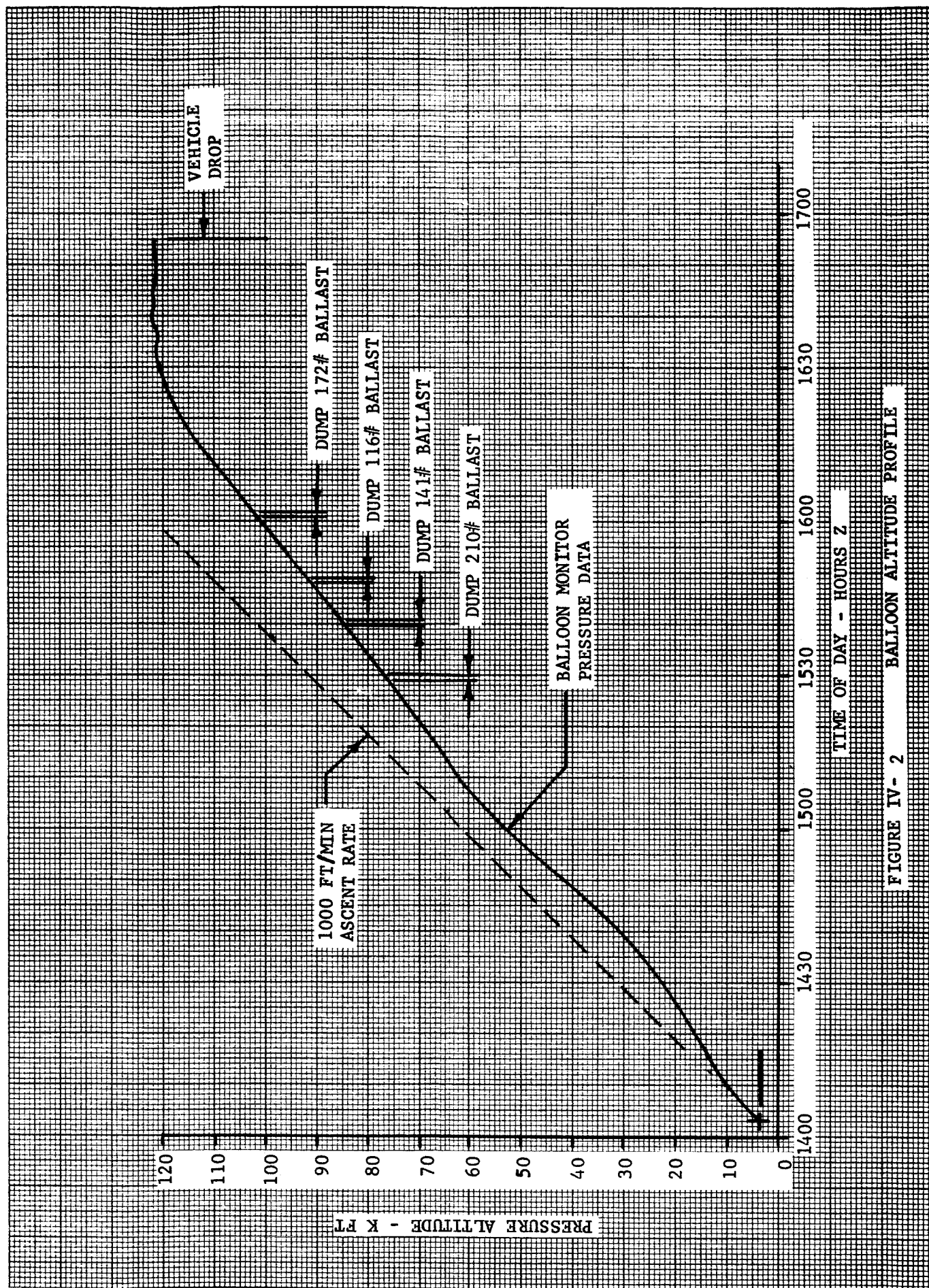


FIGURE IV-2 BALLOON ALTITUDE PROFILE

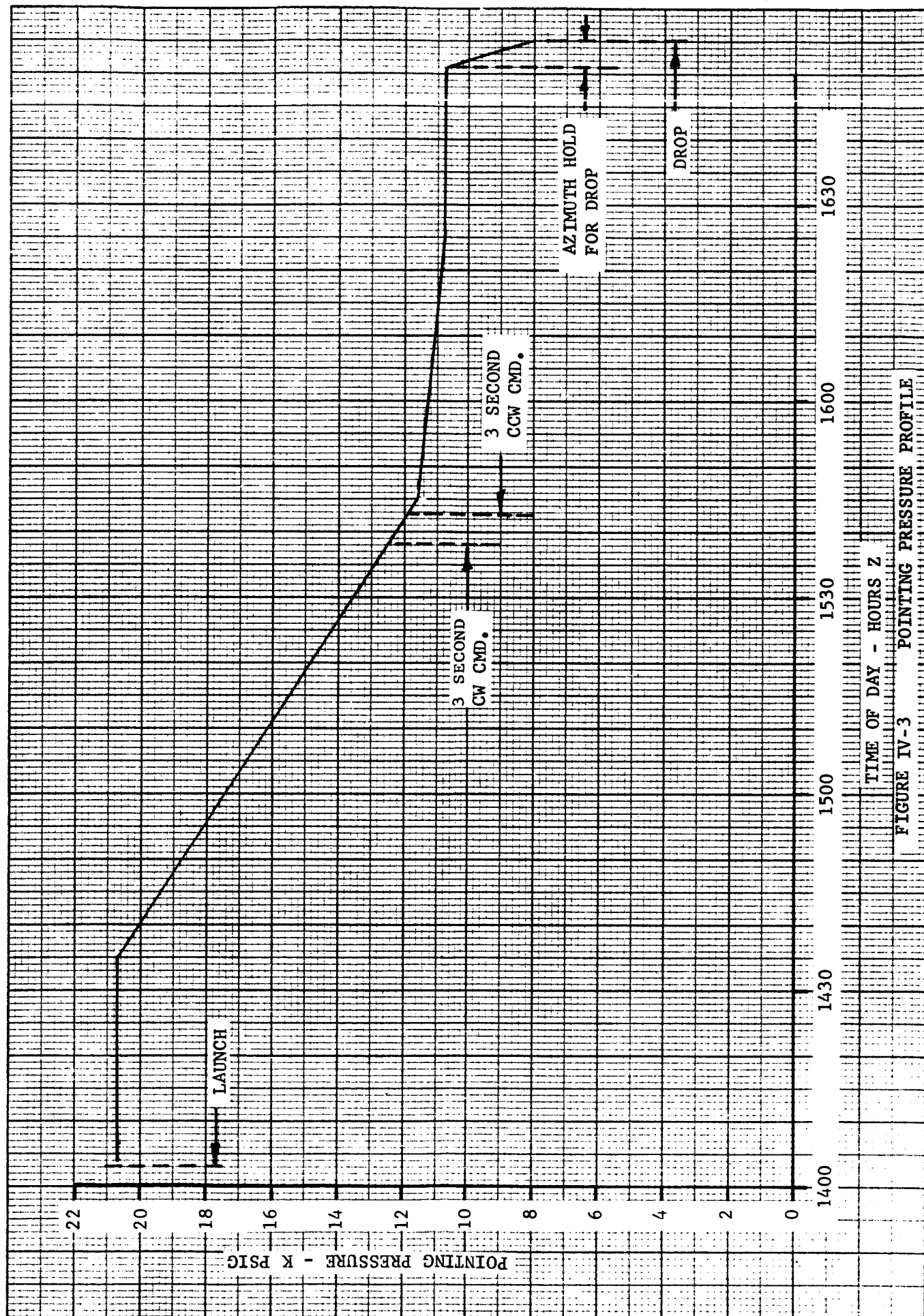


FIGURE IV-3 POINTING PRESSURE PROFILE

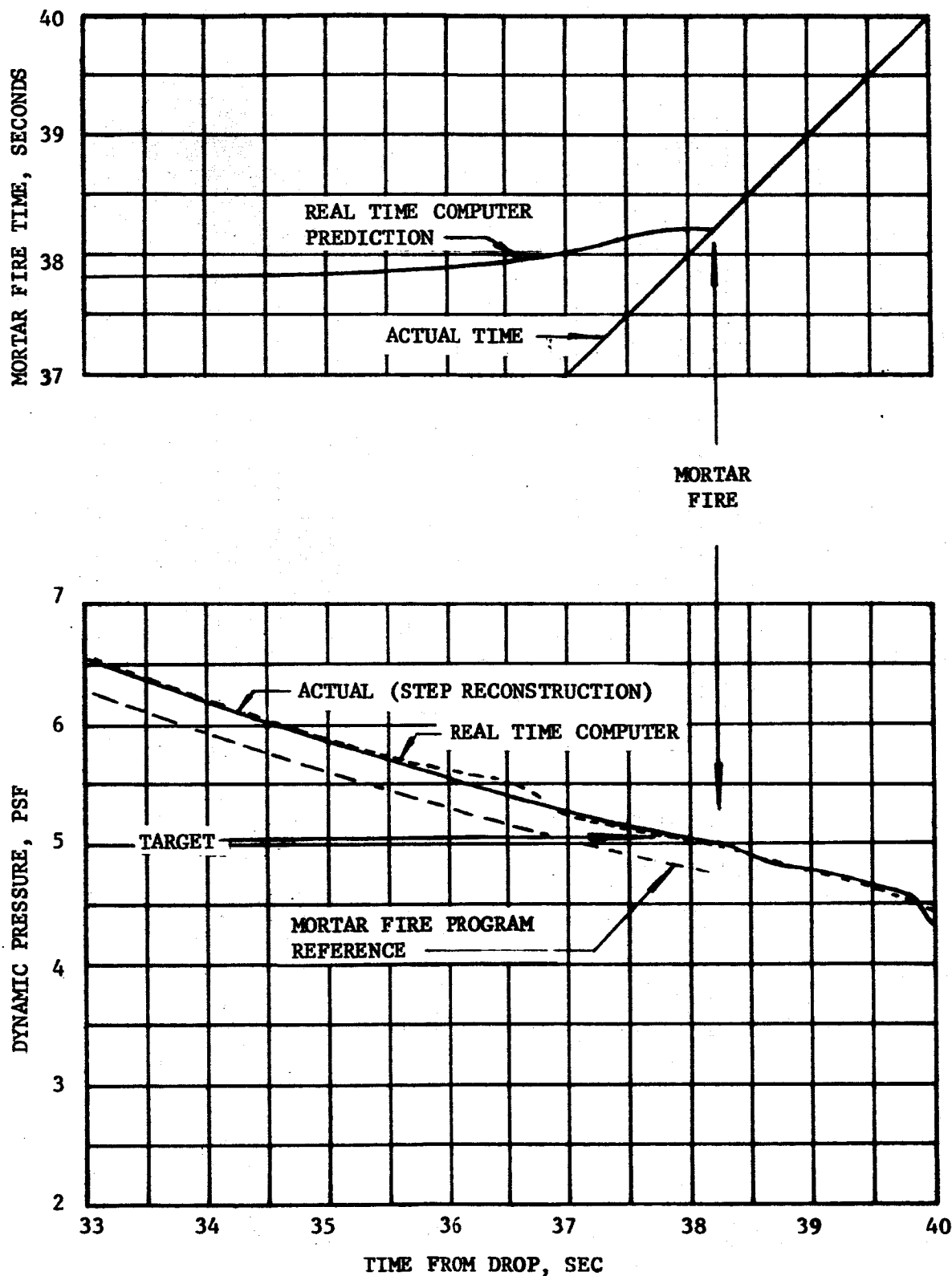


FIGURE IV-4 MORTAR FIRE COMMAND SYSTEM OPERATION

V. DECELERATOR SYSTEM ANALYSIS

A. System Description

The objective of this test of the Viking decelerator is to deploy it at a dynamic pressure lower than the lowest dynamic pressure expected on Mars as shown in Figure VI-1. This condition occurs at a transonic velocity which is also of interest. The inflation characteristics and canopy stability behind a blunt forebody are of primary concern.

The Viking decelerator is a 53-foot nominal diameter Disk-Gap-Band parachute with dimensions and general arrangement shown in Figure V-1. The parachute is fabricated entirely of Dacron type 52 except for the three-legged bridle which uses a special Goodyear proprietary fiber. The band cloth material is a 1.53 oz/sq. yd. rip-stop material having a minimum specified strength of 60 lb/in. The disk cloth is a 2.12 oz/sq. yd. rip-stop material having a minimum specified strength of 90 lbs/in. The minimum strengths of the radial tapes, circumferential tapes and suspension lines are 900 pounds, 900 pounds and 880 pounds respectively.

The parachute is packed in a deployment bag to a density of 43 lbs/ft.³ and stored in a mortar can aboard the BLDT vehicle in much the same manner as the Viking system. The BLDT vehicle itself is practically identical in shape and size to the Viking Lander Capsule. At mortar fire, the deployment bag is ejected straight back by a mortar whose reaction force is nominally oriented through the vehicle c.g. A breakdown of the ejected weight is seen in Figure V-2 to total 97 lbs. The relative velocity imparted to the deployment bag is expected from ground mortar test experience to be 112 ± 3 FPS.

Additional geometric data on the parachute are tabulated in Table V-1.

B. Mortar Fire Conditions

At mortar fire, the vehicle had a residual roll rate of -62 degrees/second and had just completed a large swing in angle of attack from -18 to +4 degrees with little change in side slip angle. Plots of angle of attack and sideslip in Figure VI-16, Section VI, show the mortar fire values to be +5.4 and -4.9 degrees respectively. Corroboration of these STEP trajectory reconstructed values is obtained by observing the mortar smoke puff in the airborne film data. At .23 seconds after mortar fire, the film data indicates an angle of attack of +5.4 degrees and a sideslip angle of -8.5 degrees. The differences between the STEP angles and the film angles are accounted for by tolerances and uncertainties in both sources of data. The aerodynamic trim angles of attack and sideslip for the BLDT vehicle at M.N. = 1.133 are -3.7 and 0. respectively. This means that the vehicle was approximately 10 degrees away from trim at mortar fire.

A summary of the important mortar fire conditions compared with expected nominal values are tabulated below:

<u>Mortar Fire Conditions</u>	<u>Nominal</u>	<u>Flight</u>
Mach Number	1.208	1.133
Dynamic Pressure, psf	5.07	5.00
Velocity, fps	1267	1194
Axial Acceleration, g's	- .41	-.40
Altitude, ft.	137500	135,368
Angle of Attack, degrees	- 8.9	5.4
Angle of Sideslip, degrees	0	-4.9
Total Angle of Attack, degrees	8.9	7.28
Spin Rate, deg/sec.	- 61.3	-62
Parachute Temperature, °F	< 80	47

The mortar fire conditions for this flight produced dynamic pressure and Mach number at first peak load which fell within the desired envelope of test conditions shown in Figure II-1, Section II.

C. Mortar Performance

The mortar performance is evaluated by observing the bag stripping process from the on-board cameras. The time at which the canopy first starts emerging from the deployment bag is identified as 1.015 seconds from mortar fire. The actual distance the deployment bag must travel for the suspension lines to be pulled from the bag is defined by the length of the lines themselves. By simulating the mortar firing process with complete aerodynamic forces on the forebody and the deployment bag, the mortar velocity can be established. The AV-2 flight conditions of Mach number, dynamic pressure and flight path angle at mortar fire are used. Assumptions were used as follows where flight data are not available:

1. Deployment bag C_D - 1.6
2. Dynamic pressure gradient behind blunt forebody (Reference 3)
3. Forebody aerodynamic coefficients (Reference 4)
4. Line and canopy stripping forces of 2 and 6 lbs. respectively (Reference 5)

Past experience has shown that under high dynamic pressure and angle of attack conditions at mortar fire, the lines bow between bag and vehicle under the influence of aerodynamic forces. The line bowing effect must then be accounted for in the simulation to obtain the proper line stretch distance. On this flight of AV-2, the dynamic pressure and angle of attack at mortar fire are so relatively low that line bowing ceases to be a significant factor. Visual evidence of this fact can be seen in the deployment

sequence of on-board camera photographs in Figure V-3 (t - 1.015 seconds). The line stripping simulation for AV-2 shows a mortar velocity of 106.5 FPS. This value does not fall within the expected range of 112 ± 3 FPS, but is above the minimum requirement of 104 FPS for BLDT established by Reference 2. The stripping process sequence derived by simulation is shown below:

<u>Time - Seconds</u>		<u>Relative Velocity-FPS</u>
Mortar Fire	0	106.5
Line Stretch	1.015	92.6
Bag Strip	1.31	83.9

The relative velocity at bag strip is seen to be more than adequate to assure positive bag strip. Bag strip is not observable on the film data from this flight because the deployment bag is behind the inflating canopy during the bag stripping process.

D. Decelerator Inflation Sequence

The on-board Milliken and Photosonic camera films were examined in detail to establish event times and to document the character of the parachute inflation. In the sequence shown below, certain events such as peak load and aeroshell separation were obtained from telemetry data: There was good correlation between film data and telemetry for common events:

<u>Sequence of Events</u>	<u>Time-Seconds</u>
Mortar Fire	0
Line Stretch	1.015
Bag Strip	1.31
Peak Load	1.62
First Full Open	1.66
Aeroshell Separation	9.10

It is noted in the above sequence that peak load occurred prior to first full inflation. This is unusual compared to the other BLDT test flights, but is a phenomenon experienced before on a bomb drop test at very low dynamic pressure (Reference 12).

Selected frames from the Milliken aft viewing camera show in Figure V-3 some of the significant events during and shortly after the inflation phase. The growth of the canopy from line stretch was obtained by tracing the projected area images from the Milliken camera and integrating these images with a planimeter. A canopy growth parameter curve of normalized area versus time is then constructed in Figure V-4. The projected area at any time is divided by the projected area observed in the final seconds of airborne film coverage. The time scale is normalized by the total filling time. The canopy growth curve for AV-2 is seen to be very similar in shape to the curve for AV-4 (the supersonic test case). The AV-2 curve does not overshoot the steady-state area with as sharp a rise rate as AV-4 near full open. This effect may be somewhat dependent upon the dynamic pressure at inflation but is not unusual for this parachute.

A plot of the projected area ratio, $S_p/S_{p \text{ final}}$, versus time from line stretch is presented in Figure V-5. The area oscillations shown are typical for a supersonic deployment of a disk-gap-band parachute except for the pronounced dip in area 1.6 seconds from line stretch. At this point flow conditions are still transonic as indicated. Close examination of the airborne film shows the canopy moving across the wake of the entry vehicle during the time interval of the dip in area. This effect has been observed before on the supersonic test flight of AV-4 (TR-3720295) and probably is the same necking down of the canopy at certain flow conditions observed in the wind tunnel test reported in Reference 7.

No correction has been applied to the projected area ratio in Figure V-5 to correct for variation in the canopy image plane under changing load conditions.

Parachute inflation was smooth and very symmetrical. The time from line stretch to first full inflation is seen in Figure V-5 to be .64 seconds. This value is plotted in Figure V-6 along with similar data from PEPP and LADT flight tests. The filling time for AV-2 falls near the lower edge of the expected uncertainty in this parameter.

E. Opening Load

Figures V-7 and V-8 show the time history of the total longitudinal parachute load recorded by the bridle attach point tensiometers for 10 and 50 seconds after mortar fire. The peak load is seen to be 9009 lbs. occurring 1.62 seconds after mortar fire (.04 seconds before first full open). This load is almost 2000 lbs. more than the 7029 lbs. obtained by simulating AV-2 deployment conditions. Since the dynamic pressure of 4.51 psf and the parachute area are relatively well defined, the mismatch in opening load prediction must be attributed to either a drag coefficient larger than experienced on other BLDT tests or to a dynamic time phasing effect associated with the low dynamic pressure. This same tendency for the opening load to be higher than anticipated at low dynamic pressure was experienced on LADT flight number 2 (Reference 12). No satisfactory explanation was ever presented for this behavior. Although not critical from the design maximum load standpoint, a better understanding of this characteristic is desirable.

The telemetered data for this flight is very noisy. The load data in Figure V-8 shows several typical noise spikes which should be disregarded.

A typical noise spike is characterized by a very narrow peak which rises unexpectedly from the general background character of the traces.

The individual tensiometer readings at each bridle leg are recorded in Figure V-9. By proper combination of the three tensiometer readings, the equivalent parachute load pull angles in pitch and yaw are obtained and plotted in Figures V-10 and V-11. These angles are the projections in the pitch and yaw planes of the total angle between the parachute load and the forebody vehicle centerline. The total pull angle is shown in Figure V-12. The structurally significant pull angle occurring at peak load is approximately 3 degrees. The character of the pull angle data is similar to what has been observed on the other BLDT flights, namely; that the onset of peak load reduces the pull angle to a minimum value.

Accelerometer readings in the X, Y and Z axis directions during the 10 and 50 second time periods after mortar fire are shown in Figures V-13, V-14 and V-15. The peak longitudinal acceleration of -5.62 g's occurs at 1.62 seconds after mortar fire and reflects a parachute opening load of 9408 lbs. This is based on subtracting out the aeroshell drag component using C_D of 1.42, a dynamic pressure of 4.55 psf, and a payload mass of 55.8 slugs. The load thus obtained is about 400 lbs. larger than the load indicated by the tensiometers. Aeroshell separation occurring 9.1 seconds after mortar fire is clearly visible on the accelerometer traces.

F. Vehicle Stability

At mortar fire the vehicle had a residual roll rate of -62 degrees/second and had just completed a large swing in angle of attack from -18 to +4 degrees with little change in side slip angle. The angles of attack and side slip were 5.4 and -4.9 degrees respectively. Pitch and yaw rates were 13 and 3 degrees/second respectively. It is apparent from these values that the vehicle was undergoing highly dynamic motions at mortar fire. Whereas these are within BLDT predictions, they represent more severe conditions than expected on Mars where a control system on the lander maintains a more stable vehicle from which the parachute is deployed. Vehicle attitude rates at parachute deployment on AV-2 are therefore expected to be high. The opening load on AV-2 was lower than the other BLDT flights, however, and this has a tendency of reducing the attitude rate transients produced in the vehicle.

The actual vehicle attitude rate time-histories in Figures V-16, V-17 and V-18 are very similar in character to the results of BLDT AV-4 flight (supersonic case). The peak rate of 92 degrees/second is somewhat lower than AV-4 but the damping characteristics are much the same. Pitch and yaw rates fall below 30 degrees/second in 22 seconds and exceed 17 degrees/second only for momentary periods after 50 seconds. The roll rate in Figure V-17 starts high at -62 degrees/second and reduces very slowly to -42 degrees/second 200 seconds after mortar fire. Noise spikes on many of the figures for this flight are very obvious in Figure V-17 and should be ignored.

G. Parachute Drag Performance

The evaluation of the drag of the parachute was conducted in two overlapping phases. The first used the reconstructed vehicle trajectory parameters at mortar fire and integrated the axial accelerometer data to obtain the subsequent trajectory. The radar data was used to resolve the acceleration vector into an L/D (lift-to-drag ratio) and roll angle. The integrated trajectory, using the L/D and roll angle shown in Figure V-19, was used to obtain the dynamic pressure for non-dimensionalizing the tensiometer and accelerometer data into a force coefficient. The conversion to an incremental parachute force coefficient was then made to the tensiometer data by adding to it the force necessary to maintain the relative velocity between the parachute and vehicle equal to zero; i.e., the acceleration force on the parachute mass.

The telemetered accelerometer data was used for this correction in the equation.

$$C_{FT} = (F_T - A_x \times W_p) / (Q S_p)$$

where: C_{FT} = Parachute Force Coefficient
 F_T = Sumation of Tensiometer data, lb
 A_x = Vehicle Axial Acceleration, g's
 W_p = Weight of the parachute, 97 lb.
 Q = Dynamic pressure
 S_p = 2206 ft.

The axial acceleration of the vehicle was converted to the incremental parachute force by removing the estimated drag of the aeroshell or base cover from Reference 4. The equation used is:

$$C_{FA} = A_x \times W_T / (Q S_p) - C_{DV} S_v / S_p$$

Where: C_{FA} = Parachute Force Coefficient
 A_x = Vehicle axial acceleration, g's
 Q = Dynamic pressure, PSF

$S_p = 2206 \text{ ft}^2$

$C_{Dy} =$ Forebody drag coefficient

$S_v =$ Forebody reference area, 103.8 ft^2

$W_T =$ Total system weight, 1897 lbs. before Aeroshell
 Separation
 1541 lbs. after Aeroshell
 Separation

This evaluation phase was conducted until 50 seconds after parachute deployment.

The second phase was begun using trajectory data from radar just after aeroshell separation and evaluated the drag coefficient necessary to obtain the radar altitude at various subsequent times. In both phases the best estimates of the meteorological data was used. During this evaluation, the parachute lift again produced irregularities in the tracking data which could not be matched with a zero lift trajectory.

Parachute force coefficients derived from accelerometer data and tensiometer data are plotted versus Mach number in Figures V-20 and V-21. The two plots are seen to be very similar in character. Both plots of parachute force coefficient show an oscillatory character reflecting the 5-8 cps natural spring mass frequency of the two body system. Another lower frequency oscillation is evident and noticeable in both figures. It starts with a drop in force coefficient between Mach .97 and .92 which is coincident with the dip in parachute projected area observed in Figure V-5. Additional low points occur at Mach .88 and .73. This behavior is tentatively identified with a canopy oscillation in and out of the forebody wake.

The expected dispersion of parachute drag from wind tunnel results (Reference 7), is superimposed over the flight results of AV-2 in both Figures V-20 and V-21. The average force coefficient is seen to be well

above the nominal expectation above Mach .6 with most of the canopy/wake interaction effects occurring where the dip in expected performance occurs.

When near steady state descent conditions are achieved, the tensiometer and accelerometer data become poor sources of parachute drag performance. The vehicle is so near equilibrium that noise on the traces becomes larger than variation in the parameter of interest. The quasi-steady state drag performance is determined by iterating on drag coefficient until the altitude change over a time increment matches the tracking radar. The drag coefficients derived in this manner ignore the effect of parachute and vehicle lift on the descent trajectory. Additional analysis is required to separate the lift and drag effects. These drag coefficients are superimposed on the plots in Figures V-20 and V-21. The steady state drag is seen to be lower than nominal between Mach .5 and .3 but still within the expected performance envelope. The drag value below Mach .07 exceeds expectation.

Plots of parachute force coefficient versus time in Figure V-22 and V-23 are included for convenience in correlating this data with time. The trajectory parameters of dynamic pressure, Mach number, and flight path angle which were used in the post mortar fire trajectory reconstruction are presented in Figures V-24, V-25 and V-26 respectively.

H. Aeroshell Separation

The aeroshell separation system on all BLDT vehicles is similar in design and construction to the system to be used on the Viking lander. The aeroshell is separated 7 seconds after mortar fire in the current Viking sequence. On BLDT, aeroshell separation is timed to occur when specific Mach number and dynamic pressure conditions occur in the Earth atmosphere.

Basically, separation is achieved by virtue of a favorable relative acceleration between bodies as indicated below:

$$\text{Relative Acceleration} = q \times \left(\frac{1}{B_{\text{chute}}} - \frac{1}{B_{A/S}} \right)$$

$$\text{where } B = \frac{M}{C_D A} \quad \text{for each body}$$

A guide rail system is used to provide positive clearance during separation. This system involves three guide rails symmetrically oriented on the aeroshell which mate with roller guides mounted on the lander body. Moment constraint is provided by two sets of roller guides separated by 6 inches for each rail. The effective length of the rail is 12 inches, the first 6 inches of which provide moment constraint and shear constraint, whereas the last 6 inches provide only shear constraint. A compression spring inside each rail provides 200 lbs. force when compressed three inches at the start of separation. Three dummy electrical disconnects were included on BLDT to simulate the Viking hardware. These disconnects are of the type which require a positive force of 50 to 150 lbs./connector to engage them. The connector force, which assists the separation, decays to near zero in one-fourth inch of travel.

The objectives of the separation demonstration are:

- (1) To determine that there are no unpredictable aerodynamic disturbances at separation that would compromise the Viking mission,
- (2) To exercise the separation hardware and concept to insure that analytical evaluations of separation dynamics are valid, and
- (3) To determine that parachute drag is adequate to produce a minimum of 50 feet of separation between aeroshell and lander in 3 seconds.

It was intended on this flight to demonstrate satisfactory aeroshell separation at the lowest value of dynamic pressure expected on Mars (1.39 psf). Actual aeroshell separation on this flight took place 9.1 seconds after mortar fire at which time the Mach number was .615 and dynamic pressure was 1.43 psf. Since the separation versus time performance is a direct function of dynamic pressure, this flight should have a slow separation.

The vehicle was pitching at 50 degrees/second during the course of the separation interval. This is considerably higher than the 30 degree/second criteria used in the design of the guide rail system.

Evaluation of the forward looking Milliken camera film shows a well behaved, predictable aeroshell separation. Separation distance versus time is obtained from this film by knowing the diameter of the aeroshell to be 11.5 feet, the horizontal field of view of the camera to be 54.9 degrees and the frame rate to be 32 frames/second. The separation distance may then be calculated by measuring the aeroshell image size on a specific horizontal field of view and correlating with the number of frames since separation:

$$\text{Separation Distance} = \frac{11.5 \times \text{H.F.V.}}{.958 \times \text{Image Diameter}}$$

The separation distance versus time plot in Figure V-27 shows 120 feet of separation in 3 seconds. Simulation of this separation using actual AV-2 flight conditions shows fair agreement with the flight results. The difference is attributed to difficulty in matching the drag performance of the parachute during this highly dynamic period. No observable change in the parachute projected area was detected during separation that would account for the reduced drag (see Figure V-3 at $t = 9.2$).

The first foot of aeroshell separation distance versus time is obtained from extensiometer data and plotted in Figure V-28. Good agreement between simulation predictions and the actual flight time-history is observed. The fact that all three extensiometer readings do not agree is an indication of relative angular rotation between bodies as they separate. In order to compute the extent of angular rotation, the guide rail and extensiometer locations must be defined as in Figure V-29. The relative angle between aeroshell and lander is plotted in Figure V-30. The maximum angle at the point where total moment constraint is lost is seen to be approximately 1 degree. This is considerably less than 1.53 degrees relative angle recorded in a ground test of the system subjected to a bending moment of 560 ft-lbs (.87 x design moment). The plot of Figure V-30 shows little evidence of any significant loads or bending moment on the rail system. There was no evidence of any damage to the aeroshell separation system.

I. Parachute Recovery Assessment

A detailed post-test inspection of the parachute was conducted by MMC and GAC. A report of this inspection by the parachute contractor is presented in Appendix C. A graphic description of canopy anomalies is included as Figure C-1 therein. In general, the parachute suffered no significant

damage and this test is therefore considered a successful qualification of the decelerator. There were several black smudge marks noted that probably came from mortar or BLDT engine exhaust residue. There was no evidence of excessive heat associated with any of the smudge marks on the canopy.

Pre-flight and post-flight parachute dimensions are recorded in Appendix D. Between pre-flight and post-flight measurement, however, the packed parachute is exposed to a heat compatibility test. Experience has shown that suspension line lengths shrink approximately 2 percent during the heat cycle. Therefore in determining the amount of suspension line length increase resulting from flight loads, we shall assume an initial suspension line length of 88 instead of 90 feet. The suspension line length increase, then, varies from a minimum of 4 inches near radial 34 to a maximum of 11 inches near radial 9. The disk radial dimension varies up to one-fourth inch and in some cases, because of shrinkage due to heat, is actually less than pre-flight measurement. The bridle leg length increases were $5/8$, $5/8$, and $3/4$ inch respectively. Other dimensional changes were minor. Taken as a whole, these dimensional changes are indicative of a very lightly loaded parachute which in fact we know from other data was the case.

TABLE V-1

PARACHUTE GEOMETRIC PROPERTIES

<u>Item</u>	<u>Relative Value</u>	<u>Value</u>
Nominal diameter	D_o	53 feet
Geometric porosity*	$0.125 S_o$	276 ft ²
Total area (S_o)**	$(\pi/4) D_o^2$	2206.2 ft ²
Disk area†	$0.53 S_o$	1169.3 ft ²
Disk diameter	$0.726 D_o$	38.5 ft
Disk circumference	$2.285 D_o$	121 ft
GAP area	$0.12 S_o$	264.7 ft ²
GAP width	$0.042 D_o$	2.2 ft.
Band area	$0.35 S_o$	772.2 ft ²
Band width	$0.121 D_o$	6.4 ft
Vent area	$0.005 S_o$	11.0 ft ²
Vent diameter	$0.07 D_o$	3.7 ft
Number of suspension lines	--	48
Length of suspension lines	$1.7 D_o$	90 ft

* Vent plus gap provide 12.5 percent geometric porosity

** Disk + gap + band

+ Includes vent

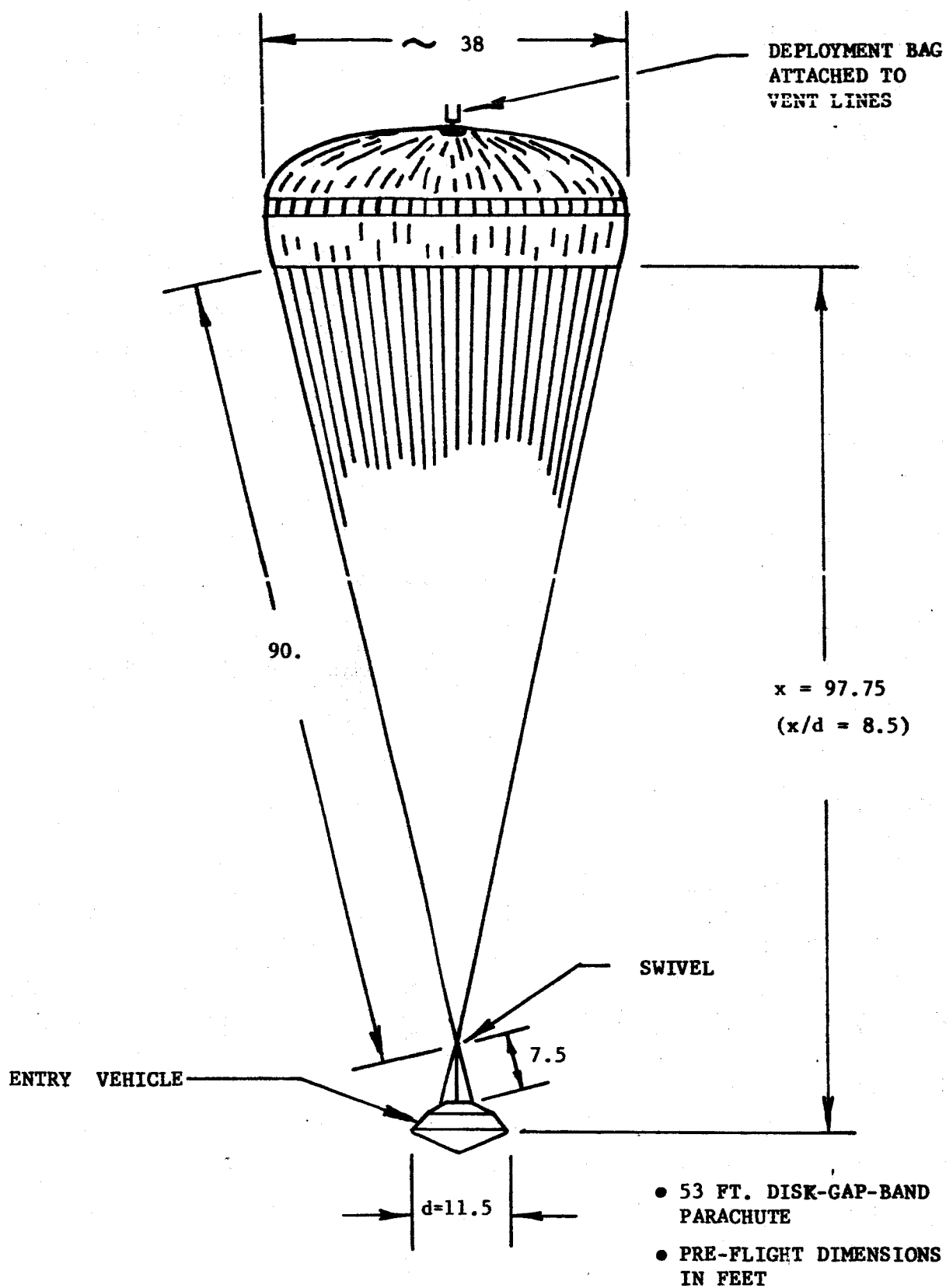


FIGURE V-1 VIKING DECELERATOR SYSTEM

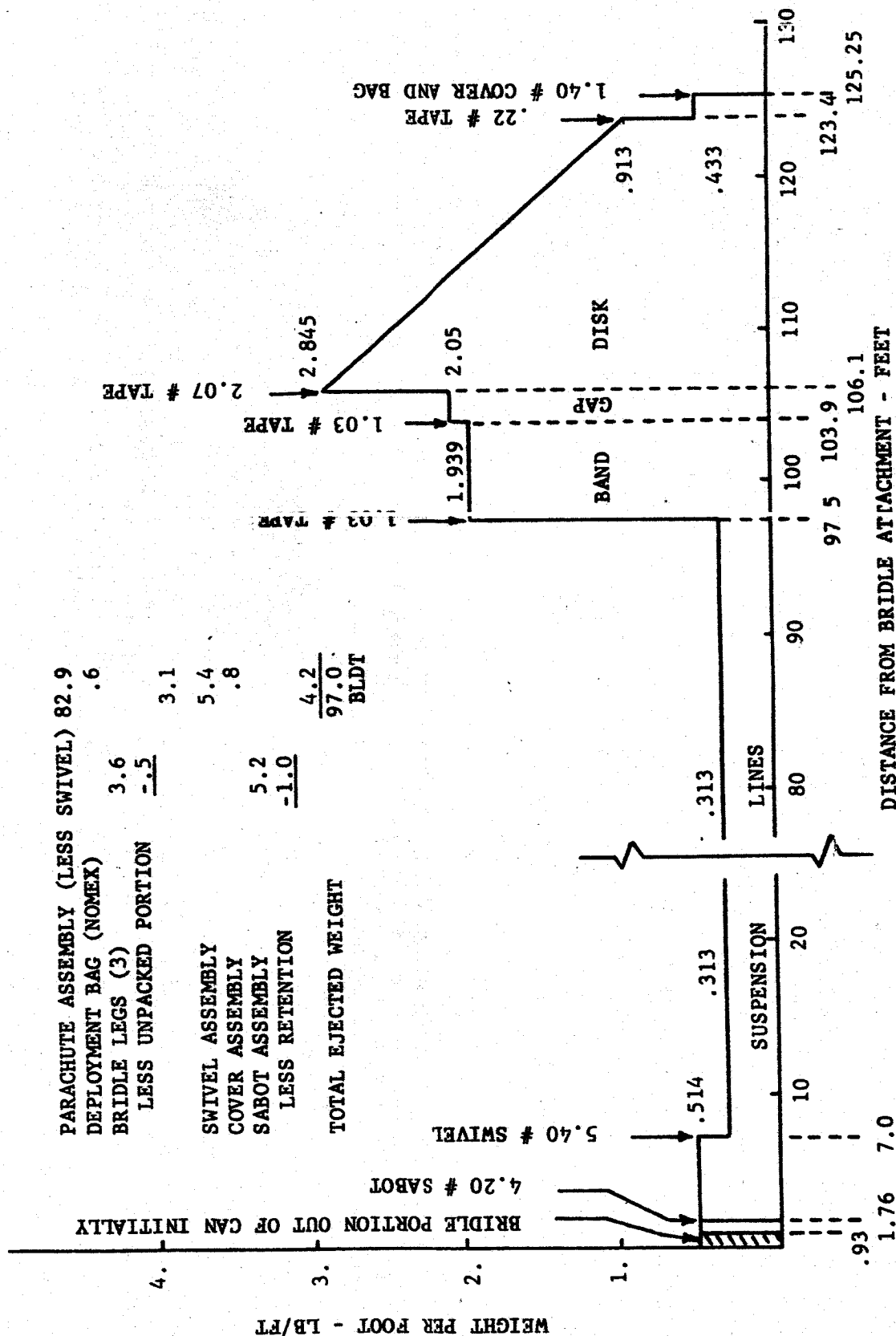


FIGURE V-2 EJECTED WEIGHT DISTRIBUTION



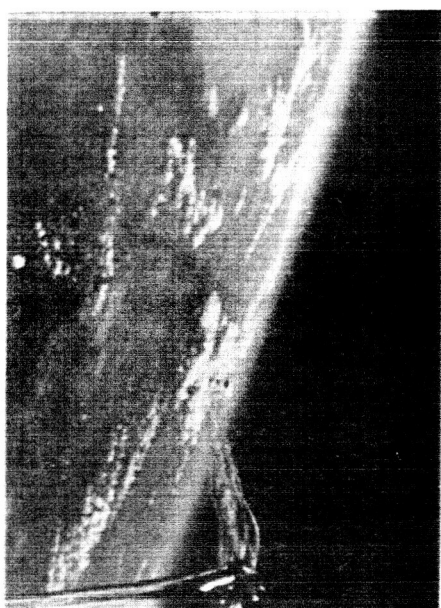
$t = .140$
BAG EMERGING



$t = .328$
STRAIGHT LINES



$t = .531$
TRAVELING WAVE ON LINES



$t = 1.015$
LINE STRETCH

FIGURE V-3 ON-BOARD CAMERA PHOTOGRAPHS



$t = 1.185$
BEGIN INFLATION



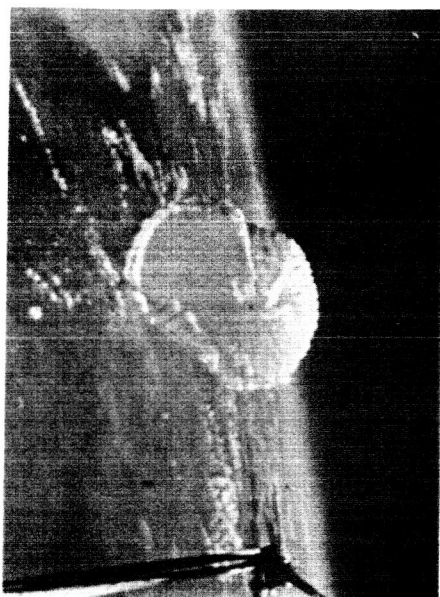
$t = 1.265$
ESTIMATED BAG STRIP



$t = 1.341$
INFLATION

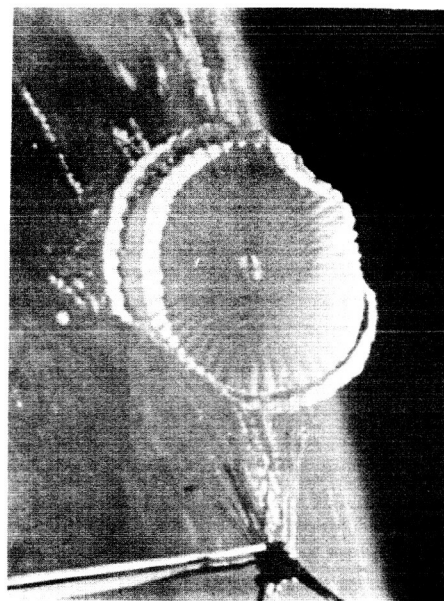


$t = 1.420$
INFLATION



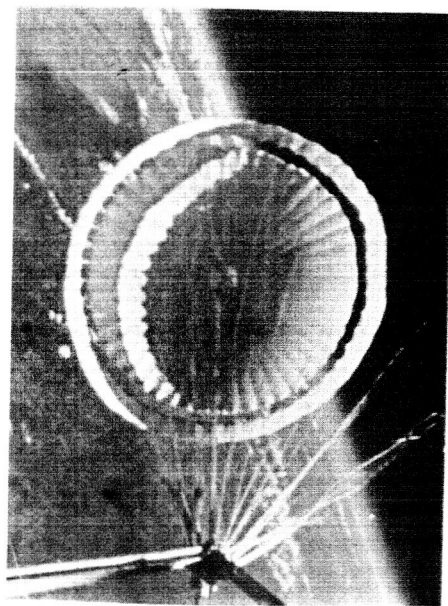
$t = 1.498$

INFLATION



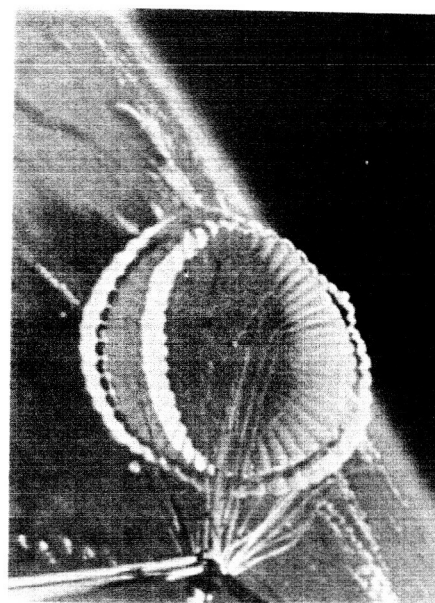
$t = 1.575$

INFLATION



$t = 1.654$

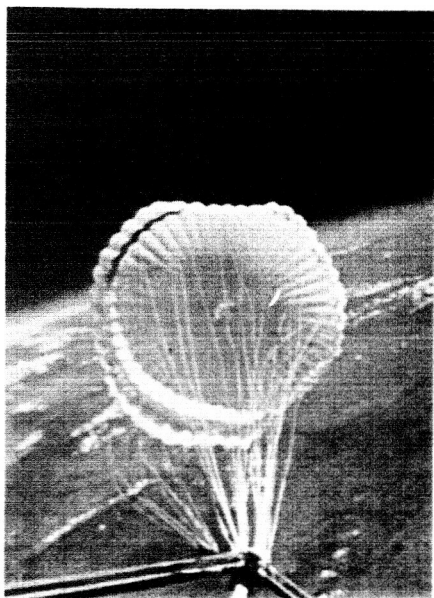
FIRST FULL OPEN



$t = 1.840$

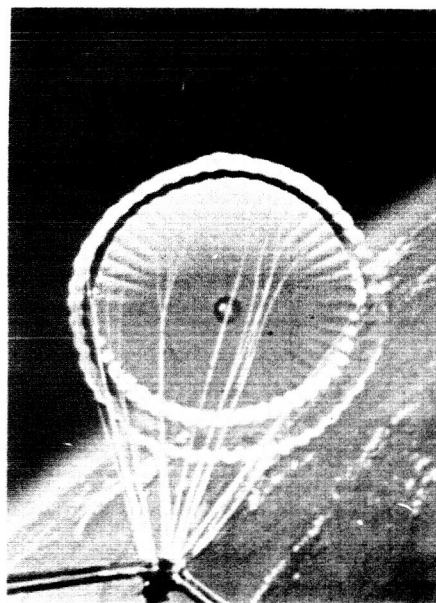
REBOUND FROM PEAK LOAD

FIGURE V-3 ON-BOARD CAMERA PHOTOGRAPHS (CONTINUED)



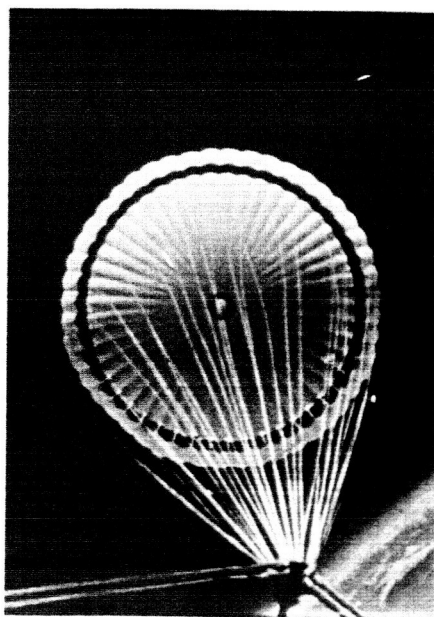
$t = 3.015$

PARTIAL COLLAPSE



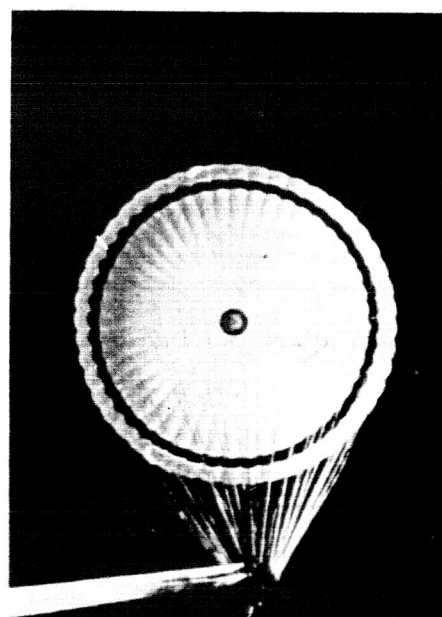
$t = 3.300$

OPEN AGAIN



$t = 9.200$

AFTER AEROSHELL SEPARATION



$t = 50.700$

FINAL VIEW

FIGURE V-3 ON-BOARD CAMERA PHOTOGRAPHS (CONTINUED)

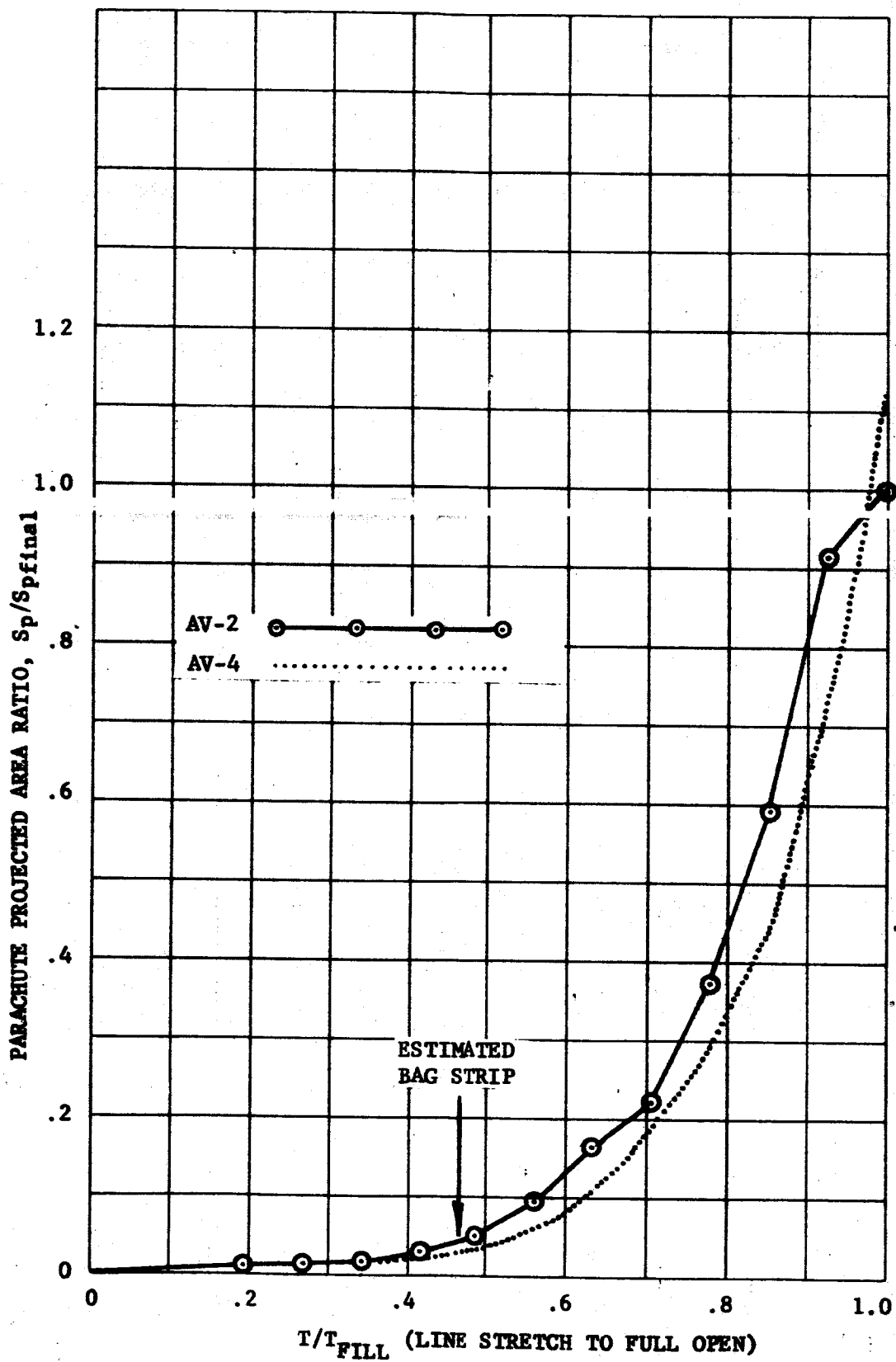


FIGURE V-4

CANOPY GROWTH PARAMETER

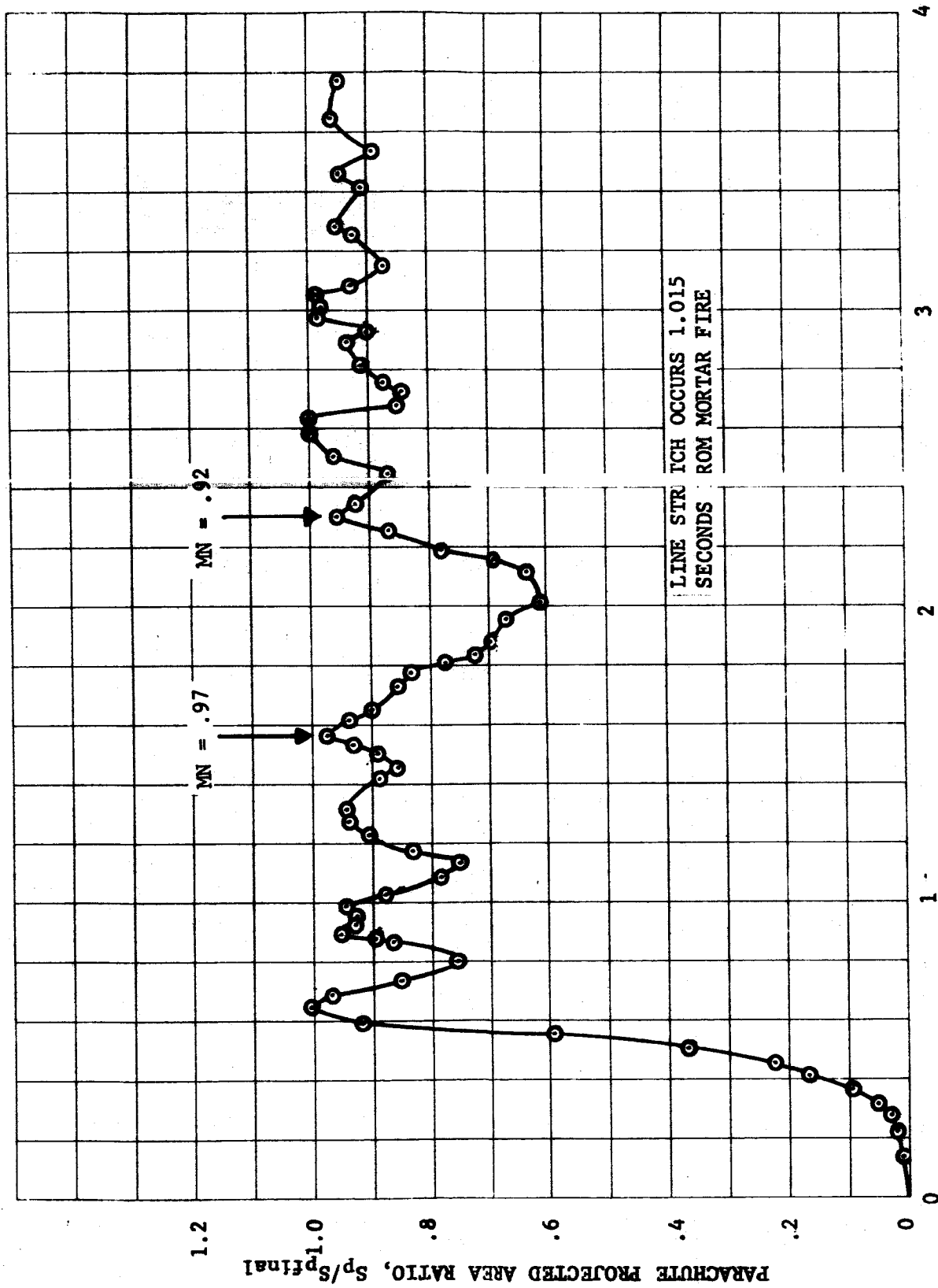


FIGURE V-5 CANOPY AREA OSCILLATIONS

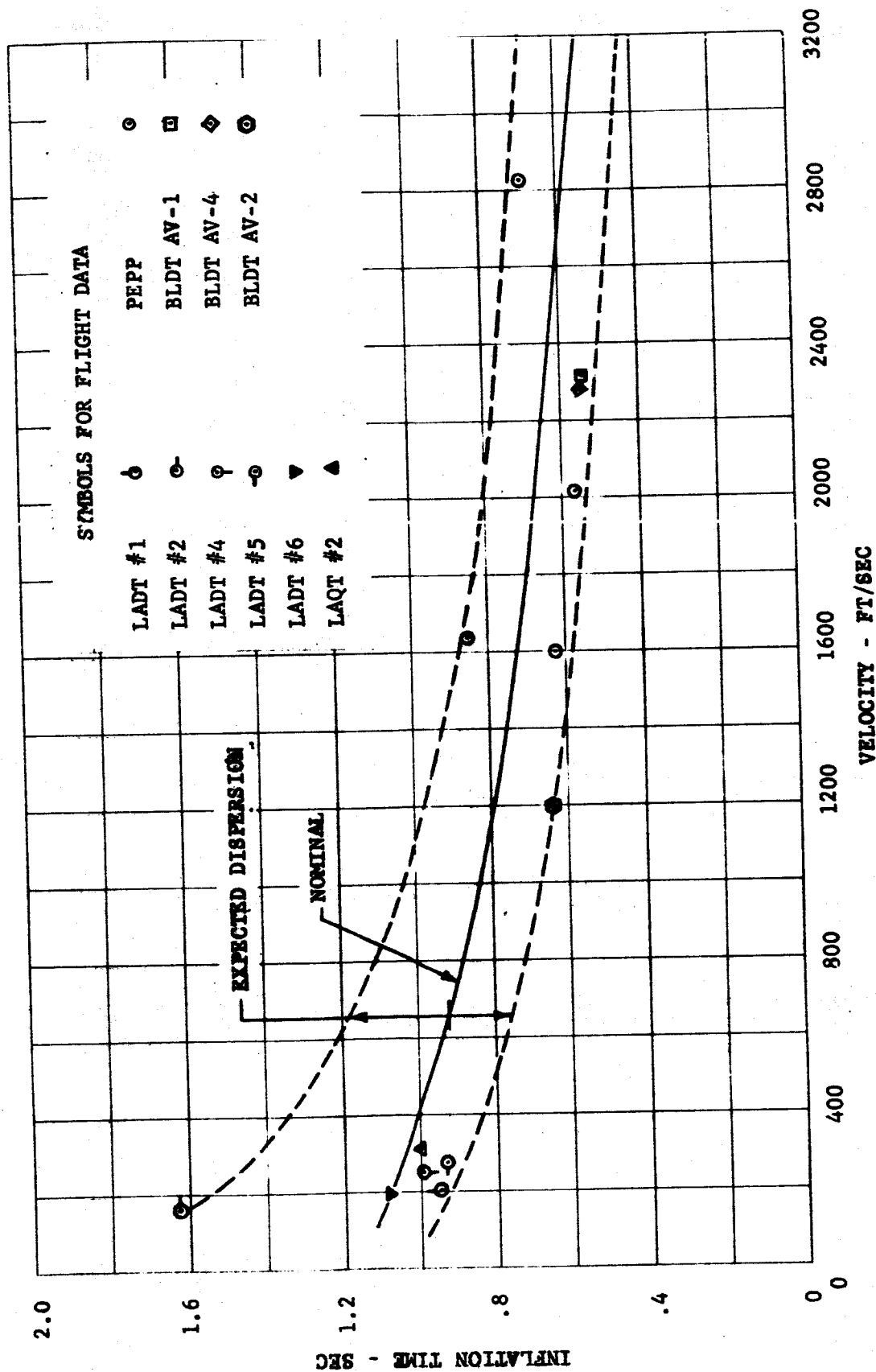


FIGURE V-6 PARACHUTE FILLING TIME FROM LINE STRETCH

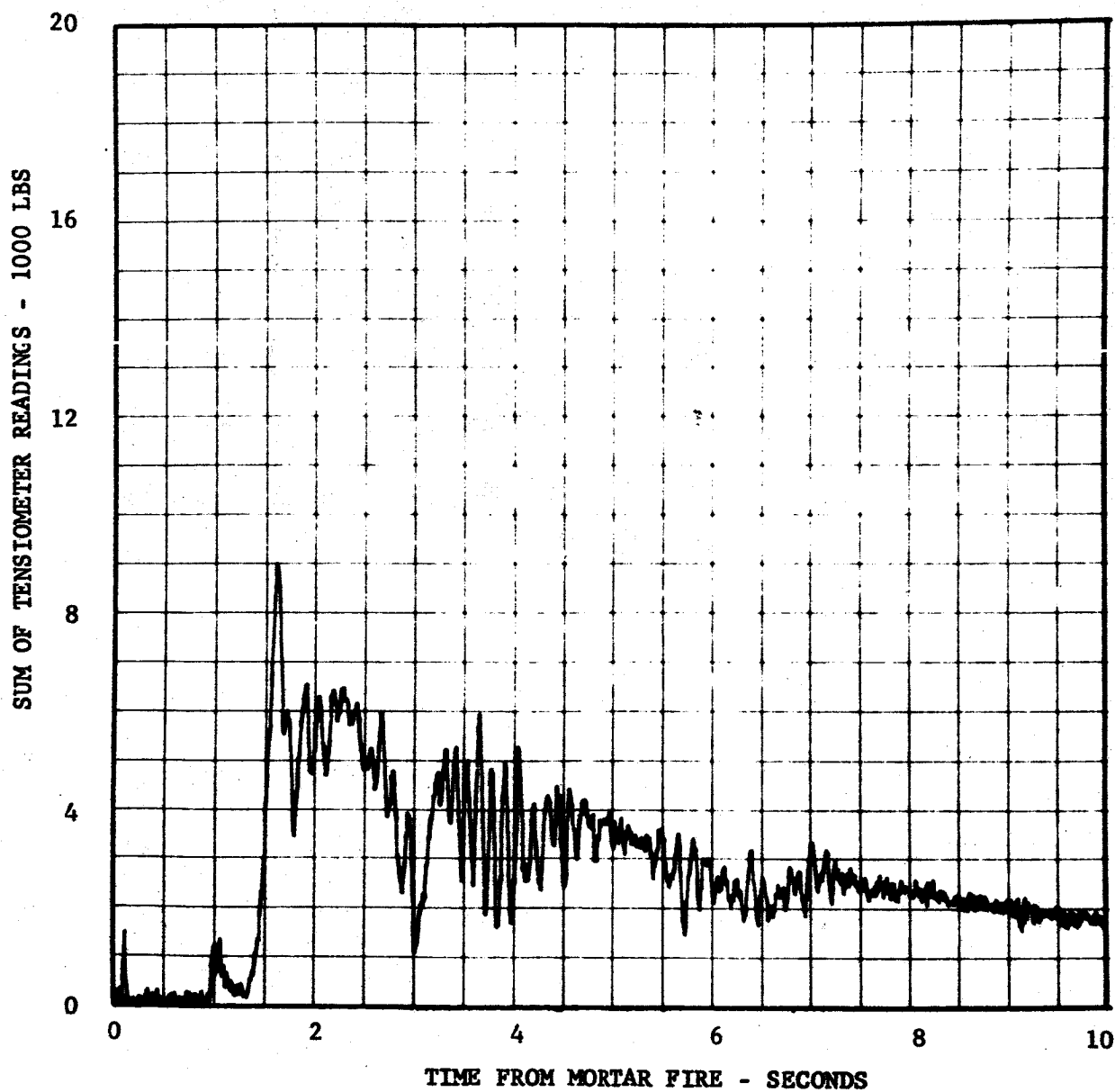


FIGURE V-7 PARACHUTE OPENING LOAD, 0-10 SECONDS

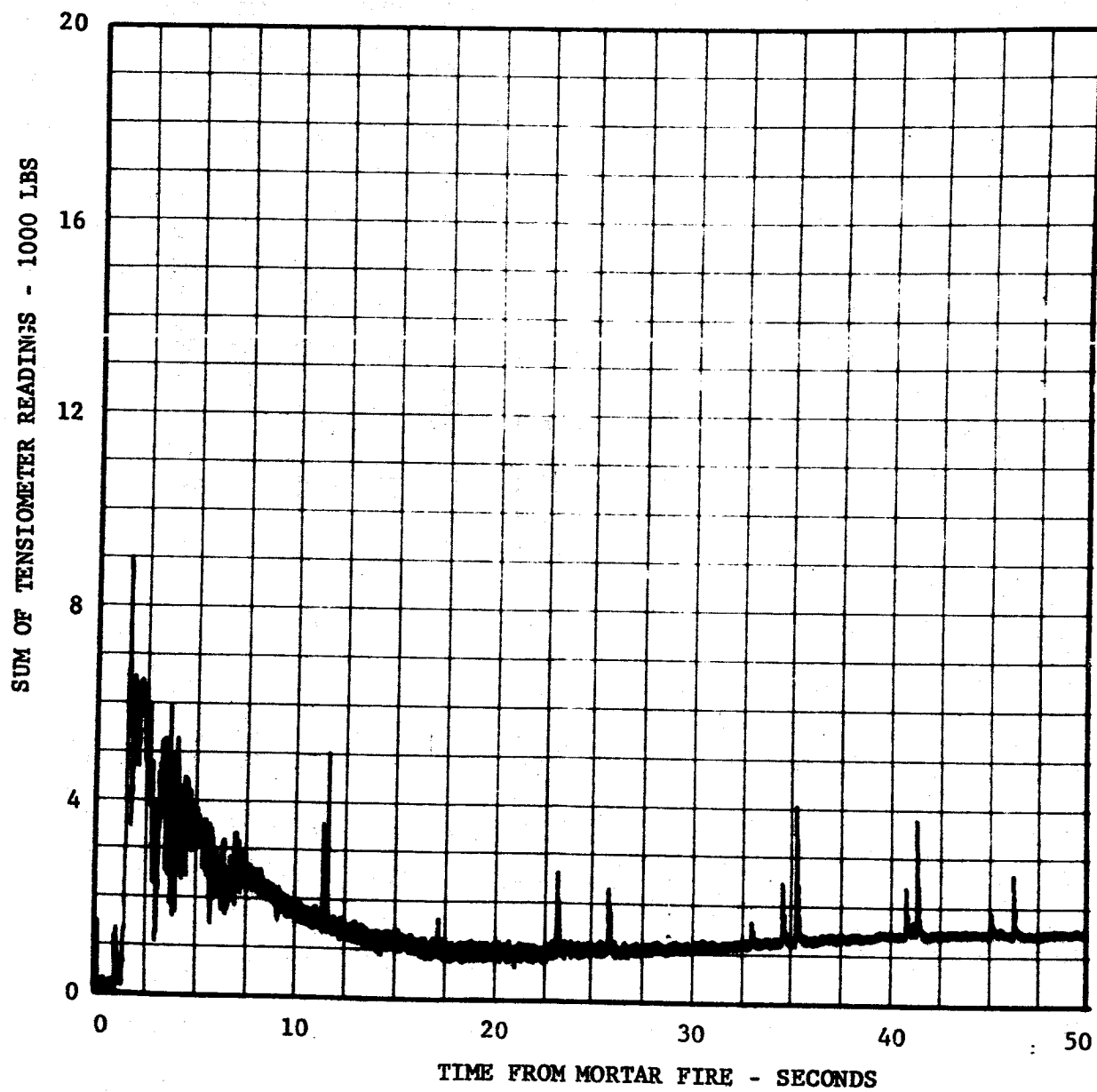


FIGURE V-8 PARACHUTE OPENING LOAD, 0-50 SECONDS

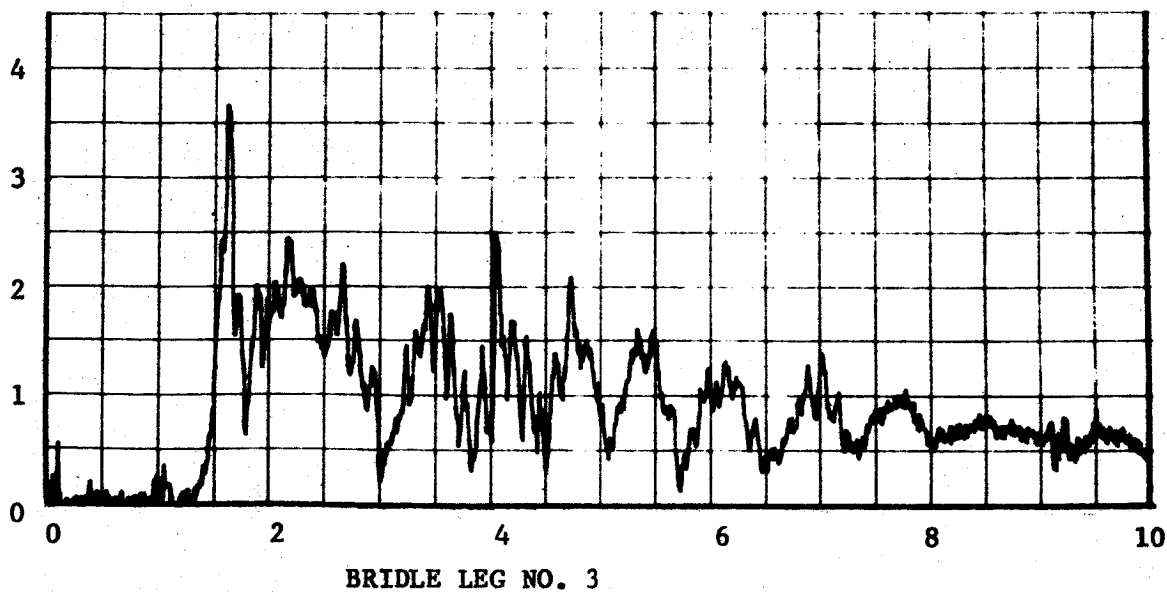
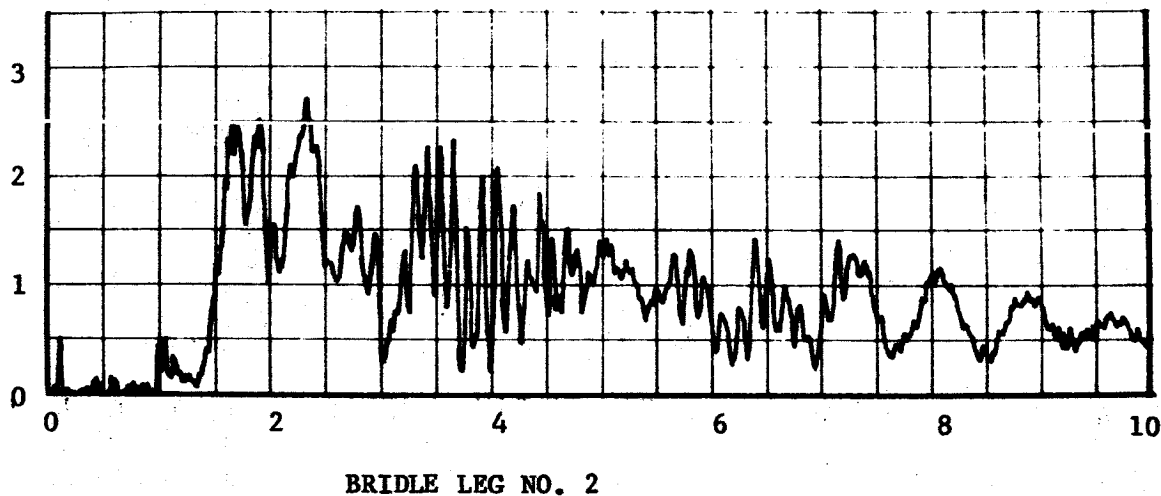
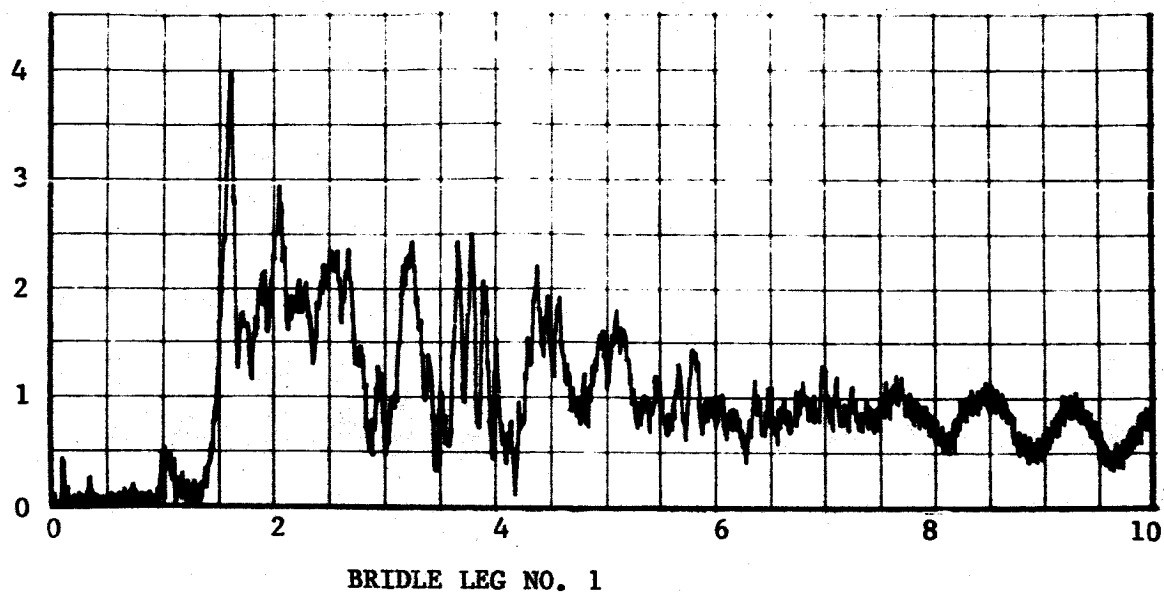


FIGURE V-9 TENSIO METER READINGS

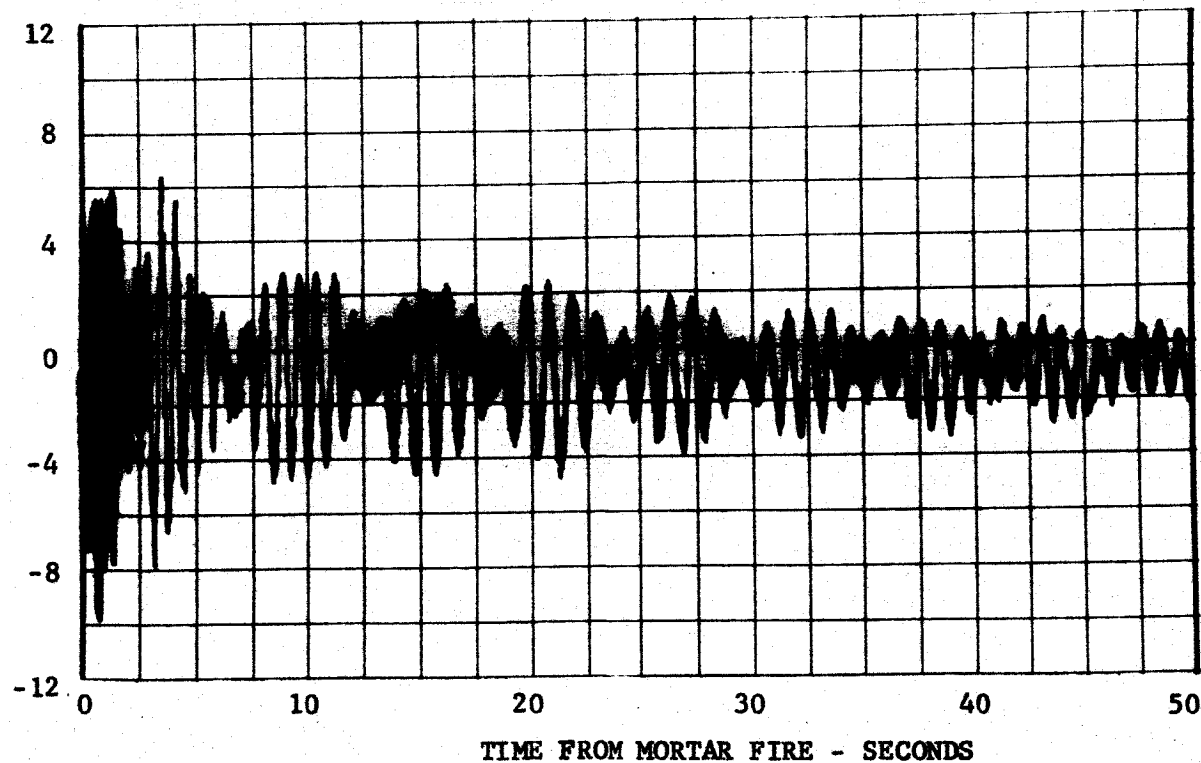
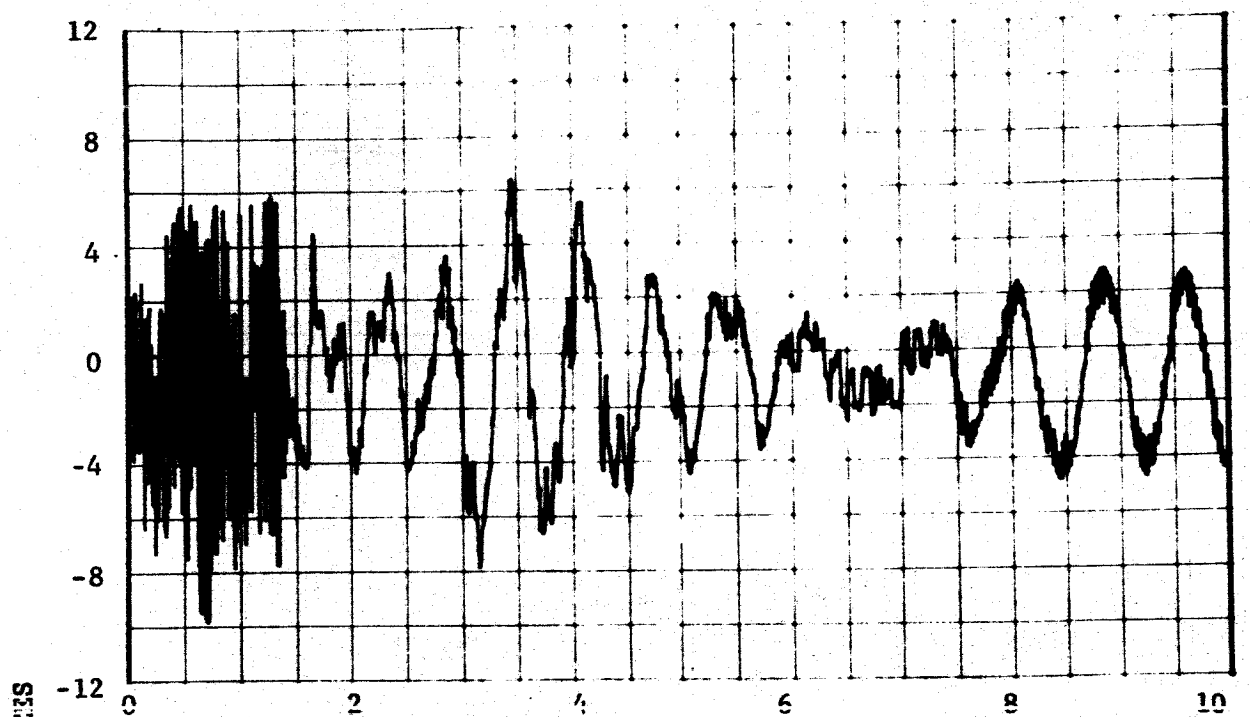


FIGURE V-10 PARACHUTE PULL ANGLE, PITCH PLANE

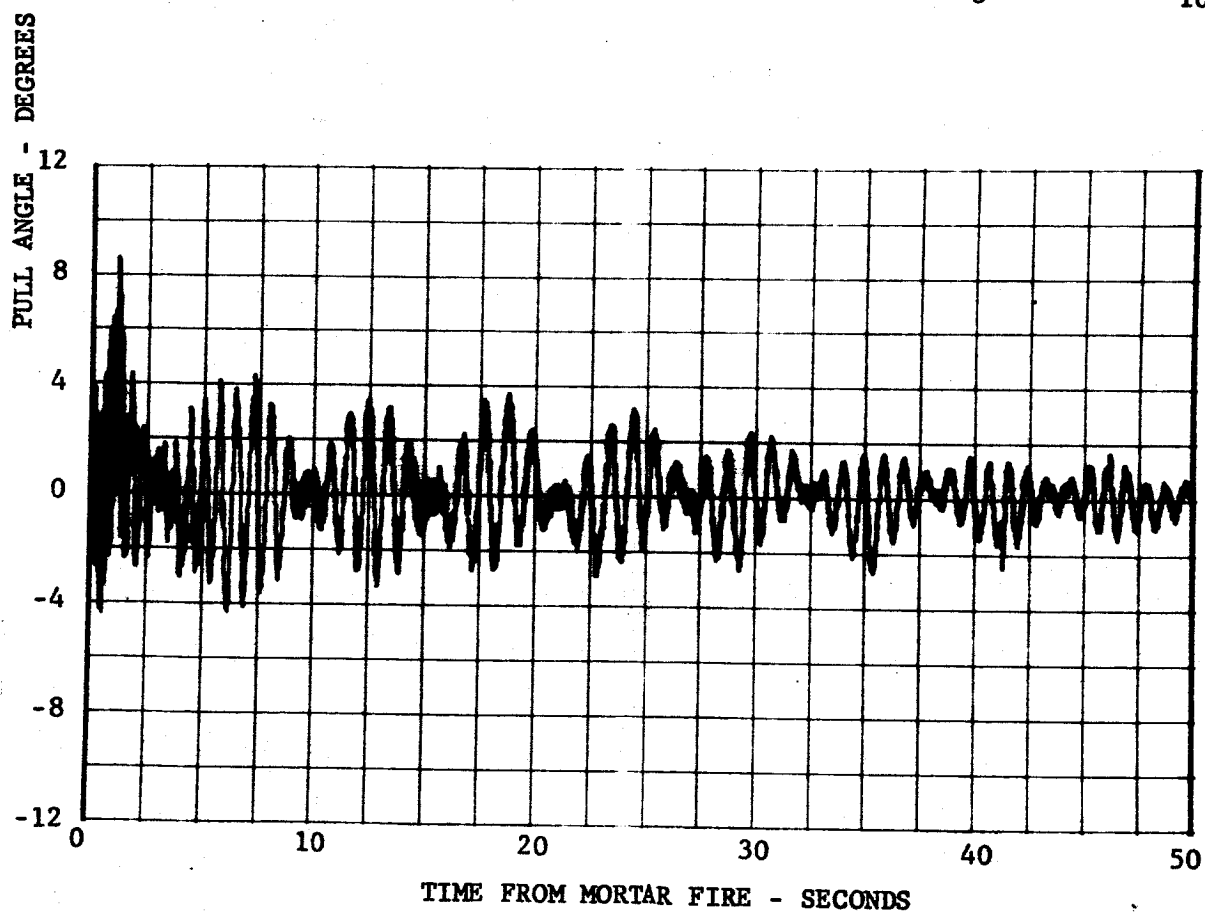
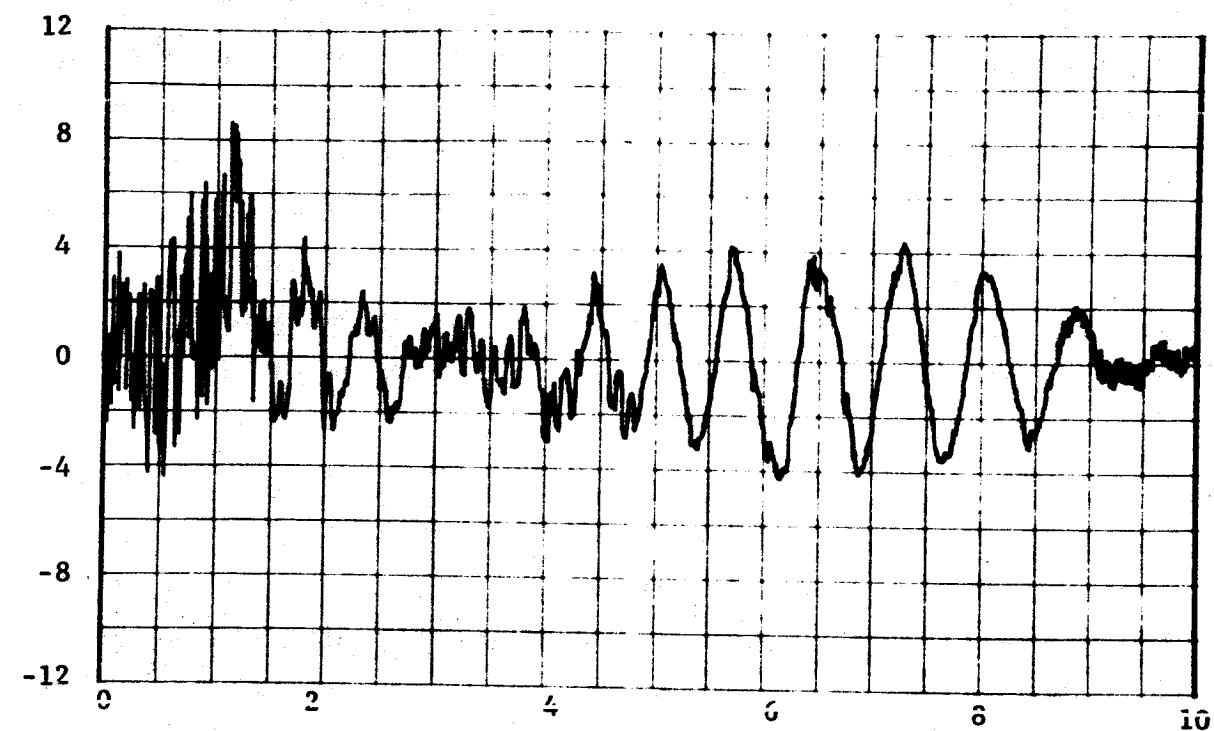
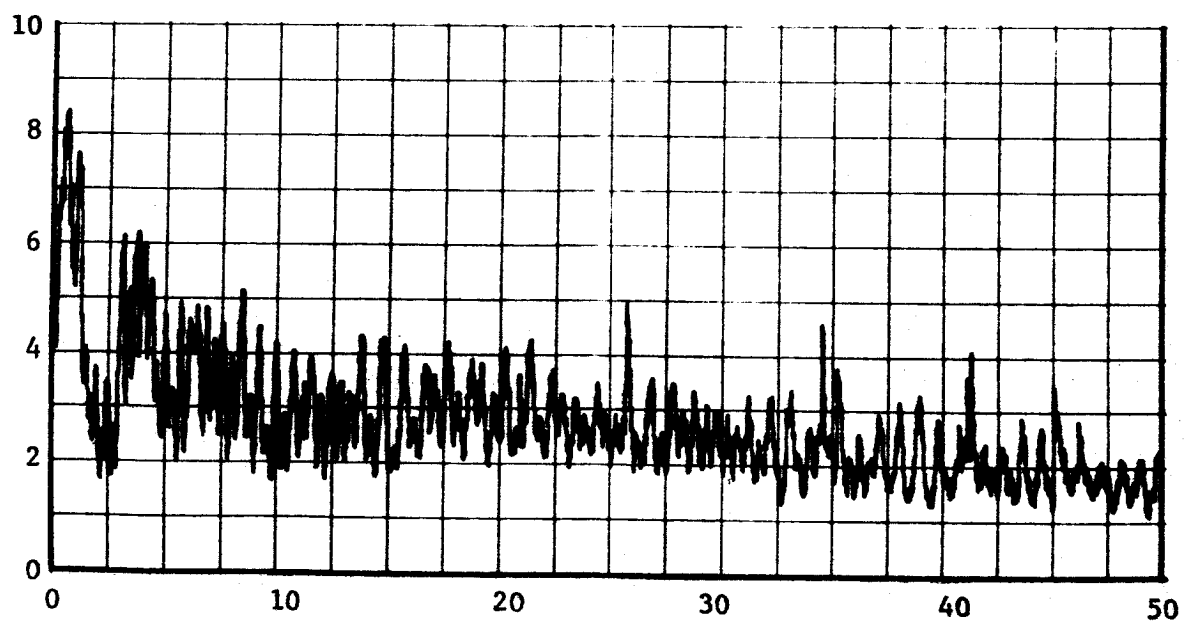
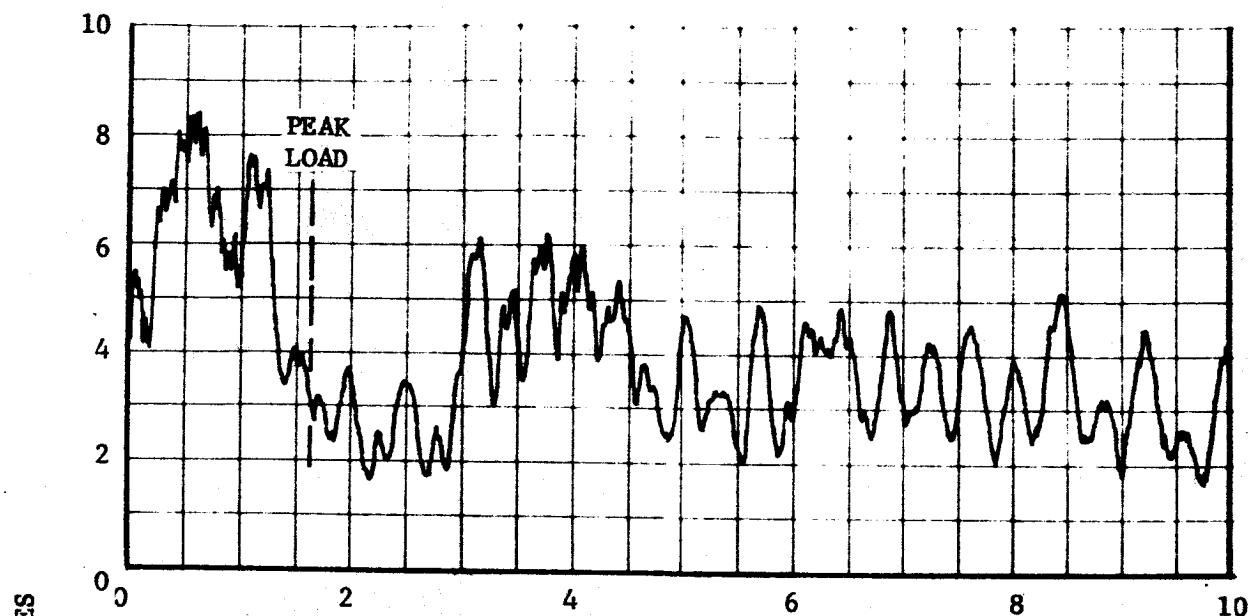


FIGURE V-11 PARACHUTE PULL ANGLE, YAW PLANE



TIME FROM MORTAR FIRE - SECONDS

FIGURE V-12 PARACHUTE TOTAL PULL ANGLE (RSS)

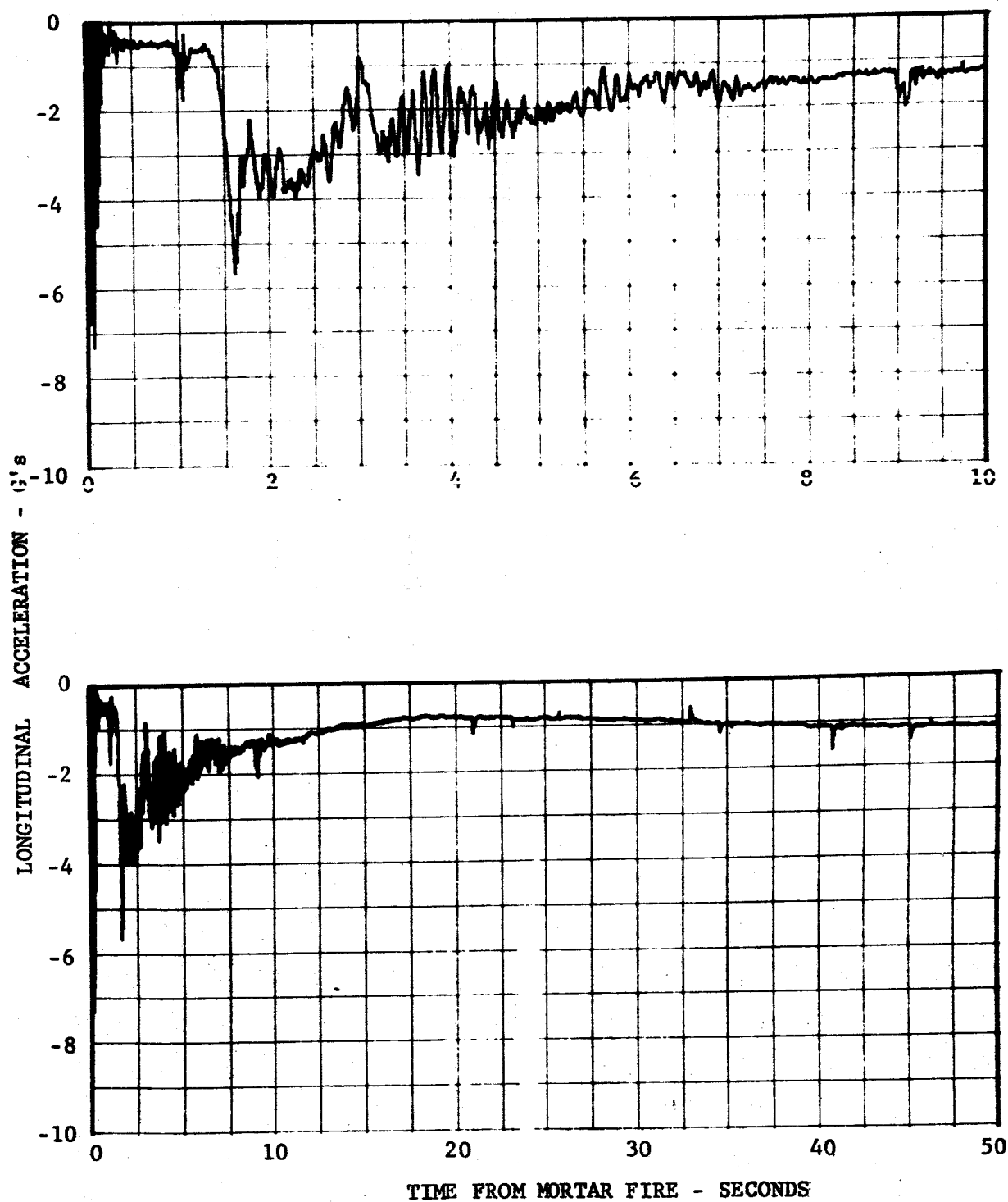
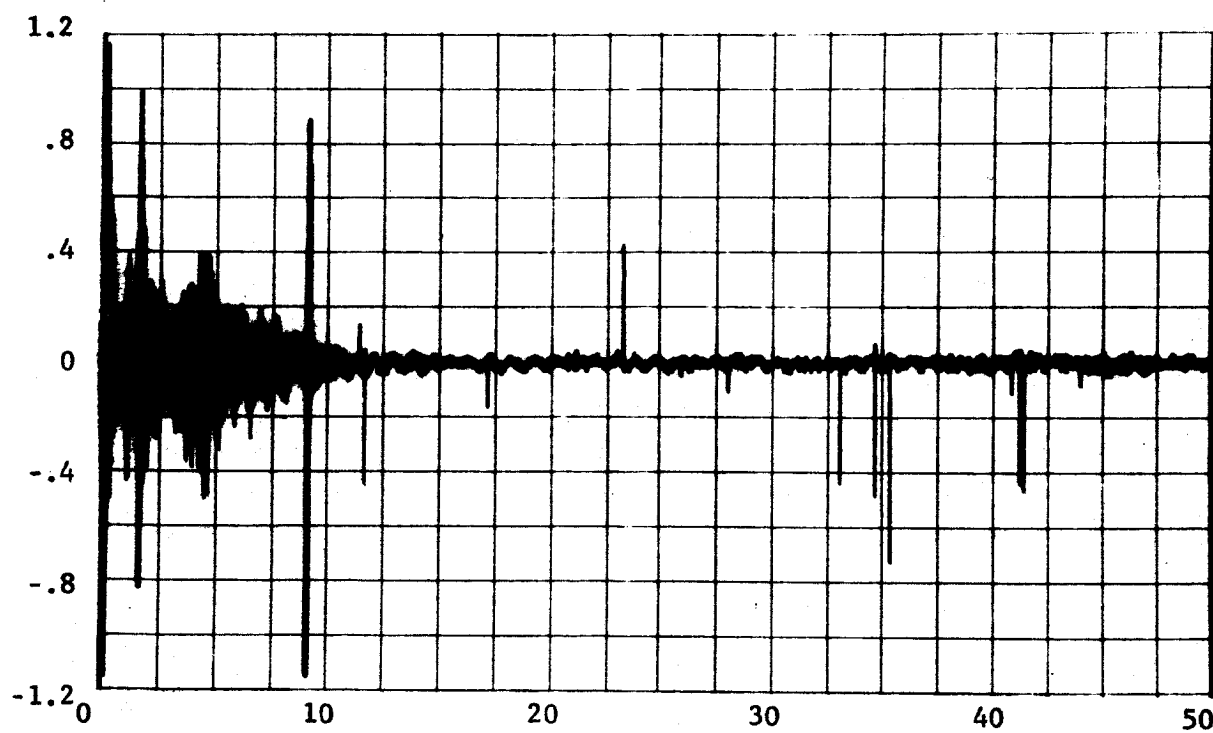
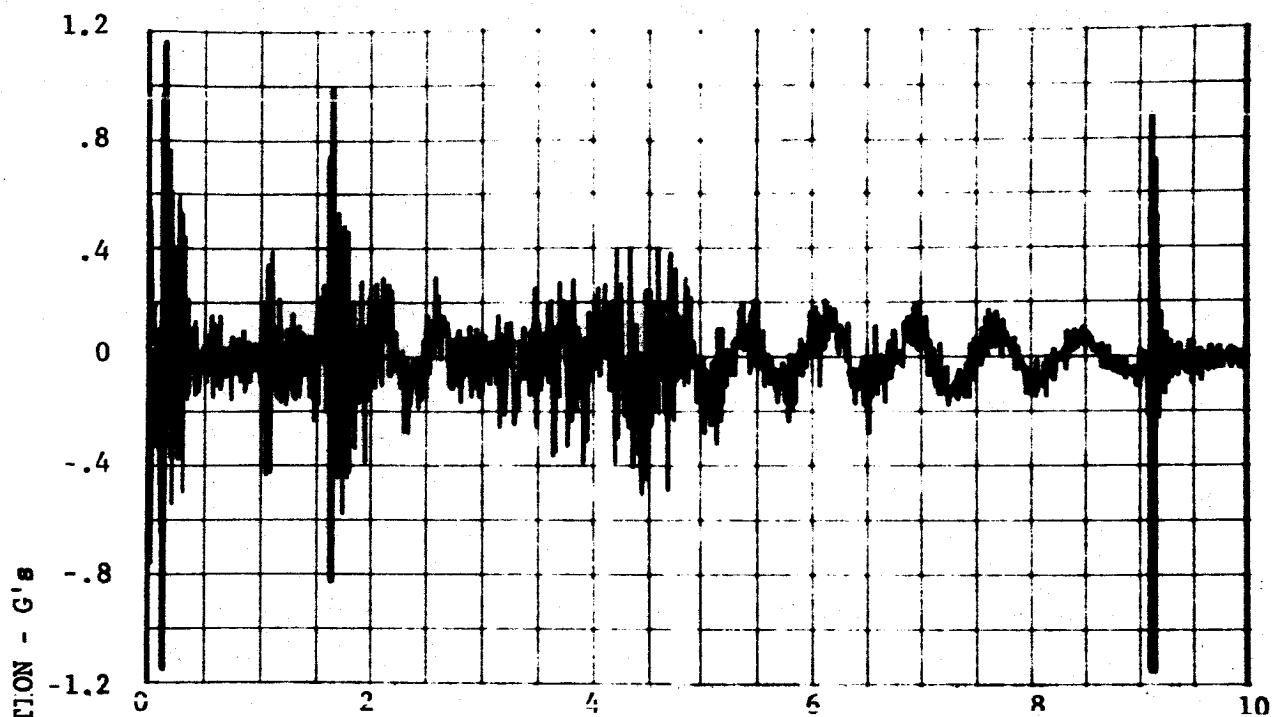
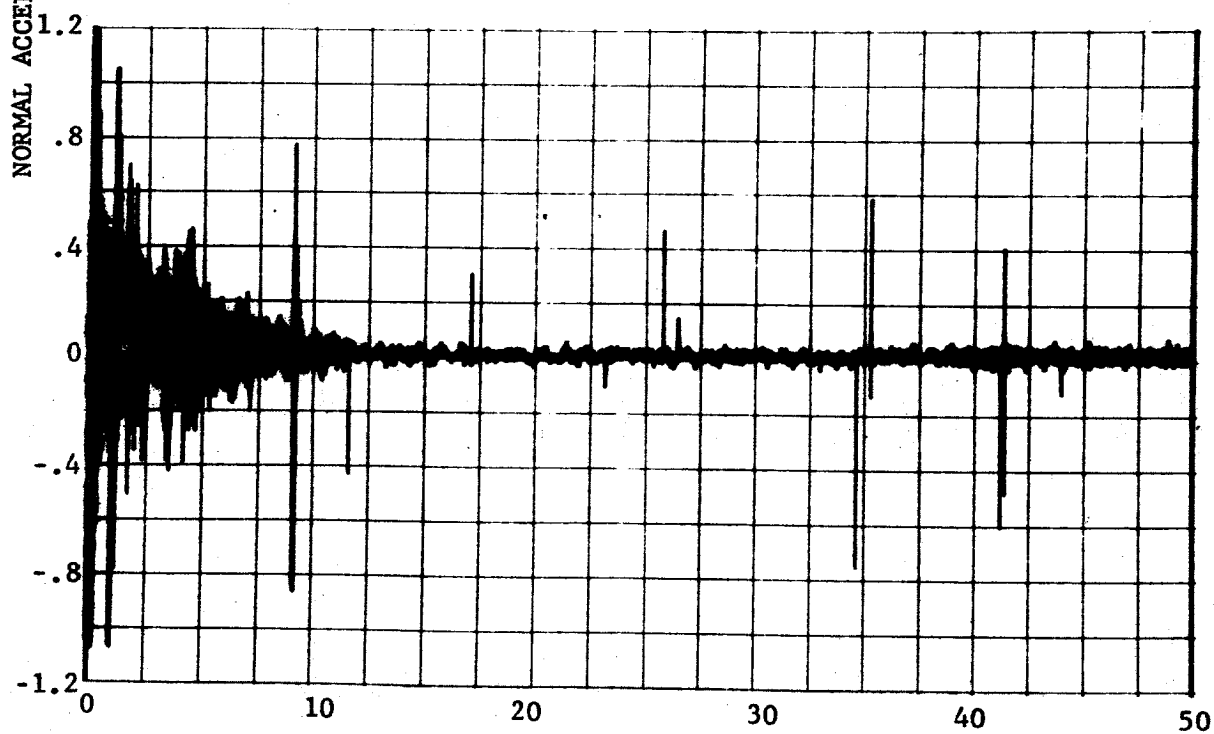
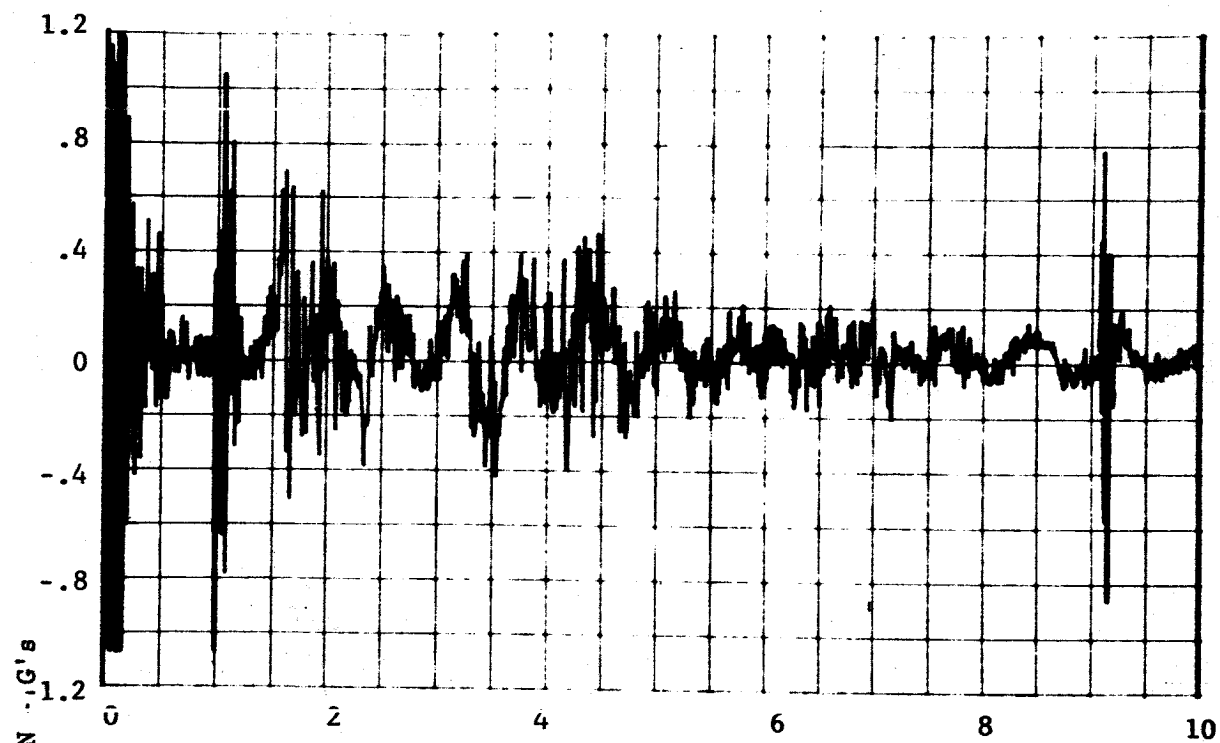


FIGURE V-13 LONGITUDINAL ACCELERATION



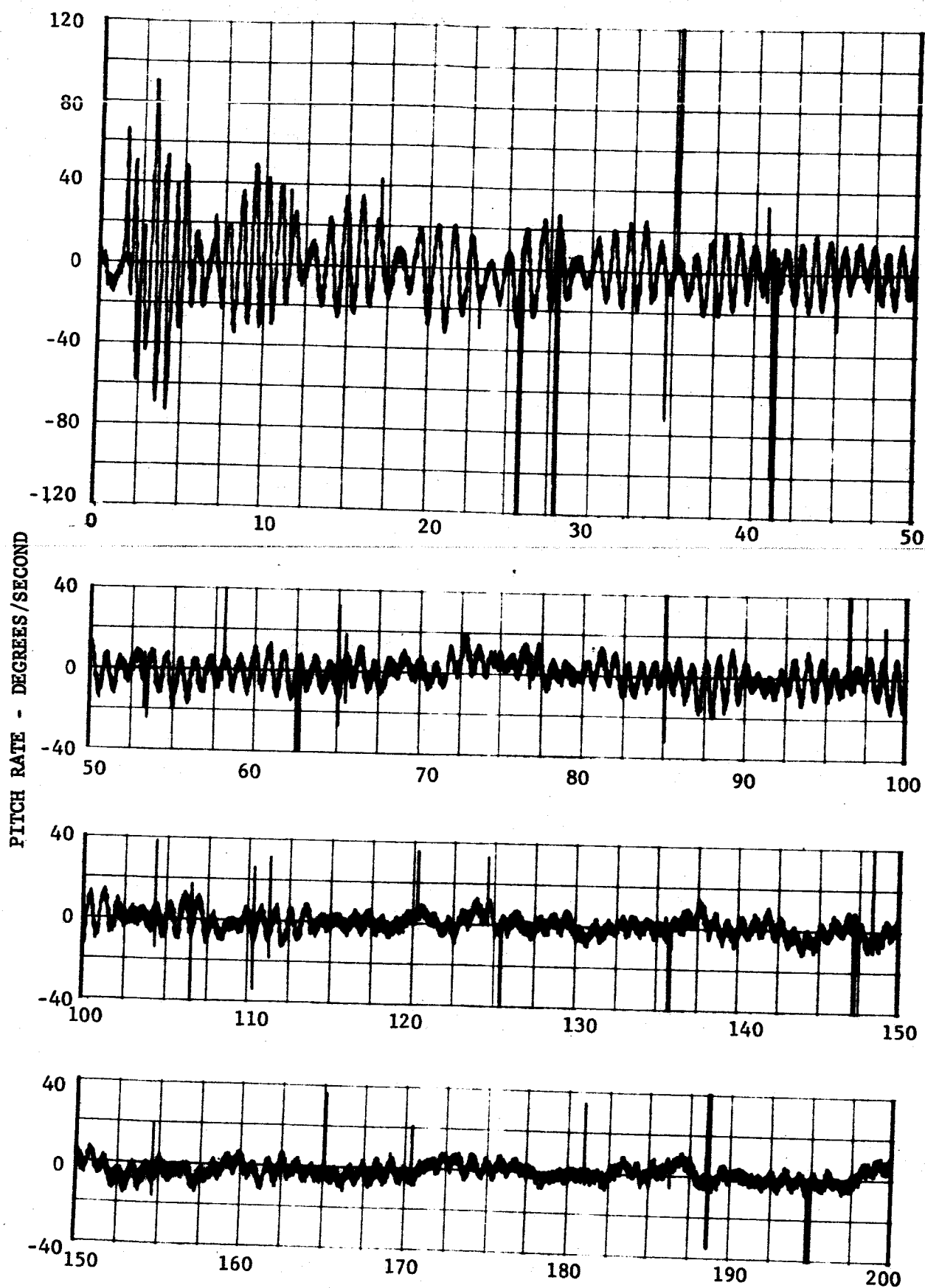
TIME FROM MORTAR FIRE - SECONDS

FIGURE V-14 TRANSVERSE ACCELERATION

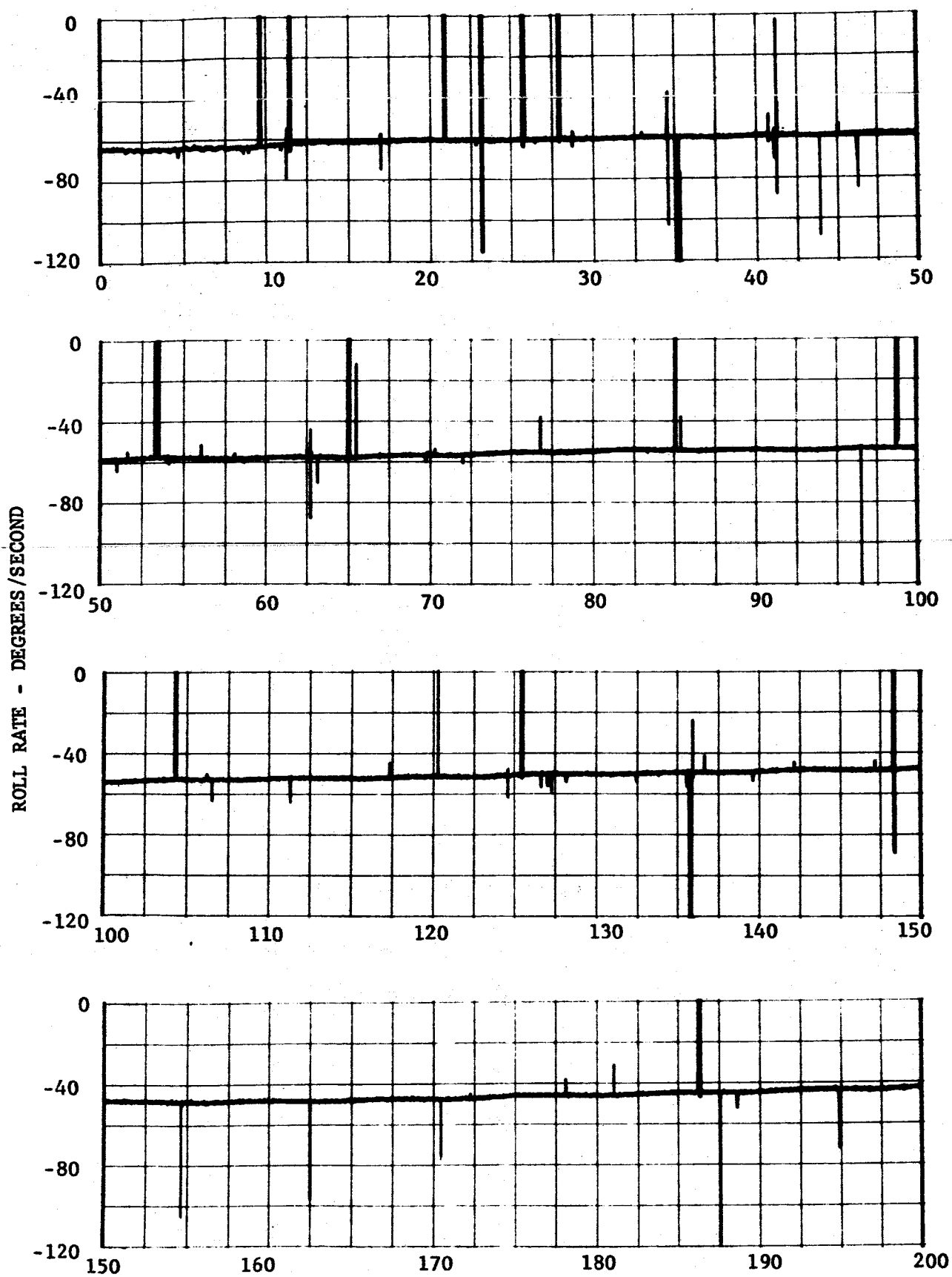


TIME FROM MORTAR FIRE - SECONDS

FIGURE V-15 NORMAL ACCELERATION

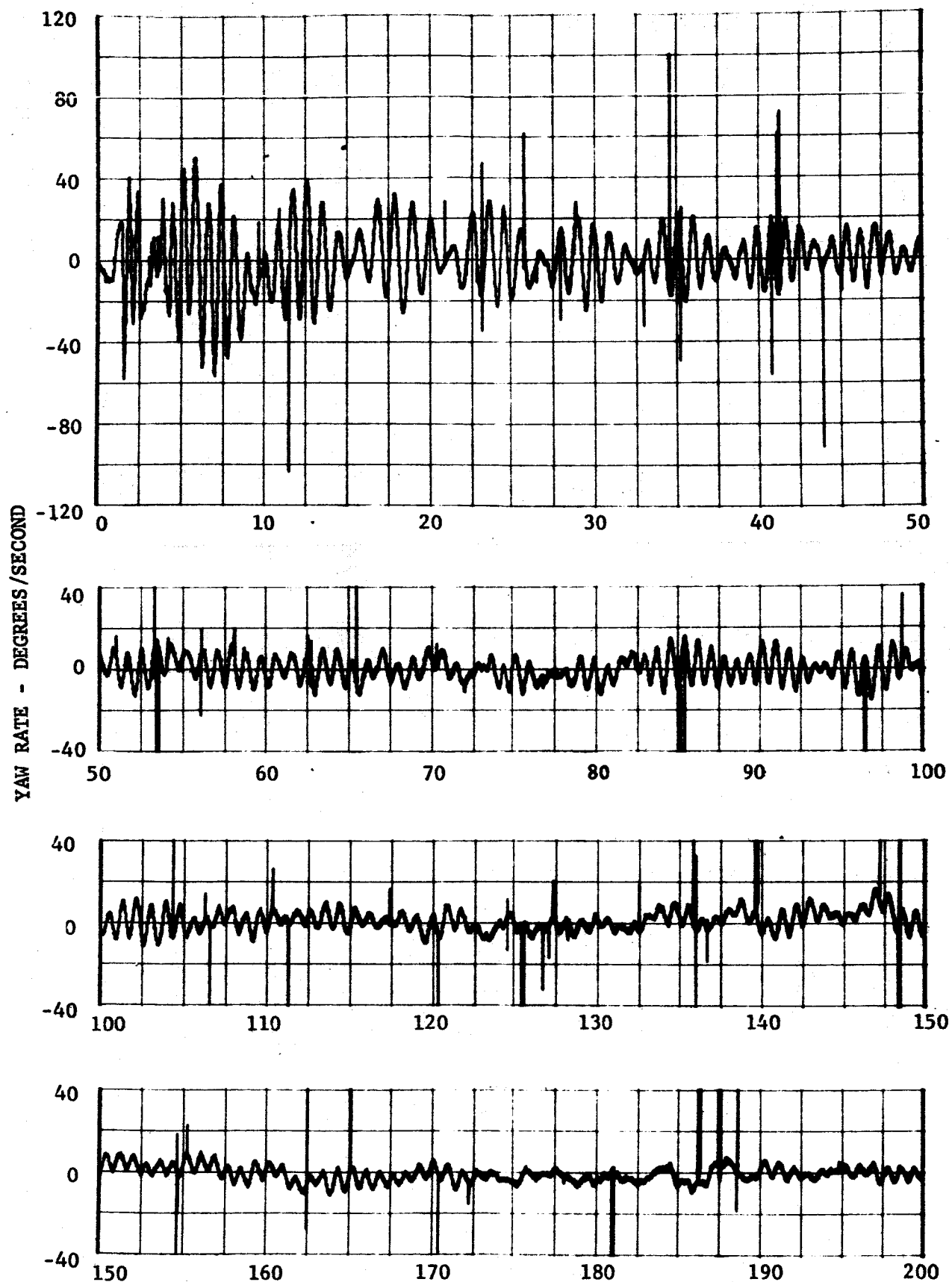


TIME FROM MORTAR FIRE - SECONDS
FIGURE V-16 VEHICLE PITCH RATE



TIME FROM MORTAR FIRE - SECONDS

FIGURE V-17 VEHICLE ROLL RATE



TIME FROM MORTAR FIRE - SECONDS

FIGURE V-18 VEHICLE YAW RATE

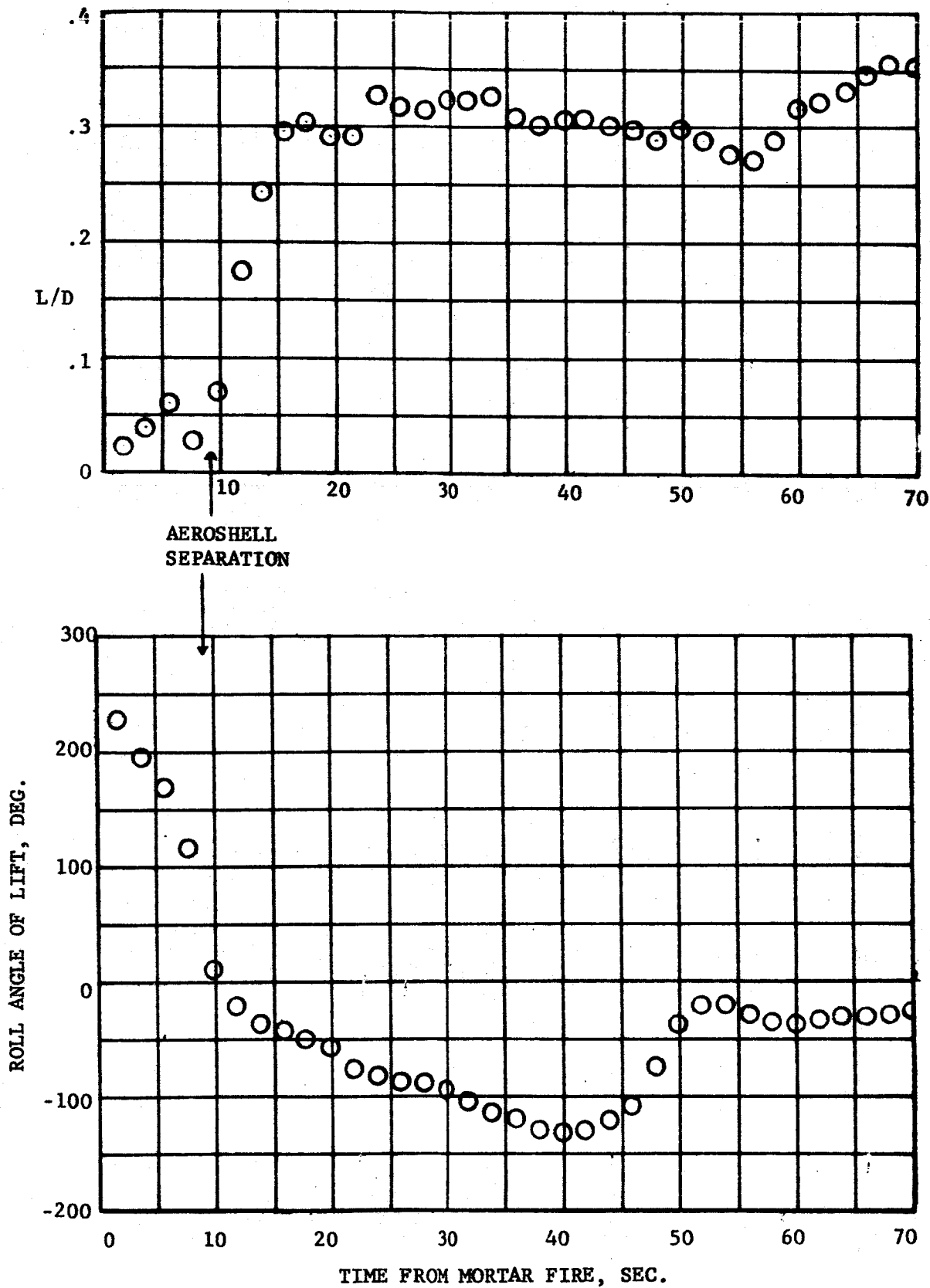


FIGURE V-19 PARACHUTE LIFTING DURING DESCENT

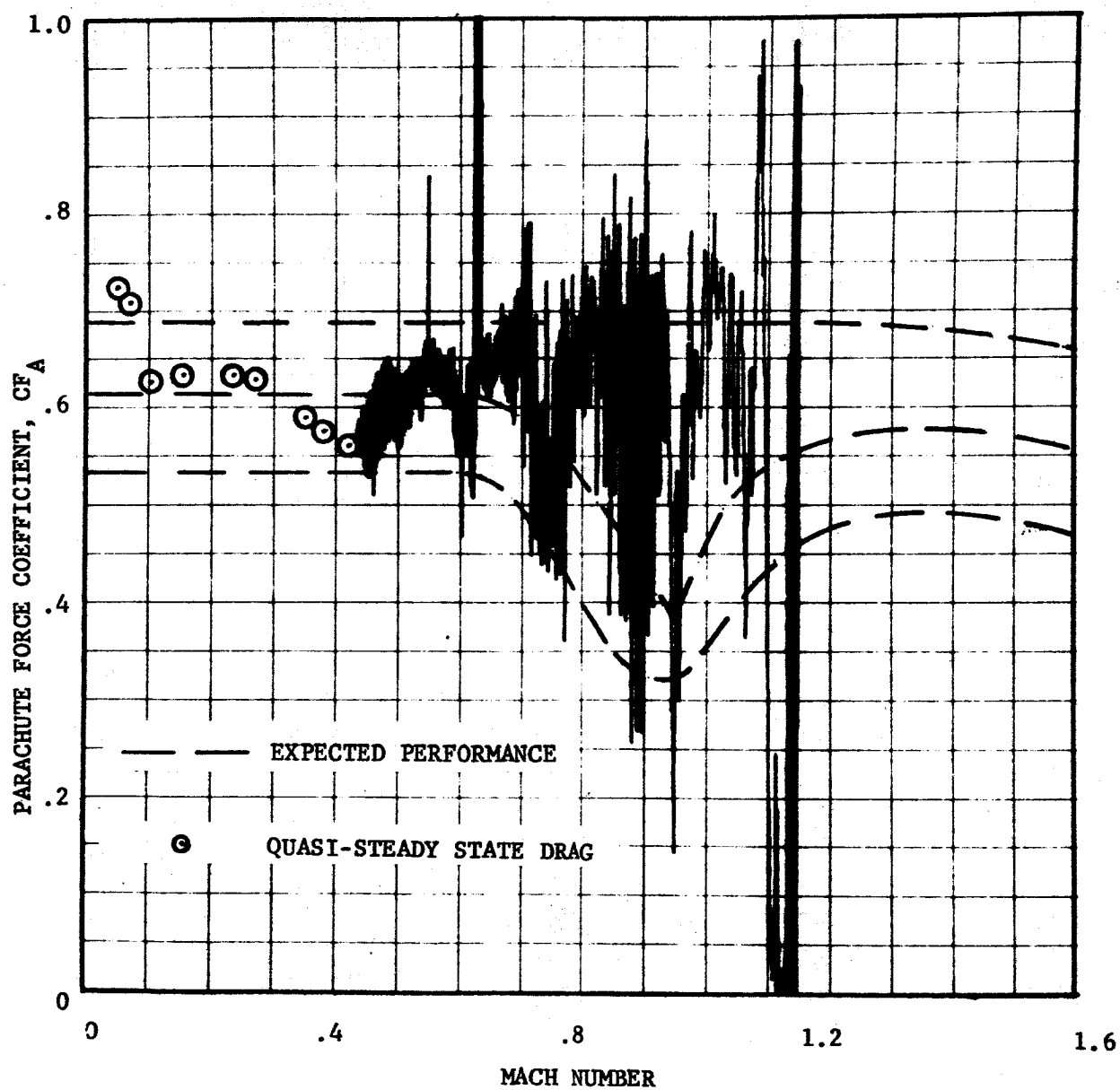


FIGURE V-20 PARACHUTE FORCE COEFFICIENT (ACCELEROMETER DATA)

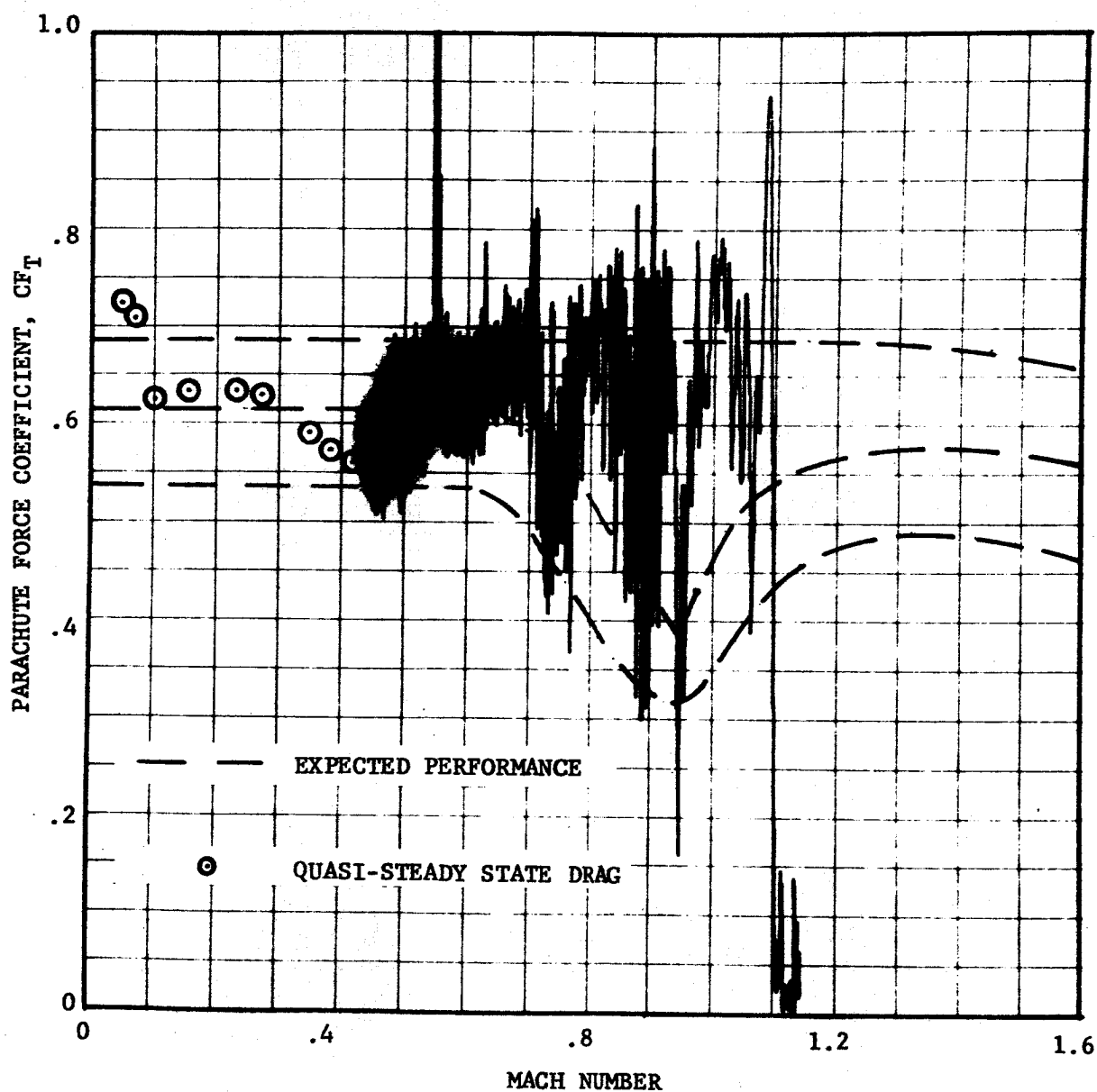


FIGURE V-21 PARACHUTE FORCE COEFFICIENT (TENSIO-METER DATA)

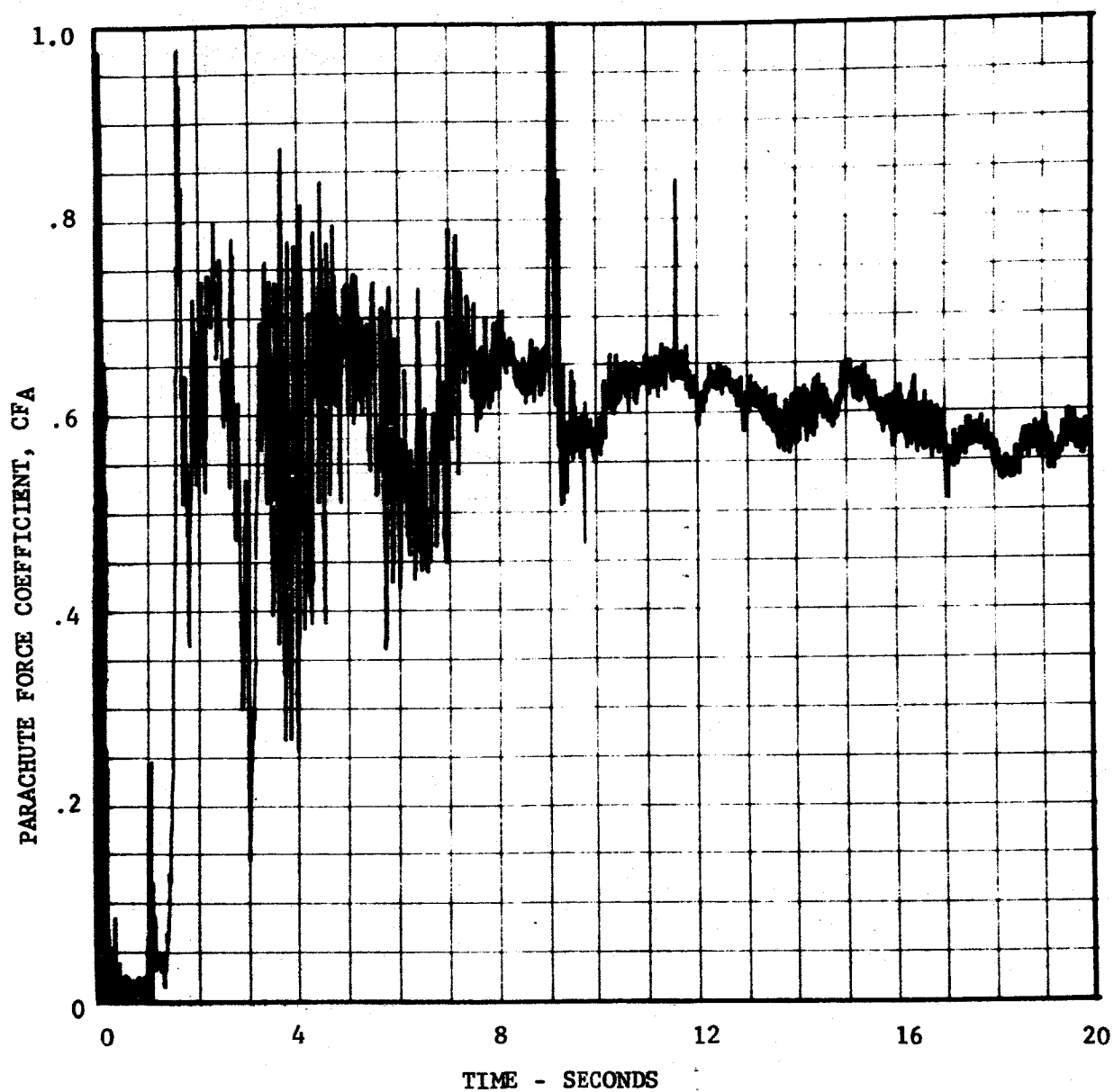


FIGURE V-22 PARACHUTE FORCE COEFFICIENT (ACCELEROMETER DATA)

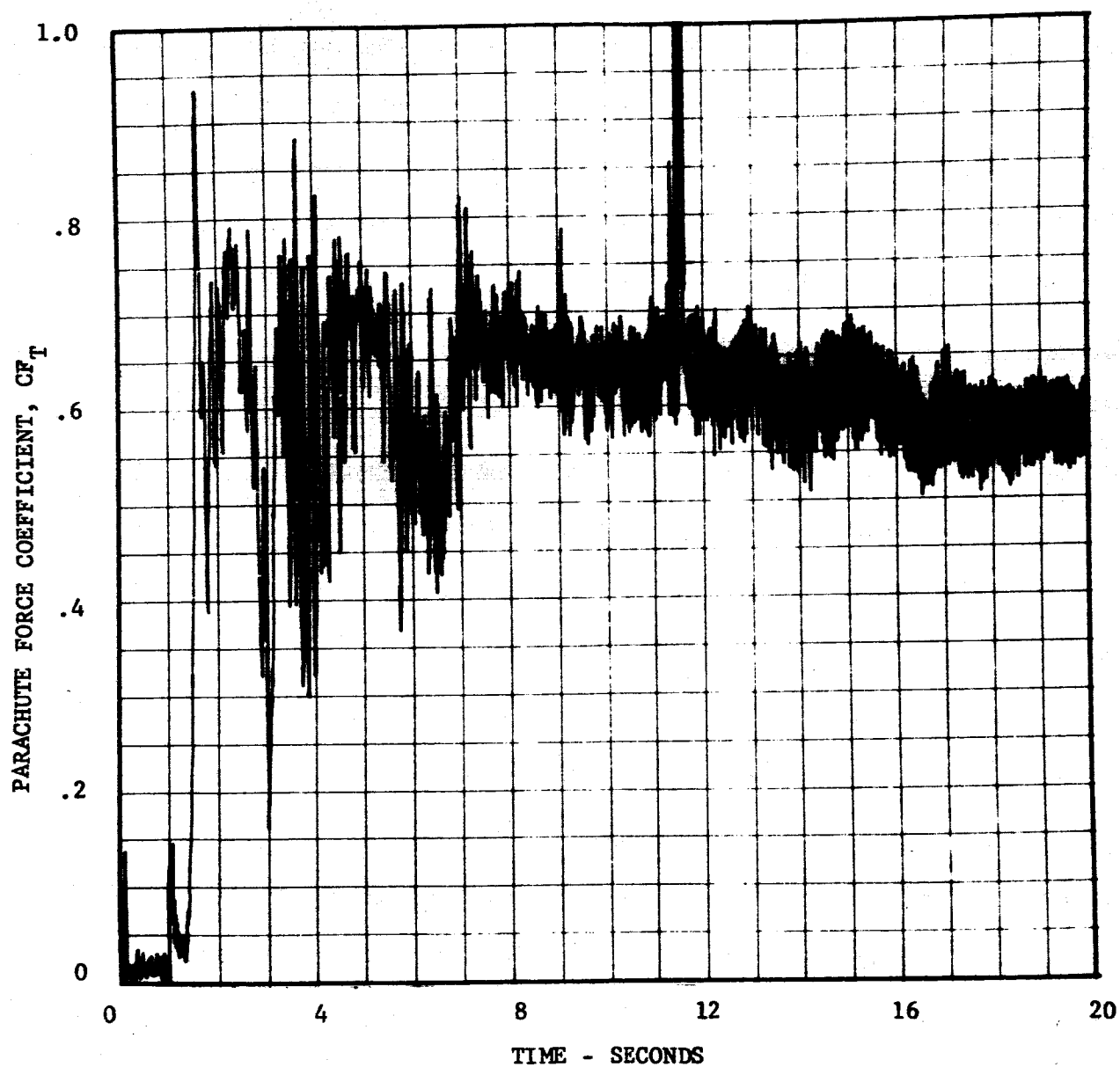


FIGURE V-23 PARACHUTE FORCE COEFFICIENT (TENSIO METER DATA)

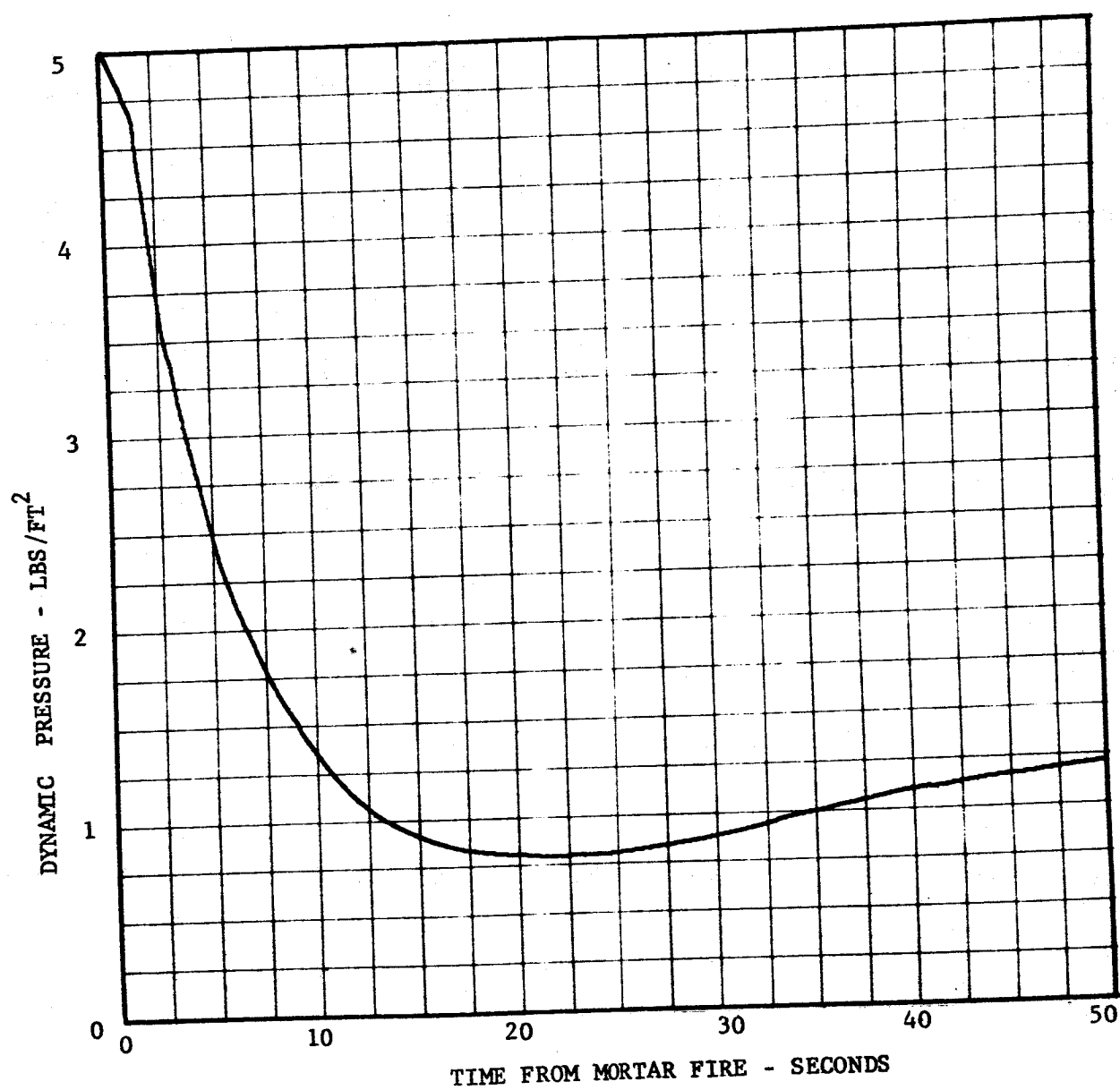


FIGURE V-24 DYNAMIC PRESSURE TIME-HISTORY

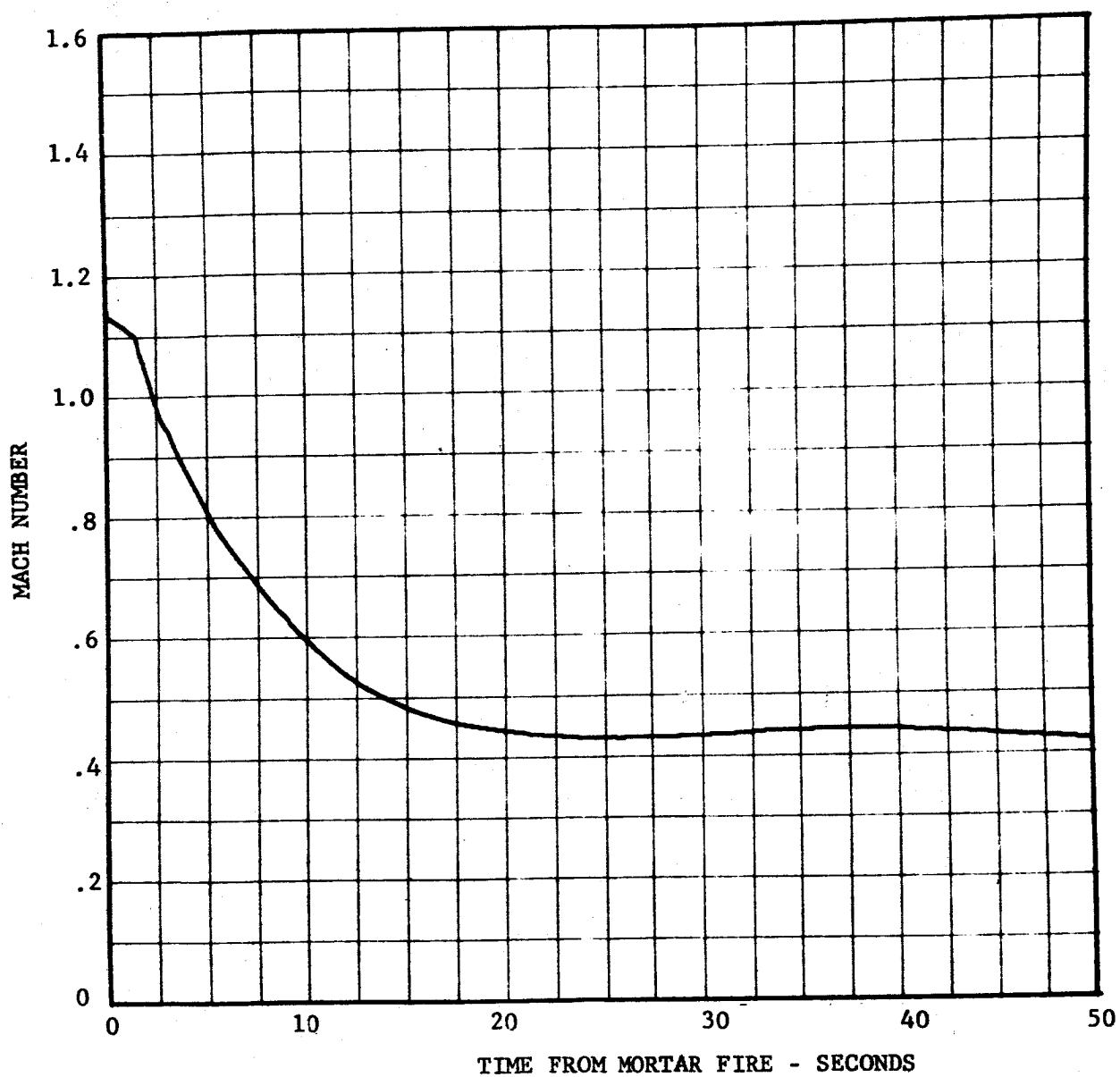


FIGURE V-25 MACH NUMBER TIME-HISTORY

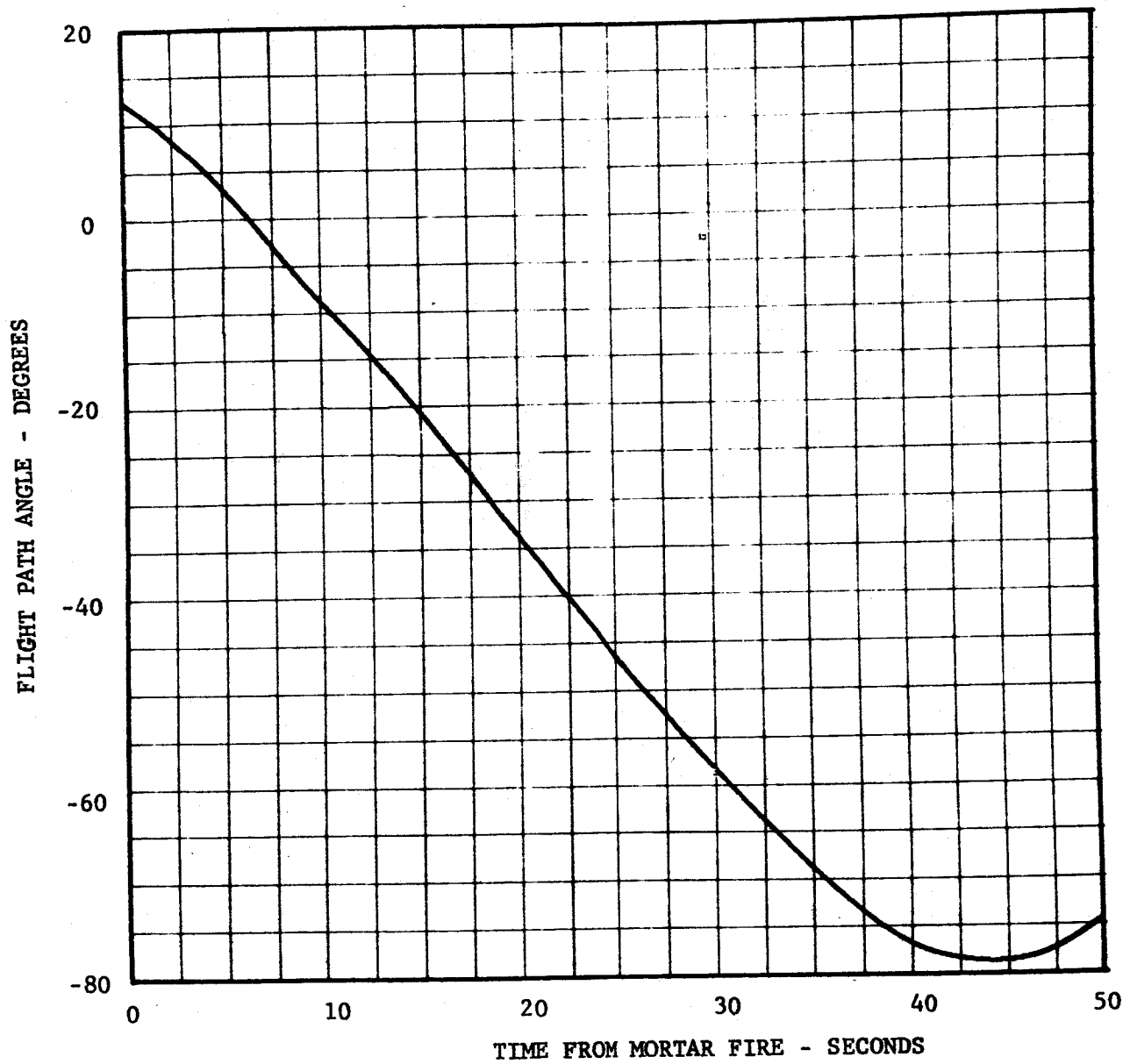


FIGURE V-26 FLIGHT PATH ANGLE

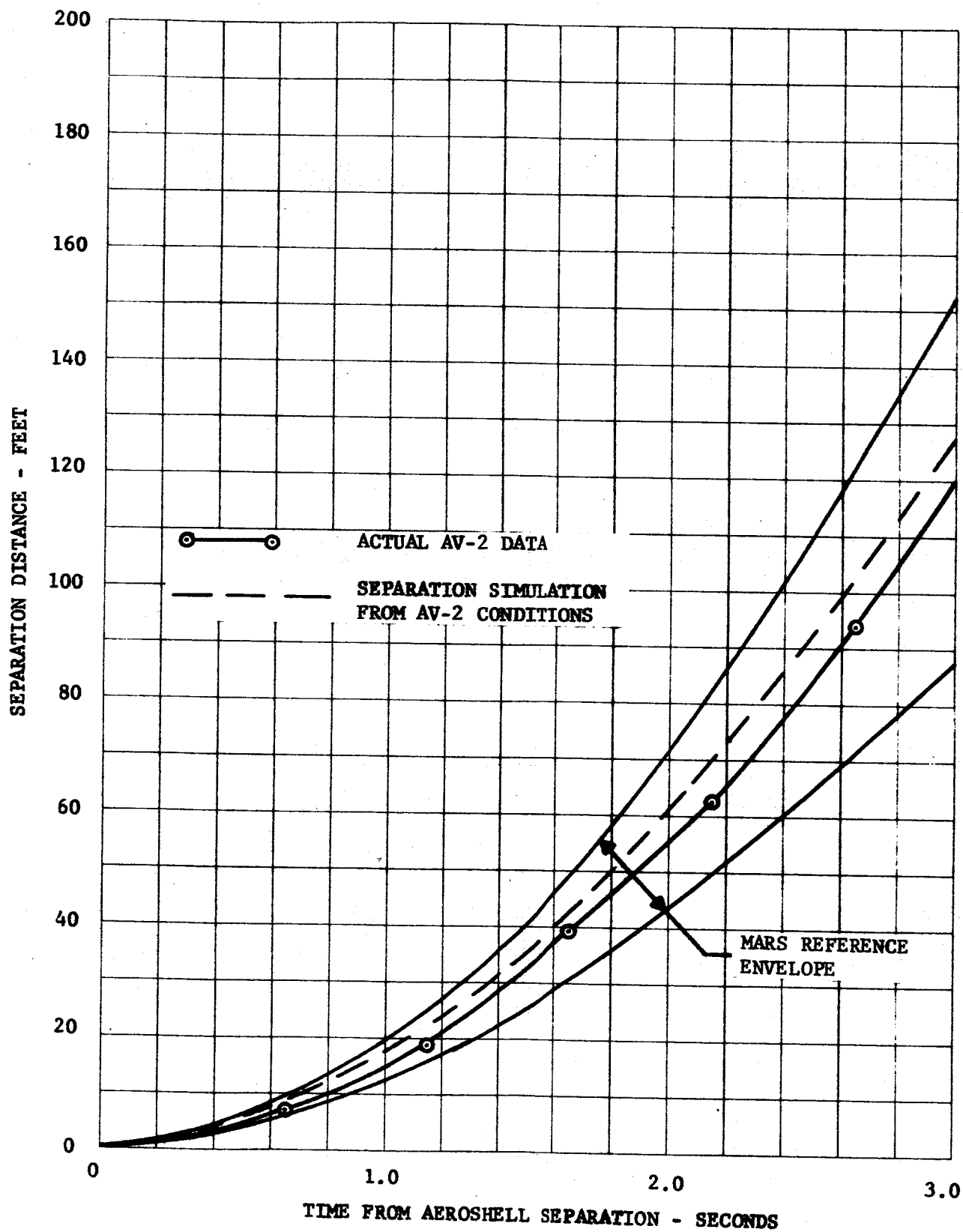


FIGURE V-27 AEROSHELL SEPARATION DISTANCE - 0-3 SECONDS

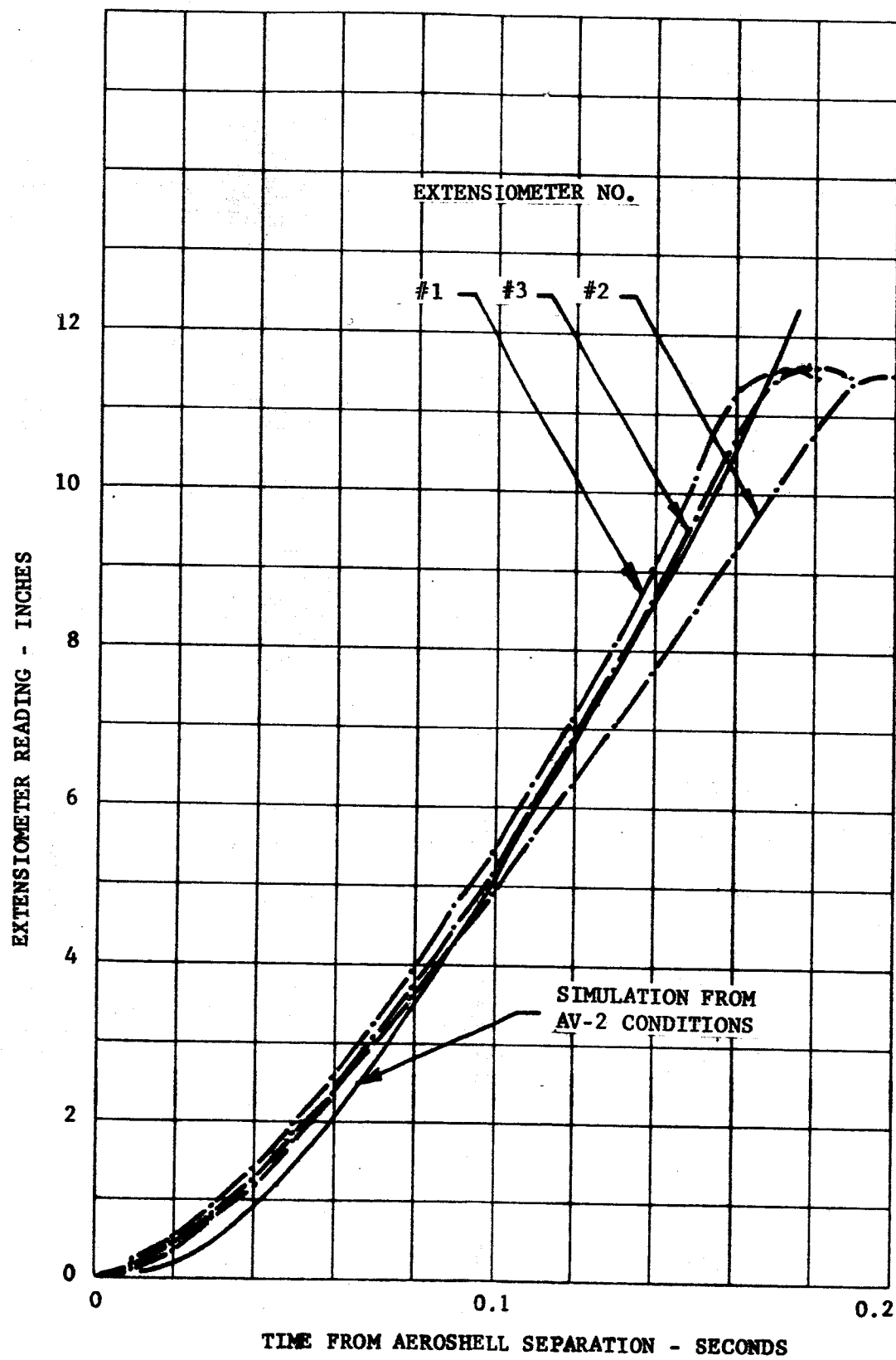


FIGURE V-28 EXTENSOMETER SEPARATION DISTANCE

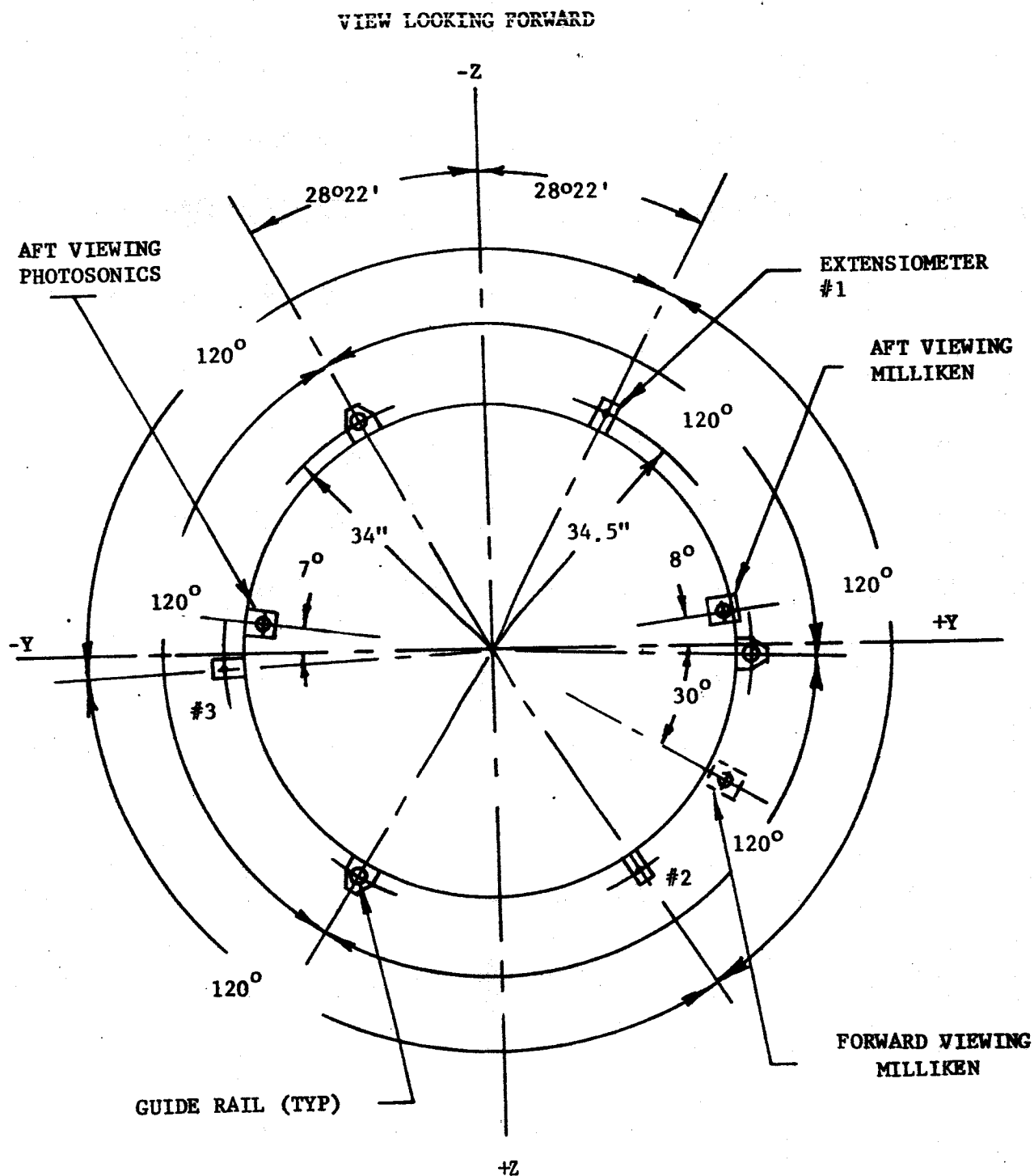


FIGURE V-29 EXTENSOMETER AND GUIDE RAIL LOCATION

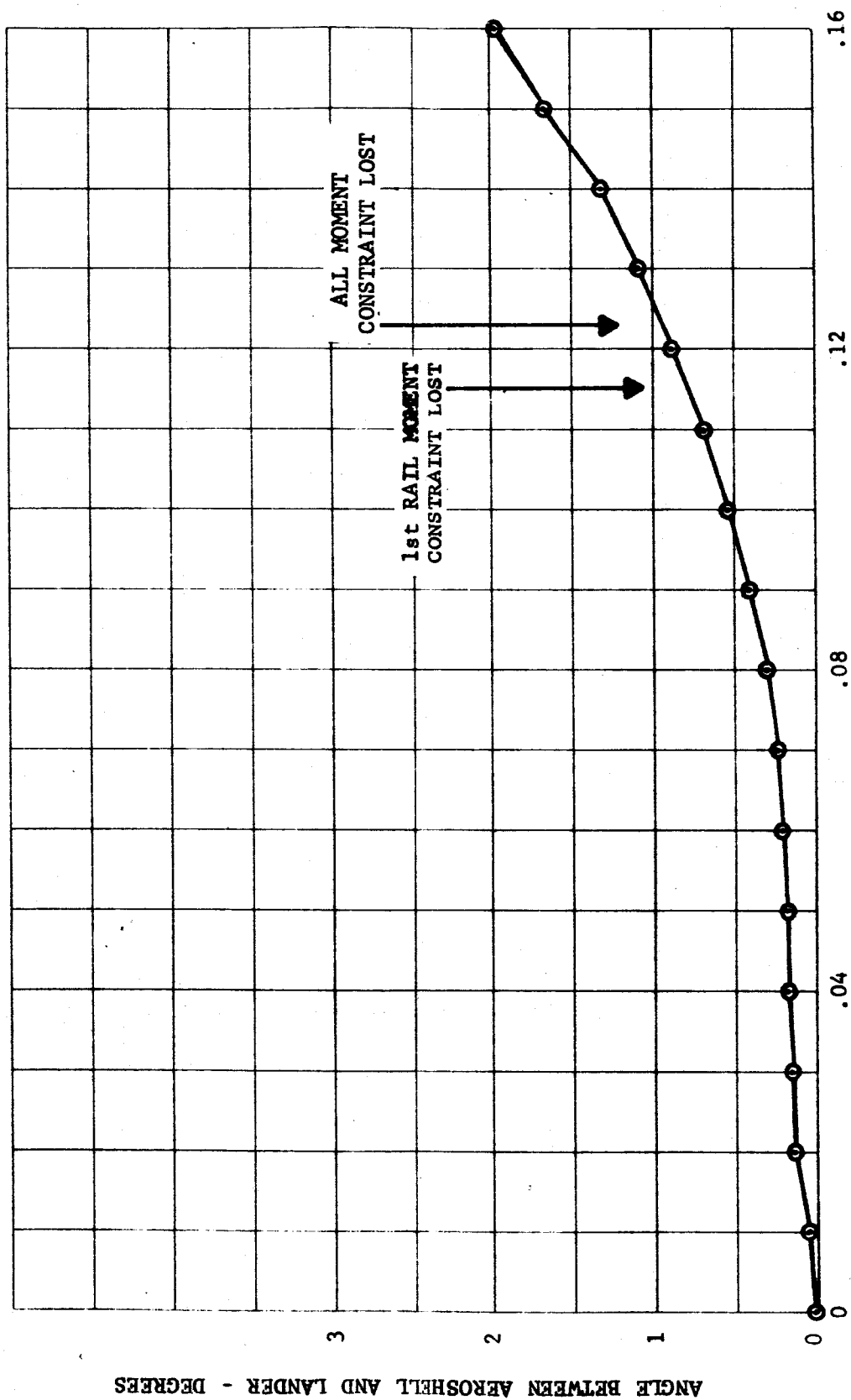


FIGURE V-30 RELATIVE ANGULAR MOTION BETWEEN AEROSHELL AND LANDER

VI. VEHICLE PERFORMANCE ANALYSIS

The following is a summary assessment of the BLDT vehicle performance.

The summary is presented by subsystem/discipline:

A. Flight Dynamics

The objective of the flight dynamics portion of the report is to establish the actual flight performance of the AV-2 vehicle from the command for vehicle release from the load bar through the command for decelerator mortar fire. It is noted that the flight of vehicle AV-2 was required to qualify the parachute in a transonic deployment domain.

The vehicle performance requirements for the transonic vehicle are established based on Mars anticipated environments and characteristics of the BLDT vehicle which might differ from the actual VLC. These performance requirements are:

1. Resultant angle of attack at mortar fire ≤ 20 degrees
2. Residual spin rate at deployment ≤ 100 degrees/second
3. Mach Number and dynamic pressure at peak load within the test envelope shown in Figure VI-1.

Figure VI-1 provides the target mortar fire and anticipated peak load conditions of:

	<u>MACH NUMBER</u>	<u>DYNAMIC PRESSURE (psf)</u>
Mortar Fire	1.208	5.07
Peak Load	1.150	4.52

The peak load requirements box is established such that the dynamic pressure is less than the lowest dynamic pressure obtainable from possible Mars entry environments and at a Mach number greater than 1.05.

1. Data Sources

The intent of this section is to evaluate the flight performance of BLDT AV-2 by reconstructing its trajectory using flight test data. The reconstruction is primarily based on three sources of data:

- o Meteorological data (density, velocity of sound, and winds);
- o Telemetry data (accelerometers, and gyros); and
- o Radar data (slant range, azimuth and elevation).

a. Meteorological Data - Meteorological data were obtained by standard WSMR radiosonde observations (RAOB) and LOKI rocket probes. The RAOB probe produced pressure, wind direction and velocity and temperature at 5000 feet intervals from surface to approximately 110,000 feet. The LOKI rocket probe produced temperature and wind data at 5000 feet intervals from 80,000 feet to approximately 150,000 feet. The combination of the RAOB and LOKI data defined the atmospheric parameters from surface to altitude. Three atmospheric profiles were obtained for the AV-2 flight as follows:

T-24 hr. data:

LOKI	launched 25 July 1972
RAOB	launched 25 July 1972

T-1 hr. data:

RAOB #128	launched 26 July 1972
LOKI #145	launched 26 July 1972

T+1 hr. data:

RAOB #211	launched 26 July 1972
LOKI #145	launched 26 July 1972

The T-24 hr. data were used by the real time computer during the actual flight to predict impact and command mortar fire. A comparison of the density of the above 3 sets of data shows that the T-1 hour data were close to the average. Therefore, the T-1 hr. data as shown in Table VI-1 were used for all flight performance analysis.

b. Telemetry Data - The flight vehicle telemetry (TM) data was transmitted via an S-band link to the WSMR receiving stations J-10 and J-67 where it was recorded and retransmitted via microwave links to the flight operations control station at building 300. These receiving stations are geographically located to provide continuous coverage of the real time mission. Their locations are shown in Figure VI-2. At Building 300, the TM data were recorded for post-flight usage and also terminated at various displays for observation and control of the mission.

The conditioned and smoothed TM accelerometer and rate gyro data, which were used for flight performance analysis, are shown in Figures VI-3 through VI-6. Figures VI-3 and VI-4 are gyro and accelerometer data respectively for the time period prior to the vehicle release from the load bar. The effect of pointing commands are reflected in the spin and yaw gyro data. Figures VI-5 and VI-6 are the same data during vehicle powered flight. It is noted that all of the accelerometer and gyro data were smoothed and conditioned except the accelerometer data prior to drop which was only conditioned. These data were filtered with a seventy (70) point standard least squares quadratic leading edge filter with exception of the pitch and yaw

rate gyros which were mid-point filtered to reduce the effect of excessive noise encountered in the pitch gyro. The conditioning was based on a two sigma (2σ) dispersion limit of the filtered data with wild points replaced by the quadratic prediction.

The initial estimates of instrumentation bias were obtained from these plots by integrating the gyro data during the float period (Figure VI-3) and adjusting the accelerometer data for zero setting during the free fall portion of flight immediately after release from the load bar (Figure VI-4). The TM instrumentation system is designed to provide a 5% end to end error tolerance limit but with the above biases it is judged that the instrumentation accuracies can be assumed to be 2%. This provides the following accuracies:

<u>FUNCTION</u>	<u>TOLERANCE</u>
Gyros	6 deg/sec
Lateral Accelerometers	0.02 g's
Longitudinal Accelerometer	0.10 g's

c. Radar Data - The BLDT vehicle was tracked by (4) WSMR FPS-16 radar sets, three (3) were beacon track and one was skin track. The beacon track radars (R123, R125 and R128) were used for continuous track of the vehicle until loss of beacon ($T + 400$ sec) at which time they switched to skin track. The skin track radar was utilized to track other system components such as balloons, load bar and aeroshell. The stated accuracy of the FPS-16 radars is 0.1 to 0.3 mils in angles and 15 to 45 feet in range, which is approximately 50 feet of space position.

The radars provided slant range (R), azimuth (A) and elevation (E) data with respect to the radar site. Only the beacon track radars were considered for performance analysis. These radar locations are shown in Figure VI-2. An analysis of the radar data consisted of transforming the (R), (A) and (E) from a given site to an (R), (A) and (E) of a second site where the derived (R), (A), and (E) were compared with the actual measured data for the second site. This analysis was completed for radar sites R123 vs. R128, R125 vs. R128 and R123 vs. R125 and the reverse of each. This analysis indicates that R123 and R125 were providing excellent tracking data with zero systematic errors and were tracking within the expected 50 feet. R128 when compared to R123 showed large systematic errors as well as large random errors. The time plots of (R), (A) and (E) differences are presented in Figure VI-7 for R123 and R125 and Figures VI-8 for R123 and R128.

The conclusion of this analysis is that both R123 and R125 radar data could be used for reconstruction of AV-2 flight.

The radar data were post-flight corrected by WSMR for systematic errors which were determined by pre-flight calibrations. Raw data of range azimuth and elevation were smoothed by standard WSMR filter techniques to produce velocity, altitude, flight path angle and azimuth. These velocity, flight path angle and altitude data are presented in Figures VI-9 and VI-11 for radar site R125. These data are earth reference measurements and are not ambient aerodynamic conditions.

2. STEP Trajectory Reconstruction

The Statistical Trajectory Estimation Program (STEP) (Reference 9) was used to determine the reconstructed trajectory. This program solves for the initial conditions (position, velocity, and attitude of the vehicle)

so that by integration of the gyros and accelerometers the trajectory matches the radar data (range, azimuth and elevation). Besides solving for initial condition it has the capability of determining the systematic errors (biases and scale factors) on the gyros and accelerometers. The program gives a minimum variance solution on the radar measurements (range, azimuth and elevation). The trajectory is considered to be the optimum when the radar data are randomly dispersed about the reconstructed trajectory and the variance of the range, azimuth and elevation is within the expected tracking accuracies of the radar.

STEP requires an estimate of the biases and scale factors on the gyros and the accelerometers. In order to obtain these biases on the gyros, the telemetry data were examined from T-45 seconds to T+0 (vehicle drop). These data are shown in Figure VI-3. At this time the vehicle had very small motions and the centers of the oscillatory motions were determined to be the biases on the gyros. These biases are:

Roll gyro (P)	-2.0 degrees/second
Pitch gyro (Q)	-.25 degrees/second
Yaw gyro (R)	-2.80 degrees/second

To determine the biases on the accelerometers, the data between T+0 and T+1 second were analyzed. These are shown in Figure VI-4. At this time the vehicle is in a near zero force field which permits establishing a zero setting. The average values of the accelerometer readings at this time were:

X-accelerometer	* -.02 g's
Y-accelerometer	-.00 g's
Z-accelerometer	-.05 g's

The scale factors on the gyros and accelerometers were initialized at unity.

The initial estimates of position and velocity at drop were obtained from smoothed radar data:

Latitude	33.4511
Longitude	-106.2321
Altitude	120900.
Velocity	94.1
Flight Path Angle (gamma)	0.0
Azimuth	276.9

The initial estimates of the body Euler angles are required for body heading (PSI), pitch (THETA) and roll angle (PHI). The initial Euler angle estimates are:

PSI	210°
THETA	65°
PHI	0°

The initial estimate for PSI was taken from the magnetometer reading at drop while THETA was estimated at 65° based on nominal value. Given these initial conditions and previously established biases and scale factors STEP was not able to provide a comparative fit to the radar data between T+0 and T+38 seconds. STEP continued to give very poor agreement with the radar data when attempts were made to revise the scale factors on the gyros. The most sensitive parameter was the scale factor on the roll gyro (P). By varying the scale factor on P between 0.98 and 1.01, STEP returned a trajectory which had systematic difference between the radars.

The reason STEP had difficulty in converging on an optimum trajectory was because of the type of trajectory the BLDT vehicle was designed to fly.

Between T+2 and T+9 seconds the vehicle has a gyroscopic turn of about 17° . During this turn STEP must have the proper roll angle history to be able to integrate the measured forces in the proper direction. An error in PHI of only a few degrees causes the reconstructed trajectory to diverge from the radar track. During the time of drop, spin up, and main engine ignition the instrumentation package is subject to high shock loads which amplify the data noise level. It is very difficult to remove only the noise due to the shock without also adding biases to the data.

In order to avoid this data noise problem, STEP was initialized at T+12 seconds with the initial position and velocity being obtained from radar data. Using Euler angles, obtained from the previous best STEP trajectories, and radar data from Radar Site R123 and R125 for every 0.2 seconds between T+12 and T+38 seconds, STEP was able to obtain a very good reconstructed trajectory. The radar track deviated from the reconstructed trajectory by the following standard deviations.

	<u>RADAR R123</u>	<u>RADAR R125</u>
$\sigma_{\text{slant range}}$	7.0 ft	6.5 ft.
σ_{azimuth}	4.8×10^{-3} deg. \approx 20 ft.	4.8×10^{-3} deg. \approx 15 ft.
$\sigma_{\text{elevation}}$	4.8×10^{-3} deg. \approx 20 ft	4.8×10^{-3} deg. \approx 15 ft.

STEP was also programmed to compute the best estimate of the biases and scale factors on the gyros and accelerometers. The only revision resulting from this analysis was to change the three gyro scale factors from 1.0 to 0.9805 and this is within the accuracy of the instrumentation system.

STEP reconstructed trajectory provides a very accurate measurement of altitude and velocity. Combining these values with the meteorological data, velocity relative to the wind, Mach number and dynamic pressure were computed.

Time history of altitude, velocity, Mach Number and dynamic pressure are shown in Figures VI-12 and VI-13. Figures VI-14 and VI-15 show the body and velocity vector orientation versus time. The conditions established by STEP at mortar fire and peak load, provided in Table VI-2, show that the flight performance did meet the requirements for dynamic pressure as required in Figure VI-1.

The angle of attack, sideslip and total angle of attack are shown in Figures VI-16 and VI-17. The total angle of attack shown on Figure VI-17 never exceeds the value of 20° after 20 seconds flight time which is less than the required value of $< 20^{\circ}$ at mortar fire.

In conclusion, the actual test conditions were within the success criteria deployment box for the transonic test, but the trajectory of BLDT AV-2 was not predicted to within 2σ dispersion limits of all the flight parameters. The deployment Mach Number/dynamic pressure test conditions were not within the designed 2σ ellipse as shown in Figure VI-1.

The actual test conditions are lower than predicted in Mach Number and appear to the left of the 2σ ellipse shown in Figure VI-1. The deviation from the nominal prediction can be attributed to any number of combinations of random deviations in the 111 independent parameters considered in the statistical analysis, which are impossible to isolate using flight data. However, the actual deviation is greater than 2σ or 89% probability indicating an excessive anomaly in a flight performance parameter. The drop altitude, which was consistently low for all missions, caused a lower than nominal Mach Number at mortar fire because of an increased atmospheric density through which the vehicle flew. The sensitivity of Mach Number at mortar fire to drop altitude is approximately .021/1000 ft. The fact that the altitude was 1760. ft. low at drop for vehicle AV-2 provides a Mach Number

shift of approximately .034 which significantly reduced the Mach Number at parachute deployment. The test conditions adjusted for the low drop altitude are included in Figure VI-1. These adjusted conditions are well within the 2σ designed dispersions.

The prediction flight conditions with respective statistical dispersions are compared below with the actual flight conditions and actual flight conditions adjusted for the low drop altitude at mortar fire:

	<u>Predicted Value</u>	<u>2σ Dispersion</u>	<u>Actual Value</u>	<u>Adjusted Actual Value</u>
Dynamic Pressure	5.07	4.67 - 5.47	5.00	5.00
Mach Number	1.208	1.156 - 1.260	1.133	1.172
Total Angle of Attack	8.9	1.4 - 15.8	7.28	7.28
Spin Rate	-61.3	-98.3 - -24.3	-62.0	-62.0
Altitude	137,500	135,860 - 139,140	135,368	137,068
Velocity	1267	1209 - 1325	1194	1240

It is noted that each adjusted flight parameter is within its 2σ predicted dispersion.

3. Body Inertial Attitude from Aft Camera

The body attitudes were obtained from the aft looking camera which was started at 33.22 seconds after drop. The method used was to measure the angle of the horizon relative to the camera frame, the angular displacement from the center of the camera frame (body X axis) to the apparent horizon and then the horizontal angular displacement of this center to the balloon image. Using the radar position of the vehicle and assuming the balloon had continued at its pre-drop velocity, allowed the vehicle inertial

azimuth to be reconstructed. The visible horizon was assumed to be 6 degrees below the local horizontal which allowed the vehicle pitch attitude to be reconstructed. The camera roll attitude relative to the vehicle body axes, shown in Figure V-29, allowed the vehicle roll attitude to be reconstructed. This data is compared to the step reconstruction of body attitude in Figure VI-18. The roll attitude shows good agreement with the STEP reconstruction, however, the heading and pitch attitudes show biases probably due to a combination of camera misalignment, balloon position uncertainty, and the indistinct visible horizon.

The smoke puff from the mortar on the film gives a measure of the velocity vector. This data point at 38.45 seconds was converted to a body attitude using the radar relative velocity and vehicle roll attitude. This data point compares favorably with both STEP reconstruction and the balloon referenced film data.

B. Capsule Aerodynamic Characteristics

The aerodynamic characteristics of the vehicle are difficult to separate from thrust misalignment effects and inertial cross coupling due to roll during the powered portion of flight. However, after despin and prior to parachute deployment, the vehicle motions and accelerations are primarily due to aerodynamic forces and moments. The axial acceleration was converted to coefficient form and is compared to the predicted from Reference 4 in Figure VI-19. The applied moments on the vehicle were extracted from the telemetered rate data using the equations:

$$PM = \dot{Q} \times I_{YY} - P \times R (IZZ - I_{XX})$$

$$YM = \dot{R} \times I_{ZZ} - P \times Q (I_{XX} - I_{YY})$$

Where:

PM = Pitch moment

YM = Yaw moment

I_{XX} = Roll moment of inertia, slug-ft²

I_{YY} = Pitch moment of inertia, slug-ft²

I_{ZZ} = Yaw moment of inertia, slug-ft²

P = Roll rate, rad/sec

Q = Pitch rate, rad/sec

R = Yaw rate, rad/sec

\dot{Q} = Pitch acceleration, rad/sec²

\dot{R} = Yaw acceleration, rad/sec²

The angles of attack and sideslip at which the predicted aerodynamics would generate these moments are compared to the STEP reconstructed angles in Figure VI-19. In addition, the body attitude from the aft looking camera data was converted to angles of attack and sideslip by using the radar relative velocity data (Figure VI-18).

The aerodynamic drag agrees well with the predicted drag just before mortar fire indicating little residual engine thrust was present during parachute deployment. The axial thrust component of the despin motors is clearly evident. The angles of attack and sideslip derived from the applied moment data indicate the aerodynamic stability of the vehicle was probably nominal.

C. Thermal Control Subsystem

The design requirements for the BLDT Thermal Control subsystem were based on maintaining previously qualified hardware within the maximum and minimum specified qualification temperatures. Except for several isolated electrical heaters, a passive thermal control system was utilized on the BLDT vehicle for ascent and float control. The passive system was based on vehicle attitude and vehicle ascent rate to float altitude with convection, solar radiation, reflected solar radiation and infrared radiation being the major heat transfer parameters being considered.

The design ascent profiles are shown in Figure VI-20 with a fast ascent rate, when integrated with the above mentioned parameters, producing the hot case and the slow ascent rate producing the cold case. Figures VI-21, VI-22, VI-23, and VI-24 show select hot and cold case predicted temperature profiles for the base cover, rocket motor support structure, aeroshell and S-band transmitter respectively. Also shown in these figures are discrete point actual temperatures, extracted from the TM data which were recorded at approximately half hour intervals. It is noted that the actual temperatures generally remain within the hot and cold case predictions and are generally close to the hot case as would be expected due to the actual ascent rate.

Presented below is a table showing the temperatures measured by the "on-board" thermistors at the time of vehicle release from the load bar and at aeroshell separation compared with the specified requirement at vehicle drop.

	SPECIFICATION REQUIREMENT (°F)		ACTUAL TEMPERATURE (°F)	
	<u>MAX</u>	<u>MIN</u>	<u>DROP</u>	<u>A/S SEPARATION</u>
Rate Gyro	125	0	78	78
Boost Motor #1	165	-65	58	167
Equipment Ballast	165	0	80	80
S-Band Transmitter #1	165	0	92	93
Instrument Beams #1	125	0	61	62
Bridle #1	210	-90	46	48
Aeroshell #1	175	-115	42	42
Boost Motor #2	165	-65	54	160
Mortar Cannister #1	80	No Min	48	85
Mortar Breech	75	25	49	87
Instrument Beam #2	125	0	59	59
Bridle #2	210	-90	46	47
Aeroshell #2	173	-115	20	21
Rocket Motor Support Structure	(No Prediction)		43	44
Mortar Cannister #2	80	No Min	45	83
Mortar Breech Flange	75	25	45	61
Bridle #3	210	-90	45	47
*Main Battery	80	50	44	44

*The thermistor titled "main battery temperature" is misnamed, it really measures rocket motor support structure temperature.

D. Structural Subsystem

The structural system provided adequate support and dynamic operation during all phases of the AV-2 mission. There was no evidence of any structural failure in the load carrying structure and the dynamic portions of the system, including flip-away lens covers and aeroshell guide rail separation system, functioned as required. It is noted that the sponge seal installed between the mortar and the BLDT structure did prohibit the flow of mortar gases into the BLDT instrument compartment.

Inspection of the recovered hardware indicated the following conditions:

1. Aeroshell - nose cap poked out and inboard skins buckled. All damage resulted from ground impact.
2. Rocket Motor Support Structure - The RMSS was undamaged except for the forward command antenna was poked from its installation with the two antenna structural brackets breaking. All damage was due to ground impact.
3. Base Cover - The base cover had two very minor dents due to ground impact.
4. Parachute Truss - No visual damage.
5. Equipment Team - No visual damage.
6. Load Bar Support Structure - No visual damage.

E. Propulsion, Azimuth Pointing and Ordnance Subsystems

The main propulsive system on the AV-2 vehicle was the 2 Rocketdyne solid rocket motors. These motors have classified performance characteristics and therefore their specific performance parameters will not be given. Solid rockets were also used to affect spin and despin of the vehicle to minimize the effect of the main rocket motor thrust vector to center of gravity misalignment. In addition to the solid rockets, a pyrotechnic ordnance was used to effect load bar separation, aeroshell separation, and camera lens cover opening. Cold gas thrusters located at the extremities of the AFCRL load bar were commanded from the ground through the command receivers onboard the vehicle. The flight performance of these subsystems will be discussed in this section.

1. Spin/Despin Motor Performance

The spin-up command generated by the onboard programmers 1.01 seconds after drop from the load bar, caused ignition of the 6 spin motors with no noticeable delay between motors. The spin rate generated was 219 degrees per second. This was 5.5% higher than predicted. The 4 despin rocket motors were ignited at 33.23 seconds and produced an incremental rate of 177 degrees/second. This was 3.5% higher than predicted. This higher performance is probably due to the plume over expanding and recirculating to produce a pressure force on the spin/despin motor bracket. The base cover near the spin motors showed some evidence of plume impingement on both the spinup and despin side.

2. Main Propulsion System

The two solid rocket motors were ignited 2.04 seconds after release from the load bar and showed no noticeable time delay between their thrust

buildup. The motors burned normally with little differential thrust and nominal total impulse. The burnout transient was smooth and produced negligible disturbance to the vehicle. Thrust damping of the motors was as predicted.

3. Azimuth Pointing Subsystem

The azimuth pointing system performed as required during flight, however shortly after T/M was acquired, the pointing pressure began to decrease. It was soon evident that there would not be sufficient pressure for pointing operations by the time the balloon reached the range. The system was therefore pulsed for 3 seconds in both directions in an attempt to stop this potentially catastrophic condition. This procedure successfully stopped most of the leakage rate after the pressure had decayed from 2070 psi to 1150 psi, midway through the flight (see Figure IV-3). When pointing operations were commenced, the available pressure for pointing had decayed to 1050 psi of which only 275 psi were required. The azimuth hold time was reduced to 3 minutes from the normal 10 minutes allowed on the previous flights both due to this low pressure and because of the experience gained on the previous flights. During ascent, the wind shears and main balloon inflating produced erratic torques to the load bar which resulted in rotational amplitudes up to 3.5 revolutions, peak-to-peak. The zero torque azimuth also varied (see Figure VI-25). Ballasting continued until 54 minutes prior to drop at which time the remaining ballast was 561 lbs. The natural damping of the system reduced the oscillations such that when the float altitude was reached, the oscillation amplitude was 410 degrees peak-to-peak. The torsional stiffness of the recovery parachute system, based on the period of oscillation, agreed well with the torsional

test measurements used for design, except during periods of ballasting, (see Figure VI-26). The oscillating amplitude decay once float altitude was reached, exhibited a damping ratio of 0.12 per cycle which is close to the predicted value of 0.1 used in design. The zero azimuth varied little during float and while the azimuth was being maintained and no difficulty was encountered with holding the proper drop azimuth within ± 2 degrees. The thrusters exhibited 12.5 ft-lb torque which was more than sufficient to counter the 1.4 ft-lb of torque generated by the 75 degrees of windup. The pointing pressure supply was consumed at a rate of 7.1 psi/sec of jet on time and the residual supply pressure was 800 psi. The last command was terminated 7.0 seconds before drop with maximum rates less than 0.2 degrees/second. The effect of pointing commands on the roll and yaw gyros can be seen in the gyro data shown in Figure VI-3 and was taken into account when the biases were evaluated.

During the flight, the magnetometer data stream from T/M through the real time computer was lost for about 10 minutes. The probable cause is a loss of synchronization between the T/M data and the real time computer. This problem was quickly corrected and adequate displays of magnetometer data were available for steering the vehicle to the required heading.

4. Ordnance Subsystem

All pyrotechnic and pyromechanical devices performed properly as programmed. Post-flight inspection revealed that all ordnance functions occurred with no damage to the flight vehicle.

F. Electrical Subsystem

The electrical power and sequencing systems operated satisfactorily during the complete mission. All battery voltages and timed events remained within predicted/required limits.

Flight batteries were activated on 7-20-72 without problems. Battery voltages were above minimum at launch and as shown in Table VI-3 during this flight.

Camera batteries operated satisfactorily as evidenced by "on-board" camera operation during flight sequence.

The actual programmer sequence times are provided in Table IV-1.

The vehicle command system operated as required and received the following commands subsequent to the 14:02:42 hours Z.

<u>TIME</u>	<u>COMMAND</u>
14:59 Hours Z	SAFE/SAFE B/U Command Check
16:49 Hours Z	Arm Vehicle
16:50 Hours Z	Power Programmers/Start Azimuth Pointing
16:55 Hours Z	Drop
16:56 Hours Z	Mortar Fire Command

G. Instrumentation Subsystem

All instrumentation hardware operated properly during the various phases of the flight.

The excessive noise which was present on some continuous channels during the flight of vehicle AV-1 was not present during the flight of vehicle AV-2. The elimination of this noise is attributed to the decrease in the transmitter deviation and adjustment of the SCO pre-emphasis taper.

H. RF Subsystem

The airborne S-Band telemetry, C-Band tracking and command control RF subsystems performed without malfunction throughout the flight.

Command system ground station checkouts were performed at Launch - 3 hours. All command transmitters were monitored at the J-67 site for center frequency, single tone deviation and triple tone execution of commands. The C-station command system checkouts were satisfactory, however the North Oscura Peak transmitter "A" experienced a failure which required 45 minutes to troubleshoot and return to operation. Consequently, the Test Conductor requested that transmitter "B" at NOP be identified as the primary NOP transmitter for the mission.

Telemetry data was monitored throughout the flight at J-67. The J-67 telemetry station personnel expressed the opinion that pre-emphasis taper was very much improved over the previous mission (AV-1).

I. TSE/OSE

The Test Support equipment and Operational Support equipment performed within the design requirements for this equipment.

At the time of vehicle connect to the van, an electrical short appeared on the instrumentation system test power meter located in the TSE Van. The electrical umbilical - E61 and the electrical power umbilical - E31 were disconnected from the vehicle and the van for inspection. When the cables were reconnected, one at a time, there was no short. Post Launch investigation of this anomaly produced a slight cut in the E31 umbilical. The umbilical was repaired prior to the next launch (AV-4).

The OSE command reception indicator panel indicated false command tones and commands during the early portion of the float phase. These were not faults in the CRIP but rather TM dropouts at the WSMR receivers which drove the CRIP to false indications.

J. Mass Properties

The BLDT vehicle mass property requirements, at decelerator mortar fire, were established based on the Viking Lander Capsule, to be as follows:

Vehicle Weight	-	$1888 \pm 12\#$
Y Axis Cg Location	-	0 OFFSET
Z Axis Cg Location	-	$-1.41 \pm 0.030"$ OFFSET
*X Axis Cg Location	-	31.7" to 33.7"

In order to fulfill the Y and Z axis cg location requirement, the AV-2 vehicle was subject to a spin balance operation at Sandia Corporation Laboratories, Albuquerque, New Mexico. During this operation, lead balance weights were fastened to the vehicle to precisely locate the vehicle cg with respect to the Y and Z axis.

The AV-2 vehicle mass properties are summarized in Table VI-4.

* Referenced to Aeroshell Theoretical Apex

TABLE VI-1

BLDT AV-2 ATMOSPHERIC PROPERTIES

<u>ALTITUDE</u> <u>(5000 FT)</u>	<u>EAST-WEST</u> <u>WIND</u> <u>(FT/SEC)</u>	<u>NORTH-SOUTH</u> <u>WIND</u> <u>(FT/SEC)</u>	<u>SPEED</u> <u>OF SOUND</u> <u>(FT/SEC)</u>	<u>DENSITY</u> <u>(SLUGS/FT³)</u>
1	2.	13.	1139.	.19173-2
2	-1.	3.	1117.	.16709-3
3	-8.	1.	1094.	.14501-2
4	-4.	4.	1075.	.12389-2
5	4.	-3.	1056.	.10554-2
6	-11.	-6.	1034.	.89529-3
7	-12.	7.	1008.	.75888-3
8	1.	4.	972.	.64925-3
9	-10.	1.	953.	.52992-3
10	-12.	-1.	934.	.42979-3
11	-10.	-2.	939.	.32909-3
12	-23.	8.	947.	.25147-3
13	-25.	6.	959.	.19152-3
14	-41.	2.	970.	.14766-3
15	-45.	4.	975.	.11506-3
16	-53.	2.	977.	.90810-4
17	-66.	2.	988.	.70551-4
18	-77.	8.	985.	.56423-4
19	-92.	5.	996.	.43916-4
20	-108.	26	1010.	.34232-4
21	-76.	17.	1008.	.27561-4
22	-90.	4.	1019.	.21719-4
23	-100.	18.	1021.	.17478-4
24	-103.	15.	1018.	.14175-4
25	-127.	2.	1028.	.11247-4
26	-144.	-5.	1043.	.88716-5
27	-151.	6.	1053.	.71098-5
28	-167.	-9.	1070.	.56559-5
29	-176.	-1.	1075.	.46139-5
30	-132.	-9.	1080.	.37786-5
31	-149.	37.	1082.	.31113-5
32	-180.	-4.	1084.	.26558-5
33	-186.	10.	1081.	.21363-5
34	-185.	11.	1077.	.17769-5
35	-203.	51.	1074.	.14755-5
36	-183.	46.	1066.	.12358-5

TABLE VI-2
STATE VECTOR DATA

BLDT AV-2

	<u>DROP</u>	<u>MORTAR FIRE</u>	<u>PEAK LOAD</u>
Time (t) - sec	00	38.2	39.8
Altitude (h) - ft	120900	135368	135731
Velocity (V) - ft/sec	--	1194.	1140.
Gamma (r) - deg	--	12.5	10.13
PSI () - deg.	210.4	-169.8	-173.57
Theta () - deg.	65°	6.94	7.14
Mach No. (MN)	--	1.133	1.080
Dynamic Pressure (q) - lb-ft ²	--	5.00	4.48
Angle of Attack () - deg.	--	+5.4	-3.1
Sideslip () - deg.	--	-4.9	-1.2
Total Angle of Attack () - deg.	--	7.28	3.27
Spin (p) - deg/sec.	--	62.	62.

TABLE VI-3
BATTERY PERFORMANCE DATA

	<u>MAIN BATTERY</u>	<u>TRANS. BATTERY</u>	<u>PYRO A BATTERY</u>	<u>PYRO B BATTERY</u>	<u>CAMERA BATTERY POSITIVE</u>	<u>CAMERA BATTERY NEGATIVE</u>
1. Activation Voltage						
a. Open Circuit	30.48	33.11	36.54	36.43	16.42	-16.48
b. 5 Second Load*	29.3	27.1	29.1	29.2	13.05	-13.05
2. Prelaunch Voltage						
No Load	30.52	32.96	33.06	32.17	16.81	-16.74
3. Float Voltage						
Drop - 2 hours	29.3	27.6	33.9	32.8	NO TM	NO TM
Drop - 1 hour	29.2	27.6	33.7	32.7	DATA	DATA
Drop - 1 minute	29.3	27.6	31.0	30.9		
4. Flight Voltages						
T + 1 minute	29.3	27.6	30.5	30.5		
T + 6 minutes	29.4	27.8	30.4	30.4		
5. Main Battery Amps.	3-6 amps					

*5 Second Load Levels - 30 amps for main battery
10 amps for all others.

TABLE VI-4
FINAL BLDT MASS PROPERTIES, AV-2

Condition	Weight (lb)	Center of Gravity (Vehicle Sta.)			Moment & Product of Inertia (Slug Ft ²)					
		X	Y	Z	I _{xx}	I _{yy}	I _{zz}	P _{xy}	P _{xz}	P _{yz}
On Load Bar	2838									
At Drop	2634	37.45	0	-1.41	505	414	369	.34	1.09	26.2
At Mortar Fire	1897	36.73	0	-1.41	435	341	331	.36	1.09	-.18
With Decelerator Deployed	1802	35.56	0	-1.41	434	329	319	.41	1.09	-.18
With Decelerator Deployed and Aeroshell Dropped	1445	39.10	0	-1.76	256	219	209	.56	3.12	-.52
Aeroshell	357	21.24	.24	.16	91	91	91			

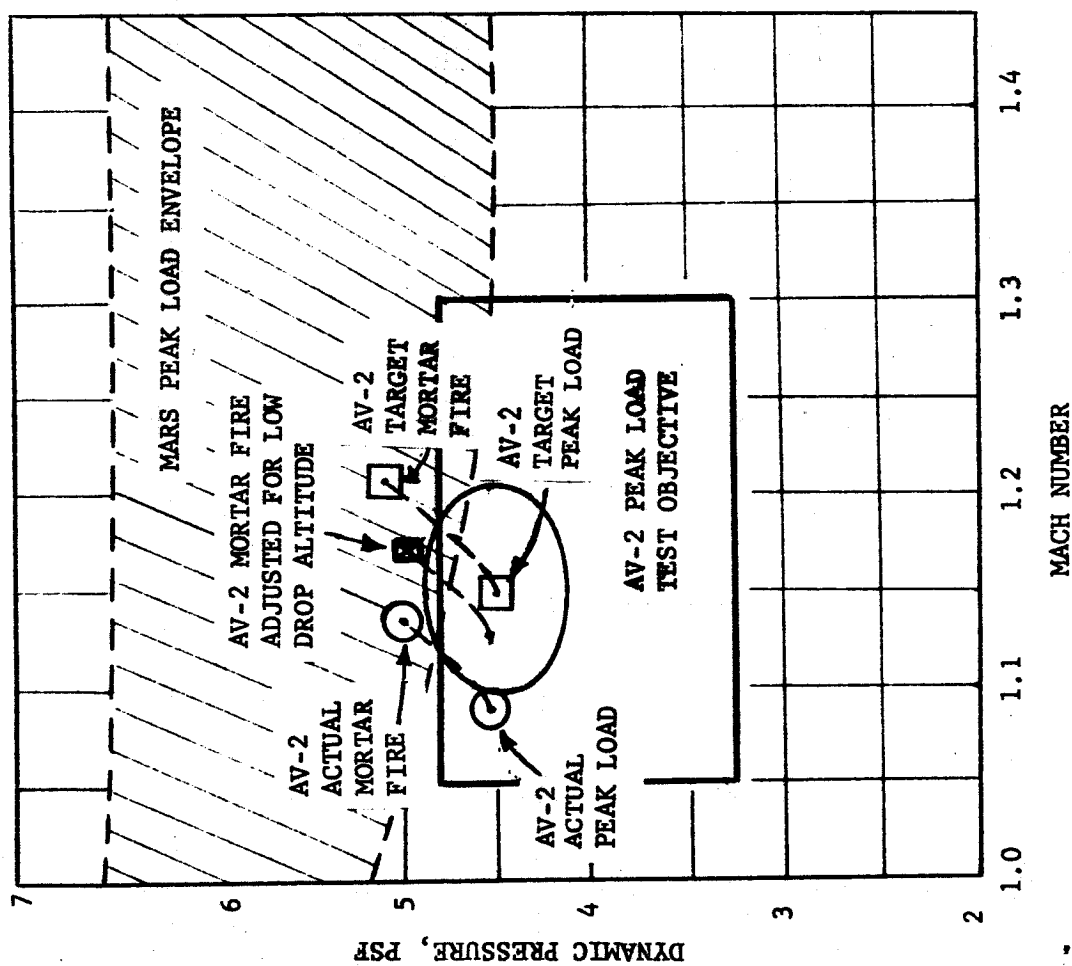
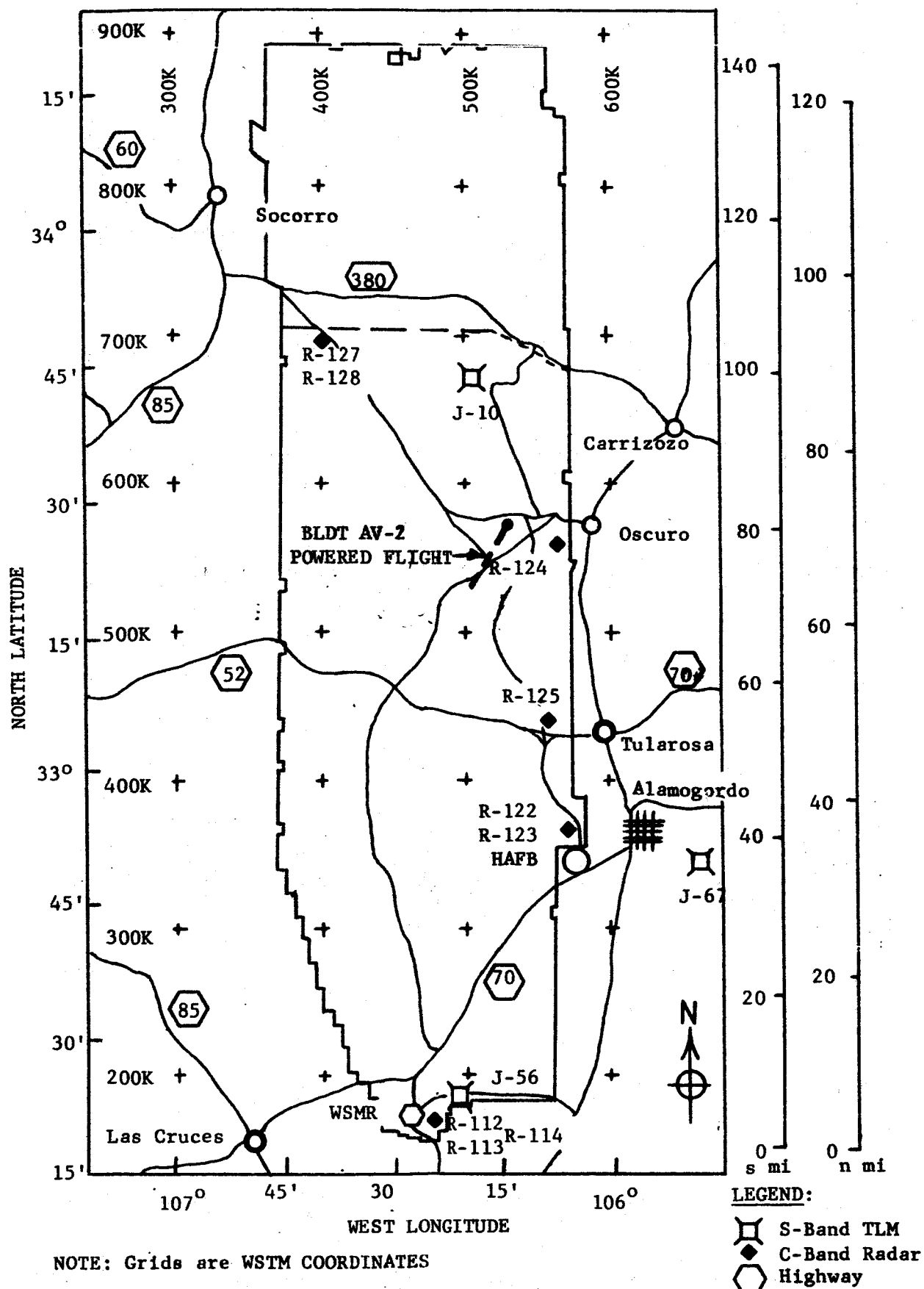
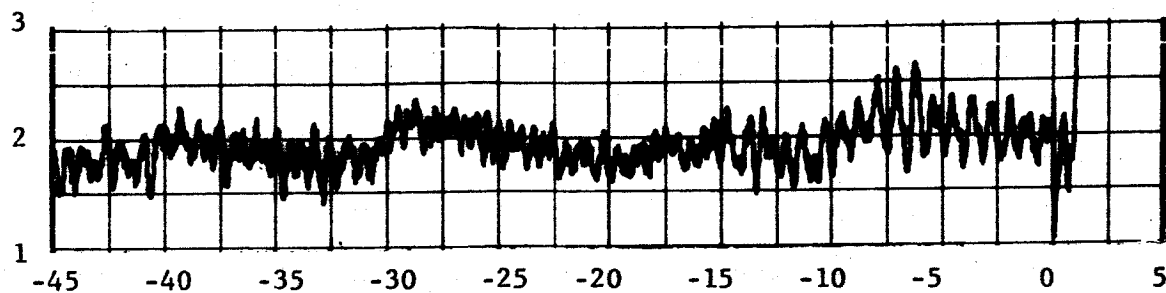


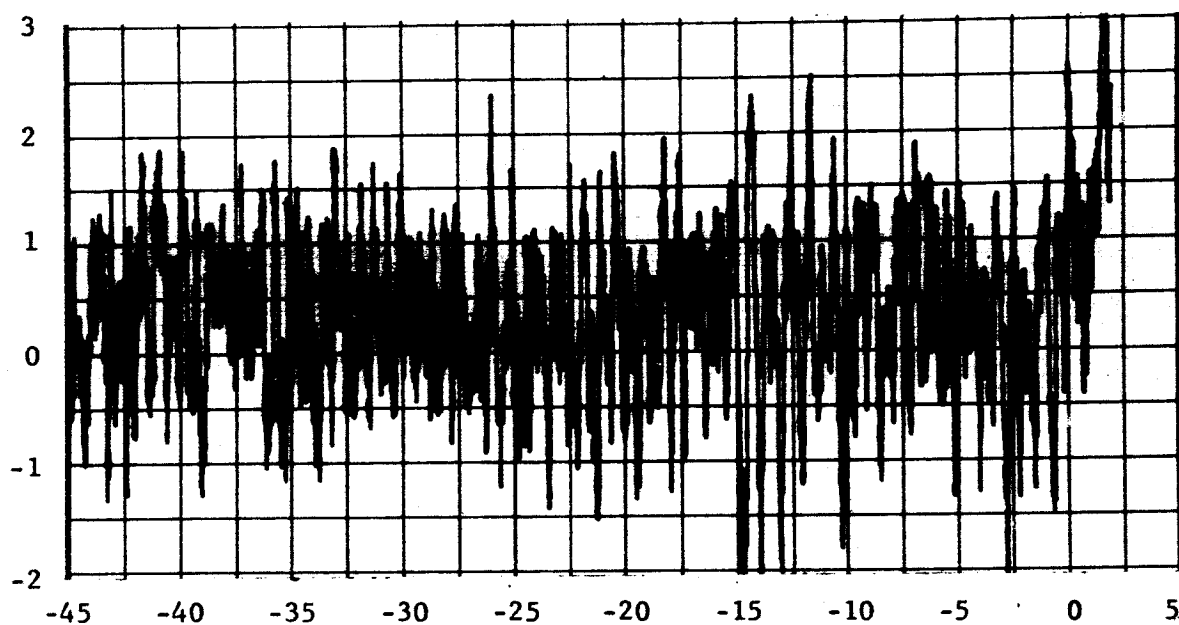
FIGURE VI-1 BLDT AV-2 TEST CONDITIONS



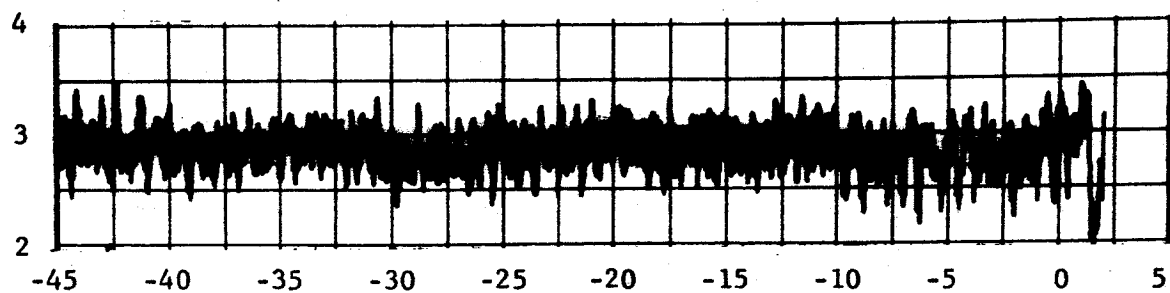
SPIN RATE (P) DEG/SEC



PITCH RATE (Q) DEG/SEC



YAW RATE (R) DEG/SEC



FLIGHT TIME - SECONDS

FIGURE VI-3 GYRO DATA PRIOR TO DROP

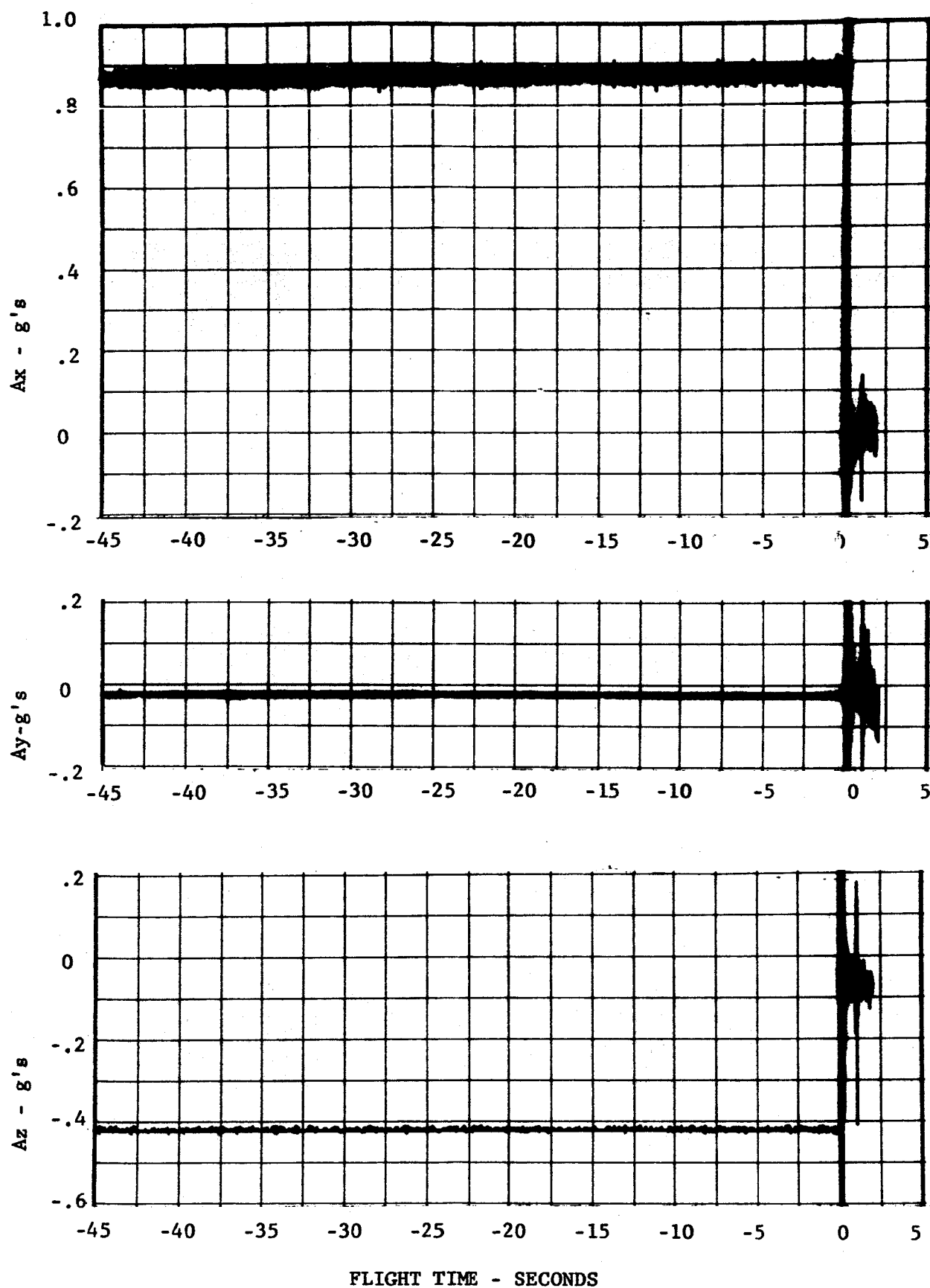


FIGURE VI-4 ACCELEROMETER DATA PRIOR TO DROP

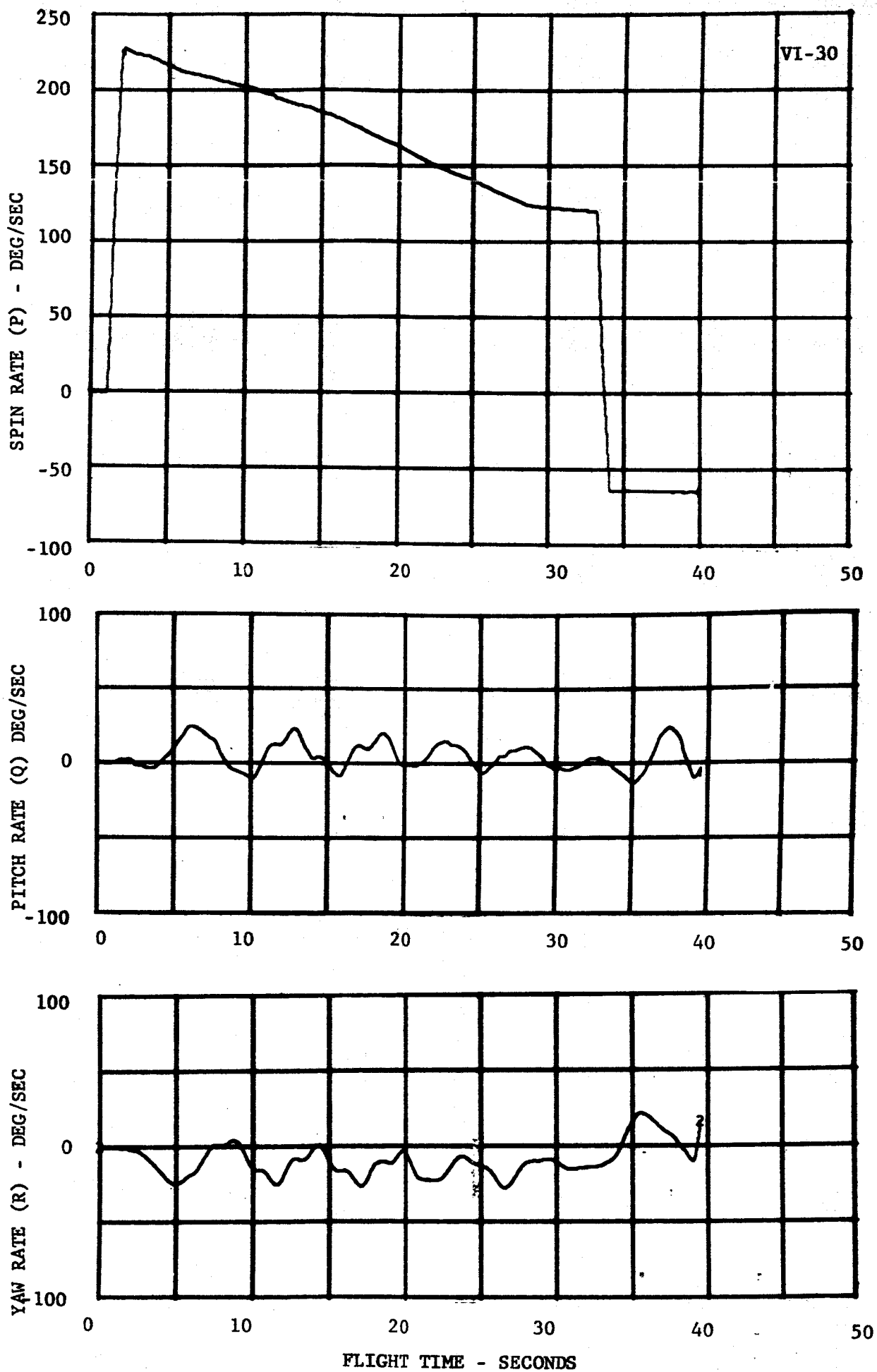
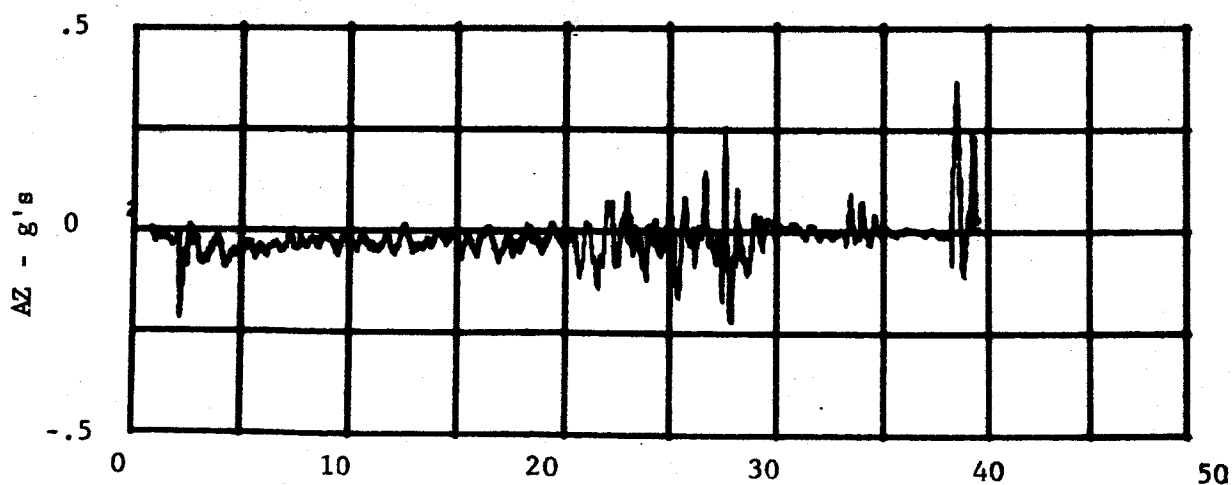
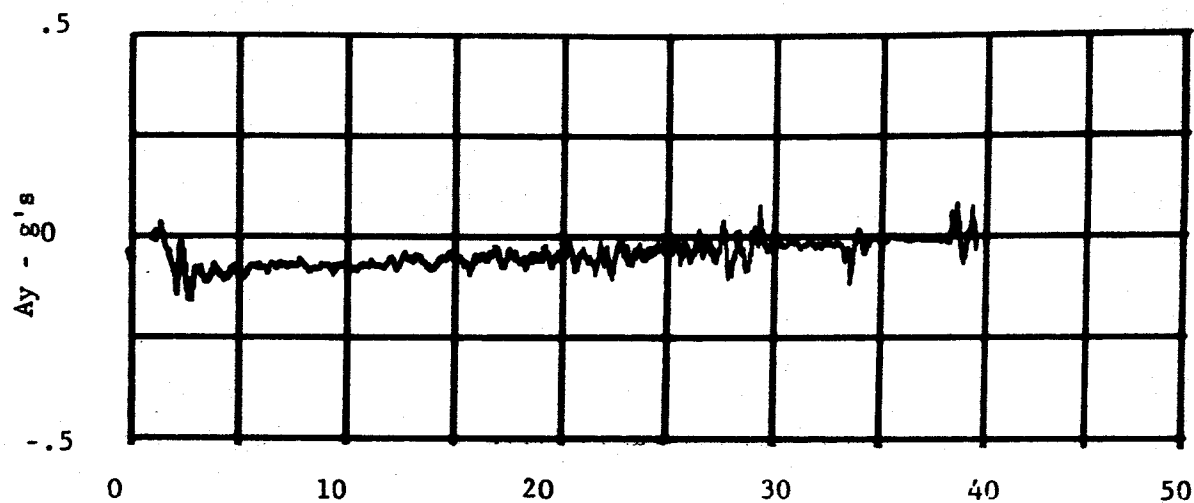
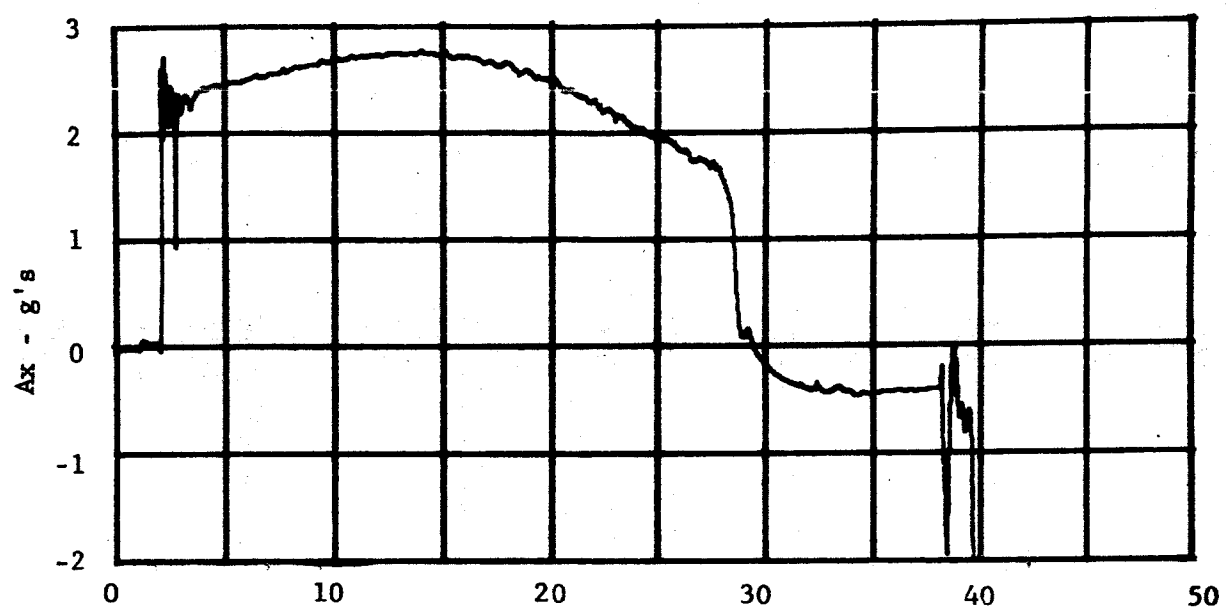


FIGURE VI-5 GYRO DATA DURING POWERED FLIGHT



FLIGHT TIME - SECONDS

FIGURE VI-6 ACCELEROMETER DATA DURING POWERED FLIGHT

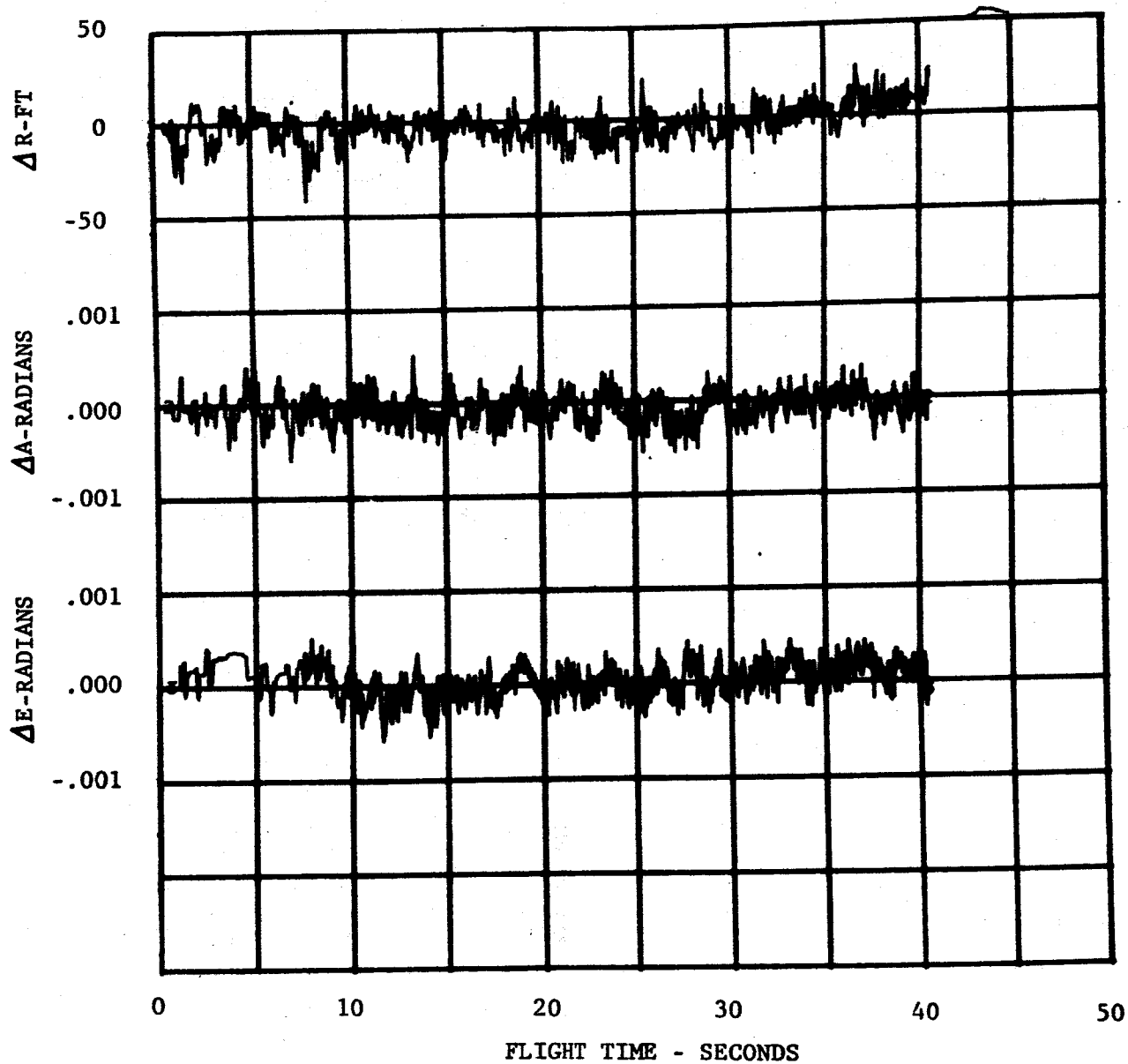


FIGURE VI-7 COMPARISON BETWEEN RADAR DATA (R125 TRANSFORMED TO R123)

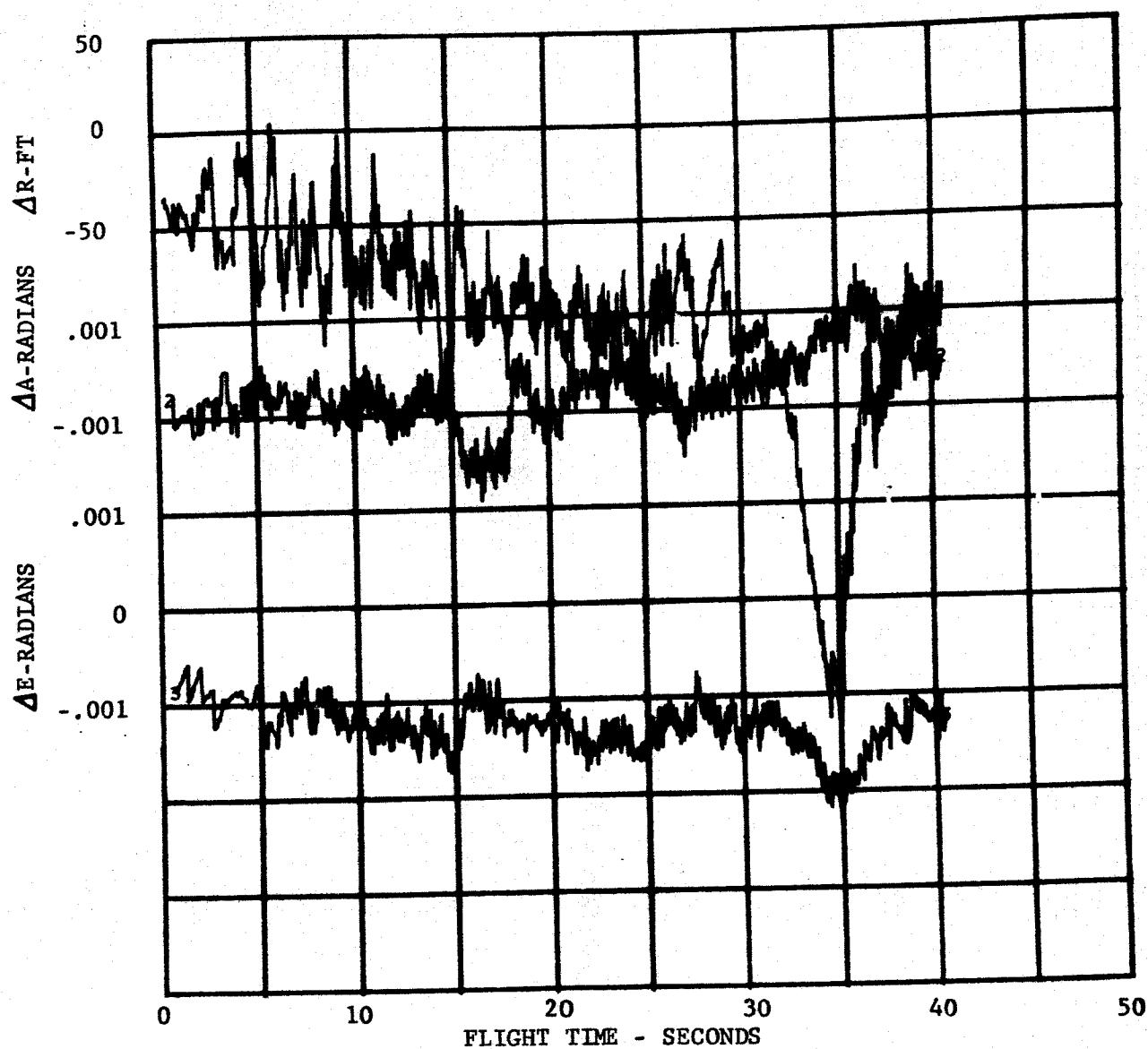


FIGURE VI-8 COMPARISON BETWEEN RADAR DATA (R128 TRANSFORMED TO R123)

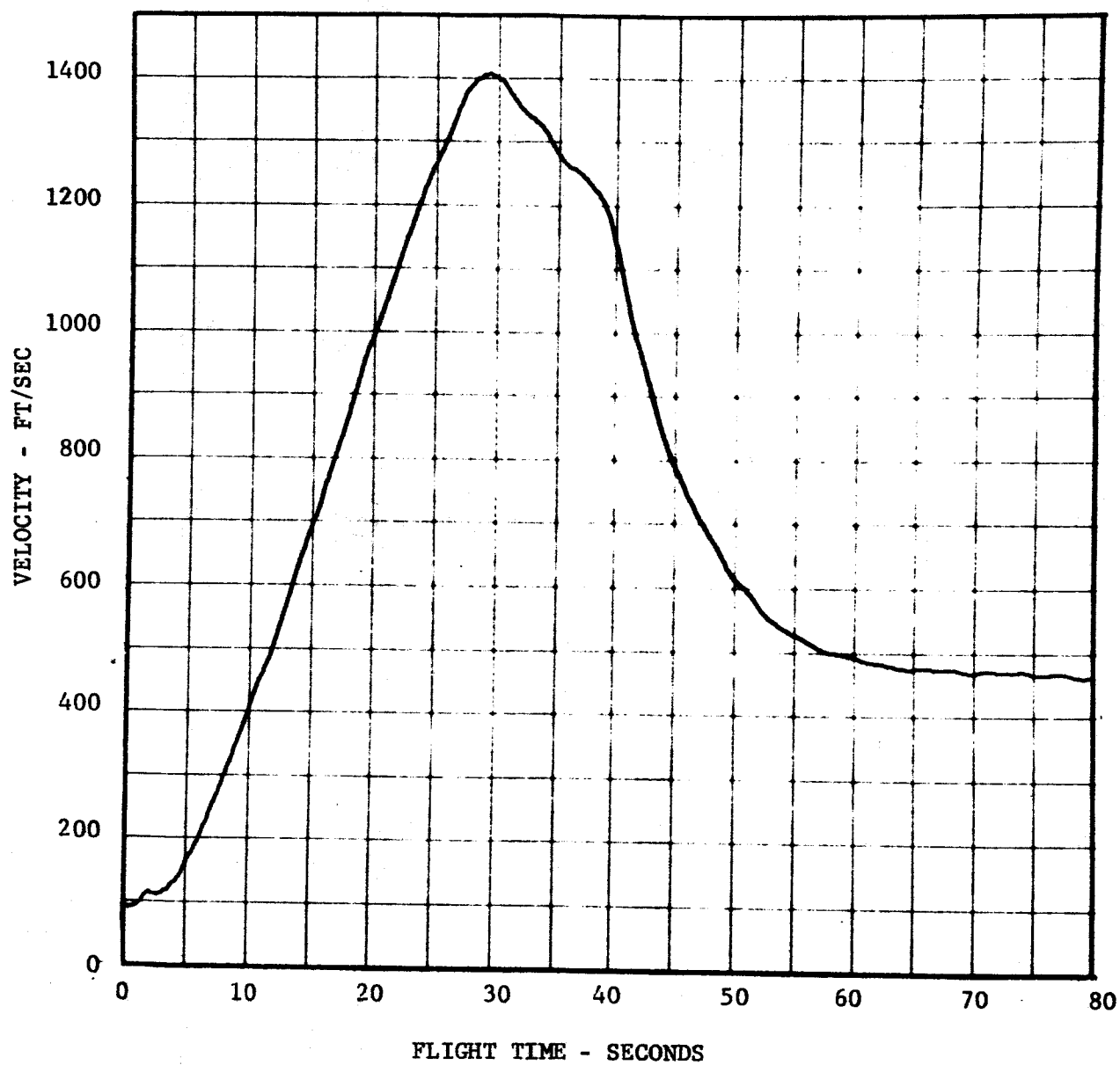


FIGURE VI-9 RADAR (R125) VELOCITY VS. FLIGHT TIME

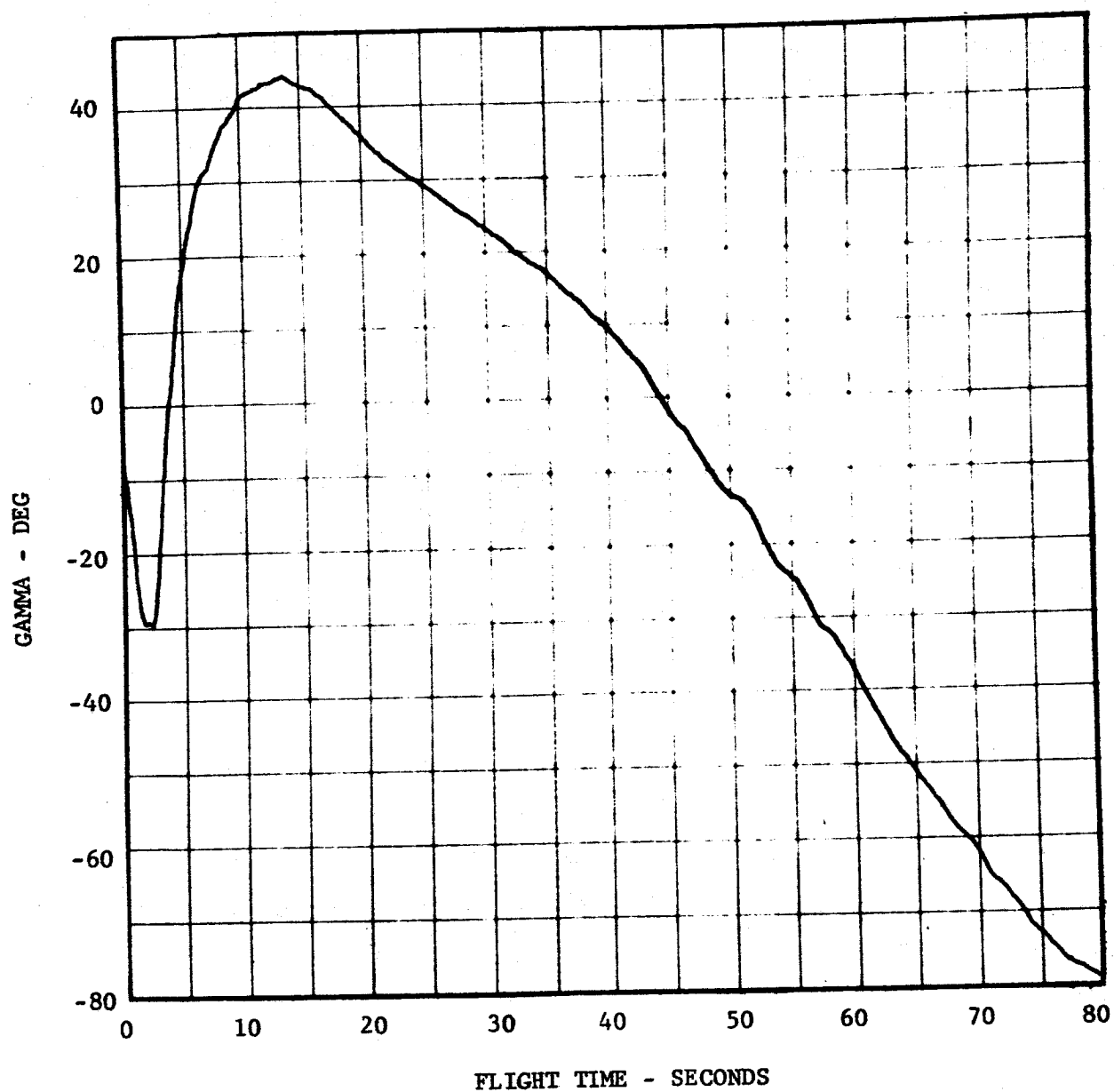


FIGURE VI-10 RADAR (R125) FLIGHT PATH ANGLE VS. FLIGHT TIME

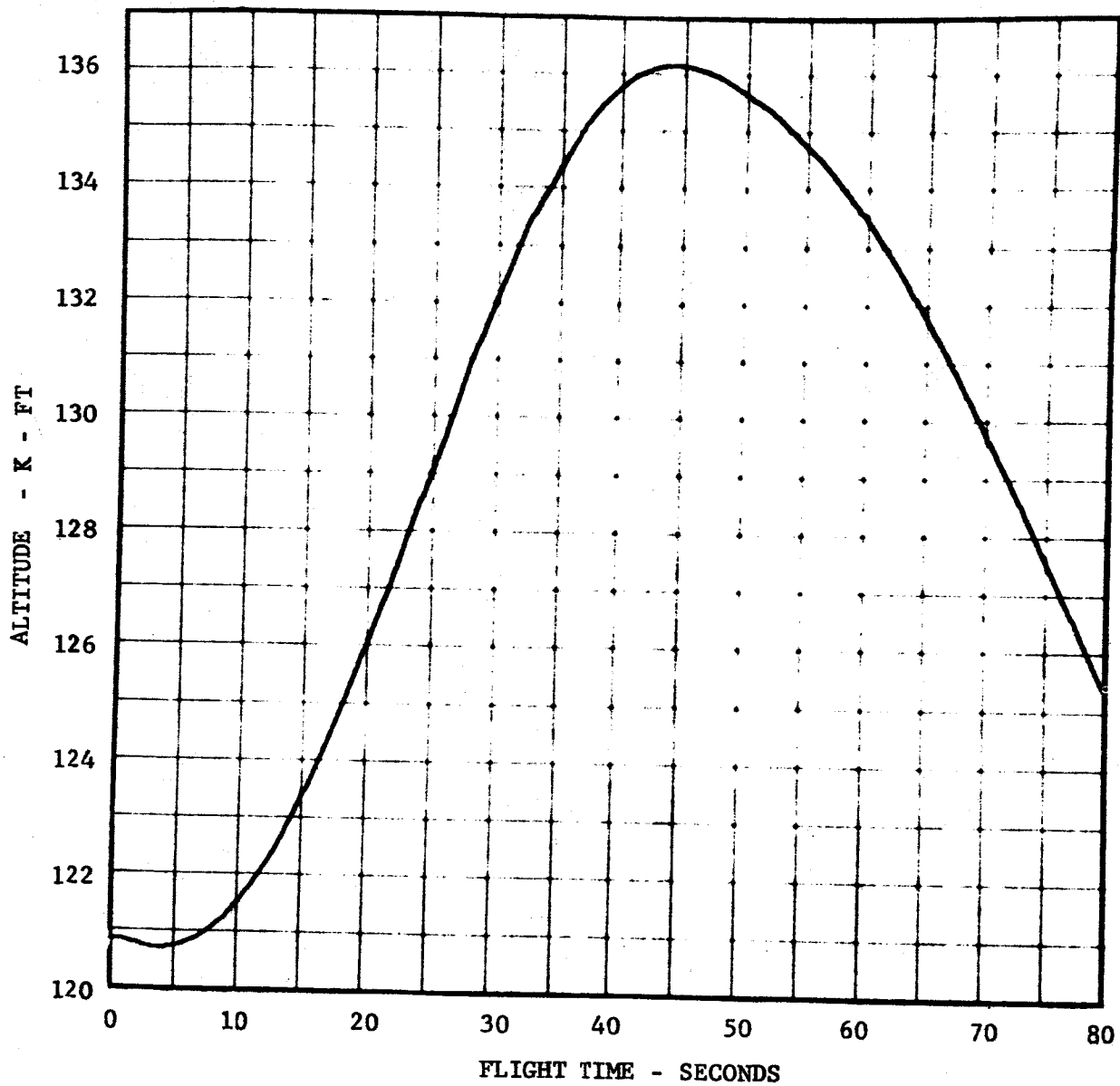


FIGURE VI-11 RADAR (R123) ALTITUDE (MSL) VS. FLIGHT TIME

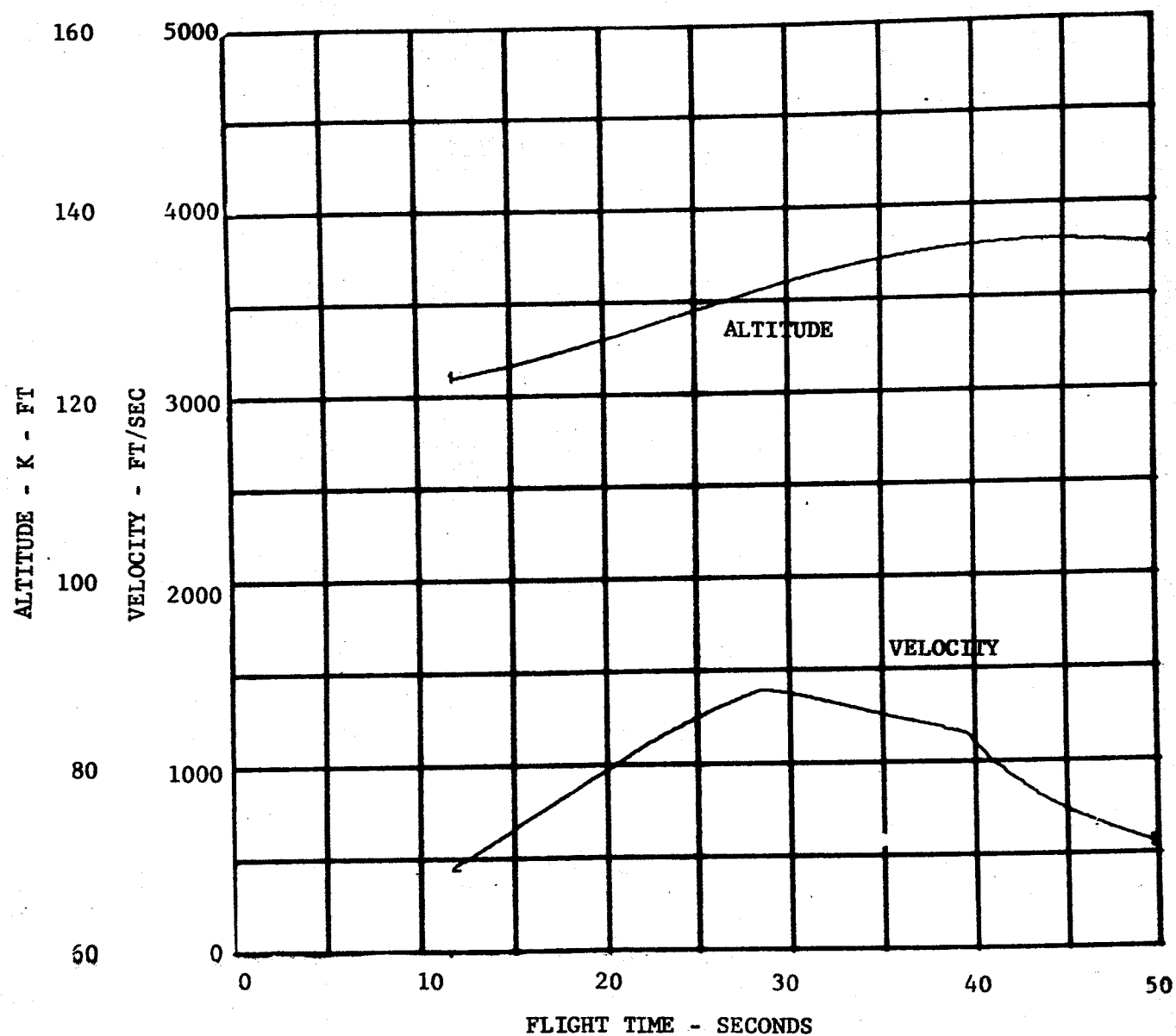


FIGURE VI-12 STEP TRAJECTORY RECONSTRUCTION OF ALTITUDE AND VELOCITY

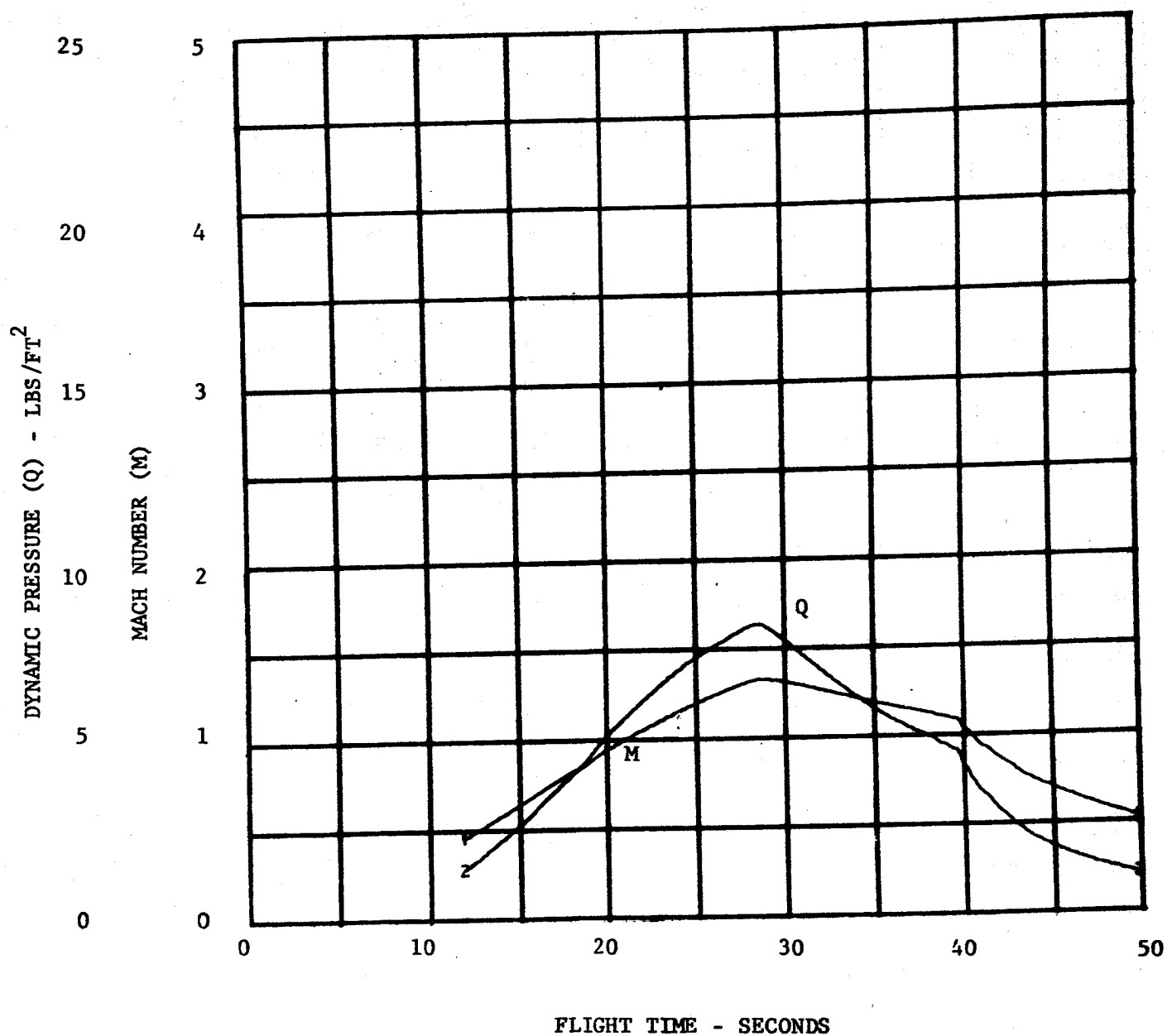


FIGURE VI-13 STEP TRAJECTORY RECONSTRUCTION OF
MACH NUMBER

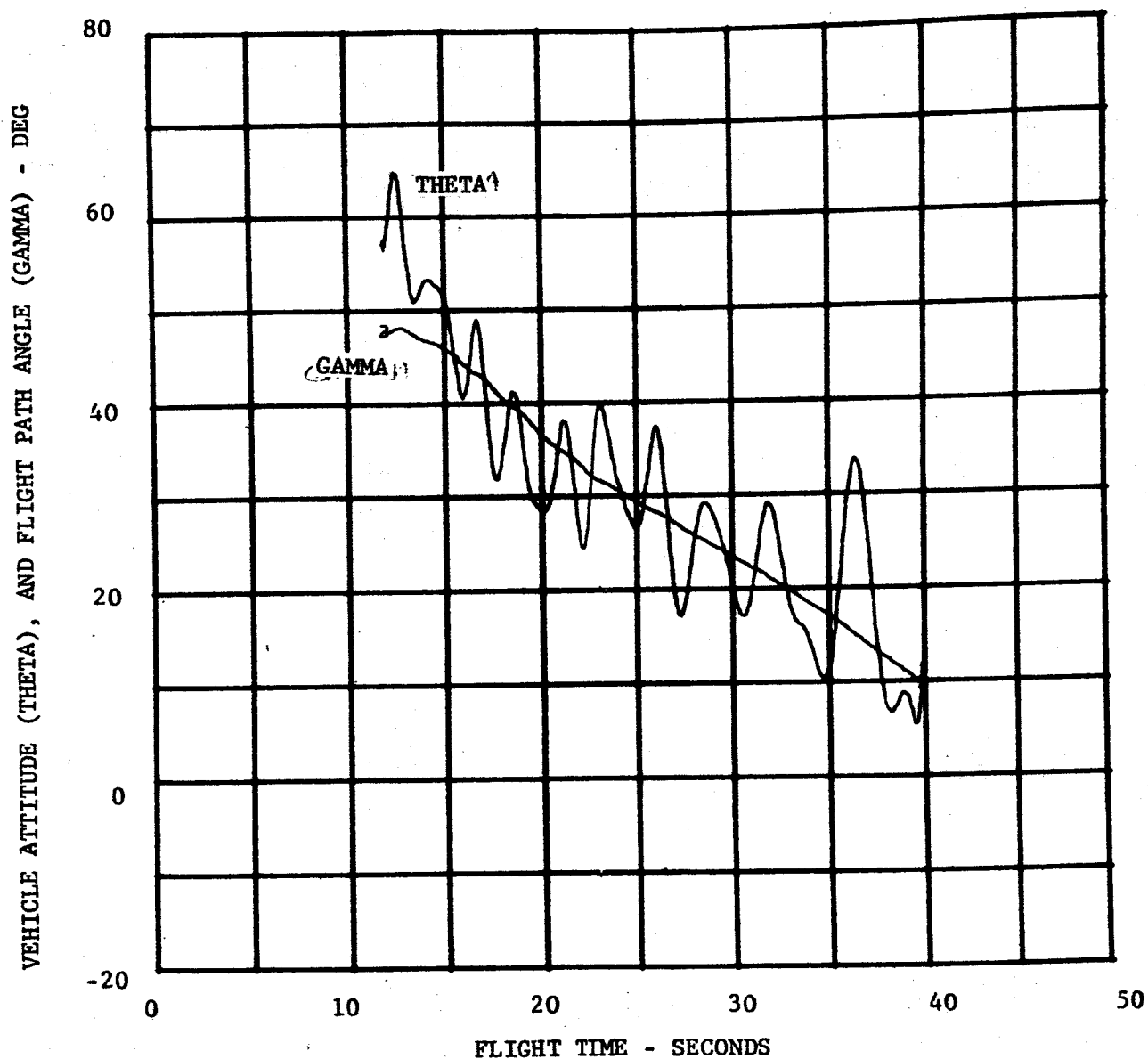


FIGURE VI-14 STEP TRAJECTORY RECONSTRUCTION OF VEHICLE ATTITUDE AND FLIGHT PATH ANGLE

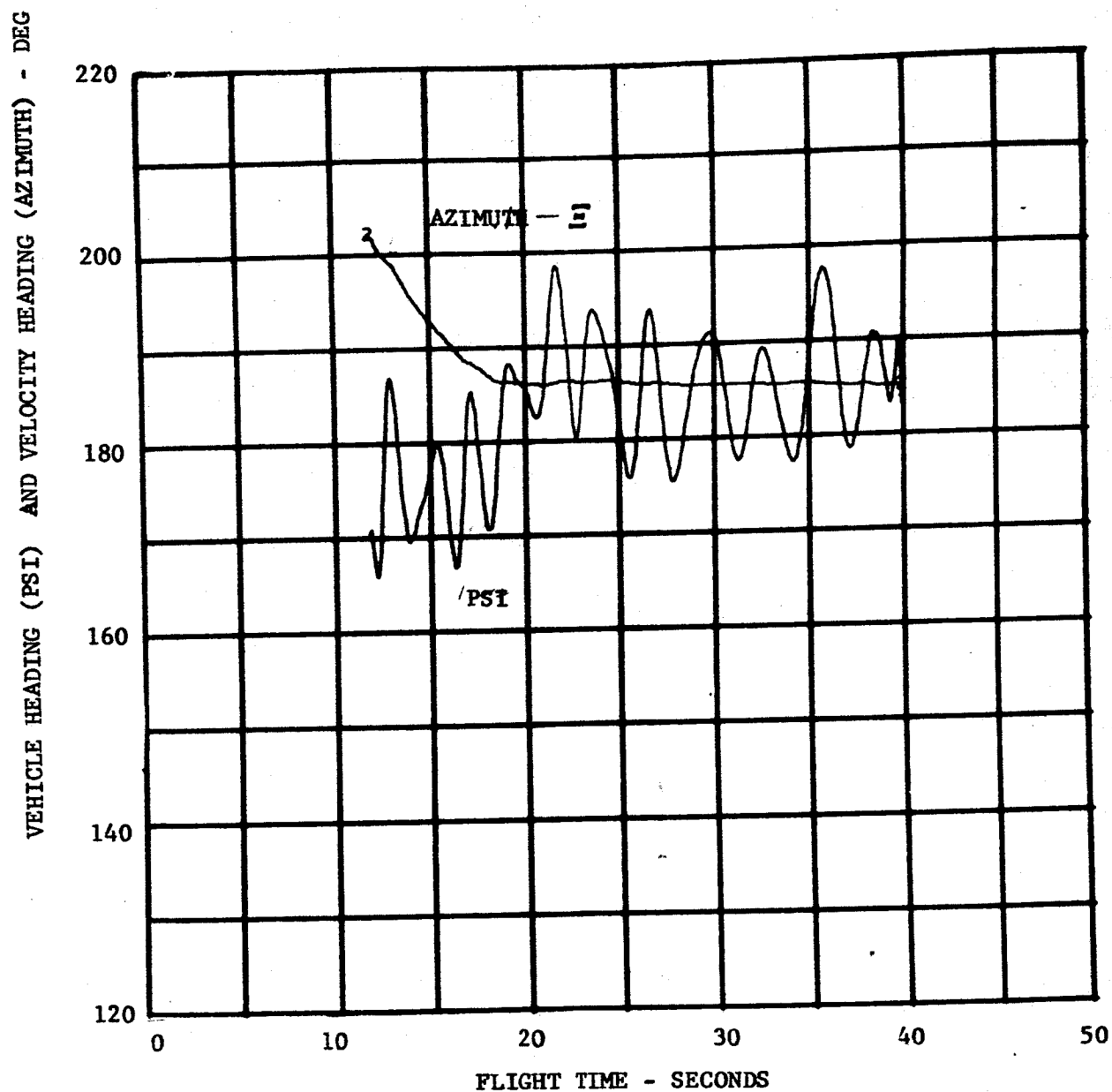


FIGURE VI-15 STEP TRAJECTORY RECONSTRUCTION
OF THE BODY HEADING AND
VELOCITY HEADING

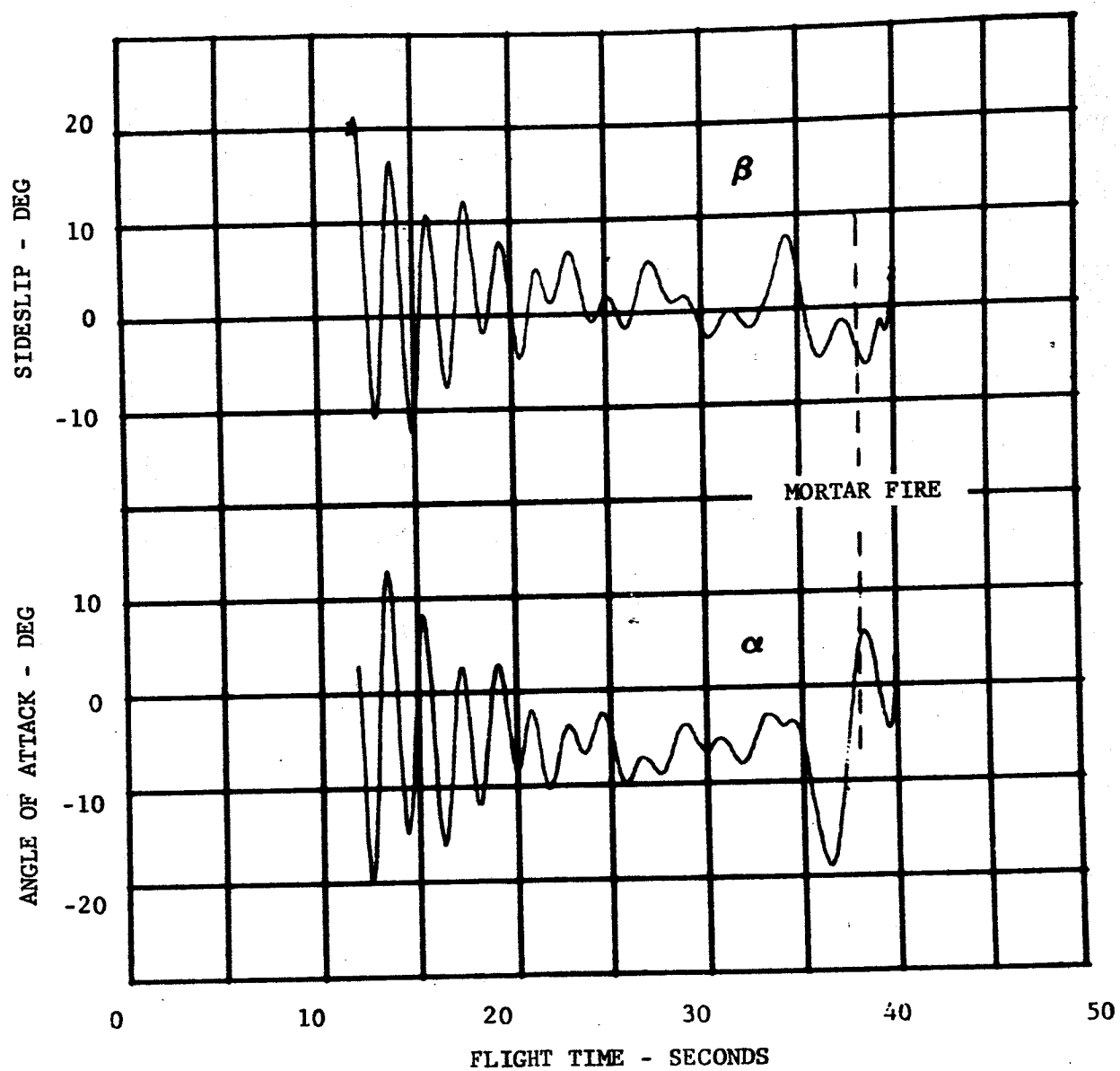


FIGURE VI-16 STEP TRAJECTORY RECONSTRUCTION OF ANGLE OF ATTACK AND SIDESLIP

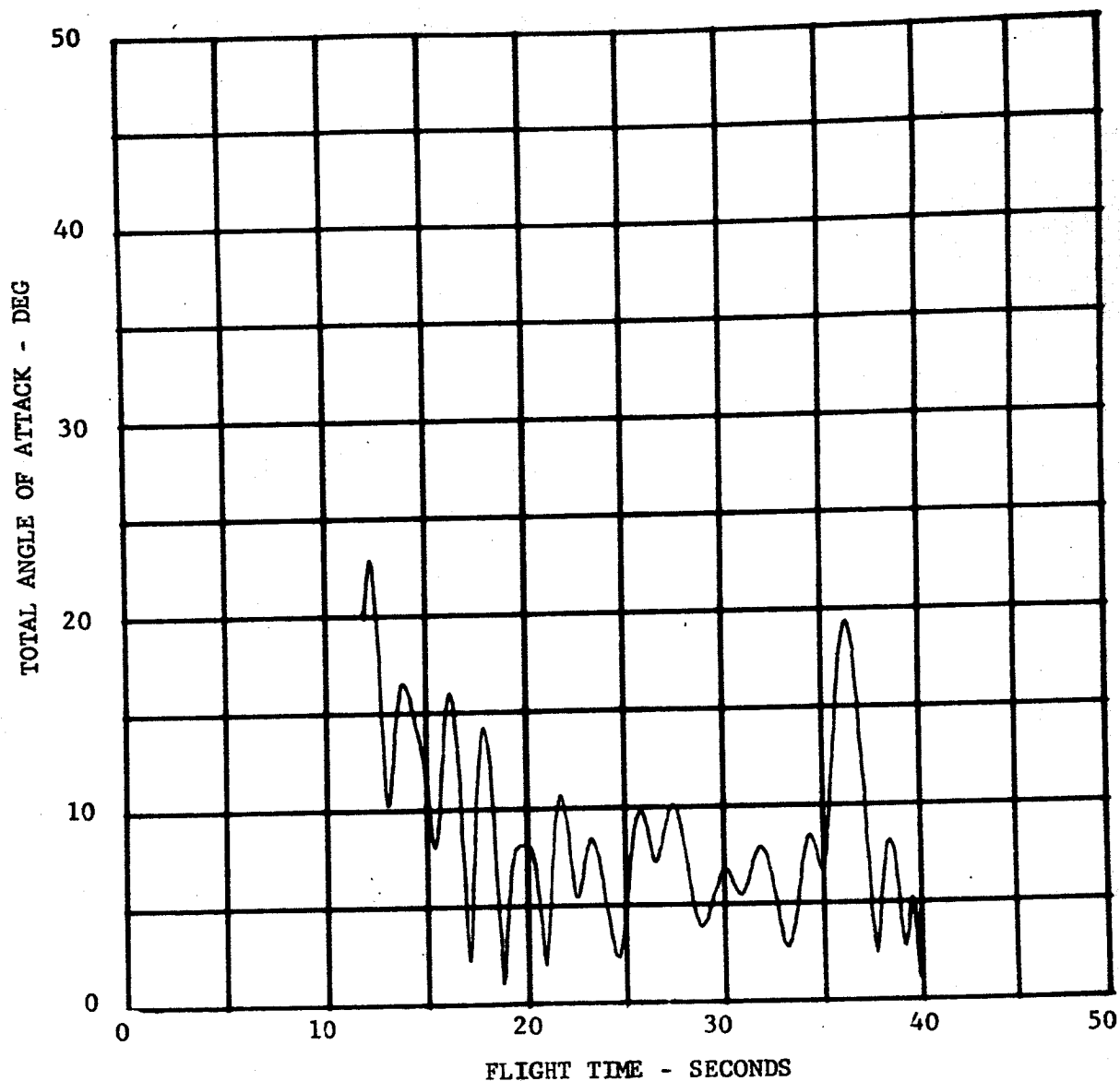


FIGURE VI-17 STEP TRAJECTORY RECONSTRUCTION OF TOTAL ANGLE OF ATTACK

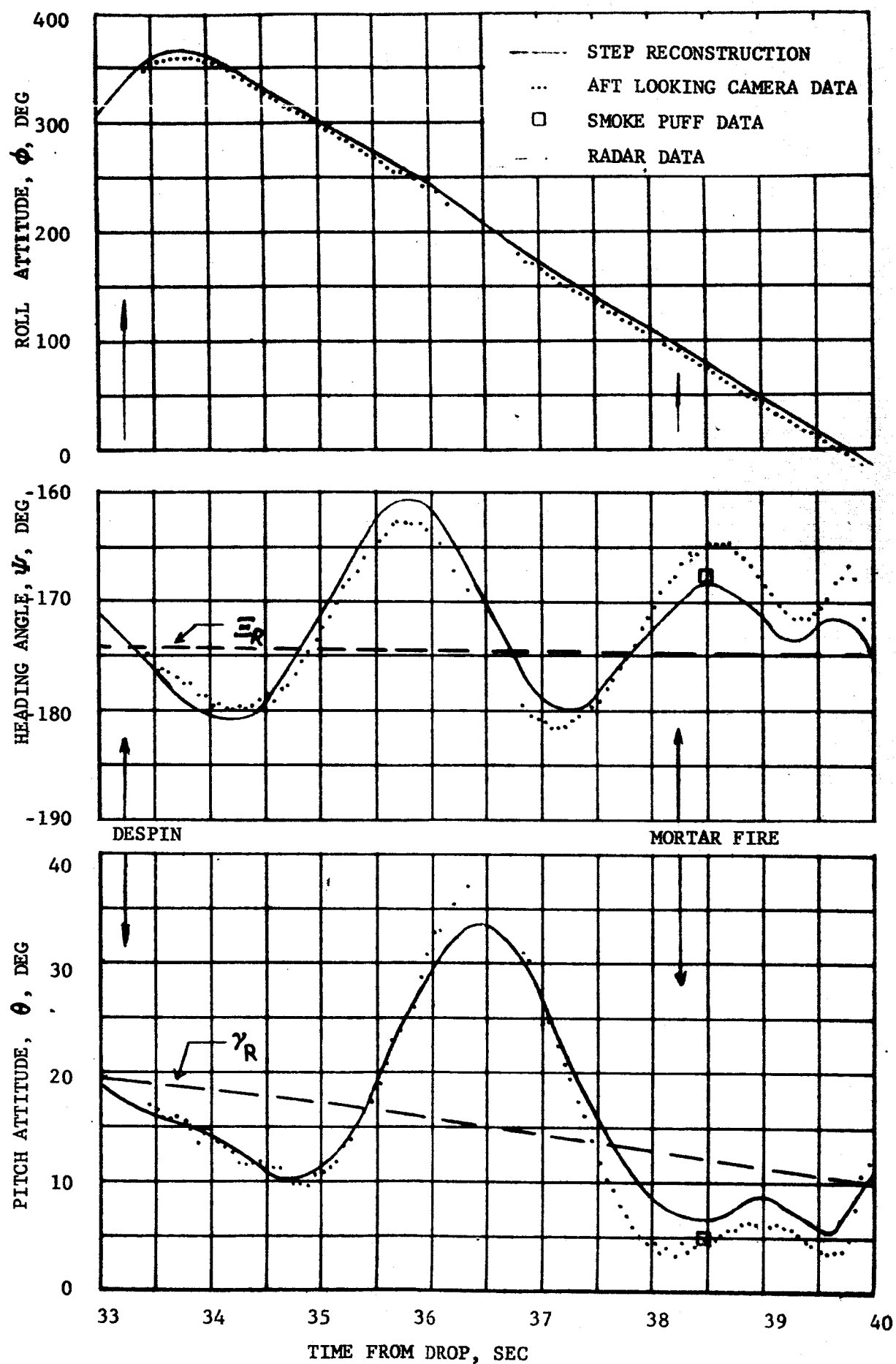


FIGURE VI-18 BODY ATTITUDES FROM AFT LOOKING CAMERA (MILLIKEN)

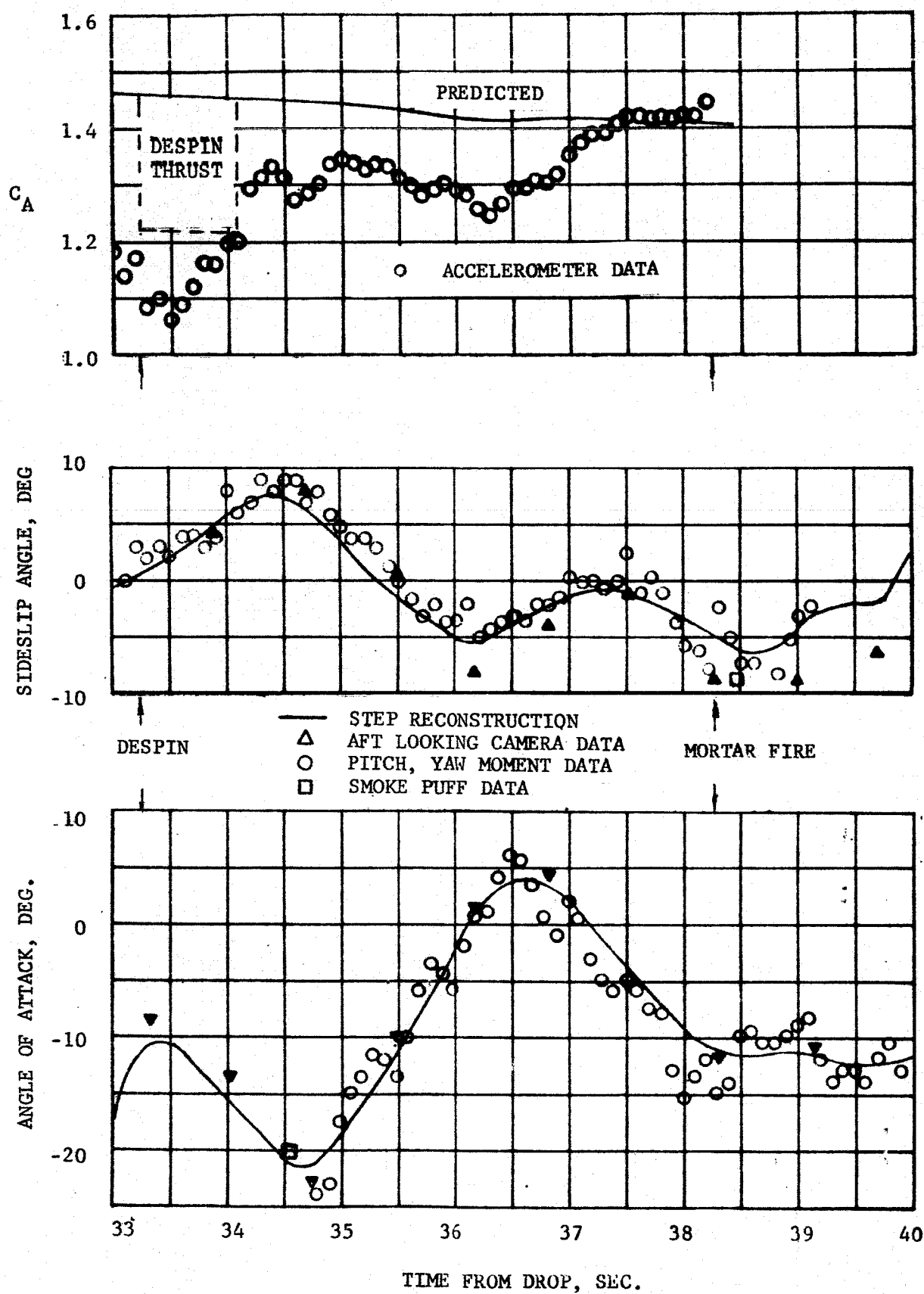
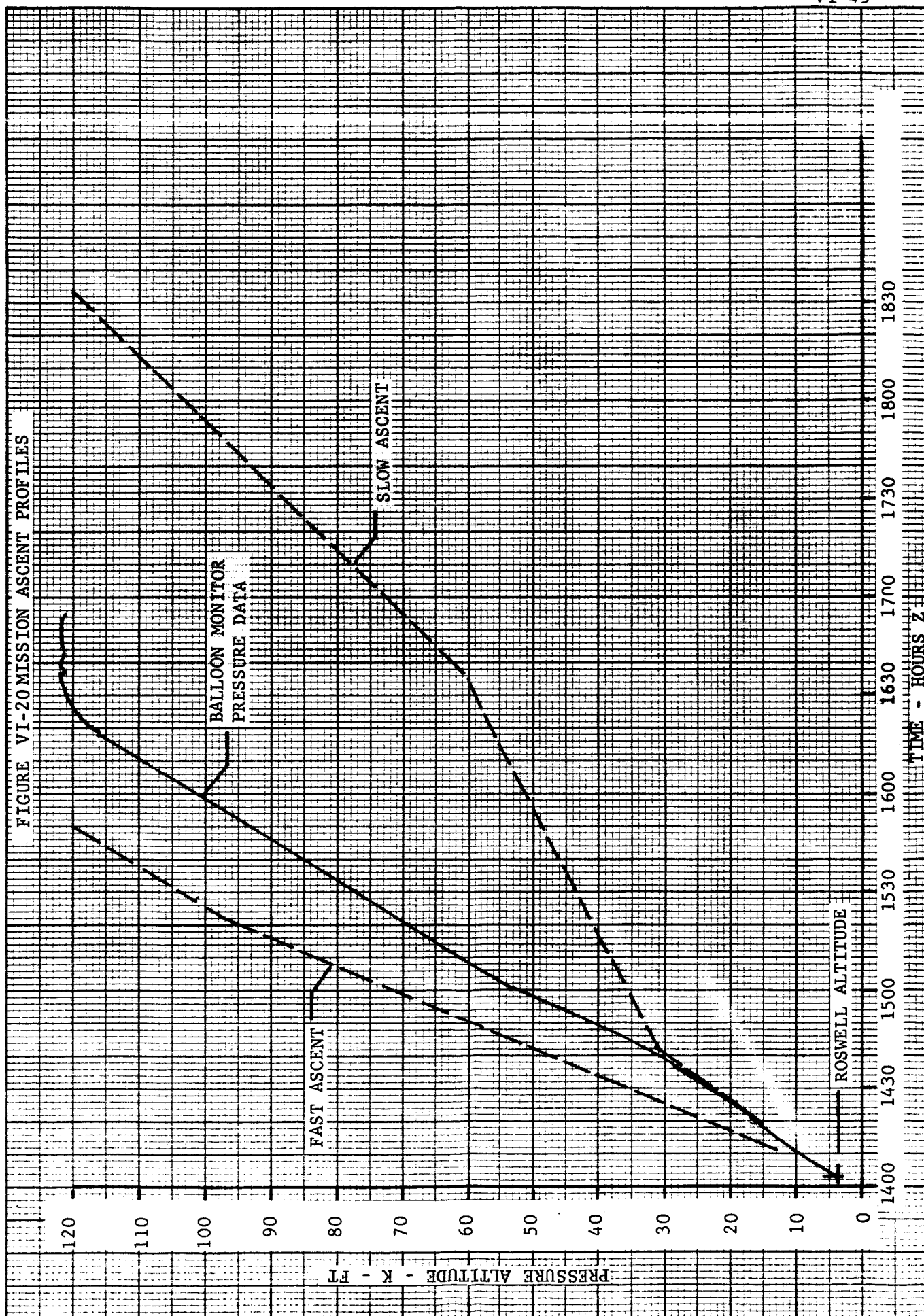
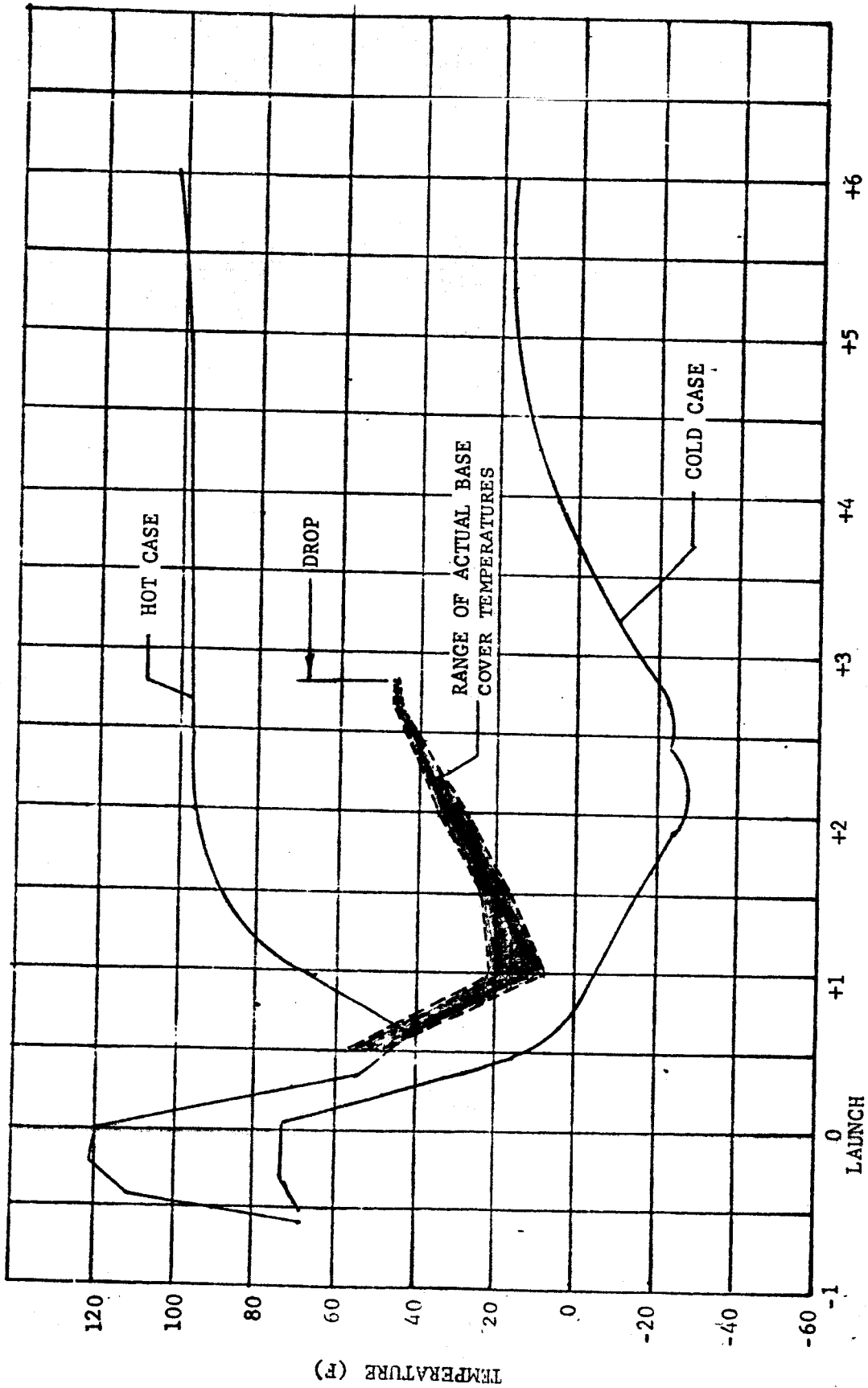


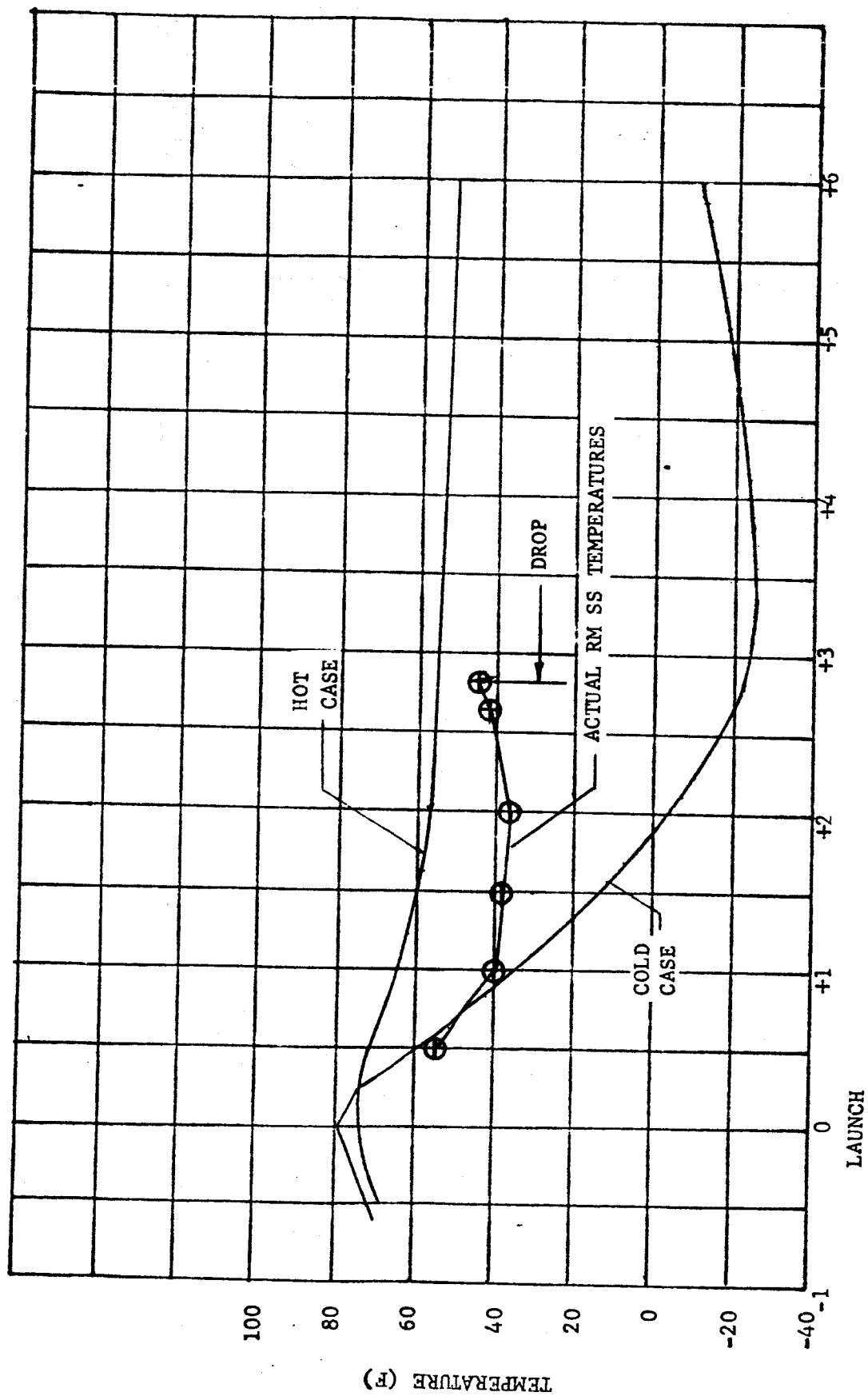
FIGURE VI-19 Angles of Attack and Sideslip and Axial Force Coefficient at Mortar Fire

FIGURE VI-20 MISSION ASCENT PROFILES





TIME FROM LAUNCH (HRS)
 FIGURE VI-21 BASE COVER TEMPERATURE HISTORY



TIME FROM LAUNCH (HRS)

FIGURE VI-22 ROCKET MOTOR SUPPORT STRUCTURE TEMPERATURE HISTORY

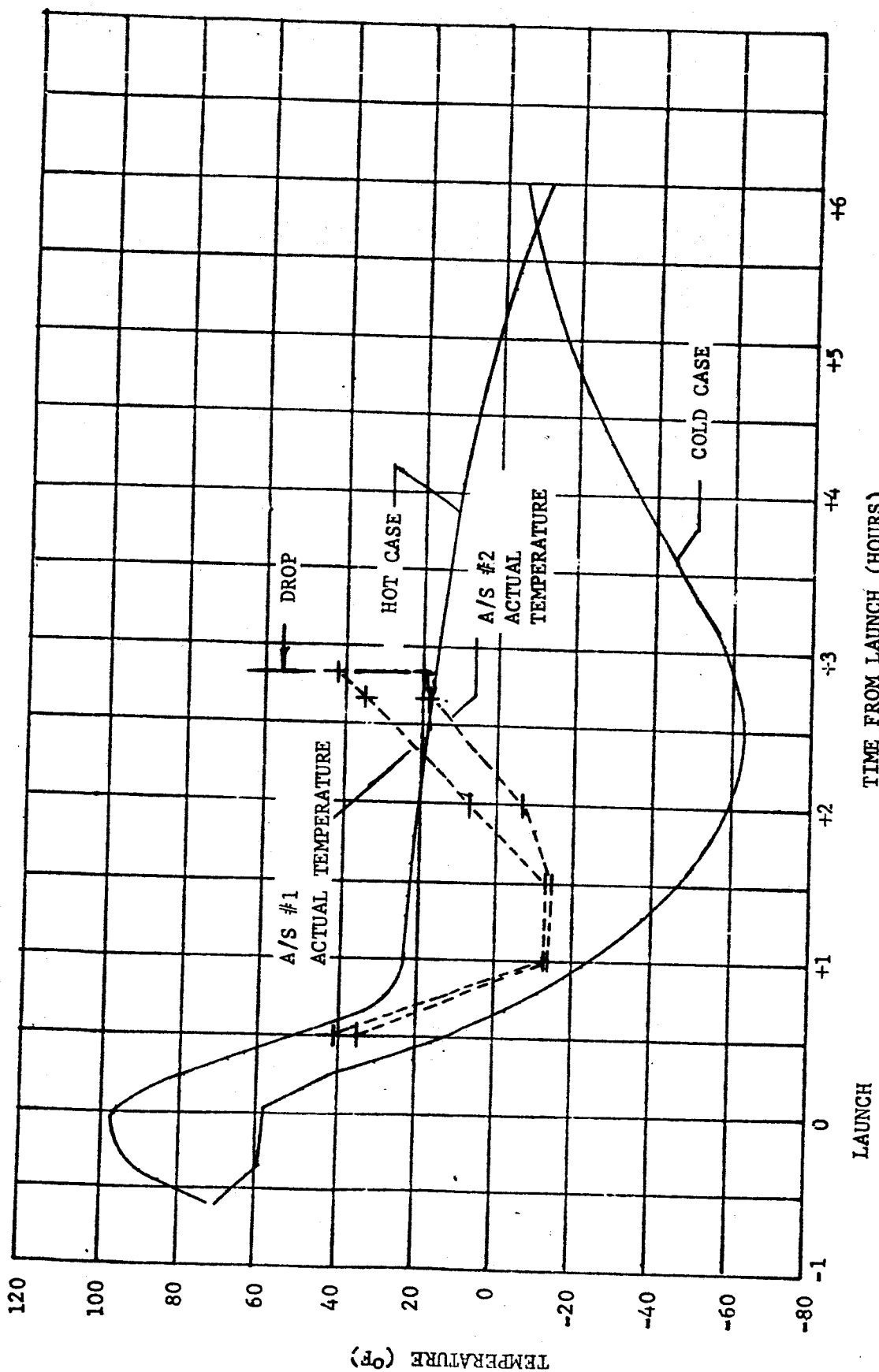


FIGURE VI-23 AEROSHELL TEMPERATURE HISTORY

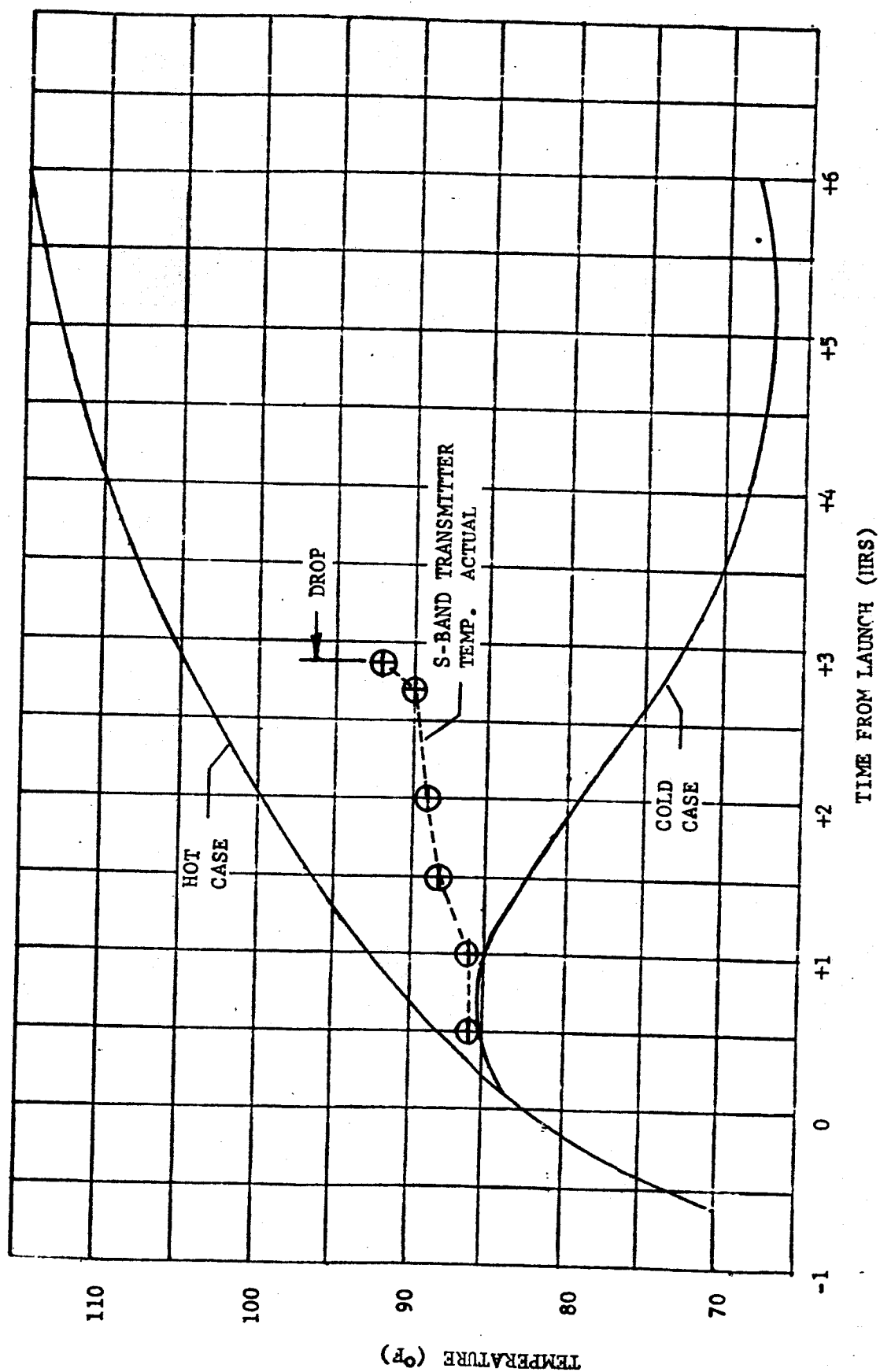


FIGURE VI-24 S-BAND TRANSMITTER TEMPERATURE HISTORY

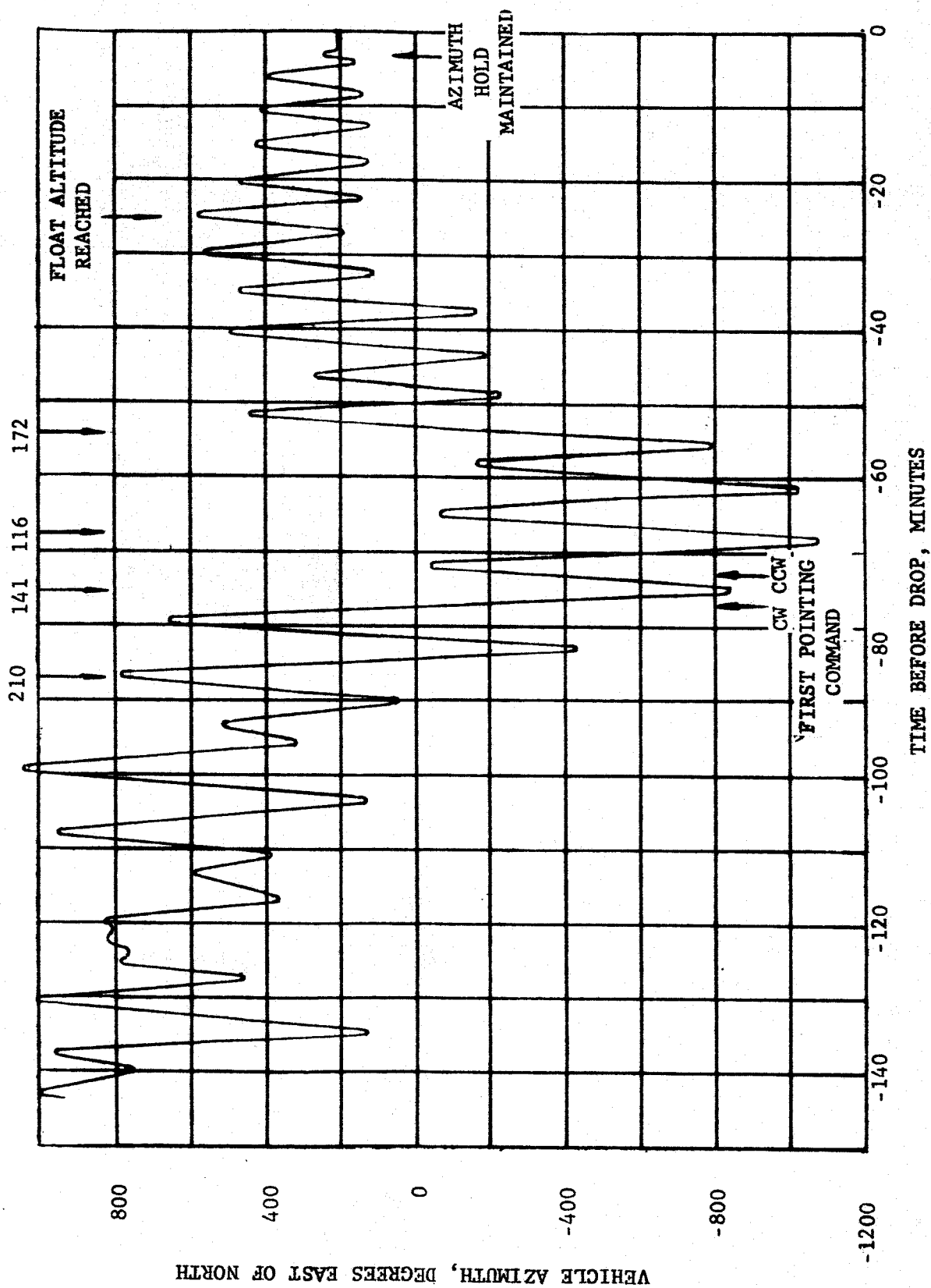
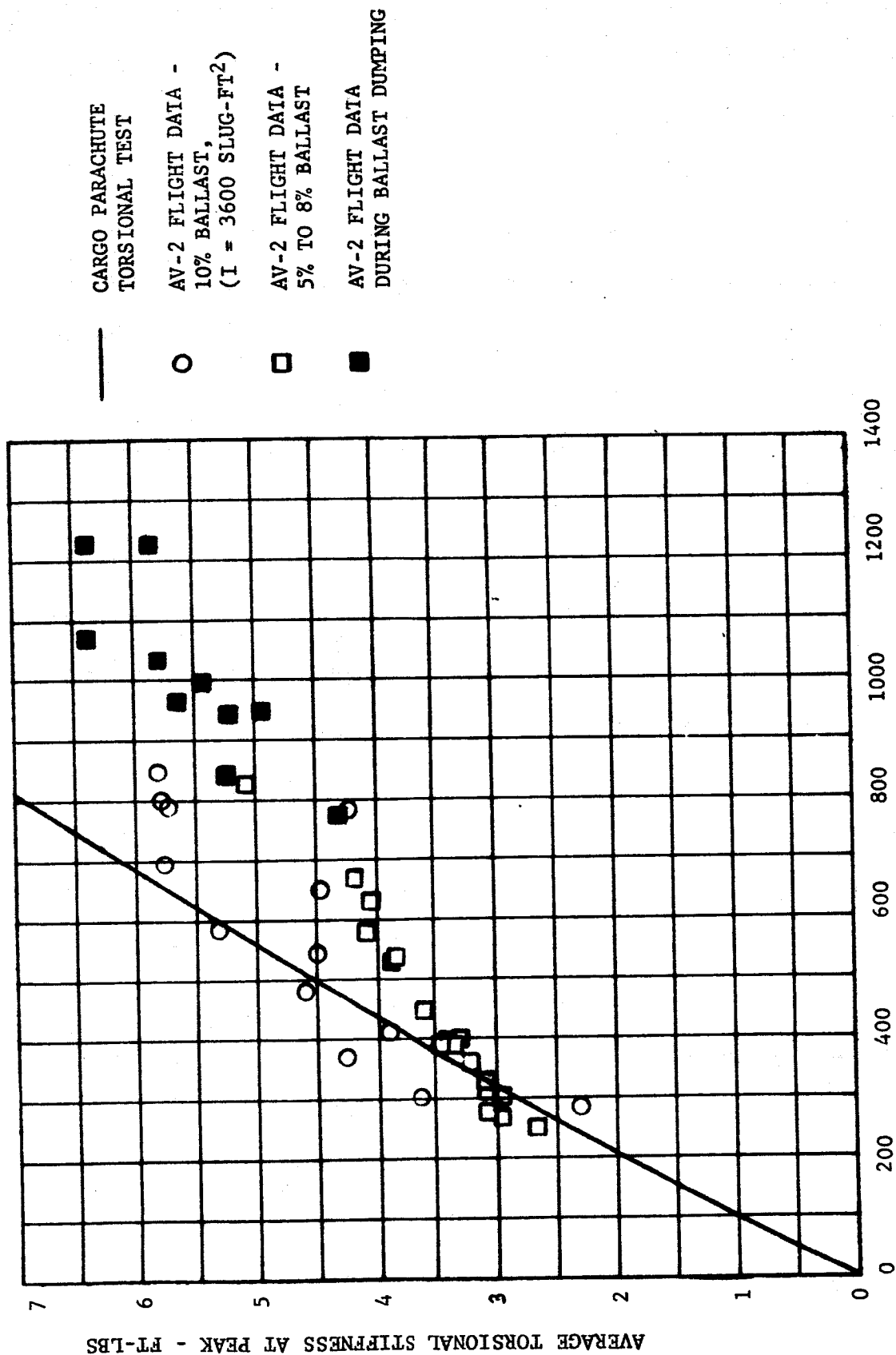
BALLASTING, 1b

FIGURE VI-25 BLDT AV-2 VEHICLE AZIMUTH HEADING



OSCILLATION AMPLITUDE (PEAK-TO-PEAK), DEG.
FIGURE VI-26 BLDT AV-2 TORSIONAL STIFFNESS

VII. CONCLUSIONS

The conclusions reached from the in-depth analysis of the AV-2 mission data and films are:

A. The flight of the vehicle was as programmed and within the predicted dispersions.

B. The dynamic pressure condition at mortar fire was slightly lower than predicted but within the tolerances required for the mortar fire command to have been issued by the ground computer based on dynamic pressure. The Mach number at decelerator actual peak load was lower than predicted but within the required performance box (See Figure II-1).

The remaining BLDT requirements which were also met are:

Resultant Angle of Attack (DEG) ≤ 21

Residual Spin Rate (DEG/SEC) ≤ 100

Decelerator Temperature ($^{\circ}\text{F}$) ≤ 80

C. The mortar fire and decelerator peak load test conditions were within the bounds required for an acceptable transonic qualification test.

D. The decelerator performed as predicted with no unusual damage. This constitutes successful qualification of the decelerator at the transonic conditions.

E. The aeroshell separation function more than adequately met the requirement for 50 feet of separation distance in 3 seconds.

VIII. REFERENCES AND OTHER DATA SOURCESA. References

1. MMC RD-3720247, Parachute Test Objectives and Requirements for BLDT Program, Dated March 29, 1972.
2. MMC TR-3720052, Viking Vehicle Dynamics Data Book, Rev. F, July 6, 1972.
3. MMC TR-3720074, Volume I, Transonic Aerodynamic Characteristics and Pressure Distributions on 8 Percent Scale Models of the Viking Lander Capsule, Aeroshell and Lander plus Base Cover, February 1971.
4. MMC TR-37209014, Viking Aerodynamics Data Book, Rev. C, June 1972.
5. GAC GER 15215, Rev. A, Viking Decelerator Design Analysis Report, March 20, 1972.
6. NASA TND-5296, Inflation and Performance of Three Parachute Configurations from Supersonic Flight Tests in a low Density Environment, July 1969.
7. MMC TR-3720181, Scale Model Test Results of the Viking Parachute System at Mach Numbers from 1 through 2.6, November 1971.
8. MMC Memorandum 8943-72-116, Viking Parachute Swivel Loads and Pull-Off Angles from Dynamic Simulation, R. D. Moog, 10 May 1972.
9. NASA CR-1482, Statistical Trajectory Estimation Programs (STEP), Volumes I and II.
10. Users Guide No. 837L7041032, BLDT Six Degrees of Freedom Trajectory Program, dated February 1972.
11. TN-3770115, Aerothermodynamics Analysis of the BLDT Vehicle (CDR Configuration) dated July 1971.
12. GAC GER-15397, Low Altitude Drop Test (LADT) of Viking Decelerator System, February 8, 1972.

B. Abbreviations

A/B	Airborne
AGC	Automatic Gain Control
A/S	Aeroshell
AV	BLDT Flight Vehicle Designator
BLDT	Balloon Launched Decelerator Test
B/U	Backup
Cg	Center of Gravity
CST	Combined System Test
CW	Clockwise
CCW	Counter Clockwise
DGB	Disk-Gap-Band
DEG	Degree
Deg/Sec	Degree/Second
fps	Feet per second
FRT	Flight Readiness Test
FT	Feet
GAC	Goodyear Aerospace Corporation
g's	Gravitational acceleration = 32.2 FPS^2
IRIG	Inter Range Instrumentation Group
K	1000
KHz	Kilohertz
LADT	Low Altitude Drop Test
MMC	Martin Marietta Corporation
NASA	National Aeronautics and Space Administration
NOP	North Oscura Peak
P	Roll Rate

PSP	Pounds per Square Foot
PSI	Pounds per Square Inch
PEPP	Planetary Entry Parachute Program
q	Dynamic Pressure
Q	Pitch Rate
R	Yaw Rate
RAOB	Radiosonde Observation Balloon
RF	Radio Frequency
RMSS	Rocket Motor Support Structure
RTDS	Real Time Data System
s	Aerodynamic Reference Area
SCO	Subcarrier Oscillation
S/N	Serial Number
STEP	Statistical Trajectory Estimation Program
T	Time
TDC	Telemetry Data Center
TM	Telemetry
VLC	Viking Lander Capsule
V	Time Rate of Change of Velocity
WSMR	White Sands Missile Range
Z,Zulu	Greenwich Mean Time

APPENDIX A

**DESCRIPTION OF
BALLOON LAUNCHED DECELERATOR
TEST VEHICLE**

APPENDIX A

DESCRIPTION OF BALLOON LAUNCHED DECELERATOR TEST VEHICLE

The BLDT Vehicle utilized for the high altitude qualification tests of the Viking Mars Lander Decelerator consisted of six (6) major subsystems which were:

- o Structural Subsystem
- o Electrical Subsystem
- o Instrumentation Subsystem
- o R. F. Subsystem
- o Propulsion/Pyrotechnic Subsystem
- o Thermal Control Subsystem

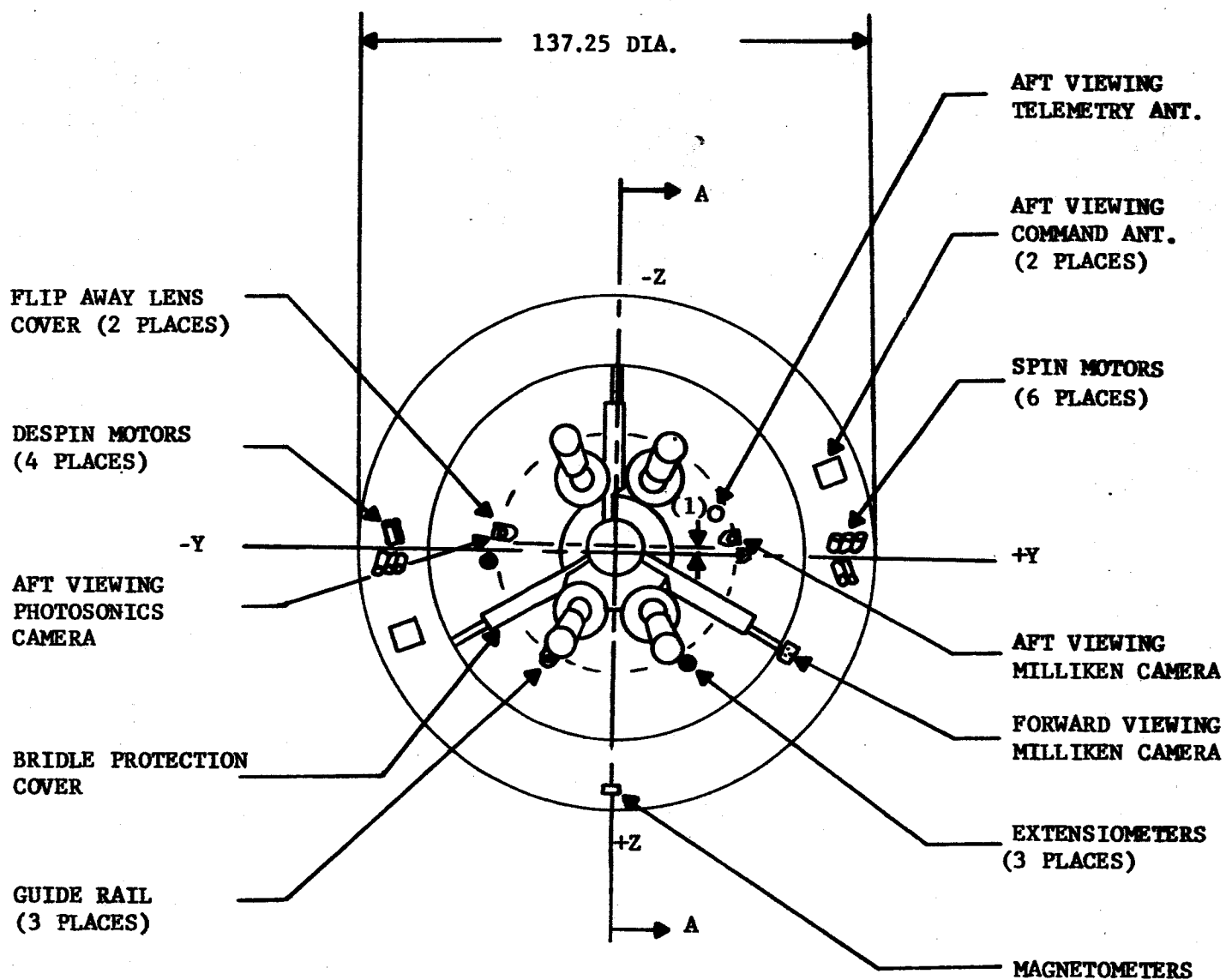
The BLDT vehicles are designed to be flown as supersonic, transonic and free fall vehicles in order to simulate the various anticipated Mars entry conditions for decelerator deployment.

A. Structural Subsystem

The vehicle structural configuration provides an external envelope which simulates the Viking Lander Capsule in order to qualify the Decelerator in the wake of a blunt body similar to the actual Mars VLC. The general configuration of the BLDT vehicle is shown in Figures A-1 through A-7.

At the initiation of the BLDT vehicle design, the test bed was to match the Mars VLC Cg and mass properties at decelerator deploy command. insofar as practical. The requirement was for the BLDT vehicle to have a weight of 1888 pounds with a Cg offset of 1.41 inches in the -Z direction at the time of decelerator mortar fire command. The final mass properties

(1) -Z AXIS Cg OFFSET = $1.41'' \pm 0.030''$

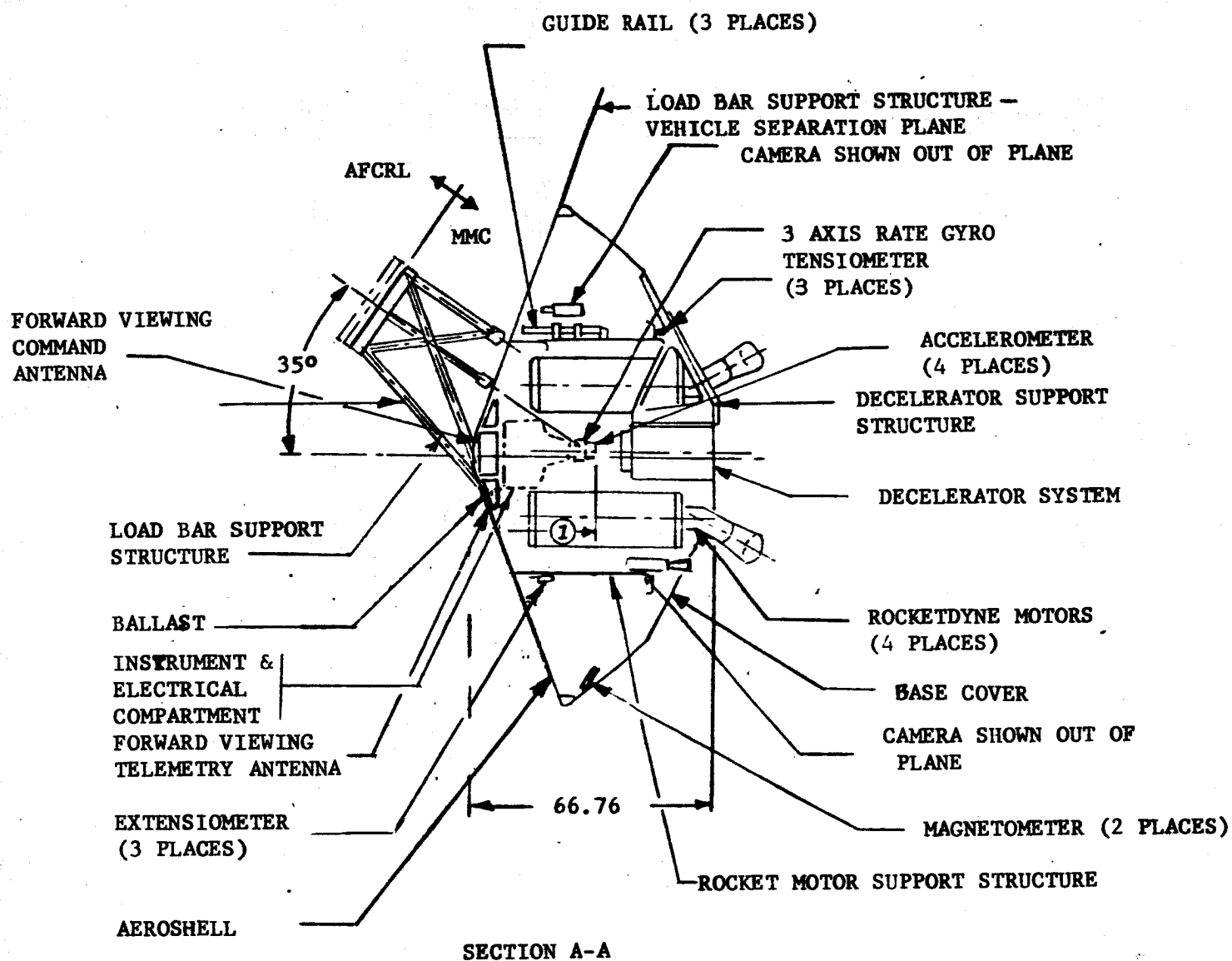


VIEW LOOKING AT AFT END
OF VEHICLE

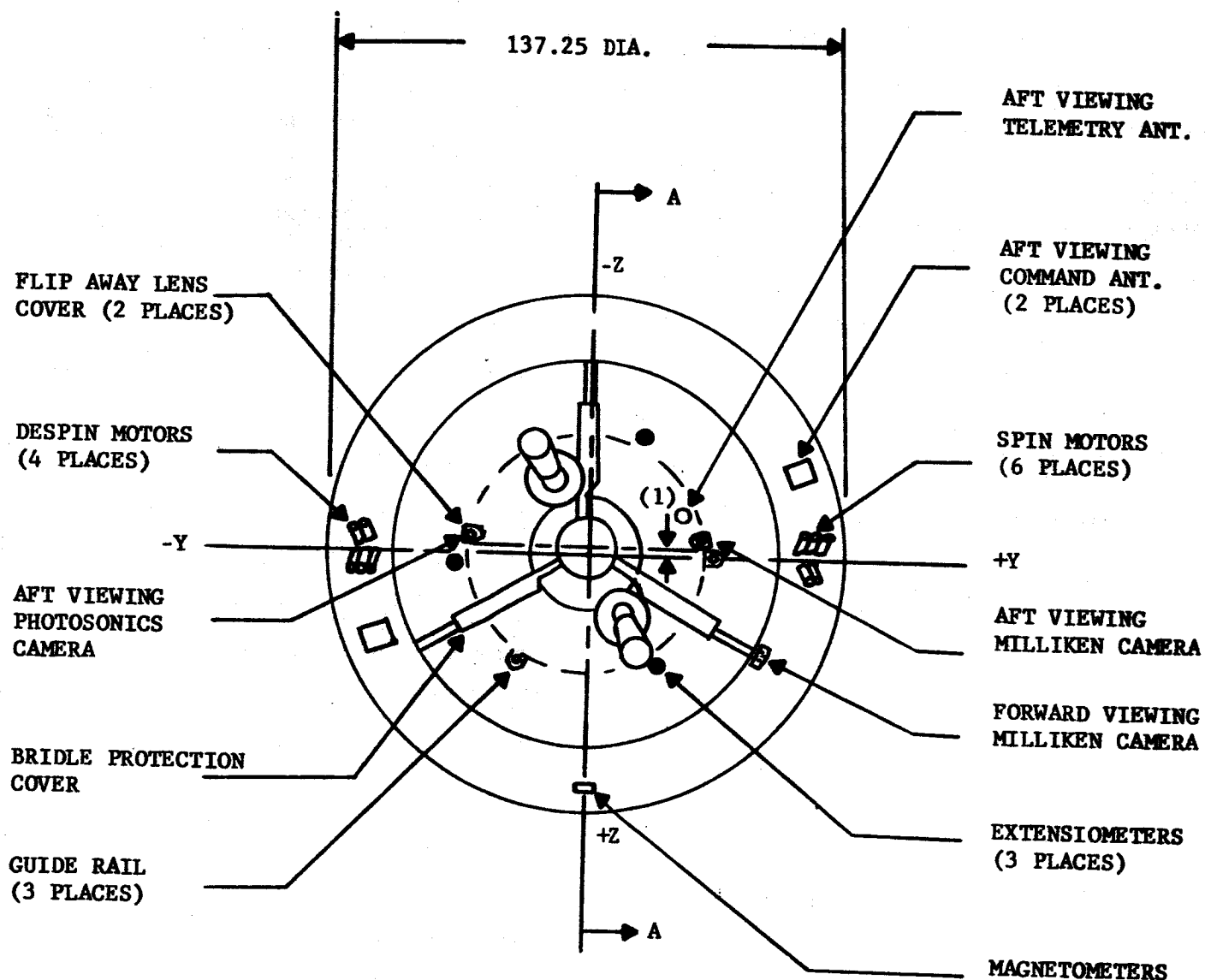
BLDT SUPERSONIC VEHICLE CONFIGURATION

FIGURE A-1

(1) X AXIS Cg AT MORTAR FIRE = 31.7" to 33.7"



(1) -Z AXIS Cg OFFSET = $1.41'' \pm 0.030''$

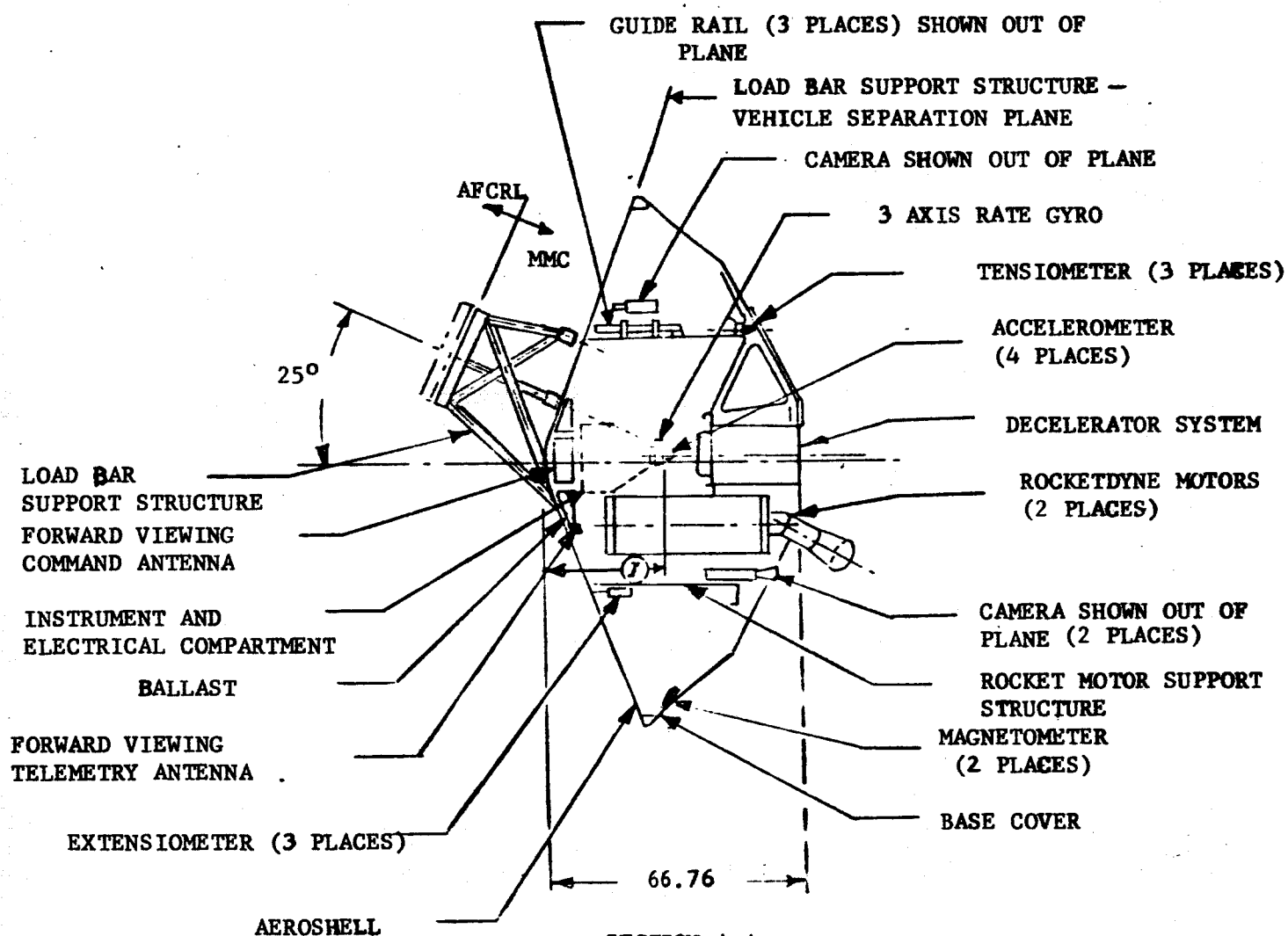


VIEW LOOKING AT AFT END
OF VEHICLE

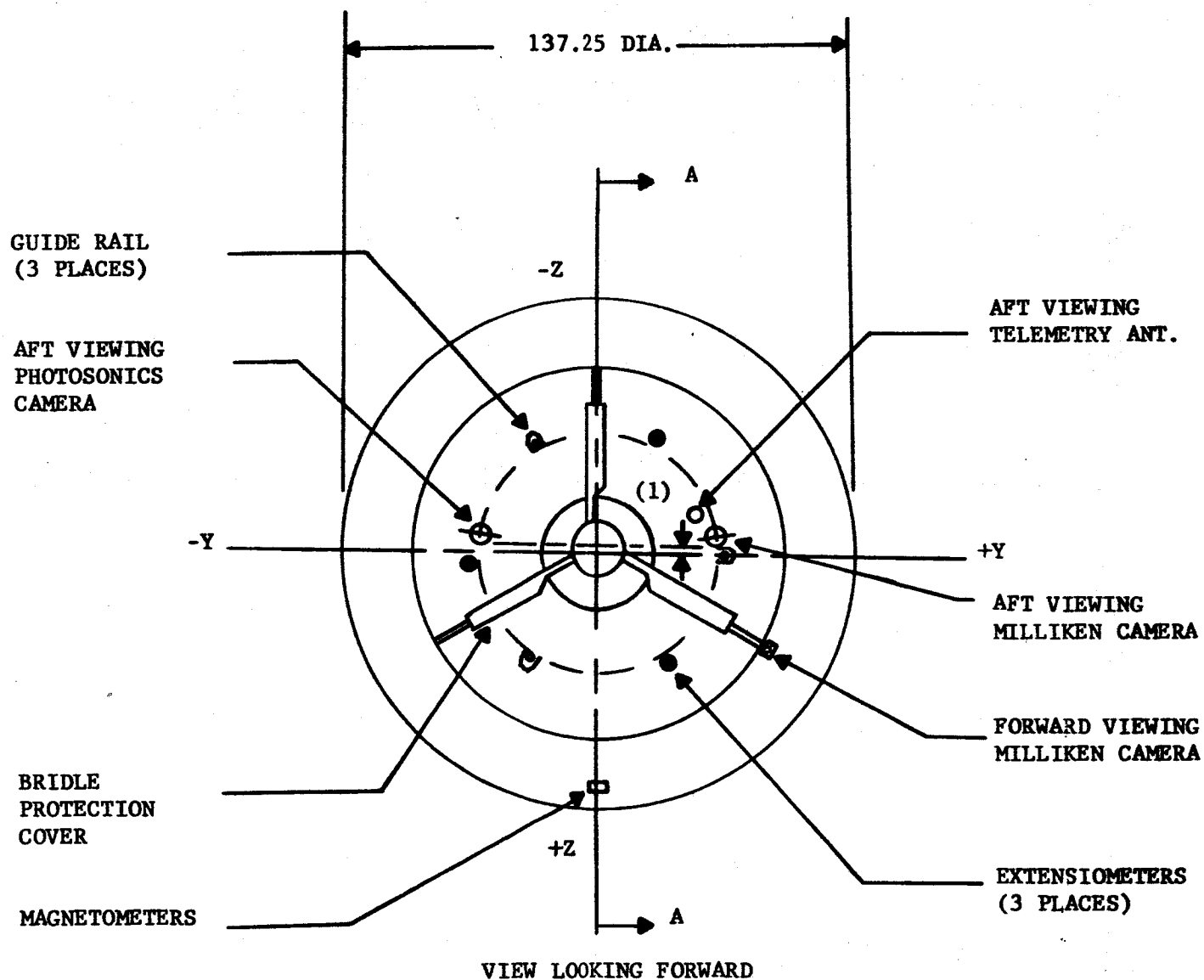
BLDT TRANSONIC VEHICLE CONFIGURATION

FIGURE A-3

(1) X AXIS C_g AT MORTAR FIRE = 31.7" to 33.7"



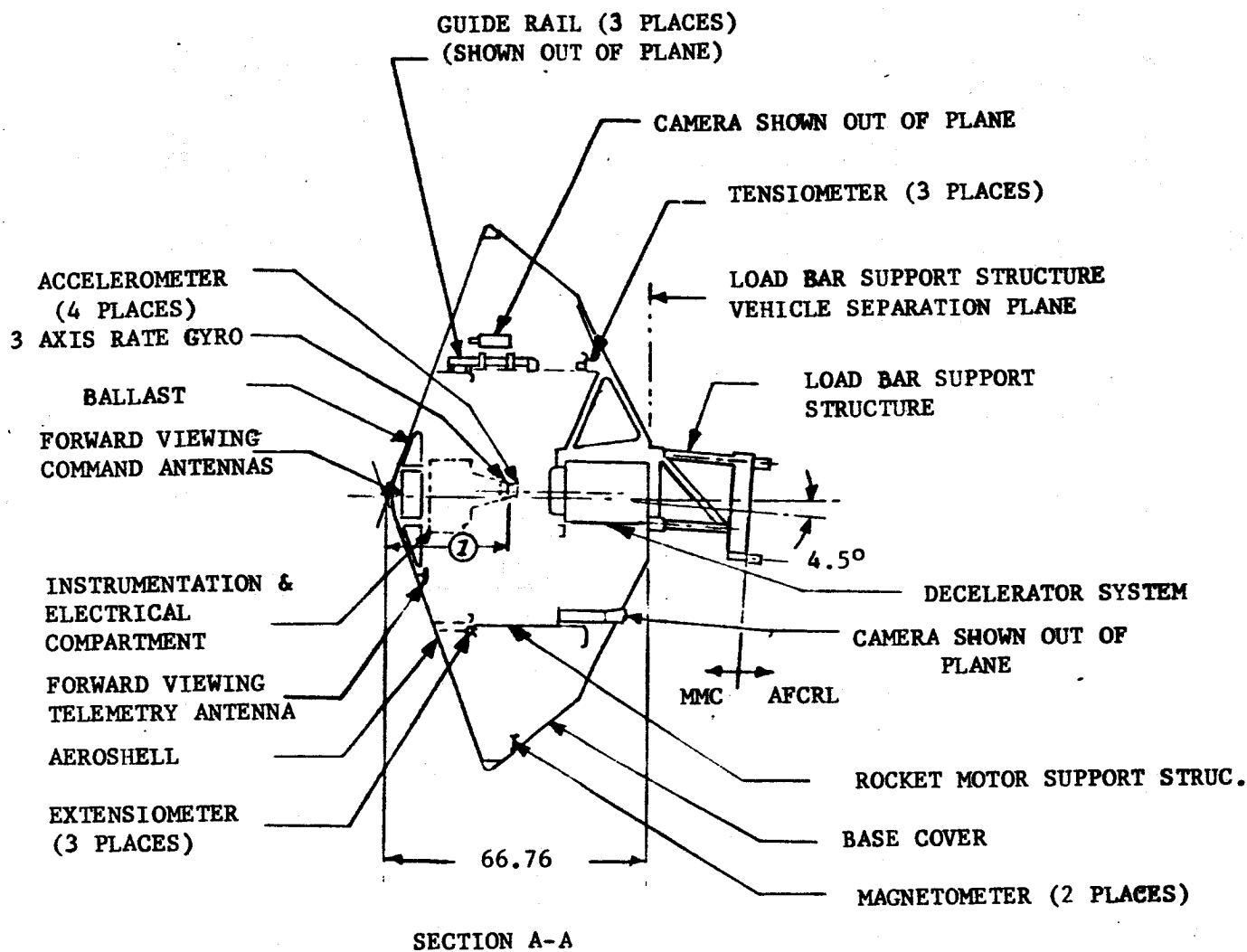
(1) -Z AXIS Cg OFFSET = $1.41'' \pm 0.030''$



BLDT SUBSONIC VEHICLE CONFIGURATION

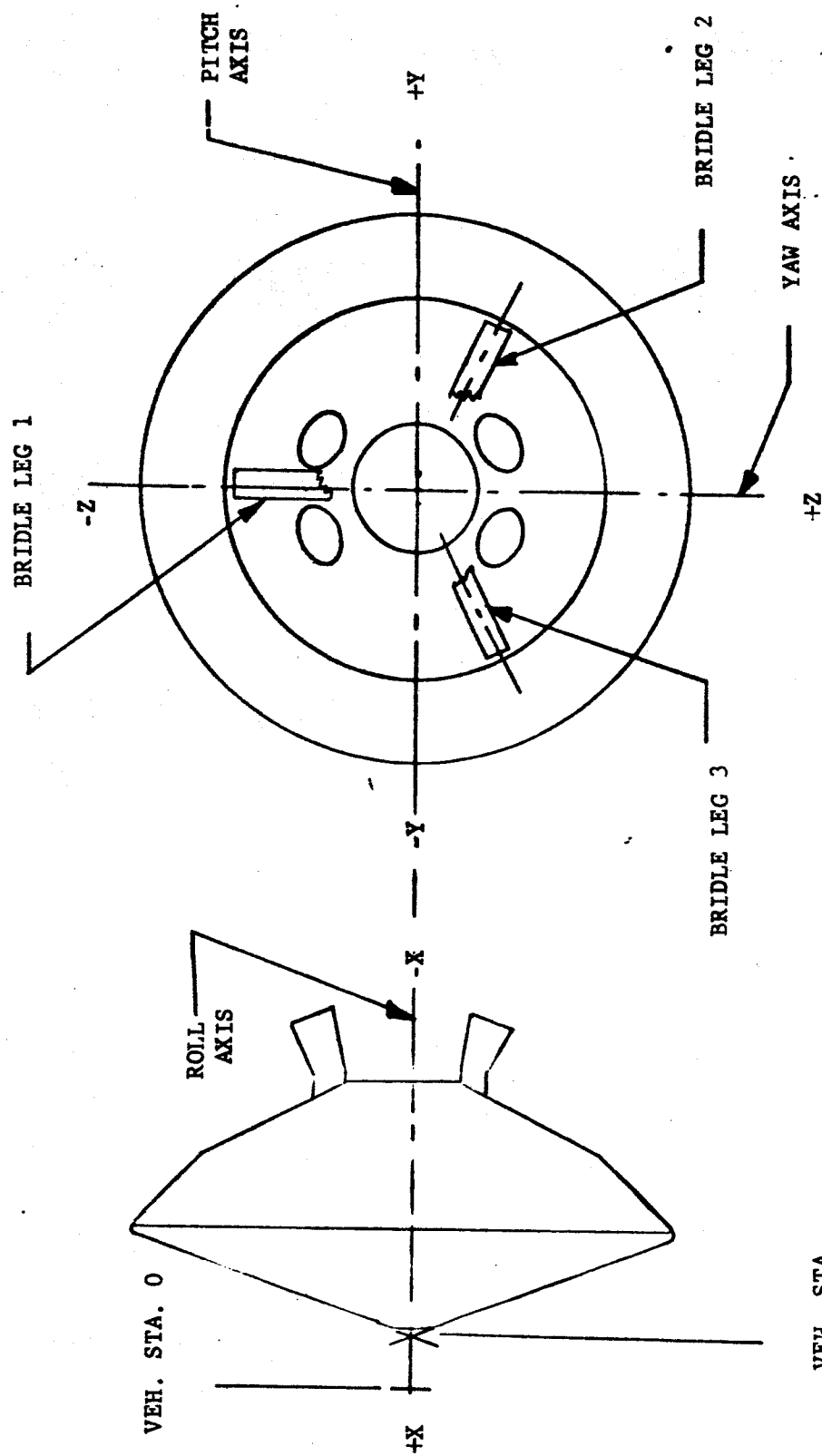
FIGURE A-5

(1) X AXIS Cg AT MORTAR FIRE = 31.7" to 33.7"



BLDT SUBSONIC VEHICLE CONFIGURATION

FIGURE A-6



BLDT COORDINATE SYSTEM
FIGURE A-7

for each vehicle, included in the individual reports, indicates the revisions which were made to the mass properties subsequent to the BLDT vehicle design.

The structural subsystem consisted of six (6) major components as follows:

1. Rocket Motor Support Structure

The rocket motor support structure is a cylindrical component, approximately 64 inches in diameter, which provides the major vehicle internal longitudinal support structure as well as providing the motor mounts for the supersonic and transonic vehicles.

2. Instrument Beam

The instrument beam is a structural beam which was tied to the forward surface of the RMSS and ran symmetrically along the Y, -Y axis. It also contained an aft facing pylon to mount the accelerometers and rate gyros at or near the vehicle longitudinal Cg.

3. Base Cover

The base cover is a lightweight external shell providing an aft configuration similar to the Mars VLC.

4. Decelerator Support Structure

The decelerator support structure is a three leg structure, similar to the Mars VLC decelerator support structure, with a cylindrical center section for mounting of the decelerator cannister parallel to the BLDT longitudinal centerline. The decelerator support structure assembled into the base cover to provide an intermediate assembly.

5. Aeroshell

The Aeroshell which is the forward surface of the vehicle provides a conical blunt aerodynamic surface approximately 11.5 feet in diameter with a 140° included angle. The aeroshell provides a forward configuration similar to the Mars VLC.

6. Load Bar Support Structure

The load bar support structure is a tubular structural member which provides the interface with the Air Force Cambridge Research Laboratory (balloon) load bar as well as providing the correct hanging pitch attitude.

B. Electrical Subsystem

The electrical subsystem provides the flight power, cabling and switching/sequencing devices required to properly sequence and activate the various functions. The electrical subsystem is shown schematically in Figure A-8.

The vehicle is powered by five (5) silver zinc batteries as follows:

1. Main Battery - 60 AH - MMC P/W PD94S0026

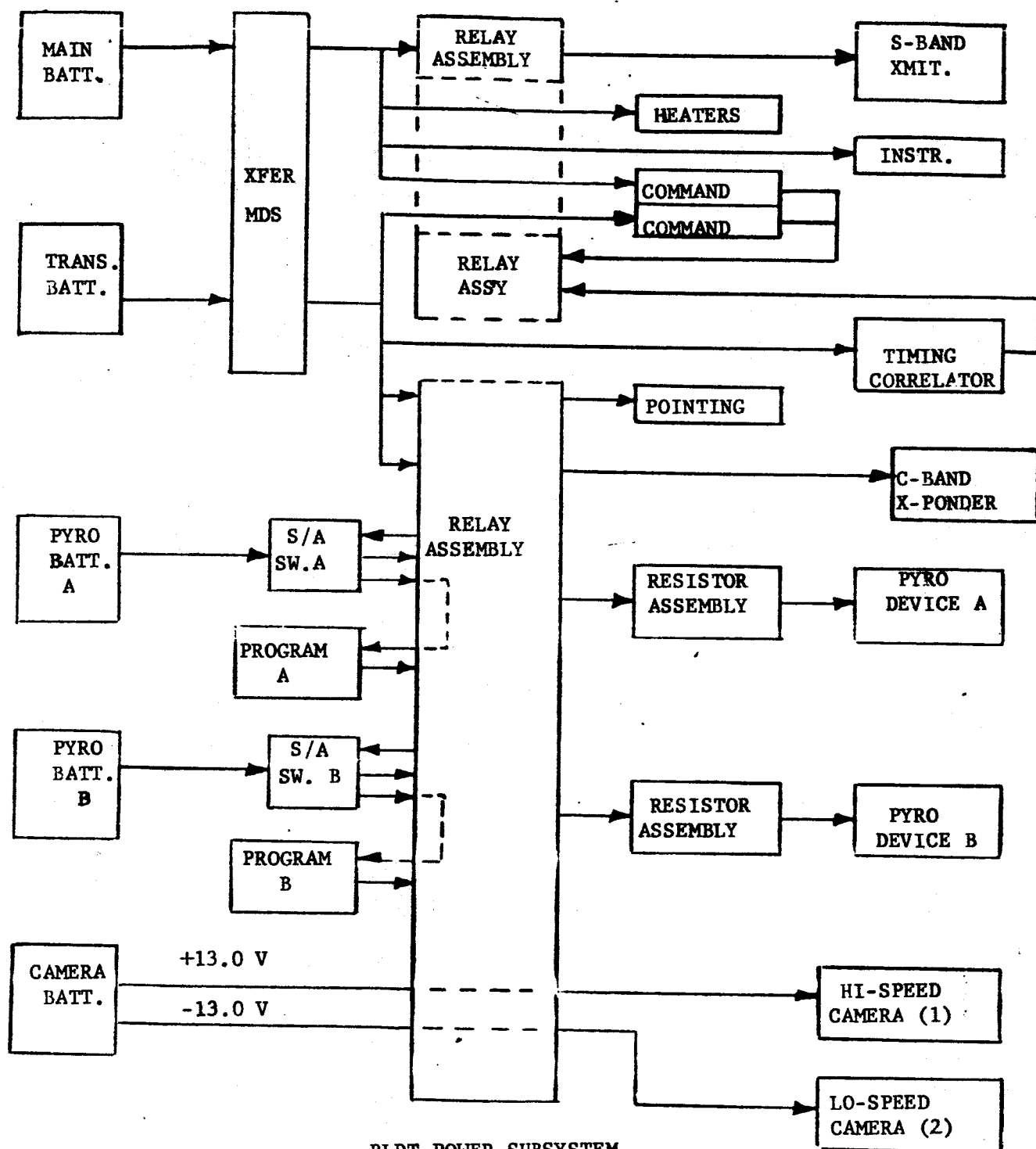
Provides power for telemetry, command system A and A/B heaters.

2. Transient Battery - 16 AH Engle Pitcher Model 4332

Provides power for timing correlator, C-band transponder and command system B.

3. Pyro Battery A - 1.0 AH - ESB Model 392

Provides power to all pyro A circuit ordnance devices and airborne programmer A.



BLDT POWER SUBSYSTEM
BLOCK DIAGRAM

FIGURE A-8

4. Pyro Battery B - 1.0 AH - ESB Model 392

Provides power to all Pyro B circuit ordnance devices and airborne programmer B.

5. Camera Battery - 1.0 AH - ESB Model 393 (Similar to model 392 except tapped at 9 cells and 18 cells).

Provide +13 volts power to onboard high speed cameras.

The electrical subsystem provides completely redundant airborne sequencing programmers and completely redundant pyrotechnic circuits.

In addition, the electrical subsystem provides all power switching relays, motor driven switches, power limiting resistors and airborne heaters.

C. Instrumentation Subsystem

The BLDT Instrumentation subsystem provides for the real time measurement and conditioning of the parameters listed in Table A-1 and provides timing correlation for the real time measurements and airborne camera. The instrumentation subsystem utilizes a PAM/FM/FM configuration as shown schematically in Figure A-9.

Additionally, the instrumentation subsystem provides the following photographic coverage:

1. Aft Looking Photosonics

Approximately 450 frames/second to record the decelerator deployment sequence.

2. Aft Looking Milliken

Sixty-four frames/second to record the decelerator deployment sequence.

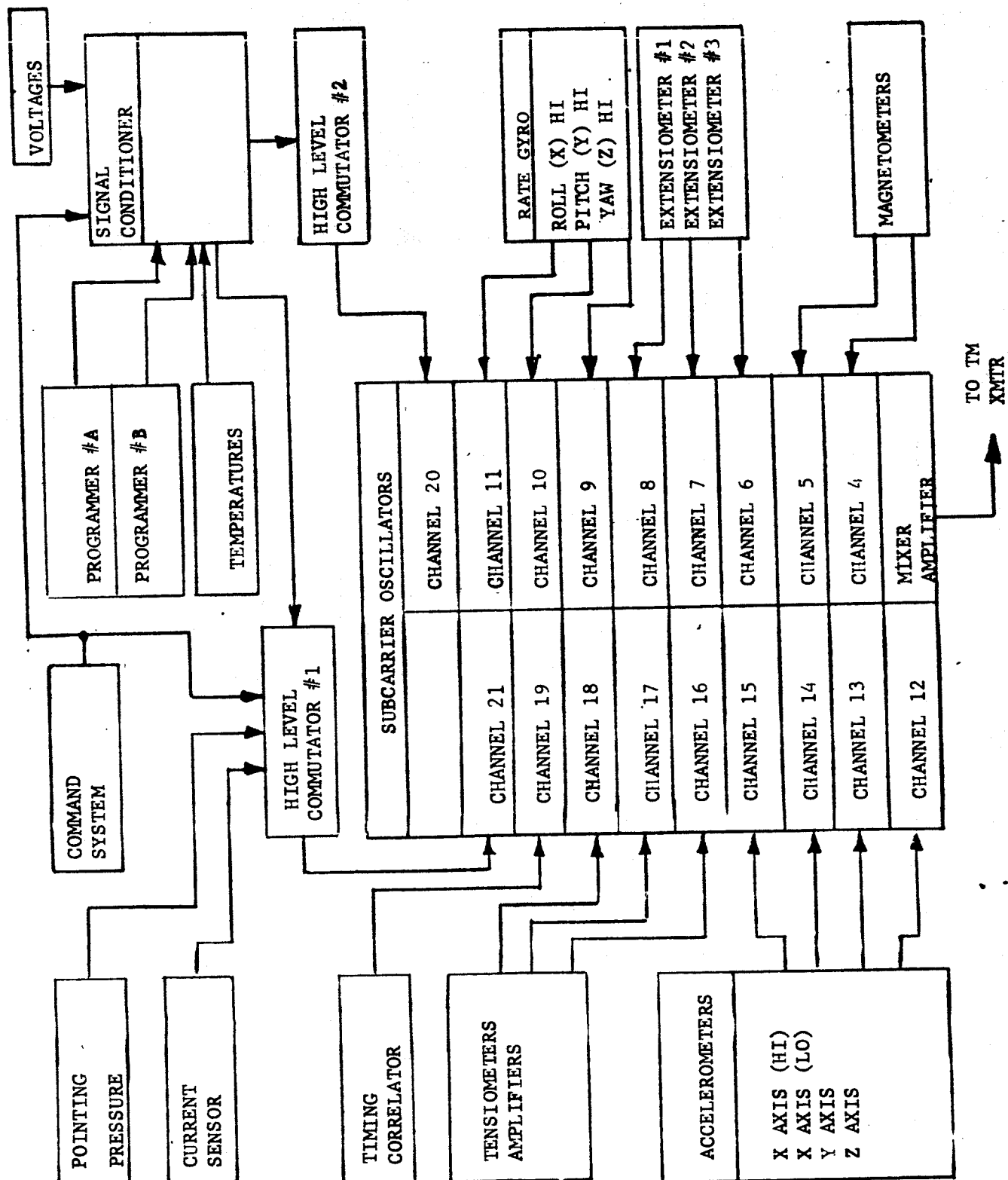


FIGURE A-9 BLDT INSTRUMENTATION SYSTEM

3. Forward Looking Milliken

Thirty-two frames/second to record the Aeroshell separation sequence and obtain a time/distance history.

D. R. F. Subsystem

The R. F. Subsystem consists of the TM transmitter, the C-Band transponder and the redundant command receiver/decoders with all of the required antenna systems.

1. TM Transmitter

The telemetry transmitter provides for the FM transmission of the composite FM data from the Instrumentation Subsystem mixer amplifier. The transmitter provides 5 watts power output in the S-Band (2285.5 MHz) range. The TM transmitter and antenna system is shown schematically in Figure A-10.

2. C-Band Tracking Transponder

The GFE tracking transponder was provided by White Sands Missile Range and is compatible with tracking radar AN/FPS-16 utilized at WSMR. The transponder and antenna system is shown schematically in Figure A-10.

3. Command Receiver/Decoder

The vehicle command system, including antenna, multicoupler, receivers and decoders, is shown schematically in Figure A-11.

The redundant receiver/decoders operate on an assigned frequency of 541 MHz and provide a 28 volt nominal decoder output for command inputs with seven command tones selected from IRIG-103-61 channels 1 through 20.

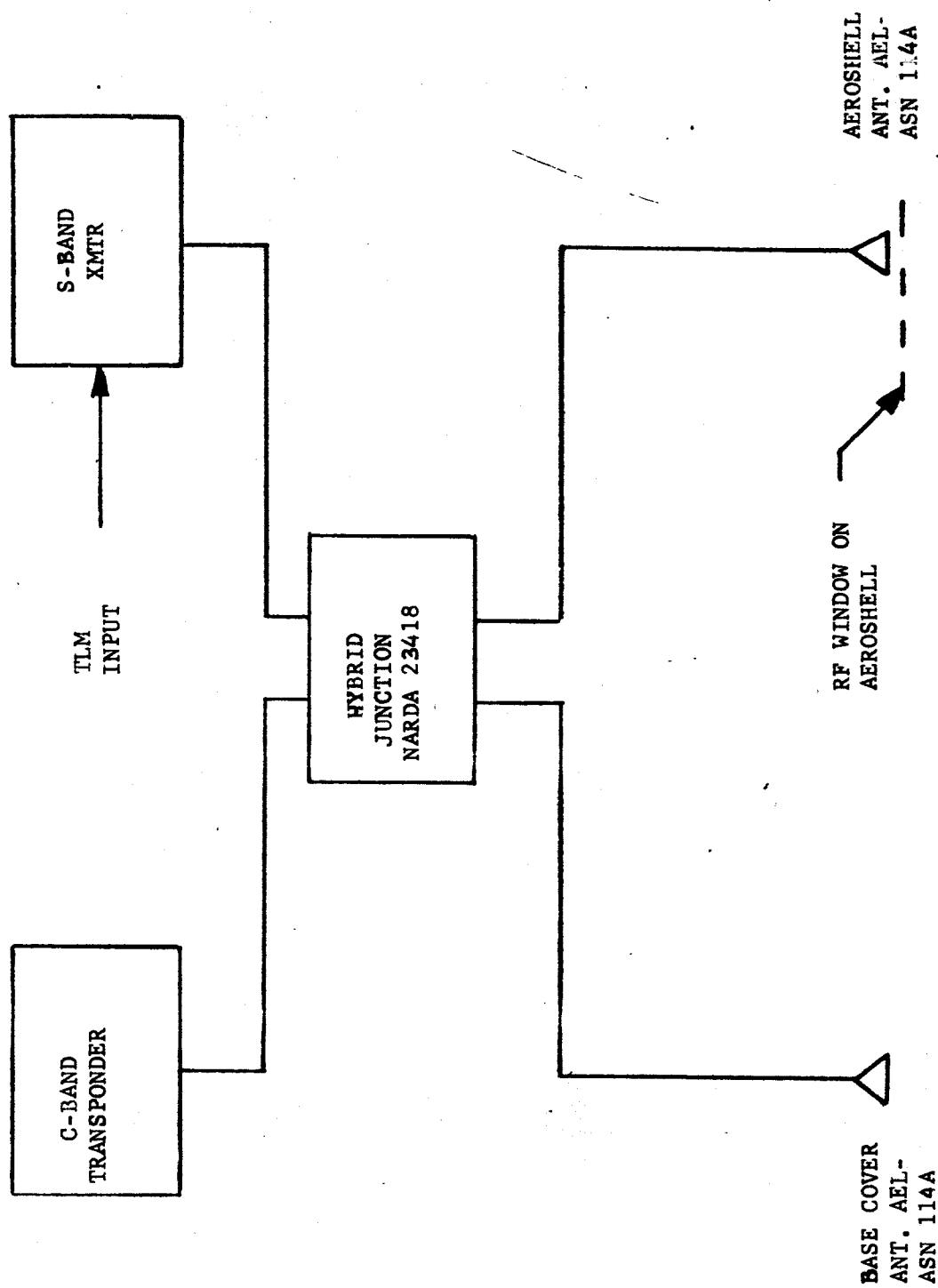


FIGURE A-10 TRACKING & TELEMETRY ANTENNA SYSTEM

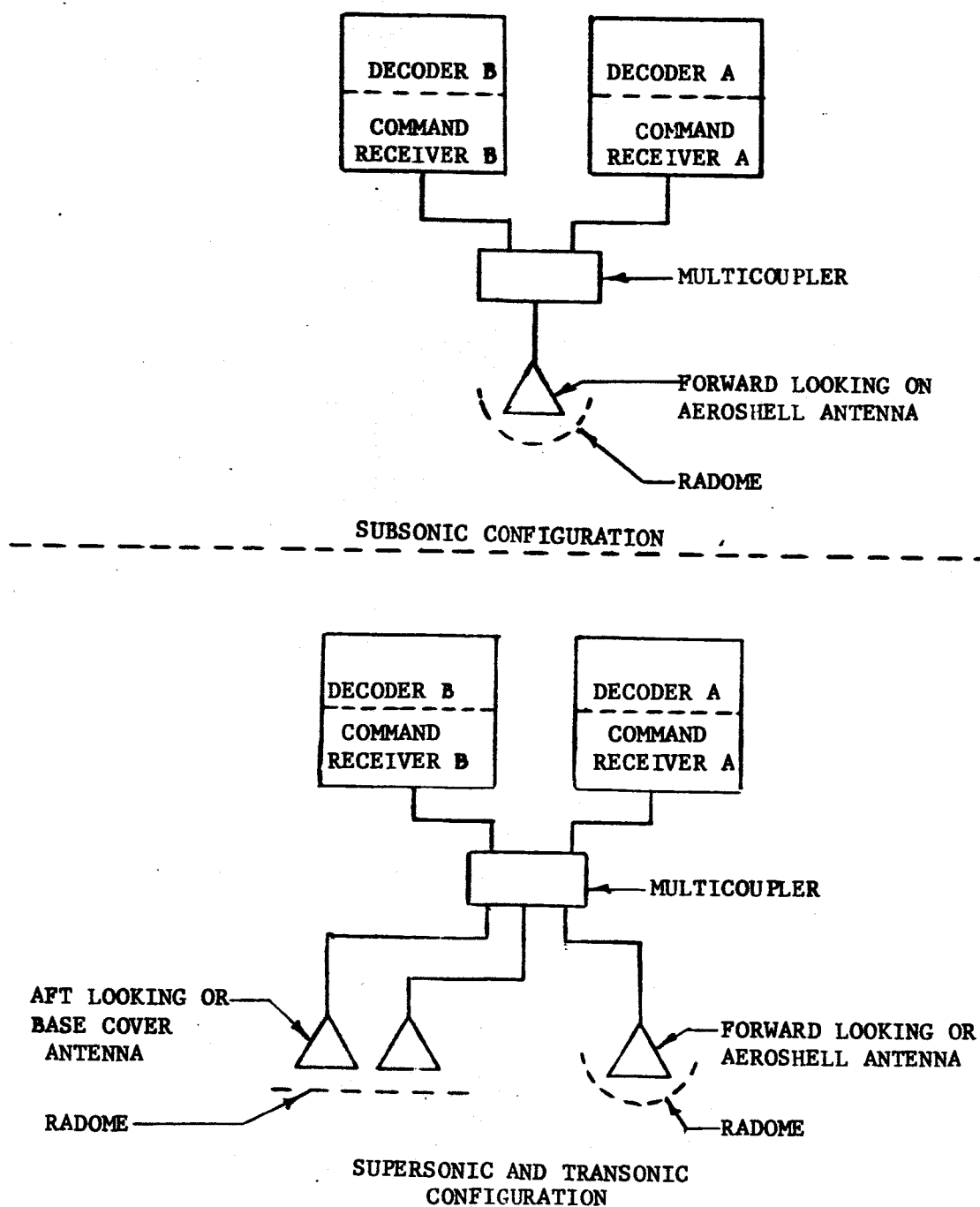


FIGURE A-11

The system coding is such that triple tone ground commands result in the following airborne functions:

<u>Function</u>	<u>Commands</u>		
	<u>Primary</u>	<u>Backup</u>	<u>Redundant</u>
Release from load bar	X		X
Mortar Fire	X		X
Arm Ordnance Bus	X		X
Safe Ordnance Bus	X	X	
Turn RF on	X		
Turn RF off	X		
Pointing, Clockwise	X	X	
Pointing, Counterclockwise	X	X	

E. Propulsion/Pyrotechnic Subsystem

The propulsion/pyrotechnic subsystem consists of the solid rocket motors required on the supersonic and transonic vehicles, the azimuth pointing system required on the supersonic and transonic vehicles and the pyrotechnic devices required on all three configurations.

The main propulsion assembly consists of a set of Rocketdyne RS-B-535 solid propellant rocket motors each having the following characteristics:

	<u>Nominal</u>	<u>3 σ Variation</u>
Total Impulse, lbf-sec	Classified	0.6%
Burn Time Avg. Thrust, lbf	Classified	1.9%
Nozzle Cant Angle, deg	35	0.1
Thrust Vector Alignment, deg**		0.2
Ignition Interval, msec	49	+27, -17
Burn Time, sec	Classified	1.8%
Loaded Weight, lbm	461.2	0.25***
Burnout Weight, lbm	91.7	3.7****

The supersonic configuration vehicles are provided with 4 of the above motors with the transonic vehicle containing 2.

The spin/despin system is required to reduce trajectory dispersions during booster burn and despin after burnout. Spin Motors having the following characteristics are used:

	<u>Nominal*</u>	<u>3 σ Variation</u>
Total Impulse, lbf-sec	76.5	3.0%
Burn Time Avg. Thrust, lbf	86.2	8.0%
Ignition Interval, msec	10.0	+10.0, -5.0
Burn Time, sec	0.87	+11.0%
Loaded Weight, lbm	1.2	0.1
Burnout Weight, lbm	0.9	0.1

* Vacuum Conditions, 70°F

** Alignment with respect to nozzle geometric centerline.

*** Actual weighing tolerance.

**** Variation from predicted value.

The supersonic and transonic vehicles utilized 6 each of the above motors for spin-up and 4 each of the above for despin.

Other pyromechanical and pyrotechnic functions included in the vehicle are:

<u>Function</u>	<u>Supersonic</u>	<u>Transonic</u>	<u>Subsonic</u>
Aeroshell Sep. Nuts	3	3	3
Load Bar Release Nuts	0	0	3
Tension Rod Separator	1	1	0
Cable Cutters	2	2	0
Decelerator Mortar*	1	1	1

* Part of Decelerator System

Also included in the propulsion subsystem is an azimuth pointing system which is used to orient the supersonic and transonic vehicle azimuth at drop in order to assure impact within the White Sands Missile Range in the event of a complete decelerator failure.

The pointing system is comprised of a gaseous nitrogen thruster system located on the balloon load bar. The system provides paired clockwise or counterclockwise rotational moments in response to ground commands. The azimuth pointing system is shown schematically in Figure A-12.

F. Thermal Control Subsystem

The thermal control subsystem consists of those passive and active components required to maintain vehicle components within the required temperature levels. These components were generally:

1. Internal and external blankets,
2. Active heaters,
3. Base cover ablative material.

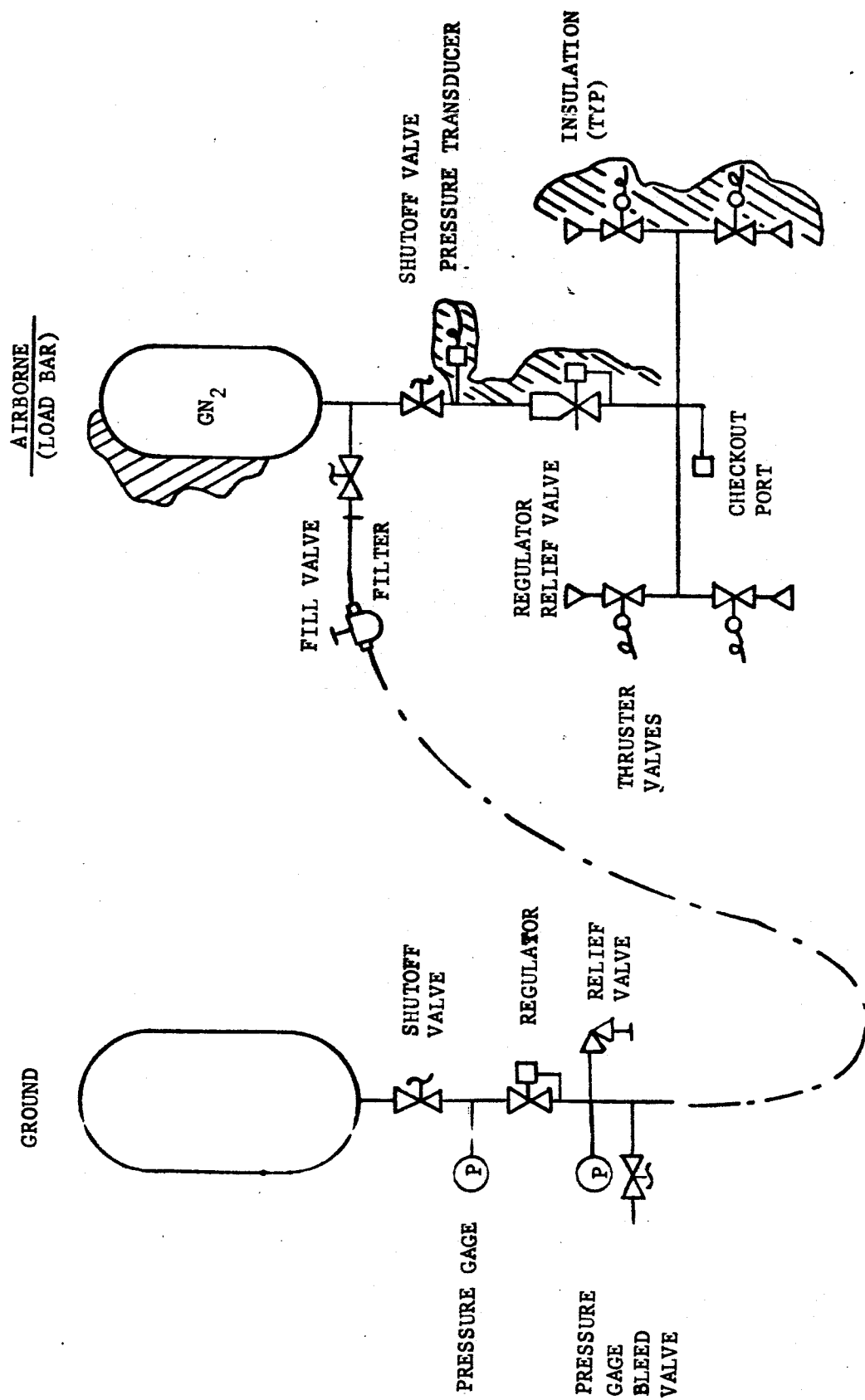


FIGURE A-12 BLDT POINTING SYSTEM

TABLE A-1

BLDT Telemetry Measurement List

No.	Measurement	Range	Accuracy		Response	Remarks
			End-to-End	Resolution		
1	Accel. X Axis	-2,+5g* -2,+3g**	5%	0.07g 0.05g	100 Hz	Low Range
2	Accel. X Axis	-15, 1g* -7, +1g**	5%	0.16g 0.08g	100 Hz	High Range
3	Accel. Y Axis	+1.0g	5%	0.01g	100 Hz	
4	Accel. Z Axis	+1.0g	5%	0.01g	100 Hz	
5	Heading	360 deg.	±5 deg.	1 deg.	5 Hz	Magnetometer No. 1
6	Heading	360 deg.	±5 deg.	1 deg.	5 Hz	Magnetometer No. 2
7	Rate Gyro, X Axis	±300°/sec.	5%	3.0°/sec	20 Hz	
8	Rate Gyro, Y Axis	±300°/sec.	5%	3.0°/sec	20 Hz	
9	Rate Gyro, Z Axis	±300°/sec.	5%	3.0°/sec	20 Hz	
10	Strain Link	0 to 12,000 lbs. ***	5%	120 lbs.	100 Hz	Parachute Linkage No. 1

* Supersonic Flight

** Transonic and Subsonic Flight

*** Amplifier will be adjusted to read 18,000 pounds full scale for supersonic flight only.

TABLE A-1 (CONTINUED)

BLDT Telemetry Measurement List

No.	Measurement	Range	Accuracy End-to-End	Resolution	Response	Remarks
11	Strain Link	0 to 12,000 lbs. *	5%	120 lbs.	100 Hz	Parachute Linkage No. 2
12	Strain Link	0 to 12,000 lbs. *	5%	120 lbs.	100 Hz	Parachute Linkage No. 3
13	Timing Pulse	25 PPS, 0 to 1.25 VDC	1%	ON/OFF	125 Hz	Camera Correlation
14	Temperature	+25 to +150°F	5%	1.5°F	10 Hz	Mortar Breech, Temp. Commuted at 30 SPS
15	Voltage	5 VDC	5%	0.05 VDC	10 Hz	Commutator #1 Full Scale Calibration at 30 SPS
16	Voltage	0 VDC	5%	0.05 VDC	10 Hz	Commutator #1 Zero Scale Calibration at 30 SPS
17	Voltage	0 to 36 VDC	5%	0.36 VDC	10 Hz	Main Battery, Commuted at 30 SPS
18	Current	0 to 16A	5%	0.16 A	10 Hz	Main Battery, Commuted at 30 SPS
19	Voltage	0 to 37 VDC	5%	0.37 VDC	10 Hz	Pyro Battery A Commuted at 30 SPS
20	Event, Cont. Step Change	0 to 14 VDC	± 50ms	(HI/LO)	10 Hz	Prog. A Reset Commuted at 30 SPS

* Amplifier will be adjusted to read 18,000 pounds full scale for supersonic flight only.

TABLE A-1 (CONTINUED)
BLDT Telemetry Measurement List

No.	Measurement	Range	Accuracy End-to-End	Resolution	Response	Remarks
21	Event, Pulse	0 to 14 VDC 0.1 sec Duration	\pm 50 ms	(ON/OFF)	10 Hz	Prog. A TM Chan. Commuted at 30 SPS
22	Event, Pulse	0 to 14 VDC 0.1 sec Duration	\pm 50 ms	(ON/OFF)	10 Hz	Prog. B TM Chan. Commuted at 30 SPS
23	Event, Cont.	0 to 4 VDC Step Change	\pm 50 ms	(HI/LO)	10 Hz	CW Point. Valve Signal Commuted at 30 SPS
24	Event, Cont.	0 to 4 VDC Step Change	\pm 50 ms	(HI/LO)	10 Hz	CCW Point. Valve Signal Commuted at 30 SPS
25	Event, Cont.	0 to 4 VDC Step Change	\pm 50 ms	(HI/LO)	10 Hz	Safe/Arm Sw. A Arm Position Comm. at 30 SPS
26	Event, Cont.	0 to 4 VDC Step Change	\pm 50 ms	(HI/LO)	10 Hz	Safe/Arm Sw. A Safe Position Comm. at 30 SPS
27	Pressure	0-2500 psia	5%	25 psi	10 Hz	Pointing system, Pressure Commuted at 30 SPS
28	Extensometer	0 to 12"	5%	0.12"	5 Hz	#1 Aeroshell Sep. Dist.
29	Extensometer	0 to 12"	5%	0.12"	5 Hz	#2 Aeroshell Sep. Dist.
30	Extensometer	0 to 12"	5%	0.12"	5 Hz	#3 Aeroshell Sep. Dist.
31	Voltage	0 to 37 VDC	5%	0.37 VDC	10 Hz	Pyro Battery B Commuted at 30 SPS
32	Voltage	0 to 33.5 VDC	5%	0.33	10 Hz	Transient Battery Commuted at 30 SPS

TABLE A-1 (CONTINUED)

BLDT Telemetry Measurement List

No.	Measurement	Range	Accuracy End-to-End	Resolution	Response	Remarks
33	Event, Cont.	0 to 4 VDC Step Change	\pm 50 ms	(HI/LO)	10 Hz	Safe/Arm Sv. B. Arm Position Comm. at 30 SPS
34	Event, Cont.	0 to 4 VDC Step Change	\pm 50 ms	(HI/LO)	10 Hz	Safe/Arm Sv. B. Safe Position Comm. at 30 SPS
35	Event, Cont.	0 to 14 VDC Step Change	\pm 50 ms	(HI/LO)	10 Hz	Programmer B Reset Commu- tated at 30 SPS
36	Deleted					
37	Temperature	-90 to +210°F	5%	3.0°F	10 Hz	Bridle Temp. #1 Commutated at 30 SPS
38	Temperature	-90 to +210°F	5%	3.0°F	10 Hz	Bridle Temp. #2 Commutated at 30 SPS
39	Temperature	-90 to +210°F	5%	3.0°F	10 Hz	Bridle Temp. #3 Commutated at 30 SPS
40	Temperature	-90 to +210°F	5%	3.0°F	10 Hz	Cannister Temp. #1 Commu- tated at 30 SPS
41	Temperature	-90 to +210°F	5%	3.0°F	10 Hz	Cannister Temp. #2 Commu- tated at 30 SPS
42	Temperature	0 to +125°F	5%	1.5°F	10 Hz	Instr. Beam Temp. #1 Commutated at 30 SPS
43	Temperature	0 to +175°F	5%	2.0°F	10 Hz	Main Battery Temp. Commutated at 30 SPS

TABLE A-1 (CONTINUED)
BLDT Telemetry Measurement List

No.	Measurement	Range	Accuracy End-to-End	Resolution	Response	Remarks
44	Temperature	-100 to +150°F	5%	2.5°F	10 Hz	Rocket Mtr. Supp. Strt. Temp. Commutated at 30 SPS
45	Event	0 or 5 VDC	± 50 ms	HI/LO	10 Hz	Command Tone #1 Commu- tated at 30 SPS
46	Event	0 or 5 VDC	± 50 ms	HI/LO	10 Hz	Command Tone #2 Commu- tated at 30 SPS
47	Event	0 or 5 VDC	± 50 ms	HI/LO	10 Hz	Command Tone #3 Commu- tated at 30 SPS
48	Event	0 or 5 VDC	± 50 ms	HI/LO	10 Hz	Command Tone #4 Commu- tated at 30 SPS
49	Event	0 or 5 VDC	± 50 ms	HI/LO	10 Hz	Command Tone #5 Commu- tated at 30 SPS
50	Event	0 or 5 VDC	± 50 ms	HI/LO	10 Hz	Command Tone #6 Commu- tated at 30 SPS
51	Event	0 or 5 VDC	± 50 ms	HI/LO	10 Hz	Command Tone #7 Commu- tated at 30 SPS
52	Voltage	0 to 4 VDC	5%	0.04 VDC	10 Hz	Command Receiver A Signal Level Commutated at 30 SPS
53	Event	0 or 28 VDC 0.1 sec duration	± 50 ms	ON/OFF	10 Hz	Mortar Fire Commutated at 30 SPS
54	Temperature	+25 to 150°F	5%	1.5°F	10 Hz	Mortar Breech Flange Temp. Commutated at 30 SPS

TABLE A-1 (CONTINUED)
BLDT Telemetry Measurement List

No.	Measurement	Range	Accuracy End-to-End	Resolution	Response	Remarks
55	Temperature	0 to +175°F	5%	2.0°F	10 Hz	S-Band Transmitter Temp. Commuted at 30 SPS
56	Temperature	-100 to +150°F	5%	2.5°F	10 Hz	Aeroshell Temp. #1 Commuted at 30 SPS
57	Temperature	-100 to +150°F	5%	2.5°F	10 Hz	Aeroshell Temp. #2 Commuted at 30 SPS
58	Temperature	0 to +175°F	5%	2.0°F	10 Hz	Equipment Ballast Temp. Commuted at 30 SPS
59	Temperature	0 to +125°F	5%	1.5°F	10 Hz	Instrument Beam (#2) Temp. Commuted at 30 SPS
60	Temperature	0 to +125°F	5%	1.5°F	10 Hz	Gyro Temp. Commuted at 30 SPS
61	Temperature	-100 to +150°F	5%	2.5°F	10 Hz	Boost Motor #1 Temp. Commuted at 30 SPS
62	Temperature	-100 to +150°F	5%	2.5°F	10 Hz	Boost Motor #2 Temp. Commuted at 30 SPS
63	Voltage	0 to 4 VDC	5%	0.04 VDC	10 Hz	Command RCVR B Signal Level Commuted at 30 SPS
64	Voltage	5 VDC	5%	0.05 VDC	10 Hz	Commutator #2 Full Scale Calibration at 30 SPS
65	Voltage	0 VDC	5%	0.05 VDC	10 Hz	Commutator #2 Zero Scale Calibration at 30 SPS

APPENDIX B

DESCRIPTION OF BLDT

SYSTEM MISSION

APPENDIX B

A. Description of BLDT System Mission1. Purpose of the System

The BLDT System is designed to subject the Viking Decelerator System to Qualification Test Requirements at simulated Mars Entry atmospheric conditions.

2. System Requirements

The Viking Decelerator System earth atmospheric test conditions which result from consideration of the variation in probable Mars atmospheres are:

	<u>Supersonic Case 1</u>	<u>Supersonic Case 2</u>	<u>Transonic Case</u>	<u>Subsonic Case</u>
Peak Load Mach No.	2.17 ± 0.17	2.06 ± 0.16	1.15 ± 0.10	0.46 ± 0.03
Peak Load Dyn. Press. (PSF)	10.09 ± 0.57	9.39 ± 0.55	4.52 ± 0.30	6.46 ± 0.80
Angle of Attack at M/F (Degrees)	≤ 17	≤ 17	≤ 20	≤ 17

The design of the BLDT test bed is constrained by the Viking Lander Capsule design to the following:

- o Vehicle weight at mortar fire - 1888 pounds.
- o Cg offset in minus Z direction - 1.41 inches.
- o Vehicle external envelope similar to VLC (See Appendix A)
- o Decelerator Temperature at mortar fire - 80°F

3. System Description

The BLDT System design which evolved from the above test requirements provides for a large volume, high lift balloon system capable of floating the BLDT Vehicles at altitudes from which the test conditions can be achieved with reduced or no propulsion capability. The predicted test altitudes and balloon lift capability involved in the system design are:

	<u>Supersonic Case 1</u>	<u>Supersonic Case 2</u>	<u>Transonic Case</u>	<u>Subsonic Case</u>
* Balloon Float Altitude (FT)	119,000	119,000	120,500	92,000
* Decelerator Mortar Fire Alt. (FT)	147,800	148,600	137,500	89,300
BLDT Vehicle Launch Weight (LBS)	3,550	3,550	2,800	2,050

The system concept provides for the launch of the balloon/flight vehicle system from the Roswell Industrial Air Center, Roswell, New Mexico with the system ascending to float altitude during the approximately 100 mile westward flight to the White Sands Missile Range. Once over the range, the flight vehicle is released from the balloon load bar to complete its flight sequence.

For the powered flight tests, the vehicle concept provides for spin rotation of the vehicle prior to solid rocket motor boost to minimize thrust dispersion effects. Following the boost phase, the vehicle is despun and allowed to coast to the correct dynamic pressure condition. For the subsonic case, the vehicle is released from the load bar and allowed to free fall until the correct velocity is attained.

* USS62 Pressure Altitude

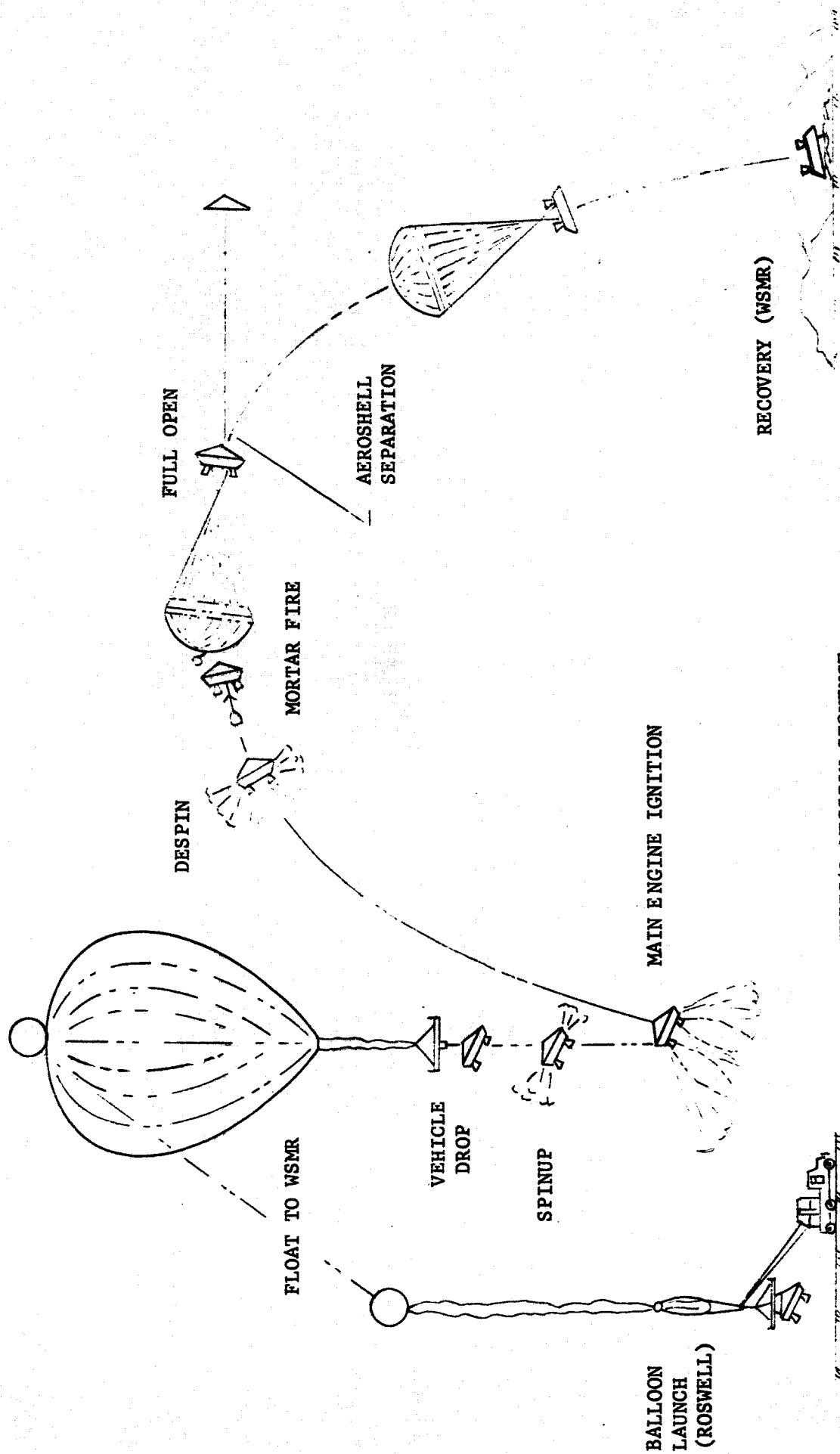
At the White Sands Missile Range, a ground computer system is programmed to receive tracking data which when integrated with predicted meteorological parameters provides the intelligence for the computer to issue a mortar fire command at the required test dynamic pressure for the powered flights. For the non-powered flight, the computer issues a timed mortar fire command following a delay for the correct velocity test conditions to be attained. In both powered and non-powered flights the vehicle incorporates an on-board programmer which provides a backup mortar fire command. Figure B-1 and B-2 depicted a typical powered and non-powered flight.

The system design includes all of the handling, checkout and control equipment necessary for prelaunch checkout, flight control and recovery of the system components.

4. Operations Description

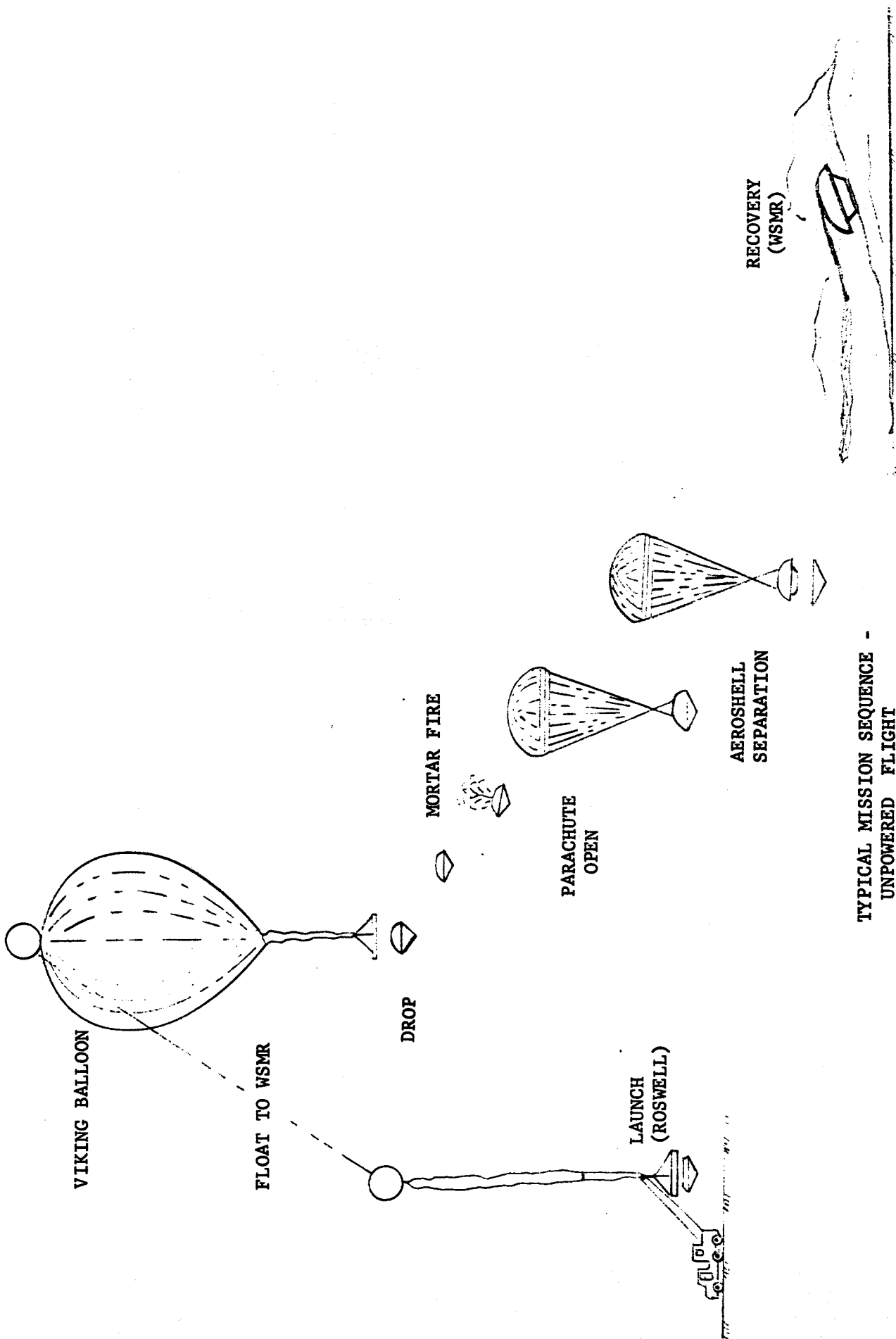
A typical sequence flow of the mission operations from assembly and checkout at Roswell, New Mexico through vehicle flight and recovery at WSMR, is shown in Figure B-3. Each of the sequence events is described below:

a. BLDT Vehicle Assembly and Checkout - This phase of the mission operation encompasses the assembly and checkout of the various system components. The BLDT vehicle, while connected to ground electrical power and in partially assembled condition, is subjected to subsystem and combined system testing in a close loop and open loop mode. The vehicle is then assembled including airborne batteries and subjected to a full flight readiness test on airborne power and in an open loop mode.



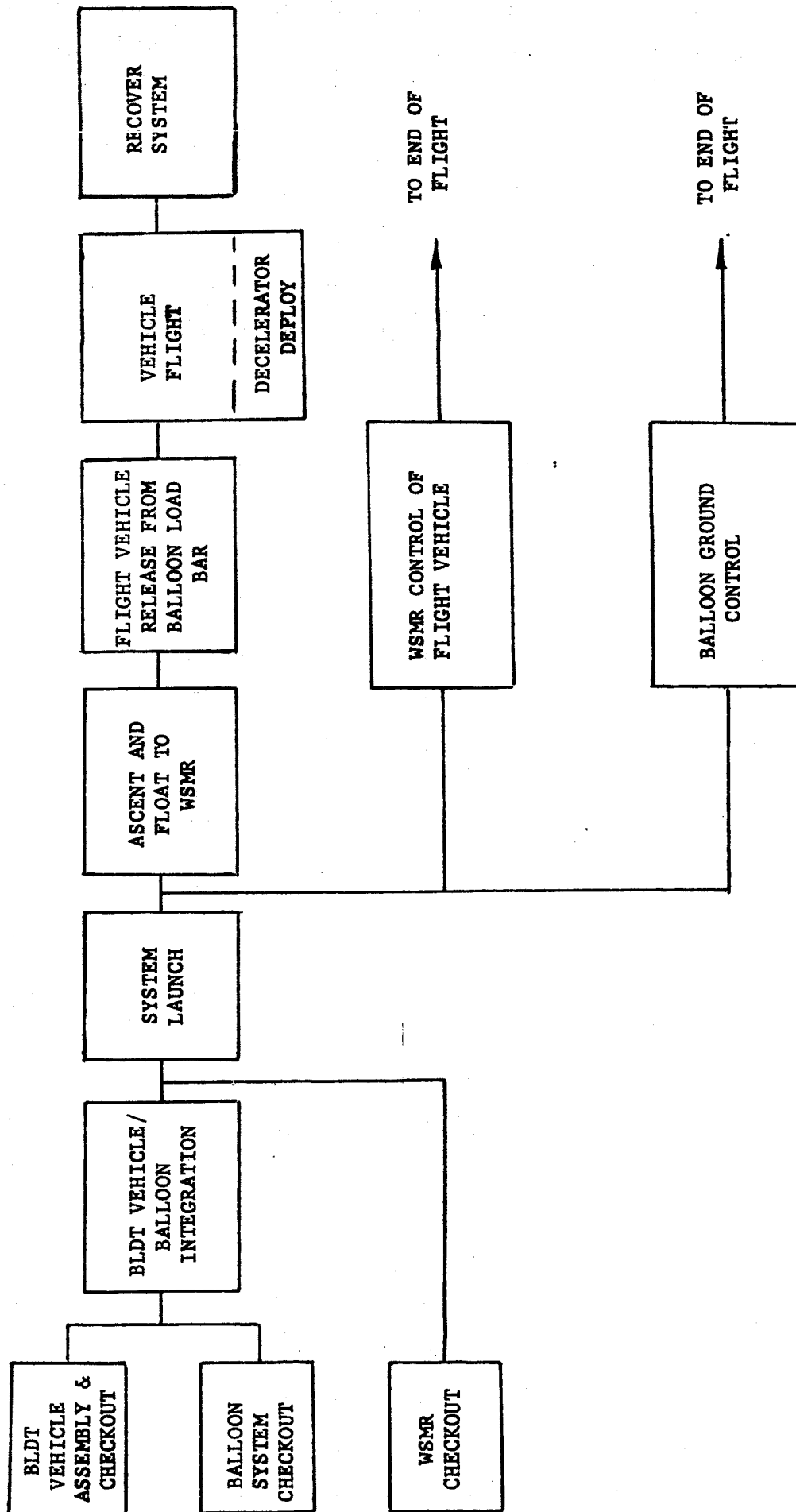
TYPICAL MISSION SEQUENCE -
POWERED FLIGHT

FIGURE B-1



TYPICAL MISSION SEQUENCE -
UNPOWERED FLIGHT

FIGURE B-2



TYPICAL OPERATIONS SEQUENCE

FIGURE B-3

While the flight vehicle is undergoing checkout and assembly, the balloon system is also being partially assembled and subjected to flight readiness testing. These checkout and assembly events were performed at the Roswell Industrial Air Center.

Coincident with the checkout of the flight system, the ground control system at the White Sands Missile Range is readied for the mission by assuring that:

- 1) The flight TM data is routed to the correct terminal data stations.
- 2) The ground command system is capable of transmitting acceptable commands.
- 3) The communications links are correctly activated.
- 4) The command station personnel are prepared to accept vehicle control.

b. BLDT Vehicle/Balloon Integration - When the prerequisite flight vehicle balloon system and WSMR Control Center checkout are completed and the meteorological constraints at the launch site and WSMR (Launch winds, float winds, local weather, etc.) are satisfactory, the flight vehicle and balloon systems are moved from the checkout hanger to the launch runway where system integration and final checkout is made.

The flight vehicle is connected to ground power and final subsystem testing is completed to assure all subsystems are functioning. The vehicle ordnance is electrically connected and the vehicle access panels are installed. In this time period the launch balloon and float balloon are layed-out and integrated with the flight vehicle, the abort recovery cargo chutes, the balloon winch and the launch crane.

When the system integration is completed, the launch stand is removed from the flight vehicle leaving the flight vehicle suspended from the balloon load bar which in turn is suspended from the launch crane. Also, the launch balloon is filled with a precisely metered quantity of helium.

c. System Launch - Following the integration of the flight vehicle and balloon into the BLDT system, the system is ready for launch.

The launch process begins with a ground winching operation in which the launch balloon is permitted to rise and which upon rising takes the float balloon (uninflated) and the cargo abort chutes from a horizontal attitude to a vertical attitude above the launch crane. Once the system is in the vertical attitude, the winch cable is separated from the balloon system through the use of an ordnance device. At this point, the two balloons with the abort cargo chutes are floating above and tethered to the launch crane with the balloon load bar and flight vehicle suspended from the crane beneath the tethered balloon. At this point, the total system for a powered flight extend from ground level to approximately 1000 feet above ground level (800 feet for a non-powered flight).

With all of the preceeding operations complete, it only remains to release the flight system from the launch crane. To do this, the launch crane is driven down wind at a velocity necessary to position the crane approximately under the balloon at which point the crane release device is actuated and the balloon floats free of the ground system taking with it the balloon load bar and flight vehicle.

d. Ascent and Float Phase - During the ascent and float phase, the balloon system, floating freely, responds to the wind directions and velocities encountered as it ascends to the design float altitude. Generally, once clear of low altitude wind influence, the balloons float in a westerly direction intersecting the WSMR at about mid-range.

As the system ascends, the helium which was loaded in the launch balloon is forced down into the float balloon which slowly inflates the float balloon and causes the system to ascend. This process continues until the float balloon becomes fully inflated at which point no further lift can be obtained. The balloon ascent to float altitude is rapid enough to arrive at the float altitude prior to intersecting the WSMR.

The balloon ascent and direction is somewhat controllable through the use of ballast dumping operations to control floating altitude and rise rates in order to take advantage of winds at the upper levels. The control of the balloon during the ascent and float phase is from the Air Force Cambridge Research Laboratory control center at Holloman Air Force Base, Alamogordo, New Mexico.

When the ascending system passes through approximately 30 K feet, the WSMR tracking radar, command networks and TM receiving stations are able to acquire the flight vehicle and start checkout. Part of the float checkout assures operation of the command nets by sending commands which do not change vehicle configuration (i.e. safe ordnance circuits, turn R.F. on, etc.) and verifying receipt of the commands through flight vehicle TM data being received at the control center.

e. Vehicle Release from Load Bar - Once the BLDT system reaches the proper float altitude and intersects the range, the vehicle ordnance circuits are armed, the vehicle flight azimuth is attained using a cold gas pointing system and the vehicle release from the load bar is commanded. All of these functions occur as a result of ground commands issued by the flight vehicle control crew at WSMR.

f. Vehicle Flight - The vehicle flight events are a function of the type of mission being flown. Table B-1 presents a sequence of

events and event times for the Supersonic, Transonic and Subsonic missions. All of the event times in Table B-1 are times from release of the flight vehicle from the balloon load bar with the exception of the ground mortar fire command for the powered flights. This command is time variable and is issued by the ground computer during the vehicle coast following despin when the vehicle achieves the correct dynamic pressure.

For the powered flights following release of the vehicle from the load bar, the vehicle is under control of the redundant airborne programmers with the exception of the issuance of the decelerator mortar fire. The vehicle functions provide a flight profile as shown in Figures B-1 and B-2.

During the vehicle powered flights, the vehicle is tracked by the WSMR tracking devices to provide the ground computer with the intelligence for issuing the mortar fire command. For all flights, tracking devices provide data for post flight analysis and to support vehicle recovery operations.

For the non-powered, free fall mission, the vehicle functions are commanded by the on-board redundant programmers except for the mortar fire which is issued as a timed output from the ground computer.

g. Recovery Operations - During this phase of the mission, all of the system components are located and moved to WSMR facilities for post flight inspection. Also during this phase the various system cameras are recovered and the film processed for post flight analysis.

TABLE B-1

VEHICLE FLIGHT SEQUENCE OF EVENTS

SUPERSONIC

<u>CASE 1</u>		<u>CASE 2</u>		<u>TRANSONIC</u>	<u>SUBSONIC</u>	<u>FUNCTION</u>	<u>SOURCE</u>
$T_D - 30$ min.	$T_D - 30$ min.	$T_D - 30$ min.	Drop - 30 min.	Drop - 30 min.	Drop - 30 min.	Attain Float Altitude	--
$T_D - 10$ min.	$T_D - 10$ min.	$T_D - 10$ min.	$T_D - 10$ min.	$T_D - 10$ min.	--	Start Azimuth Pointing	Ground Command
$T_D - 5$ min.	$T_D - 5$ min.	$T_D - 5$ min.	$T_D - 5$ min.	$T_D - 5$ min.	$T_D - 5$ min.	Arm Ordnance Bus	Ground Command
$T_D - 10$ sec.	$T_D - 10$ sec.	$T_D - 10$ sec.	$T_D - 10$ sec.	$T_D - 10$ sec.	--	Confirm Drop Azimuth	A/B T/M
T_D	T_D	T_D	T_D	T_D	T_D	Drop from Load Bar. Initiate A/B Programmer.	Ground Command
$T_D + 1$ sec.	$T_D + 1$ sec.	$T_D + 1$ sec.	$T_D + 1$ sec.	$T_D + 1$ sec.	--	Ignite Spin Motors/ Enable Boost Motor	A/B Programmer
$T_D + 2$ sec.	$T_D + 2$ sec.	$T_D + 2$ sec.	$T_D + 2$ sec.	$T_D + 2$ sec.	--	Ignite Boost Motors	A/B Programmer
--	--	--	--	--	$T_D + 12$ sec.	Start AFT Looking Camera, Enable Mortar	A/B Programmer
--	--	--	--	--	$T_D + 16$ sec.	Initiate Mortar Fire/ Start AFT Hi-Speed Camera	Ground Command
--	--	--	--	--	$T_D + 18$ sec.	Initiate M/F Backup	A/B Programmer
--	--	--	--	--	$T_D + 30$ sec.	Separate Aeroshell	A/B Programmer
$T_D + 33$ sec.	$T_D + 33$ sec.	$T_D + 33$ sec.	$T_D + 33$ sec.	$T_D + 33$ sec.	--	Ignite Despin Motors/ Release Camera Lens Covers/Start AFT Camera Enable Mortar	A/B Programmer
T_D (q cond. correct)	T_D (q cond. correct)	T_D (q cond. correct)	T_D (q cond. correct)	T_D (q cond. correct)	--	Initiate Decelerator Mortar Fire/Start AFT Hi-Speed Camera	Ground Command
$T_D + 37$ sec.	$T_D + 38$ sec.	$T_D + 38$ sec.	$T_D + 39$ sec.	$T_D + 39$ sec.	--	Initiate M/F Backup	A/B Programmer
$T_D + 47.6$ sec.	$T_D + 47.6$ sec.	$T_D + 47.6$ sec.	$T_D + 47$ sec.	$T_D + 47$ sec.	--	Separate Aeroshell	A/B Programmer

APPENDIX C

GAC POST-TEST INSPECTION

Excerpts from GAC Report No. RSE 20926-17

GAC POST-TEST INSPECTION

Viking decelerator system S/N 15 was flown as BLDT 2 (AV-2). This system incorporated S/N 16 parachute. The following constitutes the post flight inspection report.

Chute Canopy - The damage chart is presented in Figure C-1. As noted on the chart, several small black smudges are evident on various gores, primarily in the band (See Figure C-2). Most of the smudges are located in the mid-gore region. There is no evidence of excessive heat associated with the smudges. A hole, approximately 1/8 inch, is located in gore 17, panel F of the band (See Figure C-3).

Suspension Lines - No damage.

Deployment Bag - The outer surface of the deployment bag is blackened. No damage is in evidence.

Buffer - The quartz facing of the buffer is torn (approximately 1 inch) at each of the tie locations. The facing in the center of the buffer is torn at the points where the filler block is attached.

Filler Block - The filler block is missing.

Bridle Legs - The bridle legs are undamaged. Most of the basting stitches are broken. The bridle legs are blackened.

Cover Thermal Protection - Some random ruptures of the quartz facing are in evidence. The segments are blackened.

Bridle Leg Covers - The covers are blackened. No apparent damage.

Mortar - The inside of the mortar tube is blackened. The straps at the top of the mortar are all intact. The choker cord is fused to two of the straps. There is no apparent damage to the mortar.

Sabot - The sabot is blackened on the outer surface. The Teflon and stainless steel discs are still attached. The sabot retention straps are blackened but intact.

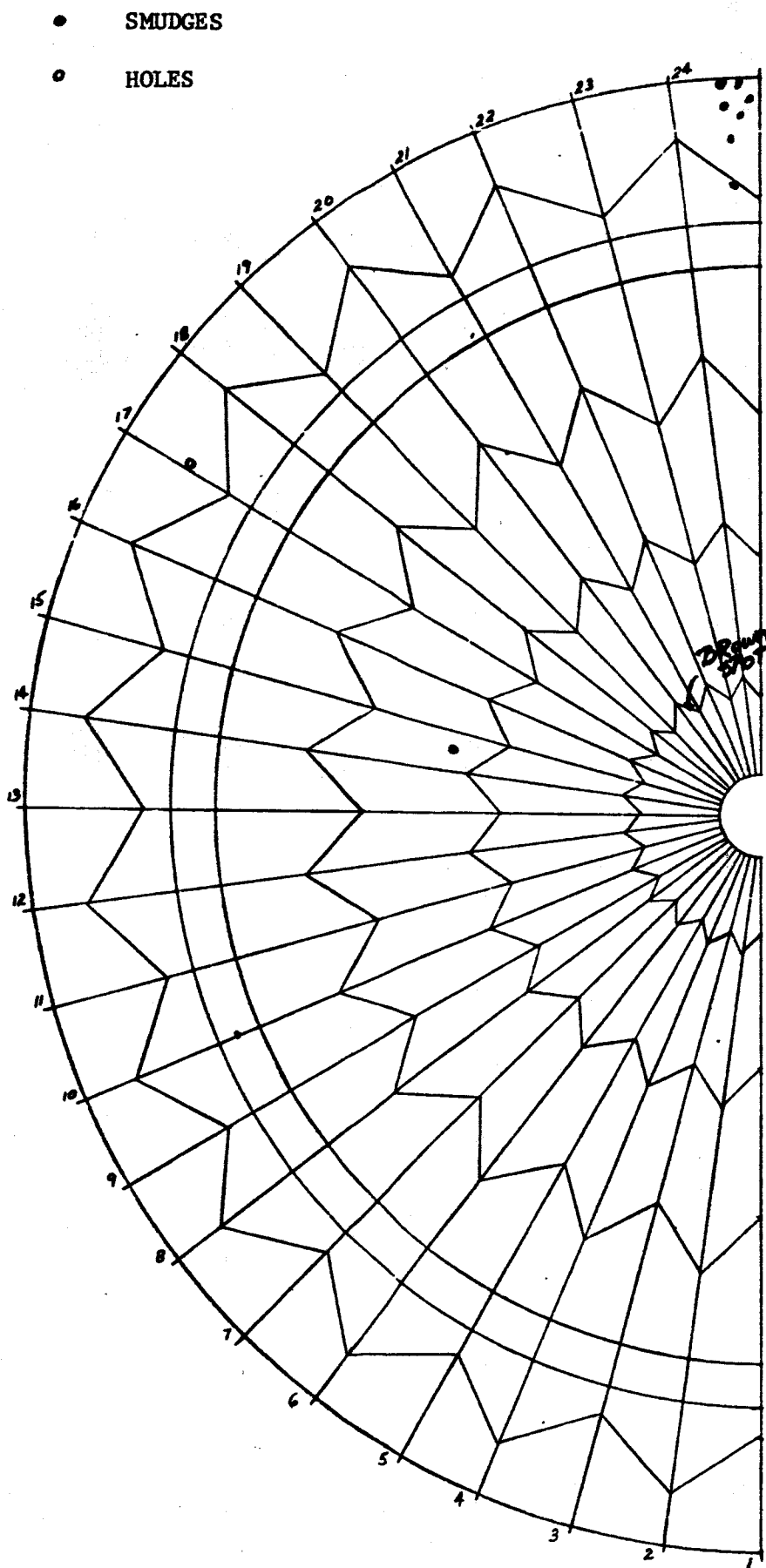


FIGURE C-1 PARACHUTE DAMAGE CHART

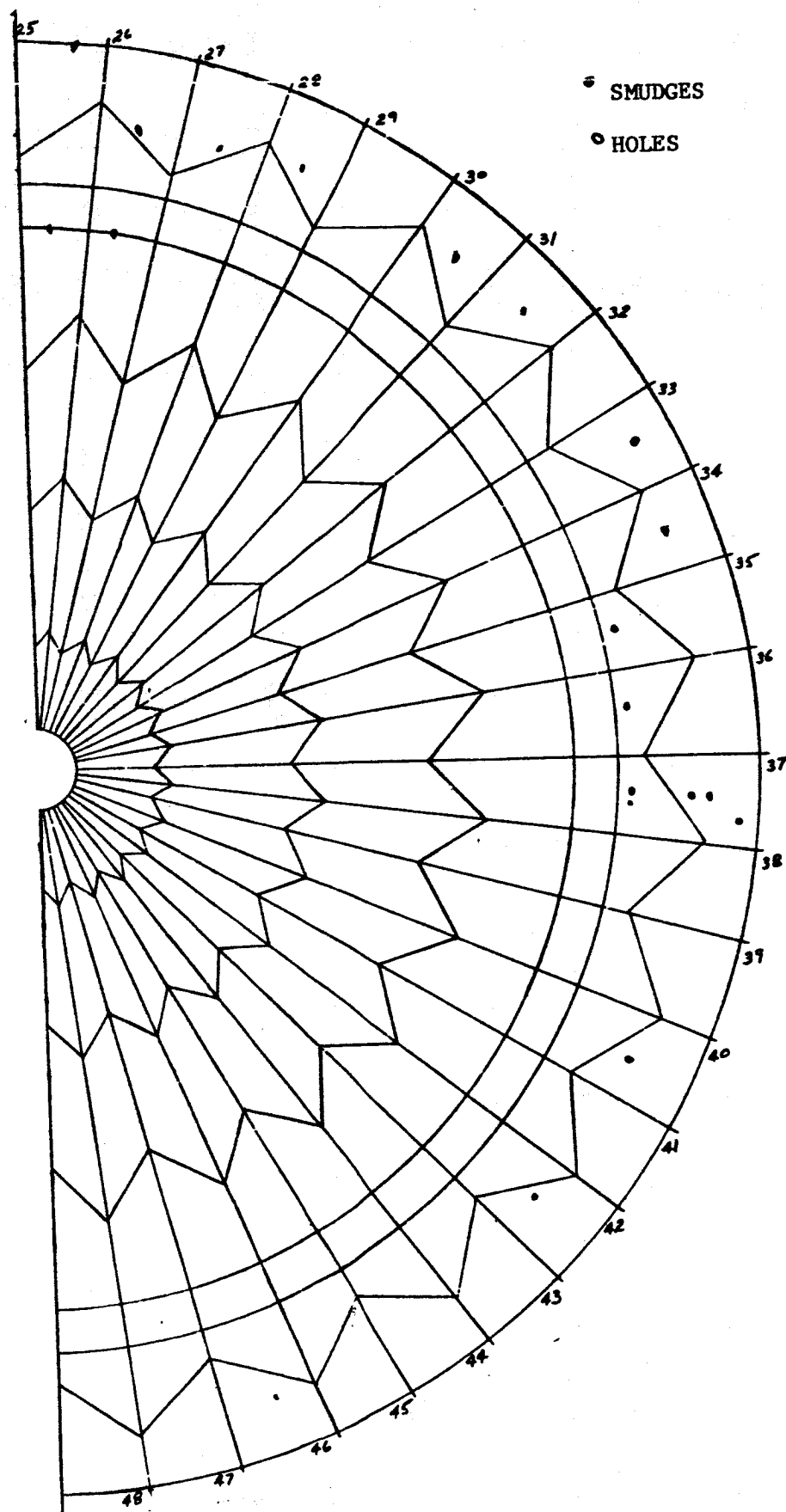


FIGURE C-1 (Continued)



FIGURE C-2 BLACK SMUDGES ON S/N 16 CHUTE

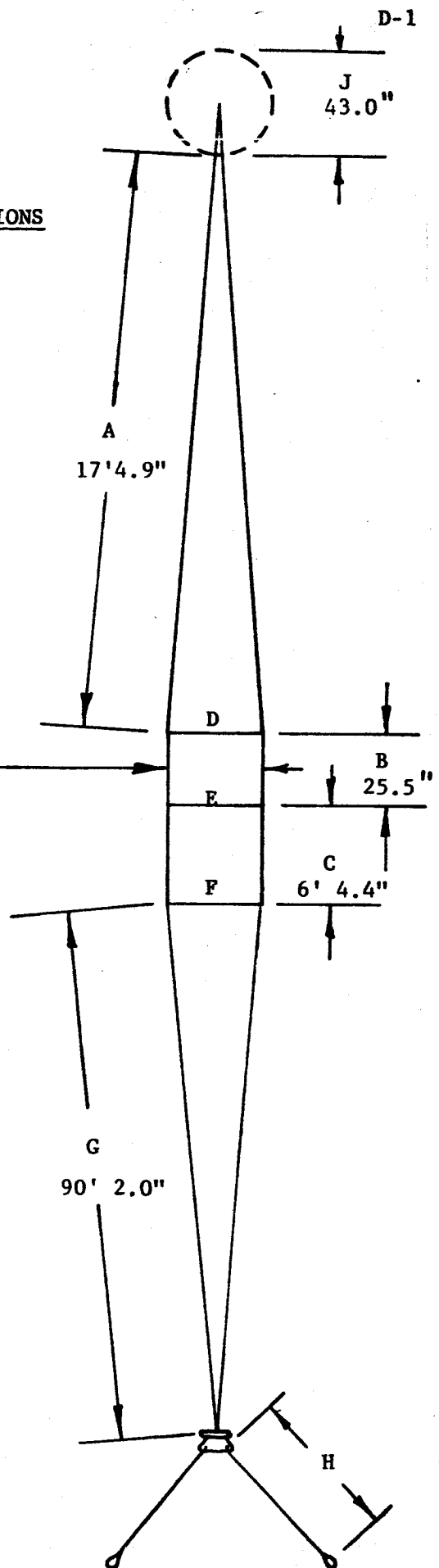
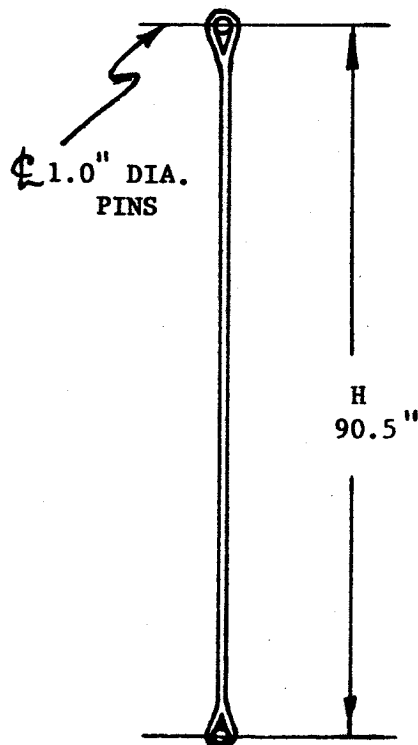
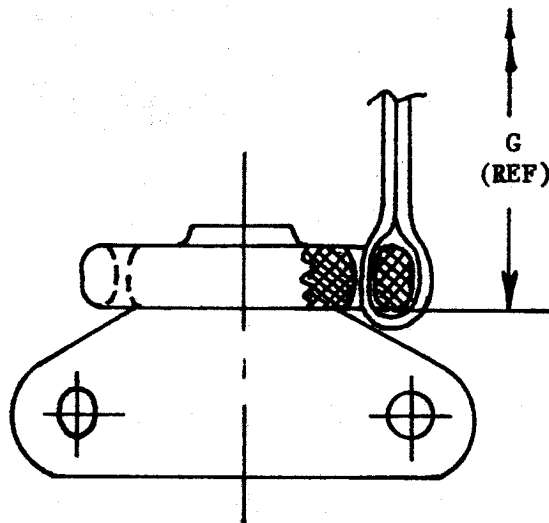


FIGURE C-3 SMALL HOLE IN GORE 17 OF S/N 16 CHUTE

APPENDIX D

PARACHUTE DIMENSIONS

30.3" D-DISK
E-BAND
F-BAND
BETWEEN RADIAL SHOWN
AND NEXT HIGHER NO.



PRE-FLIGHT AV-2

<u>RADIAL NO</u>	<u>A(DISC) FT-INCHES</u>	<u>B(GAP) INCHES</u>	<u>C(BAND) INCHES</u>	<u>D(DISC) INCHES</u>	<u>E(BAND) INCHES</u>	<u>F(BAND) INCHES</u>	<u>G(SUSP) FT-INCHES</u>
1	17-3	25-1/4	75-3/8	30	30-1/4	30-3/8	90-2 1/2
2	3 3/4	1/4	5/16	30-7/16	3/8	3/16	2 1/2
3	4 1/4	1/4	5/16	1/16	1/4	3/8	2 1/2
4	3 3/4	1/4	1/4	1/2	3/16	1/2	1 3/4
5	3 5/8	1/4	1/4	30	1/4	3/16	2
6	3 3/4	5/16	1/2	1/4	3/8	1/2	1 3/4
7	3 7/8	1/4	3/8	1/4	3/8	1/4	2
8	4 3/16	1/4	3/8	1/8	5/16	3/16	2 1/4
9	3 1/2	3/8	1/2	5/16	3/16	1/2	2 1/4
10	4	1/4	1/2	3/8	5/16	3/8	2 3/8
11	4	5/16	1/2	1/16	3/16	1/16	2 1/4
12	4 1/8	1/4	3/8	3/16	1/4	5/16	2 1/4
13	4	1/4	3/8	3/8	1/4	1/4	2 1/2
14	4 1/4	1/4	1/8	1/4	1/2	3/16	2 1/4
15	4	1/4	1/2	1/4	1/8	3/8	2 1/2
16	3 7/8	5/16	5/16	7/16	3/16	3/16	2 3/8
17	3 3/8	1/4	5/8	3/16	3/8	1/2	2 1/2
18	4 1/4	1/4	3/8	1/2	1/4	5/16	2 5/8
19	4	3/8	1/2	5/16	3/16	1/2	2 1/2
20	3 3/4	1/4	1/4	5/16	1/4	3/16	2 1/8
21	4 1/4	5/16	3/8	1/8	3/16	1/2	2
22	4 1/16	1/4	5/16	5/8	5/16	1/4	2 1/4
23	3 3/4	1/4	1/4	29-7/8	1/4	3/16	2 1/4
24	3 5/8	1/4	3/16	30-5/8	1/8	1/8	2

PRE-FLIGHT AV-2 (CONTINUED)

<u>RADIAL NO</u>	<u>A(DISC) FT-INCHES</u>	<u>B(GAP) INCHES</u>	<u>C(BAND) INCHES</u>	<u>D(DISC) INCHES</u>	<u>E(BAND) INCHES</u>	<u>F(BAND) INCHES</u>	<u>G(SUSP) FT-INCHES</u>
25	17-31/2	25-1/4	75-5/16	30-1/4	30-5/16	30-5/8	90-2
26	33/4	5/16	1/8	1/2	30	7/16	2 1/8
27	315/16	1/4	5/16	1/4	30-5/16	3/8	2 1/8
28	31/2	1/4	1/2	1/4	1/2	7/16	2
29	31/4	3/8	3/8	1/8	1/8	1/16	2 1/8
30	31/2	1/4	3/16	9/16	1/4	7/16	2
31	3	1/4	3/8	1/4	5/16	3/16	2 1/8
32	35/8	5/16	3/8	7/16	3/16	3/8	2
33	31/4	5/16	3/8	1/8	1/4	3/16	13/4
34	35/8	1/4	5/16	3/8	5/8	1/2	13/4
35	31/4	1/4	5/16	3/16	1/4	3/8	13/4
36	31/4	5/16	1/8	1/2	1/4	3/16	1 1/2
37	41/8	1/4	5/8	1/4	5/16	1/2	2
38	41/8	1/4	3/8	1/4	5/16	3/16	2 1/8
39	35/8	3/8	1/4	3/16	1/4	1/2	2
40	4	1/4	5/16	1/4	1/4	1/8	2 1/4
41	43/4	1/4	1/2	3/4	3/16	1/4	2 1/8
42	4 1/2	1/4	3/8	1/8	1/4	1/4	2 3/8
43	3 1/8	5/16	1/4	1/8	3/16	1/4	2
44	35/8	5/16	1/8	1/4	3/8	3/8	2 1/8
45	45/8	3/8	3/4	3/8	1/8	7/16	2 1/8
46	33/4	1/4	5/16	30	3/8	1/8	2 1/4
47	4	5/16	3/8	9/16	1/4	1/2	2
48	33/4	1/4	1/2	9/16	1/8	1/4	2 1/4

PRE-FLIGHT AV-2 (CONTINUED)

			VENT DIAMETER		
BRIDLE LEG	H	- INCHES	RADIAL	J	- INCHES
S/N 49	90 ⁵ / ₈		1/25	42	
S/N 50	90 ⁵ / ₈		7/31	42	
S/N 51	90 ¹ / ₂		13/37	42	
			19/43	42	

POST-TEST AV-2

<u>RADIAL NO</u>	<u>A (DISC) FT-INCHES</u>	<u>B (GAP) INCHES</u>	<u>C (BAND) INCHES</u>	<u>D (DISC) INCHES</u>	<u>E (BAND) INCHES</u>	<u>F (BAND) INCHES</u>	<u>G (SUSP) FT-INCHES</u>
1	17-3 ¹ / ₄	25-1 ¹ / ₄	75-3 ³ / ₄	29-7 ⁷ / ₈	30-1 ¹ / ₈	30-1 ¹ / ₄	88-11
2	4	3 ³ / ₈	1 ¹ / ₂	30-3 ³ / ₈	30-1 ¹ / ₄	30	101 ¹ / ₂
3	5	1 ¹ / ₄	3 ³ / ₄	30	1 ¹ / ₈	30-1 ¹ / ₈	11
4	4 ¹ / ₂	1 ¹ / ₄	1 ¹ / ₂	30-3 ³ / ₈	1 ¹ / ₁₆	1 ¹ / ₄	10
5	4 ³ / ₄	1 ¹ / ₄	1 ¹ / ₂	30	30	30	11
6	5 ¹ / ₂	1 ¹ / ₄	76	30-3 ³ / ₁₆	30-3 ³ / ₁₆	30-1 ¹ / ₄	101 ¹ / ₂
7	5 ¹ / ₄	1 ¹ / ₄	75-3 ³ / ₄	1 ¹ / ₈	1 ¹ / ₄	1 ¹ / ₈	11
8	5 ³ / ₄	1 ¹ / ₄	76	30-	3 ³ / ₁₆	30	11 ¹ / ₂
9	4 ¹ / ₄	25	75-3 ³ / ₄	30-1 ¹ / ₄	1 ¹ / ₁₆	30-3 ³ / ₈	11 ¹ / ₂
10	5	25-1 ¹ / ₄	3 ³ / ₄	1 ¹ / ₄	3 ³ / ₁₆	1 ¹ / ₄	11
11	5	1 ¹ / ₄	3 ³ / ₄	30	30	30	11
12	5	1 ¹ / ₄	3 ³ / ₄	30-1 ¹ / ₈	30-1 ¹ / ₁₆	30-1 ¹ / ₈	101 ¹ / ₂
13	4 ¹ / ₂	1 ¹ / ₄	3 ³ / ₄	1 ¹ / ₈	1 ¹ / ₁₆	1 ¹ / ₈	11
14	5 ¹ / ₂	3 ³ / ₈	3 ³ / ₄	3 ³ / ₁₆	3 ³ / ₈	30	101 ¹ / ₂
15	5	1 ¹ / ₄	3 ³ / ₄	1 ¹ / ₁₆	30	30-1 ¹ / ₈	11
16	4 ¹ / ₂	1 ¹ / ₄	1 ¹ / ₂	3 ³ / ₈	30-1 ¹ / ₁₆	30	11
17	5	1 ¹ / ₄	76	1 ¹ / ₈	1 ¹ / ₄	30-1 ¹ / ₄	101 ¹ / ₂
18	5 ¹ / ₂	1 ¹ / ₄	76	3 ³ / ₈	1 ¹ / ₈	30	11
19	5	1 ¹ / ₄	75-3 ³ / ₄	1 ¹ / ₄	1 ¹ / ₁₆	3 ³ / ₁₆	101 ¹ / ₂
20	5	1 ¹ / ₄	3 ³ / ₄	1 ¹ / ₄	1 ¹ / ₈	30	101 ¹ / ₂
21	5 ¹ / ₂	1 ¹ / ₄	76	1 ¹ / ₈	30	30-1 ¹ / ₄	101 ¹ / ₂
22	5	1 ¹ / ₄	75-3 ³ / ₄	5 ⁵ / ₈	30-1 ¹ / ₈	30	101 ¹ / ₂
23	5	3 ³ / ₈	76	29-7 ⁷ / ₈	1 ¹ / ₈	30	5
24	4 ³ / ₄	1 ¹ / ₄	75-3 ³ / ₄	1 ¹ / ₂	30	30	5

POST-TEST AV-2 (CONTINUED)

<u>RADIAL NO</u>	<u>A(DISC) FT-INCHES</u>	<u>B(GAP) INCHES</u>	<u>C(BAND) INCHES</u>	<u>D(DISC) INCHES</u>	<u>E(BAND) INCHES</u>	<u>F(BAND) INCHES</u>	<u>G(SUSP) FT-INCHES</u>
25	17-4 ³ / ₄	25-1 ¹ / ₄	75-3 ³ / ₄	30-3 ³ / ₁₆	30-1 ¹ / ₈	30-3 ³ / ₈	88-5
26	4 ¹ / ₂	1 ¹ / ₄	3 ¹ / ₄	3 ¹ / ₈	29-7 ⁷ / ₈	30-1 ¹ / ₈	5 ¹ / ₄
27	5	1 ¹ / ₄	3 ¹ / ₄	1 ¹ / ₈	30-3 ³ / ₁₆	1 ¹ / ₈	4 ¹ / ₂
28	4 ³ / ₄	1 ¹ / ₄	3 ¹ / ₄	3 ¹ / ₈	30-3 ³ / ₈	1 ¹ / ₈	5 ¹ / ₂
29	5	1 ¹ / ₄	76	30	30-1 ¹ / ₁₆	29-7 ⁷ / ₈	4
30	5	1 ¹ / ₄	76	30-3 ³ / ₈	1 ¹ / ₈	30-1 ¹ / ₈	4 ¹ / ₂
31	4	1 ¹ / ₄	75-3 ³ / ₄	1 ¹ / ₈	1 ¹ / ₈	29-7 ⁷ / ₈	4 ¹ / ₂
32	5	1 ¹ / ₄	3 ¹ / ₄	1 ¹ / ₄	1 ¹ / ₁₆	30	4 ¹ / ₂
33	4 ¹ / ₂	1 ¹ / ₄	7 ¹ / ₈	1 ¹ / ₈	30	30-1 ¹ / ₈	4
34	5	1 ¹ / ₄	7 ¹ / ₈	1 ¹ / ₄	30-1 ¹ / ₈	3 ¹ / ₈	4 ¹ / ₄
35	4 ¹ / ₄	1 ¹ / ₄	3 ¹ / ₄	1 ¹ / ₈	1 ¹ / ₁₆	1 ¹ / ₄	4 ¹ / ₄
36	5	1 ¹ / ₄	3 ¹ / ₄	1 ¹ / ₄	1 ¹ / ₈	30	4
37	4 ³ / ₄	1 ¹ / ₄	3 ¹ / ₄	3 ¹ / ₁₆	30	30-1 ¹ / ₈	7
38	5 ¹ / ₄	3 ¹ / ₈	3 ¹ / ₄	3 ¹ / ₁₆	30-1 ¹ / ₈	30	6 ¹ / ₂
39	4 ³ / ₄	1 ¹ / ₄	3 ¹ / ₄	1 ¹ / ₈	1 ¹ / ₈	30-3 ³ / ₈	4
40	4 ¹ / ₄	1 ¹ / ₄	3 ¹ / ₄	3 ¹ / ₁₆	1 ¹ / ₈	30	4
41	5	3 ¹ / ₈	3 ¹ / ₄	5 ¹ / ₈	1 ¹ / ₈	30-1 ¹ / ₈	8
42	5 ¹ / ₄	1 ¹ / ₄	3 ¹ / ₄	30	1 ¹ / ₈	30	8 ¹ / ₂
43	4 ³ / ₄	1 ¹ / ₄	3 ¹ / ₄	30-1 ¹ / ₁₆	1 ¹ / ₈	30-1 ¹ / ₈	9 ³ / ₄
44	5 ¹ / ₄	1 ¹ / ₄	7 ¹ / ₈	1 ¹ / ₈	30	1 ¹ / ₄	10
45	4 ⁷ / ₈	1 ¹ / ₄	7 ¹ / ₈	1 ¹ / ₄	30	1 ¹ / ₄	10
46	4 ¹ / ₄	1 ¹ / ₄	3 ¹ / ₄	29-7 ⁷ / ₈	30-1 ¹ / ₄	30	10
47	4 ¹ / ₂	1 ¹ / ₄	7 ¹ / ₈	30-3 ³ / ₈	1 ¹ / ₄	30-1 ¹ / ₂	10 ¹ / ₄
48	4 ¹ / ₂	1 ¹ / ₄	1 ¹ / ₂	3 ¹ / ₈	30	1 ¹ / ₈	10 ¹ / ₂

POST-FLIGHT AV-2 (CONTINUED)

BRIDLE LEG	H	- INCHES	VENT DIAMETER	
			RADIAL	J - INCHES
S/N 49	91	$\frac{1}{4}$	1/25	42 $\frac{1}{4}$
S/N 50	91	$\frac{1}{4}$	7/31	42 $\frac{3}{8}$
S/N 51	91	$\frac{1}{4}$	13/37	42 $\frac{3}{8}$
			19/43	42 $\frac{1}{2}$

APPENDIX E

BLDT COMPUTER SOFTWARE

I. PURPOSE

The control of the Balloon Launch Decelerator Test Flights at WSMR was aided through computer predictions and operations. It was the responsibility of WSMR (RTDS) personnel to develop computer software necessary to fulfill operational requirements imposed by MMC and constraints imposed by Range Safety. The purpose of this appendix is to discuss the real time computer software needed at WSMR for the BLDT mission and, in particular, describe the software furnished by MMC. The major software functions were to:

- Predict impact of flight/payload components
- Issue a precision, real time decelerator mortar fire command
- Generate real time flight information

In support of the above requirements, the following computer programs were developed by MMC for WSMR implementation:

- Vehicle Flight Azimuth Program
- Vehicle Impact Prediction Program
- Decelerator Mortar Fire Command Program

II. VEHICLE FLIGHT AZIMUTH PROGRAM

A. Program Requirements

For the BLDT powered flights, it was a Range Safety requirement that the vehicle drop azimuth be such that the vehicle, or any separated components, impact within prescribed areas of the range under all flight and failure modes including failure of the qualification decelerator to deploy. Since the failure of the decelerator to deploy results in trajectories which are greater than the width of the White Sands Missile Range, it was necessary to control vehicle flight azimuth for a period of time prior to and at release from the balloon load bar in order to assure range impact for system components and provide Range Safety with real time vehicle and separated component impact predictions.

In order to comply with the above azimuth control requirement, the Vehicle Flight Azimuth Program was generated. This program processed airborne telemetry data from a set of on-board magnetometers to provide continuous control center displays of the vehicle heading and rotational rates as well as to provide input to the Vehicle Impact Prediction Program. The real time displays of the vehicle heading and rotational rates, coupled with an airborne gas thruster impulse system, provided the necessary means for vehicle azimuth control.

B. Program Implementation

The azimuth program utilizes the telemetry output of an airborne magnetic sensing system consisting of two magnetic field sensors oriented 90° apart and mounted so as to sense only the horizontal component of the

earth's magnetic field. When the vehicle, while still connected to the balloon load bar, is rotated through a 360° arc, the output from the magnetometers provides sinusoidal curves with a 90° phase shift as shown on Figure E-1. These data are sufficient to establish the vehicle heading.

The equations for computing the vehicle heading (θ) from the TM magnetometer data is:

$$(1) \quad \theta = \tan^{-1} \left(\frac{B_2 - Y}{X - B_1} \right) + \theta_I \text{ where:}$$

θ is the heading from true north

X is the voltage from Probe 1

Y is the voltage from Probe 2

B_1 is the voltage reading of Probe 1 when perpendicular to the magnetic field.

B_2 is the voltage reading of Probe 2 when perpendicular to the magnetic field.

θ_I is a constant which combines the corrections for installation alignment and the difference between true and magnetic north.

The above equation was derived from the following relationship:

$$(2) \quad X = R \cos (\theta + \theta_I) + B_1$$

$$(3) \quad Y = R \sin (\theta + \theta_I) + B_2 \text{ where}$$

R represents the horizontal component of magnetic field strength which varies slightly with altitude.

Each vehicle was rotated over a compass rose where the magnetometer data were recorded at incremental headings from true north to provide calibration data for B_1 , B_2 and θ_I . The actual calibration values were obtained by a least square fitting of equation (2) and (3) above.

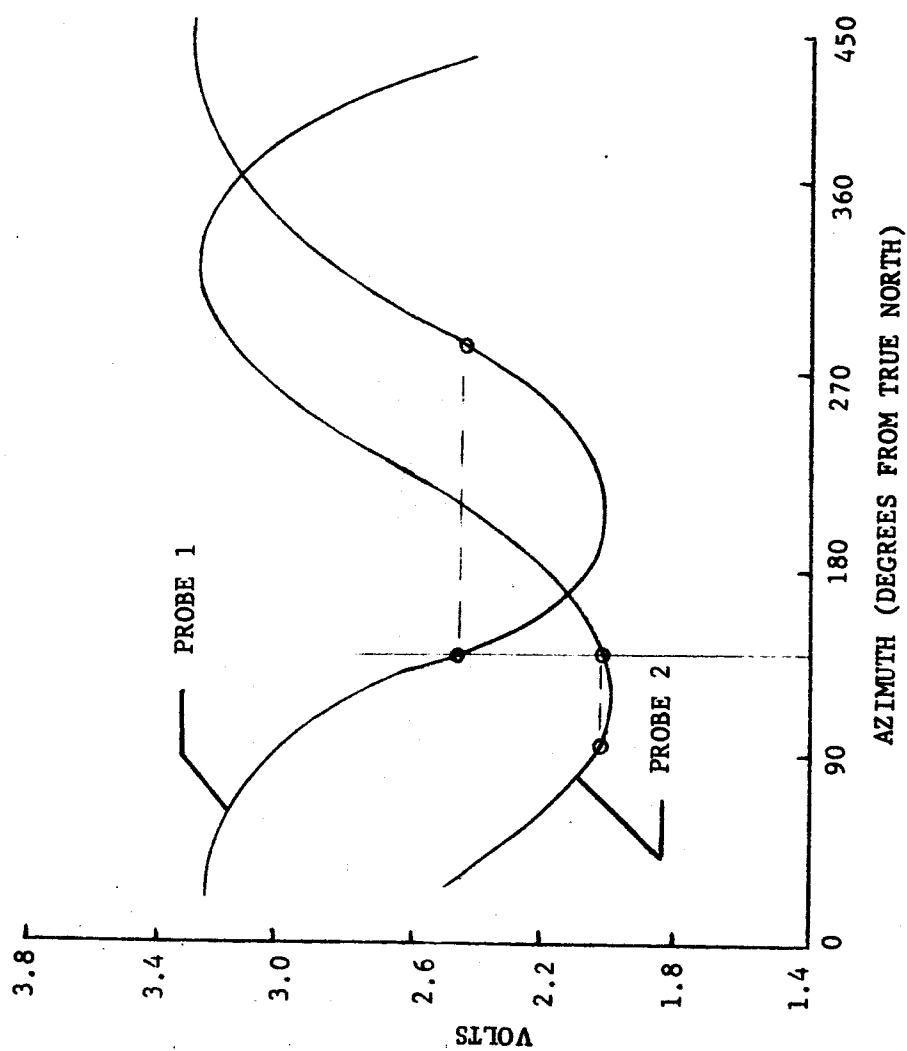
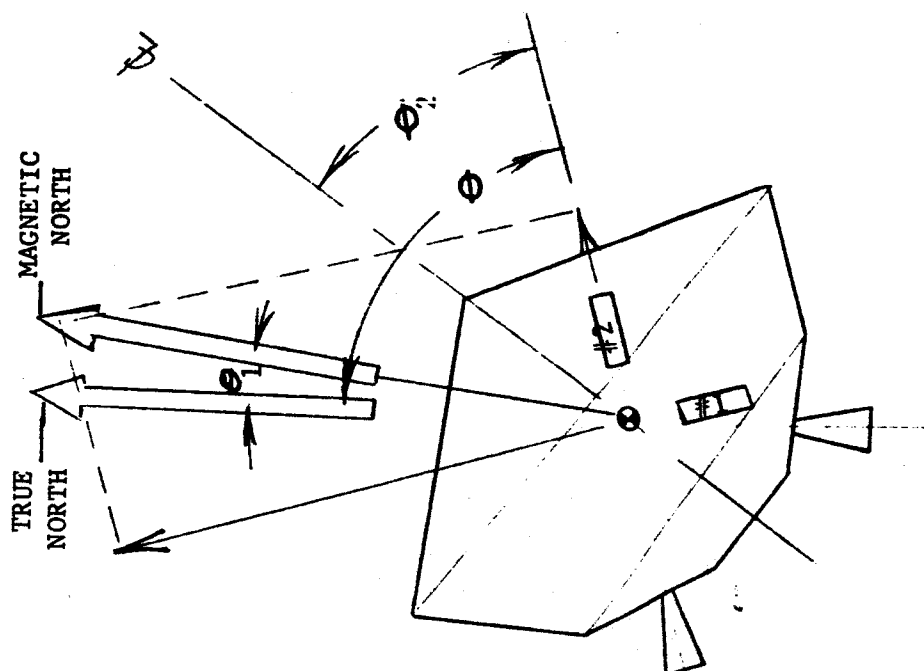


FIGURE E-1 MAGNETOMETER OUTPUT

Using the above calibration values and the TM values for X and Y, the vehicle heading can be computed using equations (1), (2), and (3). Equation (1) which uses input from both probes was normally used but in the event of a probe failure, the computer would switch to a mode which derived heading from a single probe using equations (2) or (3) depending upon which probe failed. Tests were included in the program to continuously validate each probe output by establishing acceptable minimum and maximum voltage limits. The field strength (R) was continuously calibrated to reflect its change with altitude using a gain filter to suppress noise.

To suppress inherent data noise and provide azimuth rate information, the TM data were edited and filtered with a standard, sliding 19 point, cubic polynomial, leading edge, least squares filter. The azimuth rate was obtained from the polynomial slope at the 15th point which lags real time by approximately 0.5 second. The azimuth rate data was then additionally smoothed by a 30 point summer filter which increased the lag to approximately 2 seconds.

In the event of a single probe failure, equations (2) and (3) encounter difficulty in deriving the azimuth quadrant. To circumvent this difficulty, the polynomial filter continuously extrapolates to the 20th point to predict the subsequent value of azimuth. This predicted value is used to determine the quadrant while the remaining probe data are used to compute the heading. For a condition of temporary TM drop-out, the azimuth is obtained directly from the filtered prediction.

The program listing is included in Table E-1. This computer program provided the intelligence to drive two (2) XY plotters (vehicle heading and vehicle azimuth rate) plus vehicle heading and azimuth rate digital

displays. It was these displays which were monitored while manually sending clockwise and/or counter clockwise commands to change or control the vehicle heading during the drop operations.

SUBROUTINE AZCOMP
C THIS ROUTINE COMPUTES AZIMUTH AND AZIMUTH RATE FROM TELEMETRY DATA.

```

COMMON /STATUS/ IRN,ITG,IPG,IRBC,LOCTAB(M),LIGHTS(4),IDNAME,
1 IDDATE,NUNRDR(6),IPRISC(6,2),LOEN,IBOEN,LORECT,BURECT,TENPER,
2 IDEINP,IDEQ,MSLTGT(6,2),WDFLAG,IVERNO,ISPLL,IOREQ,IDRUMQ,
3 IPRINT(7),ITWOUT,IVDQ(6),FREQCN(2),FREQCT,GPDATA(32),IDFSET
4 ,NVPAS,NSTAT
EQUIVALENCE (TLOREC,LORECT)
END
INCLUDE AZCMH,LIST
COMMON /AZCMH/ AZC,AZRATE,ICK,P,AZN
END
EQUIVALENCE (V1,GPDATA(3)),(V2,GPDATA(2)),(AZD,AZRATE),(AZC,AZ)
DIMENSION Y(20),Z(151)
DATA INIT,B1,B2,RMAX,RMIN,RC,RAD,GR/
1 0,2.5498,2.3551,3.87,1.03,1.0193,57.295779,.0001/
DATA S1,S2,S3,S4,S5,S6,D/86575020.,-17739540.,758100.,
1 4589754.,-216600.,10830.,146919780./
DATA AZ1,RCH,RCHN,IN/-32.65,1.25,0.80,0/
1,SAZD,A,B,C/4*0.0/
C *** V1 = R * COS (AZ+AZ1) + B1
C V2 = R * SIN (AZ+AZ1) + B2
C
C *** CHECK MAG READINGS
CA=(V1-B1)/RC
SA=(B2-V2)/RC
IF (RMAX-V1) 6,6,1
1 IF (RMIN-V1) 2,6,6
2 IF (RMAX-V2) 9,9,3
3 IF (RMIN-V2) 4,9,9
C *** BOTH MAGS ARE GOOD
4 ICK=0
R=SQRT(CA*CA+SA*SA)*RC
IF (R.GT.RCHX.OR.R.LT.PCMN) GO TO 10
RC=RC+GR*(R-RC)
5 AZ = RAD*ATAN2(SA,CA)+AZ1
GO TO 11
C *** MAG 1 IS BAD
6 IF (RMAX-V2) 10,10,7
7 IF (RMIN-V2) 8,10,10
8 ICK=1
AP=(A+20.*B+225.*C)/D-AZ1
CA=COS(AP/RAD)
CK=1.0-SA*SA
IF (CK.LE.0.) CK=1.E-20
CA=SIGN(SQRT(CK),CA)
GO TO 5
C *** MAG 2 IS BAD
9 ICK=2
AP=(A+20.*B+225.*C)/D-AZ1
SA=SIN(AP/RAD)
CK=1.-CA*CA
IF (CK.LE.0.) CK=1.E-20
SA=SIGN(SQRT(CK),SA)
GO TO 5

```

```

C ***   BOTH MAGS ARE BAD
10      ICK=3
        AZ=(A+20.*B+225.*C)/D
11      INIT = INIT+1

        Y(INIT) = AZ
        IF(INIT.NE.20) GO TO 16
        INIT=19

C * * *   QUADRANT CHECK
        DEL=AZ-AZZ
        ADEL=ABS(DEL)
        IF(ADEL.LT.180.) GO TO 21
        SD=SIGN(1.,DEL)
        DO 12 I=2,19
12      Y(I)=Y(I)+360.*SD
        AZZ=AZZ+360.*SD
        DEL=AZ-AZZ
        ADEL=ABS(DEL)
21      IF(ADEL.LT.6.) GO TO 13
        Y(20)=AZZ+3.*SIGN(1.,DEL)
C * * *   LEAST SQUARES FIT
13      SUM1=0.0
        SUM2=0.0
        SUM3=0.0
        DO 14 I=1,19
        Y(I) = Y(I+1)
        SUM1=SUM1+Y(I)
        SUM2=SUM2+I*Y(I)
14      SUM3=SUM3+I*I*Y(I)
        A = SUM1*S1+SUM2*S2+SUM3*S3
        B = SUM1*S2+SUM2*S4+SUM3*S5
        C = SUM1*S3+SUM2*S5+SUM3*S6
        AZZ=(A+19.*B+361.*C)/D
        AZ=AZZ
        IF(AZ.LT.0.) AZ=AZ+360.
        AZD=10.*(B+30.*C)/D
        IN=MOD(IN,150)
        IN=IN+1
        SAZD=SAZD-Z(IN)+AZD
        Z(IN)=AZD
        AZD=SAZD/150.
        RETURN
16      AZZ = AZ
        A=AZ
        RETURN
        END

```

TABLE E-1 (CONTINUED) AZIMUTH PROGRAM LISTING

III. IMPACT PREDICTION PROGRAM

A. Program Requirement

As previously discussed in IIA, it is a requirement to provide impact information to Range Safety in order to select a drop point and corresponding flight azimuth. Additionally, the impact data are used to select the best impact area to expedite recovery of the spent hardware and to direct the recovery crew to the predicted impact area.

The program is required to operate in two modes as follows:

1. A static mode in which drop parameters are selected and impact analysis are performed using range intersect predictions.
2. A dynamic mode in which real time drop parameters are used and real time impact predictions are derived.

The mode of operation is manually selected and requires only a change in the source of input data.

B. Program Implementation

The Impact Prediction Program is based upon a nominal trajectory (perturbed by current wind conditions), latitude and longitude of drop and vehicle heading at drop.

The software reflects two modes of flight; accelerated flight (powered flight and decelerator transients); and equilibrium descent, where the aerodynamic drag is nearly equal to the system weight and the rate of descent is a direct function of the atmospheric density. The point of impact is obtained by first computing the wind effect to the nominal, zero wind, accelerated flight trajectory and then adding the wind drift effect of the equilibrium descent.

1. Accelerated Flight Mode

The vehicle position, at the completion of accelerated flight, is computed by adding wind corrections to a nominal zero wind trajectory which is represented by a nominal range (R) for each vehicle configuration and a nominal azimuth shift (ΔA_Z) which occurs because of vehicle spin. The time equivalents of the nominal trajectory and wind velocities are tabulated as functions of altitude at intervals of 5000 feet. The position corrections due to wind are computed by multiplying the wind velocity (W_i) by the time (t_i) required to transverse each of the 5000 foot intervals of altitude.

The position (X_a, Y_a) at the completion of accelerated flight is given by the equations:

$$(4) \quad X_a = X_D + R \sin (A_Z + \Delta A_Z) + \sum_{i=1}^N t_i (W_{x_i})$$

$$(5) \quad Y_a = Y_D + R \cos (A_Z + \Delta A_Z) + \sum_{i=1}^N t_i (W_{y_i})$$

where: A_Z is the drop heading
 X_D, Y_D is the range drop position.

The position location (X_a, Y_a) is the starting location for the equilibrium descent portion of the computation which follows.

2. Equilibrium Descent

During equilibrium descent, the vehicle weight counterbalances aerodynamic drag as shown in the relationship:

$$(6) \text{ Weight} = \text{Drag}$$

$$\begin{aligned} wt &= q C_D A \\ &= 1/2 \rho \left(\frac{dh}{dt} \right)^2 \end{aligned}$$

where: q is dynamic pressure

C_D is aerodynamic drag coefficient

ρ is atmospheric density

$\frac{dh}{dt}$ is rate of descent

It is noted that the atmospheric density (ρ) is considered constant over each altitude interval.

Rearranging equation (6), the time spent during any altitude interval can be computed as:

$$(7) \Delta t_i = \left(\frac{\rho C_D A}{2 wt} \right)^{1/2} \cdot 5000$$

The summation of the displacements obtained by multiplying the Δt by the corresponding wind velocity for each 5000 feet altitude interval gives the increment of vehicle displacement (X_b, Y_b) for the equilibrium descent portion of the impact prediction. This summation is represented by:

$$(8) X_b = \sum_{i=1}^N \Delta t_i (w_{x_i})$$

$$(9) Y_b = \sum_{i=1}^N \Delta t_i (w_{y_i})$$

The displacements given by equations (8) and (9) are added to the position computed by the accelerated flight operations to obtain the impact position (X_p, Y_p). The equations for this operation are:

$$(10) X_p = X_a + X_b$$

$$(11) Y_p = Y_a + Y_b$$

The impact prediction is computed separately for each of the possible flight conditions which are:

- o Powered flight followed by payload decelerated descent to impact.
- o Powered flight followed by aeroshell descent to impact.
- o Powered flight without decelerator deployment (abort mode).

The impact prediction program drove an XY plotted which displayed impact locations of the above flight articles superimposed on a map of the White Sands Missile Range. During the dynamic mode of operation, where the heading angle was fed directly to the impact prediction program from the azimuth program, the impact prediction was displayed continuously for the abort mode which was the most critical case due to its extended trajectory. This continuous impact display provided assurance to Range Safety that the overall azimuth control operation was adequate and stable and since the display was for the worst case (abort), Range Safety was assured that all flight articles would impact within an acceptable area.

IV. DECELERATOR MORTAR FIRE COMMAND PROGRAM

A. Program Requirement

The airborne command receiver was used to allow the ground computer to fire the decelerator mortar at the proper flight conditions. This real time command system minimized the effect of vehicle dispersions on the parachute qualification dynamic pressure test condition. The vehicle programmers were set to open a time window for this signal to prevent inadvertent mortar fire prior to despin and also to backup the ground command in the event this command link failed.

The ground computer compared real time information from all available radar sites and automatically selected the best radar tracking information. The velocity and altitude data were then used with the current atmospheric density and winds to compute the dynamic pressure. The dynamic pressure data were then compared to the nominal predictions and the flight deviation converted to an effective time shift in the mortar fire time for the powered flights. The subsonic flight mission used a fixed time from initiation of drop, due to the predictable nature of the gravitational acceleration.

B. Program Implementation

The generation of the ground mortar fire command is based on flight deviations from a reference trajectory. The radar data subsequent to drop is used in conjunction with current atmospheric density and wind velocity data to compute the dynamic pressure and ascent rate. The deviations from the reference trajectory are used with sensitivity coefficients to predict the time increment from nominal when the desired dynamic pressure will

probably occur. The predicted mortar fire time was continuously calculated after drop and filtered such that the latest information was weighted most heavily. The equation for predicting the mortar fire time is:

$$(12) \quad T = T_N + S_Q \left(\frac{Q - Q_N}{Q + DQ} \right) + S_H (H - H_N) + \Delta t$$

where: S_Q , S_H , Q_N , H_N are time varying functions.

The various elements are individually discussed below.

1. Nominal Trajectory Parameters (Q_N , H_N)

The reference trajectory was determined from the best estimate of the "as built" vehicle performance and the US Standard 1962 atmosphere.

2. Sensitivity Coefficients (S_Q , S_H)

The correlation between the deviations of randomly dispersed trajectories from the nominal trajectory and the deviation in the time from nominal at which these trajectories attain the desired dynamic pressure was used to generate the sensitivity coefficients. The two parameters, dynamic pressure and ascent rate, were evaluated separately. The dynamic pressure sensitivity coefficient (S_Q) is expressed as a percent variation and to avoid possible division by zero, early in flight when Q is small, it was incremented by a constant DQ .

3. Radar Track Data (Q, \dot{H})

The radar track furnished the position and rate of change of position data which when coupled with current atmospheric data defined dynamic pressure (Q). Ascent rate (\dot{H}) was obtained directly from the radar data.

4. Filter Constants

A dual filter was used to suppress the effect of random noises on the radar tracking data.

Variation in mortar fire time comes primarily from erratic velocity derived from radar position data, however, systematic variations in velocity are averaged and used to bias the mortar fire late such that a lower dynamic pressure is obtained. The primary filter was given a shorter time constant to respond to the latest data on dynamic pressure and still give a margin based on the overall variability in the data. This filter used a 5 second time constant on the variability of the mortar fire time with a 2 second time constant when the predicted mortar fire is shifting earlier and a 1 second time constant when shifting late. This filter is initialized by setting the initial value of mortar fire time equal to T MAX (dispersed backup programmer setting). This bias is reduced by a .5 second time constant as soon as valid data becomes available.

5. Nominal Mortar Fire Time (T_N)

Although a 6.0% (2σ) dispersion on mortar fire dynamic pressure was assumed, this value represents in part radar data uncertainties which are to some degree detected by the mortar fire program and used to bias the mortar fire time late. The nominal time is therefore selected based on the expected meteorological data uncertainty only. It is made up of two parts, density and winds. The density uncertainty is expected to be $\pm 3.5\%$ (3σ) and the winds 1.53% (3σ). The resultant 2σ dynamic pressure bias below the 30% overload dynamic pressure is 2.5%.

5. Time Delay (ΔT)

The transmission time delay from ground to air effects the mortar fire program in two ways. First, the mortar fire program uses a reference drop time which would be earlier than actual drop time due to the combined transmission and pyro delay. The second is the time delay between the commanding of mortar fire on the ground and the flight occurrence of mortar fire. To some degree, these delays are compensatory except that the radar data does not have this delay and therefore the actual trajectory and the reference nominal trajectory will not be time correlated. For this reason, care was taken to make the mortar fire program insensitive to time delays. A mortar fire transmission time delay of .03 seconds was included.

In the event the predicted mortar fire time is outside an acceptable mortar fire window, the data is assumed to be bad and the current mortar fire time estimate is slowly moved later. This rate of change was evaluated such that if acceptable data is never obtained, the mortar fire time would revert to the airborne backup programmer time.

The Fortran source programs for computing mortar fire command time are given in Table E-2.

```

FUNCTION FIRE(T,Q,HD)
*****
*
*       MORTAR FIRE REAL TIME CALCULATION PROGRAM
*       TRANSONIC FLIGHT
*****
T = TIME FROM DROP , SECONDS
Q = DYNAMIC PRESSURE , PSF
HD= VERTICAL VELOCITY, FPS (POSITIVE UPWARD)
TDEL=SYSTEM TIME DELAY
SIGT=INITIAL VALUE OF NOISE
SIGQ=Q BIAS TO PREVENT DIVISION BY 0.0
TMIN=EARLIEST MORTAR FIRE TIME
TMAX=LATEST MORTAR FIRE TIME
TNOM=TIME NOMINAL TRAJECTORY ACHIEVES DESIRED MORTAR FIRE Q
DTBD=OUT OF RANGE DATA BIAS ON TIME
COMMON /DATA/D(170)
EQUIVALENCE (D(161),G1 ),(D(162),G2 ),(D(163),G3 )
1,(D(164),)TBD),(D(165),TDEL),(D(166),SIGT),(D(167),SIGQ)
2,(D(168),TMIN),(D(169),TMAX),(D(170),TNOM)
DATA G1 ,G2 ,G3 ,DTBD ,TDEL,SIGT,SIGQ,TMIN,TMAX,TNOM/
, 0.02,2.0,0.05,0.012,0.10,2.00,2.00,33.5,39.5,37.0/
IF(T.GT.1.0) GO TO 2
SDT=SIGT
TMFL=TNOM+SDT
TMFC=TMFL
1 FIRE=TMFC-TDEL
RETURN
2 IF(T.GT.4.) GO TO 1
CALL TABNOM(T,HN,QN,HS,QS)
TMF=TNOM+1S*(HD-HN)+QS*(Q-QN)/(Q+SIGQ)
IF(TMFC.GT.TMAX) GO TO 3
IF(TMFC.GT.TMIN) GO TO 4
3 TMF=TMFC+TBD
GO TO 5
4 DT=ABS(TMFC-TMFL)-SDT
SDT=SDT+G1*DT
TMFL=TMF
TMF=TMF+SDT
5 IF(TMFC.GT.TMAX) TMF=TMAX
DT=TMF-TMFC
IF(DT.GT.0.0) DT=G2*DT
TMFC=TMFC+G3*DT
GO TO 1
END

```

TABLE E-2 MORTAR FIRE COMMAND LISTING

SUBROUTINE TABNOM(T,HN,QN,HS,QS)

*
* NOMINAL FLIGHT VERTICAL VELOCITY (HN),DT/DV (HS),
* DYNAMIC PRESSURE (QN),DT/DQ (QS) TABLE INTERPOLATION
*

COMMON /DATA/D(170)

DIMENSION HN1(40),QN1(40),HS1(40),QS1(40)

1, HN2(39),QN2(39),HS2(39),QS2(39)

EQUIVALENCE (D(2),QN1(2),QN2(1)),(D(42),HN1(2),HN2(1))

1, (D(82),QS1(2),QS2(1)),(D(122),HS1(2),HS2(1))

IT=1

DT=0.0

IF(T.LT.1.0) GO TO 1

IT=39

DT=1.0

IF(T.GE.40.) GO TO 1

IT=T

DT=IT

DT=T-DT

1 HN=HN1(IT)+DT*(HN2(IT)-HN1(IT))

QN=QN1(IT)+DT*(QN2(IT)-QN1(IT))

HS=HS1(IT)+DT*(HS2(IT)-HS1(IT))

QS=QS1(IT)+DT*(QS2(IT)-QS1(IT))

RETURN

END